NATO Science for Peace and Security Series - C:
Environmental Security

Safety, Reliability and Risks Associated with Water, Oil and Gas Pipelines

Edited by
Guy Pluvinage
Mohamed Hamdy Elwany

Springer

NATO OTAN

This publication is supported by:

The NATO Science for Peace and Security Programme

Safety, Reliability and Risks Associated with Water, Oil and Gas Pipelines

NATO Science for Peace and Security Series

This Series presents the results of scientific meetings supported under the NATO Programme: Science for Peace and Security (SPS).

The NATO SPS Programme supports meetings in the following Key Priority areas: (1) Defence Against Terrorism; (2) Countering other Threats to Security and (3) NATO, Partner and Mediterranean Dialogue Country Priorities. The types of meeting supported are generally "Advanced Study Institutes" and "Advanced Research Workshops". The NATO SPS Series collects together the results of these meetings. The meetings are co-organized by scientists from NATO countries and scientists from NATO's "Partner" or "Mediterranean Dialogue" countries. The observations and recommendations made at the meetings, as well as the contents of the volumes in the Series, reflect those of participants and contributors only; they should not necessarily be regarded as reflecting NATO views or policy.

Advanced Study Institutes (ASI) are high-level tutorial courses intended to convey the latest developments in a subject to an advanced-level audience

Advanced Research Workshops (ARW) are expert meetings where an intense but informal exchange of views at the frontiers of a subject aims at identifying directions for future action

Following a transformation of the programme in 2006 the Series has been re-named and re-organised. Recent volumes on topics not related to security, which result from meetings supported under the programme earlier, may be found in the NATO Science Series.

The Series is published by IOS Press, Amsterdam, and Springer, Dordrecht, in conjunction with the NATO Public Diplomacy Division.

Sub-Series

A.	Chemistry and Biology	Springer
B.	Physics and Biophysics	Springer
C.	Environmental Security	Springer
D.	Information and Communication Security	IOS Press
E.	Human and Societal Dynamics	IOS Press

http://www.nato.int/science
http://www.springer.com
http://www.iospress.nl

Series C: Environmental Security

Safety, Reliability and Risks Associated with Water, Oil and Gas Pipelines

edited by

Guy Pluvinage
University Paul Verlaine,
Metz, France

and

Mohamed Hamdy Elwany
University of Alexandria,
Egypt

Published in cooperation with NATO Public Diplomacy Division

Proceedings of the NATO Advanced Research Workshop on
Safety, Reliability and Risks Associated with Water, Oil and Gas Pipelines
Alexandria, Egypt
4–8 February 2007

A C.I.P. Catalogue record for this book is available from the Library of Congress.

ISBN 978-1-4020-6525-5 (PB)
ISBN 978-1-4020-6524-8 (HB)
ISBN 978-1-4020-6526-2 (e-book)

Published by Springer,
P.O. Box 17, 3300 AA Dordrecht, The Netherlands.

www.springer.com

Printed on acid-free paper

TABLE OF CONTENTS

PREFACE

Pipes are of major importance for transport of liquids and gas mainly for water, natural gas and oil. In Western Europe, the distribution of drinking water has been achieved 20 years ago and the problem of renewal of the networks is now considered as an accurate question in terms of money and time. From the quantitative point of view, it has been shown that the quality of the networks is highly perfectible: the primary rate is about 70% that means about 30% of water is lost by leak or break. In Mediterranean countries the rate is lower and sometimes more than 80% is lost by leaks, breaks and illegal withdrawing. From the qualitative point of view, a degradation of the distributed water has been pointed out, which is due to pollution of resource and damage of the network.

Length of the water networks is greatly different from one country to another. Total gas pipes length in the world is estimated to 1 million km for gas transport (pipes of diameter 80–1,000 mm), in the USA 450,000 km, in Russia 235,000 km, in Canada 71,300 km, in France 30,815 km. In China, the construction of the natural gas pipelines has gained its initial scale. By the end of 2003, the total length of the national natural gas pipe was about 21,000 km, represented by such long-distance gas pipelines as WEP, Shaan-Jing (Jingbian-Beijing), Se-Ning-Lan (Sebei-Xining-Lanzhou) and Ya13-1- Hong Kong pipelines.

The pipelines are of capital importance for the landlocked countries. Currently, only crude exports of Russia towards Europe completely depend on the pipelines. The pipeline of Drushba, for instance, is built on a distance of 3,640 km, from the area of Samara in Russia to the refinery of Leuna in Germany, with 34 stations of pumping.

The pipelines of long distance have a great geopolitical importance. It is the case, for instance, for the area of the Caspian Sea, where all the plans of export of oil starting from this area primarily depend on the construction of pipelines. The pipeline remains the mean of transcontinental transport least expensive compared to the rail-bound or ground transport. It constitutes under this aspect an important mean of transport between the USA and Canada, but also between the various European countries where the pipelines are relatively of short distance. One of the biggest is Trans-Alaska oil pipe (TAPS) of length 1,270 km. This pipeline connects the Arctic coast to the Western coast of Alaska. It transports 2 million oil barrels per day.

It became increasingly paramount to ensure the safe utilisation of such plants in order to prevent economical, social and ecological losses. From a

technical point of view, pipelines are complicated 3D structures that include straight pipes, nozzles, pipe-bends, dissimilar welded joints, etc. In addition, their operating conditions can be quite severe, that is, internal pressure and cyclic loading (vibration) combined with the influence of internal and external corrosive environments. The potential synergy of such parameters can lead to an increase in the risk of damage and unexpected fracture of these structures during their long-term exploitation.

Leak and fracture of pipes is assumed to be achieved by initiation and propagation of a defect and final failure when defect reaches a critical length. To have a precise idea of life duration of the water pipes the three following components need to be precisely described:

1. Defect initiation
2. Crack propagation
3. Final failure

Defect Initiation

Initial defect is assumed in one case as being corrosion pitting and, in the second case, scratches, gouges, etc., made during implementation or service life.

When local corrosion is the principal mode of damage, due to the statistical character of corrosion pits, it needs to be characterised by a probabilistic distribution such as Weibull's or Gumbel's laws in order to determine the probability of the most severe damage or the deepest corrosion crater. Scratches, gouges or dents are now considered as more frequent damage than corrosion. They do not appear at the beginning, but at an uncertain part of the life. They are due to impact with foreign objects such agriculture or civil engineering equipments. Statistical distribution on geometry and orientation are needed to determine also the probability of the most severe defect. In both cases, this gives the initial defect size a_i for a reference time and its probability of occurrence. This initial defect can be related with the defect detected during inspection, if it occurs.

Crack Propagation

In service, cyclic variation of internal pressure is present, but also bending coming from soil movement or repeated vehicles passage, which generate fatigue loading. An initial defect is growing under mechanical and environmental conditions. The current status, in terms of prediction of failure, is based on corrosion studies of unstressed components and fracture and fatigue of pipes within non-aggressive environments. This approach has a number of fundamental limitations: corrosion effects are influenced by applied stress state and damage is not constant over the duration of stress–corrosion interaction; the description of the stress field around corrosion defects is not adequately

described and therefore the fracture criterion may be non-conservative. Furthermore, corrosion science studies have shown that differences in electrochemistry exist between a pit cavity and an open smooth surface.

Final Failure

An initial defect is growing under mechanical and environmental conditions. Fracture occurs when defect has reached its critical size corresponding to service conditions $a_{cr,1}$. Under over-pressurised conditions the critical defect is $a_{cr,2}$, which has a size smaller than $a_{cr,1}$. For a well-controlled and programmed replacement of the water grids, it is necessary to know kinetics of crack growth of the defect size between $a_{cr,2}$ and $a_{cr,1}$. From this, it is possible to know the residual life duration of the examined water pipes.

A more conservative approach consists in taking into account the possibility of crack extension of surface defects. A surface crack can be extended under fatigue, corrosion or combined corrosion and fatigue and reach a critical size with wall perforation behind crack front. Crack growth until this size is possible as far as length and crack opening displacement are insufficient to ensure a detectable leak, or until the critical crack size to lead to brittle fracture is not reached. In any case, used method to apply the "Leak Before Break" concept needs to ensure a given conservatism given by experimental data.

This book presents papers, which were delivered at the NATO Workshop "Safety, reliability and risks associated with water, oil and gas pipelines" held in Helnan Palestine Hotel, Alexandria (Egypt), 4th–8th February 2007, under the auspices of the NATO Science for Peace and Security Program. The organisers acknowledge the Program Committee for attribution of a support grant. Three major defect assessment tools for pipes are presented:

(a) Failure assessment diagram and particularly the SINTAP
(b) Limit analysis
(c) Strain design approach

Repairing methods are based on results of investigation. Methods such as welded sleeve, clamped composite sleeve, grinding and pipe replacement are described.

Professor Guy Pluvinage
Professor Mohamed Hamdy Elwany

GENERAL APPROACHES OF PIPELINE DEFECT ASSESSMENT

G. PLUVINAGE
Laboratoire de Fiabilité Mécanique
ENIM-UPV Metz (France)

Abstract: In this paper the three major defect assessment tools for pipes are presented: (i) the failure assessment diagram and particularly the SINTAP procedure, (ii) a notch adapted failure assessment diagram by modification of the SINTAP using the volumetric method, (iii) different pipe limit analysis and their comparison for the same kind of defects.

Keywords: failure assessment diagram, SINTAP, notch, limit analysis

1. Introduction

Pipelines have been employed as one of the most practical and low price method for large oil and gas transport since 1950. The pipe line installations for oil and gas transmission are drastically increased in last three decades. Consequently, the pipeline failure problems have been increasingly occurred. The economical and environmental and eventually in human life considerations involve the current issue as structural integrity and safety affair. The explosive characteristics of gas provide high wakefulness about the structural integrity. Therefore, the reliable structural integrity and safety of oil and gas pipelines under various service conditions including presence of defects should be warily evaluated. The external defects, e.g., corrosion defects, gouge, foreign object scratches and pipeline erection activities are major failure reasons of gas pipelines. A typical example of a corrosion defect is given in Figure 1. According to numerous design codes, this kind of defects is considered as a semi-elliptical crack-like surface defect of aspect ratio a/c. The aspect ratio varies in range [0.1–1] depending on corrosion rate anisotropy. Another example of dents produce by impact of foreign object (IFO) is presented in Figure 2.

G. Pluvinage and M.H. Elwany (eds.), Safety, Reliability and Risks Associated with Water, Oil and Gas Pipelines, 1–22.

Several types of pipes failures can be distinguished as longitudinal, circumferential or helicoidally failures. These types depend mainly on pipe diameter. For small diameter pipes, where bending stresses are predominant, circumferential failure occurs. For large diameters, hoop stresses are more important than bending stresses and longitudinal failure appears. When bending and hoop stresses are of the same importance, fracture path becomes spiraled.

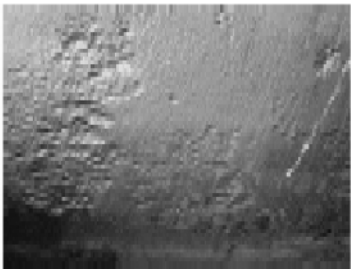

Figure 1. Example of corrosion defect on pipe.

Figure 2. Example of dent on pipe.

Pipe steels have yield stress up to 700 MPa for the most recent quality in order to ensure enough ductility and weldability. Failures emanating from the above mentioned defect are elasto-plastic fracture or plastic collapse. For these two situations, defect assessment is made generally by two tools: failure assessment diagram (FAD) and limit analysis.

According to numerous design codes, all defects are considered as a semi-elliptical crack-like surface defect of aspect ratio a/c. This is a very conservative approach. Trends are now to take into account the real geometry of the defect and particularly its finite tip radius. For this reason, tools like the FAD need to bee modified.

In this paper the two major defect assessment tools for pipes are presented:

1. The FAD and particularly the Structural Integrity Assessment Procedure (SINTAP) [1]
2. A notch-adapted failure assessment diagram (NFAD) by modification of the SINTAP using the volumetric method
3. A comparison of different limit analysis for the same kind of defect is given in the third part.

2. Sintap Procedure for Crack-Like Defect

In a FAD, the basic fracture mechanics relationship with three parameters: applied stress (σ_{app}), defect size (a) and fracture toughness (K_{IC} or J_{IC}) is

replaced by a two parameters relationships f(k_r, S_r). Stress and defect size are combined into the applied stress intensity factor K_{app} or applied J parameter J_{app} and the parameter k_r and S_r are non-dimensional according to the following initial definitions:

$$k_r = \frac{K_{app}}{K_{Ic}} \text{ and } S_r = \frac{\sigma_{app}}{Rm} \tag{1}$$

where Rm is the ultimate strength. In the plane {S_r; k_r}, a given relationship $k_r = f(S_r)$ delimits the safe zone and the failure zone (Figure 3).

Initially, the relationship between non-dimensional stress intensity factor and non-dimensional stress was issued from a plasticity correction able to describe any kind of failure continuously from brittle fracture to plastic collapse.

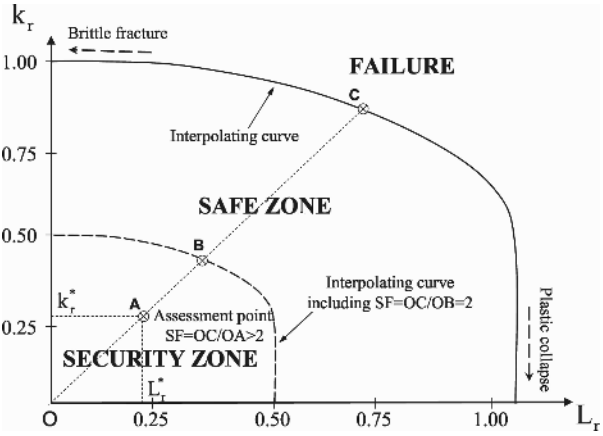

Figure 3. Typical presentation of failure assessment diagram (FAD). Definition of safety factor.

A typical representation of a FAD is given in Figure 3. On the same figure, the load safety factor F_s is defined according to:

$$F_S = \frac{OB}{OC} \tag{2}$$

The advantages to the use of FAD are:

- The use of an unique tool for any critical situations (in other way, several failure criteria need to be used from LFM, EPFM and LA)
- To get, for any non-critical situation the safety factor F_s.

The SINTAP procedure is derived from the initial FAD. However, definitions of non-dimensional parameters are little different: k_r parameter is derived from the applied J_{ap} parameter and fracture toughness J_{Ic}

$$k_r = \sqrt{\frac{J_{ap}}{J_{Ic}}} \tag{3}$$

and the S_r parameter is replace by the L_r parameter

$$L_r = \frac{P}{P_L} = \frac{\sigma_{ref}}{\sigma_0} \tag{4}$$

where P is the applied load, P_L the limit load. The material behaviour is assumed to follow the Ramberg–Osgood relationship:

$$\frac{\varepsilon}{\varepsilon_0} = \frac{\sigma}{\sigma_0} + \alpha\left(\frac{\sigma}{\sigma_0}\right)^n \tag{5}$$

where ε_0 and σ_0 are respectively the reference strain and stress and n the strain hardening exponent. The reference stress is given by:

$$\sigma_{ref} = \frac{P}{P_0}\sigma_0 \tag{6}$$

where P_0 is the reference load.

The applied J parameter is obtained by assuming proportionality between J_{app} and the elastic value of J parameter J_{el}. The coefficient of proportionality is derived from the constitutive non-dimensional stress–strain relationship of the material.

The relationship between k_r and L_r is considered as a limit curve obtained from numerous experimental data. This limit curve is more physically an interpolation curve between brittle fracture representative assessment point and plastic collapse. In these methods, failures near plastic collapse are represented by data in the "tail" of the diagram.

There are several similar FAD procedures, i.e., EPRI in the USA, R6 in the UK, RCCMR in France with small and more and less conservative difference in the safe zone area. The SINTAP is the result of a European project of a multidisciplinary approach in order to get a unify multilevel method useful for SME to large companies. The level hierarchy depends on knowledge of description of stress–strain curve and fracture toughness. Lower levels are used with simple description of stress–strain curve but with higher conservatism.

The mathematical expressions of SINTAP for the lowest and more conservative (default level) is given as below:

$$f(L_r) = \left[1 + \frac{L_r^2}{2}\right]^{\frac{-1}{2}} \left[0.3 + 0.7 \times e^{\left(-0.6 \times L_r^6\right)}\right], \quad \text{for } 0 \le L_r \le 1 \text{ where } L_r^{max} = 1 + \left(\frac{150}{\sigma_Y}\right)^{2.5} \tag{7}$$

where $f(L_r)$, L_r, L_r^{max}, σ_Y, are interpolating function, non-dimensional loading parameter, maximum value of non-dimensional loading or parameter, yield stress, respectively.

In this paper, SINTAP Level 1 has been used to determine the safety factor and the reliability factor for a boiler tube (Figure 4) exhibiting a longitudinal defect inside the tube weld, applying deterministic and probabilistic methods [2]. The influence of temperature is discussed.

The material is a steel used for boiler pipes. Its mechanical properties for five different temperatures are reported in Table 1.

TABLE 1. Mechanical properties of a boiler steel for five different temperatures.

T [c°]	20	400	520	540	560
K_{Ic}[MPa√m]	167.1	160.7	117.9	106.5	94.1
$R_{p0,2}$ [MPa]	380	275	275	255	240
R_m [MPa]	500	470	420	400	380

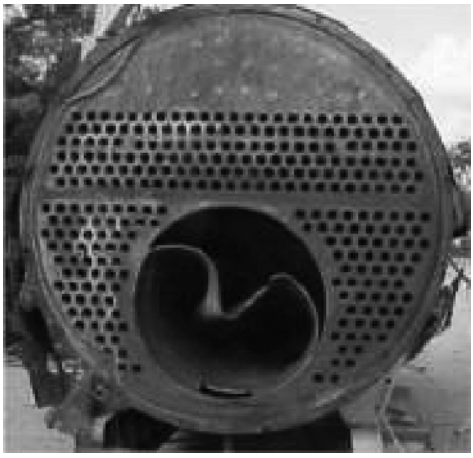

Figure 4. Example of a boiler with the different tubes.

The boiler pipe has an external diameter of 273 mm and a wall thickness of 24 mm. The pipe is welded and the butt weld is assumed to exhibit a

longitudinal semi-elliptic surface defect of depth a = 2.25 mm, its great axis is 2c = 15 mm and its aspect ratio a/2c = 0.15.

Under the effect of internal pressure the hoop stress of 77 MPa is produced in the tube. The stress intensity factor for a semi-elliptic surface defect is given in code SINTAP in the following form:

$$K_I = \frac{PR_m}{t}\sqrt{\pi a}\; F\left(\frac{R_i}{t}, \frac{2c}{a}, \frac{a}{t}\right) \tag{8}$$

R_i is the internal half diameter, t is the wall thickness of the pipe and R_m its mean half diameter.

The value of the geometrical correction for this defect is equal to $F\left(\frac{R_i}{t}, \frac{2c}{a}, \frac{a}{t}\right) = 1.445$. Variations of F with small variation are small and F is considered as constant in the present study.

3. Probabilistic Approach of Safety Factor by Coupling Sintap and FORM/SOTM Method

First-Order Reliability Methods (FORM) and Second-Order Reliability Methods (SORM) are general methods of structural reliability theory [2]. These methods are based on linear (first-order) and quadratic (second-order) approximations of the limit state surface $g(X) = 0$ tangent to the closest point of the surface to the origin of the space. The determination of this point involves non-linear programming.

The FORM/SORM algorithms involve several steps:

- In the first step, the space of uncertain parameters x is transformed into a new N-dimensional space u consisting of independent standard Gaussian variables. The original limit state $g(x) = 0$ then becomes mapped onto the new limit state $g_u(u) = 0$ in the u space.
- In the second step, the point on the limit state $g_u(u) = 0$ having the shortest distance to the origin of u space is determined using an appropriate non-linear optimization algorithm. This point is referred to as the design or β-point, and has a distance β_{HL} to the origin of the u space.
- In the third step, the limit state $g_u(u) = 0$ is approximated by a surface tangent to it at the design point. Lets such limit states be $g_L(u) = 0$ and $g_Q(u) = 0$, which correspond to approximating surfaces of hyperplane (linear or first-order) and hyperparabolic (quadratic or second-order), respectively.

The probability of failure P_F is thus approximated by

$$P_{F,1} = \phi(-\beta_{HL})$$

$$P_{F,2} \approx \phi(-\beta_{HL}) \prod_{i=1}^{N-1} (1-\kappa_i \beta_{HL})^{-1/2} \tag{9}$$

$$\phi(u) = \frac{1}{\sqrt{2\pi}} \int_{-\infty}^{u} exp(-\frac{1}{2}\xi^2) d\xi \tag{10}$$

$\phi(u)$ is the cumulative distribution function of a standard Gaussian random variable, and k_i' are the principal curvatures of the limit state surface at the design point. FORM/SORM are analytical probability computation methods. Each input random variable and the performance function $g(x)$ must be continuous.

Until the 19th century, all constructions were conceived and carried out mainly in an empirical way. The introduction of the steel construction required development of strength of materials. The principle of safety initially adopted consisted in making sure that the maximum stress in the most critical section of construction remained lower than a working load L obtained by dividing the resistance of material R by conventionally accepted safety factor F_s The engineers realized gradually the disadvantage of this design approach, and this contributed to develop the reliability concept based on a probabilistic approach. According to new approach, a structure is considered safe if probability of its failure is lower than a conventional accepted value, value that depends on many factors like the expected life of the structure, consequences generated by its failure, risks of obsolescence, relevant economic criteria like the costs of replacement, maintenance costs.

Instead of imposing a safety factor based on the material resistance or on load or on defect size or all the three, the probabilistic approach introduces the reliability factor as quantitative criterion of a low failure probability.

Within the chosen procedure, the following parameters are treated as random parameters:

- Fracture toughness
- Yield strength
- Ultimate tensile strength
- Defect distribution
- Pressure distribution

These random parameters are treated as not being correlated with one another. The parameters can follow a normal, log-normal, Weibull or some special distributions (for the defects).

The coefficient of variation CV_x is an excellent indicator of the homogeneity of the analyzed unit. This one will be declared homogeneous if CV < 1/3, concerning the properties of materials, if the mechanical tests were carried out carefully, the coefficient of variation is an excellent indicator of the manufactures quality, thus, the manufacture of low carbon steel leads to a coefficient of variation CV = 0, 1, for ultimate strength, yield stress and fracture toughness. The pressure distribution obeys to the same coefficient of variation. We notice that for exponential distribution the coefficient of variation is necessary taken as unit. The presentation of the method will be arrived out with the value of coefficient of variation.

The fracture toughness is assumed to be a Weibull's distribution. The Weibull's probability density function has the following form:

$$f(K_{IC}) = C \times m \times K_{\rho,c}^{m-1} \exp\left(-C \times K_{\rho,c}^{m}\right) \tag{11}$$

where C (scale) and m (shape) are the Weibull's distribution parameters. μ (mean) and σ (standard deviation) are the input data into the program and are related to the Weibull's distribution parameters as follows:

$$\begin{aligned} \mu &= \frac{C^{-1}}{m * \Gamma\left(1+\frac{1}{m}\right)} \\ \sigma &= C^{\frac{-2}{m}}\left[\Gamma\left(1+\frac{2}{m}\right)-\Gamma^2\left(1+\frac{1}{m}\right)\right] \end{aligned} \tag{12}$$

where $\Gamma(Z)$ is the gamma function, defined by the following integral:

$$\Gamma(Z) = \int_0^{\infty} t^{Z-1} e^{-t}\, dt \tag{13}$$

Yield strength ultimate, tensile strength and internal pressure can be mainly assumed as a normal distribution. The normal probability density function has the following form:

$$F(X) = \frac{1}{\sigma\sqrt{2\pi}} \exp\left[-\frac{1}{2}\left(\frac{X-\mu}{\sigma}\right)\right] \tag{14}$$

For defect, depth a is assumed to follow an exponential distribution. The probability density function has the following form:

$$F(X) = \lambda \exp\left(-\lambda a\right) \tag{15}$$

where λ is the exponential distribution parameter. μ (mean), the standard deviation, σ is related to λ as below:

$$\mu = \sigma = \frac{1}{\lambda} \tag{16}$$

We can calculate the probability of rupture by using methods FORM/ SORM. The results show that the probability of rupture decreases when the temperature grows at constant stress. The following Table 2 gives the fracture stress for a probability of 10^{-6} for different temperatures.

TABLE 2. Evolution of the fracture stress corresponding to a probability of failure Pf $=10^{-6}$ with temperature.

Stress (MPa)	150	110	100	95	90
Temperature (C°)	20	400	520	540	560

From obtained results it is possible to find the reliability factor F_s which decreases with increasing temperature T according to the following equation:

$$F_s = 2.7879\ T^{-0.1167} \tag{17}$$

4. Modified Sintap for Fracture Emanating from Notches

In the present section, the structural integrity of corroded pipes is addressed [3]. The semi-spherical defects, semi-elliptical defects and long blunt notch are taken into account and are not considered as crack-like defects. Pipes are made in API X52 which is considered as following as exhibiting strain hardening behaviour. The obtained stress distributions at defect tip yield the notch stress intensity factor and stress parameters which are needed to assess structural integrity by the notch-adapted SINTAP.

4.1. MECHANICAL PROPERTIES OF API X52

API X52 was the most common gas pipeline material for transmission of oil and gas during 1950–1960. The chemical composition of API X52 is shown in Table 3.

TABLE 3. Chemical composition of API X52 (Weight %).

C	Mn	Si	Cr	Ni	Mo	S	Cu	Ti	Nb	Al
0.22	1.22	0.24	0.16	0.14	0.06	0.036	0.19	0.04	<0.05	0.032

In Table 4, the mechanical properties of API X52 are presented.

TABLE 4. Mechanical properties of API X52.

E (GPa)	ν	σ_Y (MPa)	σ_U (MPa)	A%	n	K (MPa)	K^*_C (MPa√.m)
203	0.30	410	528	32	0.164	876	116.6

where E, ν, σ_Y, σ_U, $A\%$, n, K and K_C^* are Young's modulus, Poisson's ratio, yield stress, ultimate stress, relative elongation, hardening exponent, hardening coefficient and fracture toughness, respectively.

4.2. VOLUMETRIC METHOD

The volumetric method [4] is a local fracture criterion, which assumed that the fracture process requires a certain volume. This volume is assumed as a cylindrical volume with effective distance as its diameter. Physical meaning of this fracture process volume is "the high stressed region" where the necessary fracture energy release rate is stored. The difficulty is to find the limit of this "high stressed region". This limit is a priori not a material constant but depends on loading mode, structure geometry and load level. The size of the fracture process reduced to the effective distance according to the above mentioned assumptions is obtained by examination of the stress distribution.

The bi-logarithmic elastic-plastic stress distribution (Figure 2) along the ligament exhibits three distinct zones which can be easily distinguished. The elastic-plastic stress primarily increases and it attains a peak value (zone I) then it gradually drops to the elastic-plastic regime (zone II). Zone III represents linear behaviour in the bi-logarithmic diagram. It has been proof by examination of fracture initiation sites that the effective distance correspond to the beginning of zone III which is in fact an inflexion point on this bi-logarithmic stress distribution. A graphical method based on the relative stress gradient χ associated the effective distance to the minimum of χ.

The relative stress gradient is given by:

$$\chi(r) = \frac{1}{\sigma_{yy}(r)} \frac{\partial \sigma_{yy}(r)}{\partial r} \tag{18}$$

where $\chi(r)$ and $\sigma_{yy}(r)$ are the relative stress gradient and maximum principal stress or crack opening stress, respectively.

The effective stress for fracture is then considered as the average volume of the stress distribution over the effective distance. However stresses are multiply by a weight function in order to take into account stress gradient due to geometry and loading mode.

The stress distribution is given by:

$$\sigma_{eff} = \frac{1}{X_{eff}} \int_0^{X_{eff}} \sigma_{yy}(r) \times (1 - r \times \chi(r))\, dr \tag{19}$$

Therefore, the notch stress intensity factor is defined as a function of effective distance and effective stress:

$$K_\rho = \sigma_{eff} \sqrt{2\pi X_{eff}} \tag{20}$$

where K_ρ, σ_{eff} and X_{eff} are notch stress intensity factor, effective stress and effective distance, respectively.

Description of this kind of stress distribution at notch tip and the procedure with the help of the relative stress gradient is given in Figure 5.

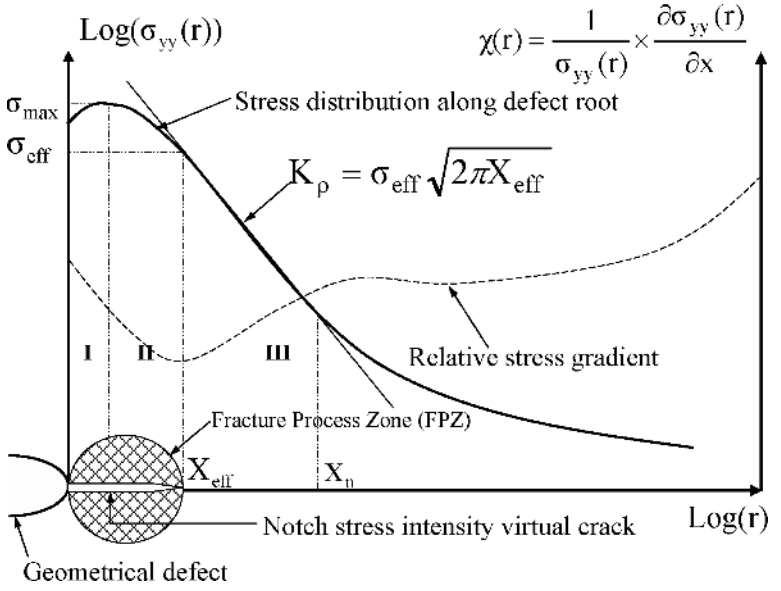

Figure 5. Schematic elastic-plastic stress distribution along notch ligament and notch stress intensity virtual crack concept.

4.3. NOTCH-ADAPTED FAILURE ASSESMENT DIAGRAM (NFAD)

An example of NFAD is given by Matvienko [5]. The parameter k_r is defined as the ratio of the applied notch stress intensity factor and fracture toughness K_{IC}.

$$k_r = \frac{K_\rho}{K_{Ic}} = \frac{\sqrt{1-\left(\frac{\sigma_g}{\sigma_{coh}}\right)^2}}{\sqrt{\left[1-\left(\frac{\sigma_g}{\sigma_{coh}}\right)^2 \cdot \frac{1}{(k_t)^2}\right]}}. \tag{21}$$

The interpolation curve is taken from the cohesive zone model and the criterion of average stress in the cohesive zone head of the notch tip as indicates in [5]. However the critical stress intensity factor is shown as to be a decreasing function of the elastic stress concentration factor and consequently failure assessment curve is notch radius dependant (Figure 6). In order to get a NFAD interpolation curve independent of the notch radius, the parameter k_r is defined as follows:

$$k_r = \frac{K_{\rho,app}}{K_{\rho,c}(\rho)} \tag{22}$$

where the fracture toughness $K_{\rho,c}$ is a function of notch radius.

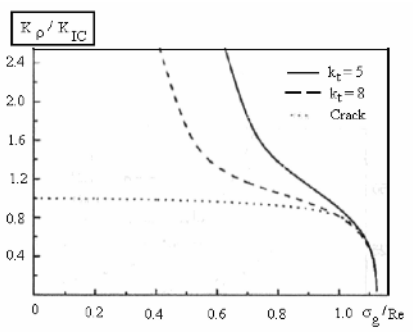

Figure 6. NFAD according to Matvienko [5].

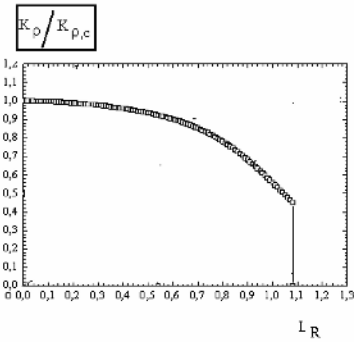

Figure 7. NFAD independent of notch radius [4].

L_r parameter keeps the same definition. By assumption, the interpolation curve is independent of notch radius and is the same that the crack's one. Consequently, the SINTAP interpolation curves were used in the NFAD (Figure 7).

4.4. DEFECT GEOMETRY

In Figure 8 a, b and c, the geometrical configuration of current defects is presented. In the present paper, the defect depth for all models is equal to one half of pipe wall thickness and the defect length over defect depth ratio is considered as ten ($L/d = 10$). Using the same defect depth and length-depth ratio allows comparison of the geometrical features on the stress distribution and stress gradient around the chosen defects.

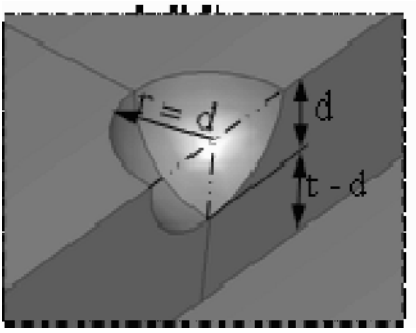

Figure 8-a. Central semi-spherical defect (t = 6.1mm, d = t/2).

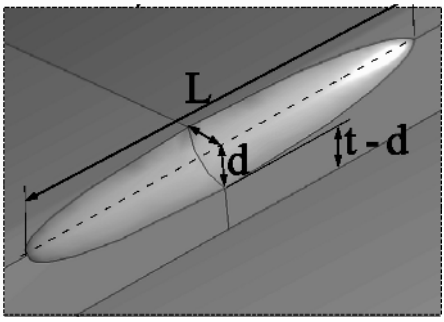

Figure 8-b. Central semi-elliptical defect (t = 6.1 mm, d = t/2, d/L = 0.1)

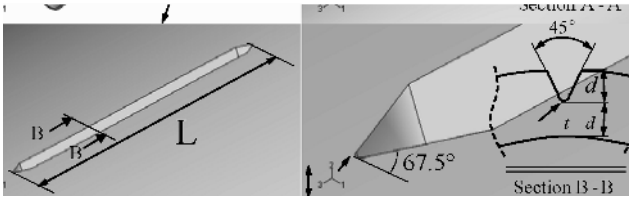

Figure 8-c. Central longitudinal notch (t = 6.1 mm, d = t/2, d/L = 0.1, ρ = 0.15 mm).

4.5. BI-LOGARITHMIC STRESS DISTRIBUTION AT DEFECT TIP

In Figure 9, the stress distribution along the radial and longitudinal directions of the three kinds of defects are plotted in bi-logarithmic graphs Then the elastic-plastic relative stress gradient method is applied to specify the effective distance and the effective stress.

The obtained notch stress intensity factors and applied internal pressure are utilized to define the required assessment points which are used in the failure assessment prediction of the SINTAP.

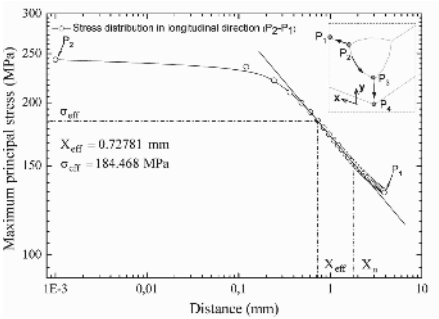

Figure 9-a. Semi-spherical defect in longitudinal direction.

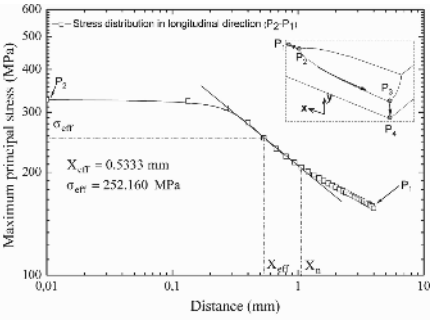

Figure 9-b. Semi-elliptical in longitudinal direction.

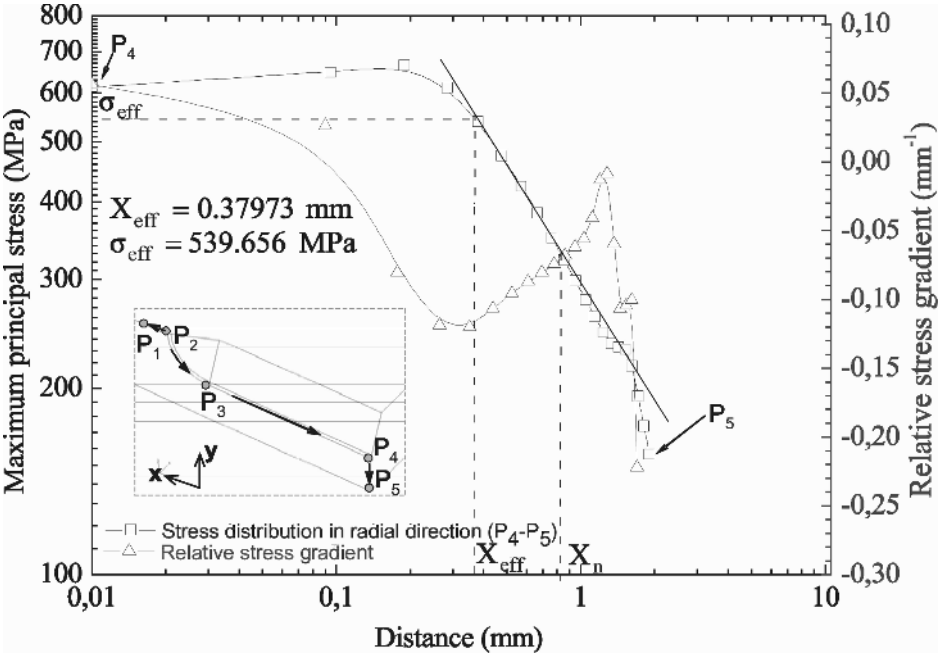

Figure 9-c. Blunt notch in radial direction.

The safety factor has been determined on the FAD according to the procedure described in Figure 2. Two SINTAP level has been used (Level 0 and Level 1). Characteristics of these two levels are given in Table 6.

TABLE 5. Effective stress, effective distance and notch intensity factors along radial and longitudinal direction using 70 bars as applied internal pressure.

Defect type	Radial direction		
	Effective distance (mm)	Effective stress (MPa)	K_ρ (MPa.√m)
Semi-spherical	0.42	202.7	10.4
Semi-elliptical	0.67	343.4	22.3
Blunt notch	0.38	539.6	26.3
Defect type	Longitudinal	direction	
	Effective distance (mm)	Effective stress (MPa)	K_ρ (MPa√.m)
Semi-spherical	0.72	184.4	12.4
Semi-elliptical	0.53	252.1	14.5
Blunt notch	0.63	311.4	19.7

TABLE 6. SINTAP levels 0 and 1 description.

Level	Data needed	When to use
Default level		
Level 0	Yield or proof strength	When no other tensile data available
Standard levels		
1. Basic	Yield or proof strength: ultimate tensile strength	For quickest result. Mismatch in properties less than 10%

The mathematical expression of the interpolation curve f(Lr) are given in formulae (22) and (23)

LEVEL 0

$$f(L_r) = \left[1 + \frac{L_r^2}{2}\right]^{\frac{-1}{2}} \left[0.3 + 0.7 \times e^{\left(-0.6 \times L_r^6\right)}\right], \quad \text{for} \quad 0 \le L_r \le 1 \text{ where } L_r^{max} = 1 + \left(\frac{150}{\sigma_Y}\right)^{2.5} \tag{23}$$

LEVEL 1

TABLE 7. Safety factors according to the SINTAP.

Type	SINTAP 0B	SINTAP 1B
Semi-spherical	4.095	4.106
Semi-elliptical	3.407	3.750
Blunt notch	3.186	3.583

$$f(L_r) = \begin{cases} \left[1 + \dfrac{L_r^2}{2}\right]^{\frac{-1}{2}} \left[0.3 + 0.7 \times e^{\left(-\mu \times L_r^6\right)}\right], & 0 \le L_r \le 1 \\ \left[1 + \dfrac{1}{2}\right]^{\frac{-1}{2}} \left[0.3 + 0.7 \times e^{(-\mu)}\right] \times L_r^{\frac{N-1}{2N}}, & 1 < L_r \le L_r^{max} \end{cases}$$

where
$$\mu = \min\left[0.001 \times \frac{E}{\sigma_Y}, 0.6\right], \qquad (24)$$

$$L_r^{max} = \frac{1}{2}\left(\frac{\sigma_Y + \sigma_U}{\sigma_U}\right), \; N = 0.3\left(1 - \frac{\sigma_Y}{\sigma_U}\right)$$

In Table 7, different safety factors according to the SINTAP are presented.

We notice that all values of the safety factor are above the conventional value of 2 and consequently all the defect sizes are acceptable.

5. Assesment of Defect by Limit Analysis

The structural integrity of corrosion defects is substantially studied (see Figures 10 and 11). In Figure 10, a list of methods available for corrosion defect assessment is presented. They are grouped vertically by their type, codified methods or others and horizontally by their applicability, pressure or combined loading, etc.

5.1. ASME B31G AND MODIFIED ASME B31G

ASME B31G [6] is a code for evaluating the remaining strength of corroded pipelines. It is a supplement to the ASME B31 code for pressure piping. The code was developed in the late 1960s and early 1970s at Battelle Memorial Institute and provides a semi-empirical procedure for the assessment of corroded pipes. Based on an extensive series of full-scale tests on corroded pipe sections, it was concluded that pipeline steels have adequate toughness and the toughness is not a significant factor. The failure of blunt corrosion flaws is controlled by their size and the flow stress or yield stress of the material. The input parameters include pipe outer diameter (D) and wall thickness (t), the specified minimum yield strength (σ_Y), the maximum allowable operating pressure (MAOP), longitudinal extent of corrosion (L_c) and defect depth (d).

According to the ASME B31G code, a failure equation for corroded pipelines was proposed by means of data of burst experiments and expressed with consideration of two conditions below:

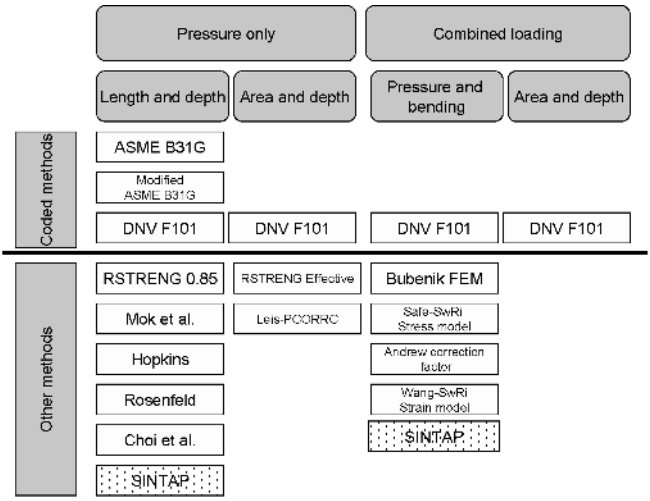

Figure 10. Methods for corrosion assessments.

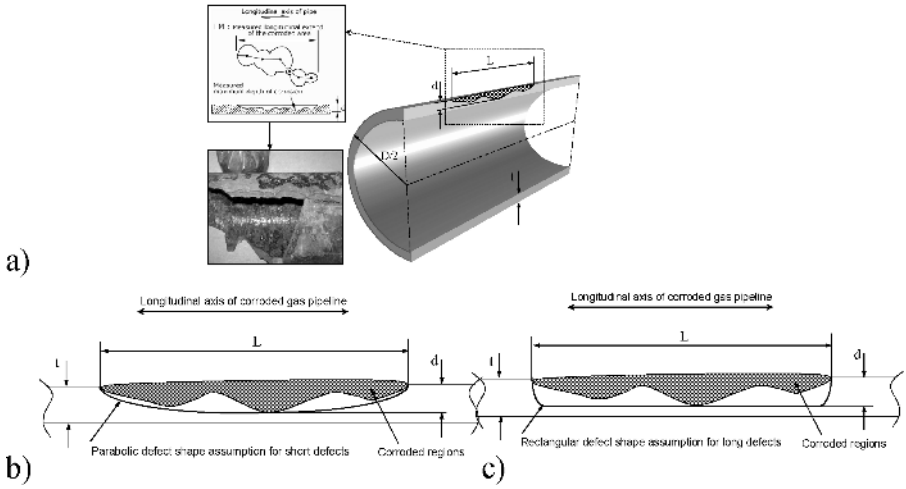

Figure 11. (a) Typical illustration of corrosion defects (longitudinal axis). (b) Short corrosion defect simplified as a parabolic curve (ASME B31G). (c) Long corrosion defects simplified as a rectangular defect.

First, the maximum hoop stress cannot exceed the yield strength of the material ($\sigma_{\theta\theta} \le \sigma_Y$). Second, relatively short corrosion is projected on the shape of a parabola and long corrosion is projected on the shape of a rectangle. The failure pressure equation for the corroded pipeline is classified by parabola and rectangle as shown in Figure 10.

Parabolic defects

$$P_f = \frac{2(1.1\sigma_Y)\times t}{D}\left[\frac{1-(2/3)\times(d/t)}{1-(2/3)\times(d/t)/M}\right], \tag{25}$$

where $M = \sqrt{1+0.8\left(\frac{L}{D}\right)^2\left(\frac{D}{t}\right)}$, for $\sqrt{0.8\left(\frac{L}{D}\right)^2\left(\frac{D}{t}\right)} \le 4$

Rectangular defects

$$P_f = \frac{2(1.1\sigma_Y)\times t}{D}\left[1-(d/t)\right], \tag{26}$$

where $M = \infty$,

for $\sqrt{0.8\left(\frac{L}{D}\right)^2\left(\frac{D}{t}\right)} > 4$

where, P_f, D, d, t, M, σ_Y and L are the failure pressure, outer diameter, maximum corrosion depth, wall thickness, bulging factor, yield stress and longitudinal corrosion defect length, respectively. Due to some problems associated with the definition of flow stress a new flow stress was proposed as:

$$\sigma_f = 1.1\times\sigma_Y + 69 \ \text{(MPa)} \tag{27}$$

The modified ASME B31G including this new modified flow stress and bulging factor is a follows:

$$P_f = \frac{2(1.1\sigma_Y + 69)\times t}{D}\left[\frac{1-0.85\times(d/t)}{1-0.85\times(d/t)/M}\right],$$

where $M = \sqrt{1+0.6275\left(\frac{L}{D}\right)^2\left(\frac{D}{t}\right)-0.003375\left(\frac{L}{D}\right)^4\left(\frac{D}{t}\right)^2}$, (28)

for $\left(\frac{L}{D}\right)^2\left(\frac{D}{t}\right) \le 50$

$$P_f = \frac{2(1.1\sigma_Y + 69)\times t}{D}\left[\frac{1-0.85\times(d/t)}{1-0.85\times(d/t)/M}\right], \tag{29}$$

where $$M = 3.3 + 0.032\left(\frac{L}{D}\right)^2\left(\frac{D}{t}\right)$$

for $$\left(\frac{L}{D}\right)^2\left(\frac{D}{t}\right) > 50$$

It is necessary to recall that ASME B31G is limited to low stress concentration factors and internal pressure loading conditions. In the assessment procedure, one considers the maximum depth and longitudinal extent of the corroded area, but ignores the circumferential extent and the actual profile. If the corroded region is found to be unacceptable, B31G allows the use of more rigorous analysis or a hydrostatic pressure test in order to determine the pipe remaining strength. Alternatively, a lower MAOP may be imposed.

5.2. DNV RP-F101

DNV RP-F101 is the first comprehensive and extensive code for pipeline corrosion defect assessment. It provides guidance for internal pressure and combined loading. It covers all loading types, e.g., pressure only and combined loading. Furthermore, it provides codified formulations for pressure, bending and area depth. DNV RP-101 proposes two methods to find the failure pressure. The first is based on the partial safety factor and the second is classified as allowable stress design. Both methods entail information on the pipe outside diameter (D), wall thickness (t), ultimate tensile strength (σ_U), MAOP, longitudinal extent of corrosion (L_c) and defect depth (d). The allowable stress design method considering non-interacting defects is discussed here. The exact procedures for the partial safety factor method and interacting defects can be found within the DNV code.

To pursue the design procedure via DNV RP-101, it is required to determine the loading type (pressure only and combined loading) and consequently, the failure pressure can be obtained as:

$$P_f = \frac{2(\sigma_U)\times t}{D-t}\left[\frac{1-(d/t)}{1-(d/t)/Q}\right], \tag{30}$$

where $$Q = \sqrt{1+0.31\left(\frac{1}{\sqrt{Dt}}\right)^2}$$

where P_f, D, d, t, Q and σ_U are the failure pressure, outside diameter, corrosion depth, wall thickness, correction factor and ultimate tensile strength, respectively. According to DVN RP-101, the failure pressure should not exceed the MAOP, otherwise, the corroded pipe will be repaired or replaced before returning to service.

5.3. CHOI'S METHOD

Based on limit load analysis assumptions and finite element analysis of corroded pipelines, Choi et al. [7] proposed a limit load solution as a function of R/t, d/t, $L/\sqrt{Rt}$ as follows:

$$P_f = \begin{cases} 0.9 \times \dfrac{2(\sigma_U) \times t}{D_i}\left[C_0 + C_1\left(\dfrac{L}{\sqrt{Rt}}\right) + C_2\left(\dfrac{L}{\sqrt{Rt}}\right)^2\right], \\ \dfrac{L}{\sqrt{Rt}} < 6\ , \\ 1 \times \dfrac{2(\sigma_U) \times t}{D_i}\left[C_3 + C_4\left(\dfrac{L}{\sqrt{Rt}}\right)\right],\ \dfrac{L}{\sqrt{Rt}} \geq 6 \end{cases}$$

where

$$\left\{ \begin{array}{l} C_0 = 0.06\left(\dfrac{d}{t}\right)^2 - 0.1035\left(\dfrac{d}{t}\right) + 1, \\ C_1 = -0.6913\left(\dfrac{d}{t}\right)^2 + 0.4548\left(\dfrac{d}{t}\right) - 0.1447,\ C_2 = 0.1163\left(\dfrac{d}{t}\right)^2 - 0.1053\left(\dfrac{d}{t}\right) + 0.0292, \\ C_3 = -0.9847\left(\dfrac{d}{t}\right) + 1.1101,\ C_4 = 0.0071\left(\dfrac{d}{t}\right) - 0.0126 \end{array} \right\} \tag{31}$$

where P_f, σ_U, D_i, d, t and R are the failure pressure or maximum pressure, ultimate tensile strength, inside diameter, defect depth, wall thickness and average pipe radius, respectively. In general, the corrosion pits are idealized into a semi-elliptical shape rather than rectangular and semi-spherical shapes.

where

$$\left\{\begin{array}{l} C_0 = 0.06\left(\frac{d}{t}\right)^2 - 0.1035\left(\frac{d}{t}\right) + 1, \\ C_1 = -0.6913\left(\frac{d}{t}\right)^2 + 0.4548\left(\frac{d}{t}\right) - 0.1447,\ C_2 = 0.1163\left(\frac{d}{t}\right)^2 - 0.1053\left(\frac{d}{t}\right) + 0.0292, \\ C_3 = -0.9847\left(\frac{d}{t}\right) + 1.1101\ ,\ C_4 = 0.0071\left(\frac{d}{t}\right) - 0.0126 \end{array}\right\} \tag{32}$$

The failure pressure is extracted by means of the maximum failure pressure according to the above-mentioned codes (ASME B31G, Modified ASME B31G, DNV RP-101 and Choi's method).

The safety factors have been also extracted via SINTAP safety margins and assessment points. The safety factor is determined by means of the applied pressure P_{app} over failure pressure P_f as:

$$F_S = \frac{P_{app}}{P_f} \tag{33}$$

In Table 8, different safety factors according to the SINTAP and limit load analysis methods are computed using implemented MATLAB code.

TABLE 8. Calculated safety factors using mentioned coded and other methods.

Type	SINTAP 0B	SINTAP 1B	ASME B31G
Semi-spherical	4.0	4.1	3.5
Semi-elliptical	3.4	3.7	3.4
Blunt notch	3.1	3.5	N/A
Type	mASME B31G	DNV RP F-101	Choi et al.
Semi-spherical	4.0	4.2	3.3
Semi-elliptical	3.9	4.2	2.8
Blunt notch	N/A	N/A	N/A

As expected earlier, the SINTAP 0B is more conservative than SINTAP 1B. Nevertheless, ASME B31G, modified ASME B31G, DNV RP F-101 and Choi's method do not offer any structural integrity formulae for blunt notch defects and DNV RP F-101 does not exhibit any variation in safety factor for the chosen semi-spherical and semi-elliptical defects. The comparison of computed safety factors emphasizes that DNV RP F-101 and Choi's method provide the upper-bound and lower-bound margins.

6. Conclusion

The structural integrity of corroded pipelines subjected to internal pressure is studied in this paper. The semi-spherical, semi-elliptical and blunt notch defects are examined under this loading and safety factors are evaluated by means of the SINTAP which is modified using a NFAD. The ASME B31G, mASME B31G, DNV RP F-101 and Choi's method have been also utilized.

References

1. SINTAP: Structural Integrity Assessment Procedure, Final Report EU project BE95-1462 Brite Euram Programme Brussels (1999)
2. S. Jallouf, Lj. Milović, G. Pluvinage, A. Carmasol, and S. Sedmak, Determination of safety margin and reliability factor of boiler tube with surface crack, *Structural Integrity and Life* **5**(3), pp. 131–142 (2005)
3. C. Schmitt, E. Hadj-Taieb, G. Pluvinage, and R. Akid, Water pipeline failure due to water hammer effects, *Fatigue and Fracture of Engineering Materials and Structures*, **29** p. 1075 (December 2006)
4. G. Pluvinage Fracture and Fatigue emanating from stress concentrators Kluwer (2003)
5. Y. U. Matvienko, Local fracture criterion to describe failure assessment diagrams for a body with crack/notch, *International Journal of Fracture* **124**, pp. 107–112 (2003)
6. American National Standard Institute (ANSI)/American Society of Mechanical Engineers (ASME), Manual for determining strength of corroded pipelines, ASME B31G (1984)
7. J. B. Choi, B. K. Goo, J. C. Kim, Y. J. Kim, and W. S. Kim, Development of limit load solutions for corroded gas pipelines, *International Journal of Pressure Vessel and Piping* **80**(2), pp. 121–128 (2003)

APPLICATION OF SINTAP TO THE FAILURE ASSESSMENT OF GAS PIPES

NENAD GUBELJAK*
University of Maribor, Faculty of Mechanical Engineering
Smetanova 17, SI-2000 Maribor, Slovenia

Abstract: The fracture behavior of structures depends on loading conditions, geometry of component and material properties. Therefore, in those cases when loading conditions and geometry of component are known, the material should ensure the integrity of the structure and ductile fracture behavior of component. Therefore, it is necessary to select right material for structure regarding to flaw's size and position and as well loading condition. It is especially important for safety, reliability, and integrity of pipes, where materials are exposed to different environmental influences and material-ageing processes. Fracture mechanics-based flaw assessment concepts are increasingly used in industrial regulations and standards for ensuring structure integrity. A considerable number of different guidelines and procedures are available which are partly based on the same bases but also exhibit significant differences. The European Union sponsored Structural Integrity Assessment Procedure (SINTAP), an interdisciplinary Brite–Euram project. SINTAP is useful engineering tool, in order to find appropriate material or maximum loading capacity of structural component with crack. Parts of the structure are also deformed during manufacturing and installation. The aim of this chapter is demonstrate the use of SINTAP in order to find maximum internal pressure capacity of gas pipe, regarding to two materials degradation. The results of analysis show that decrease in mechanical properties and fracture.

Keywords: integrity of structure, crack driving force, stress intensity factor, pipeline, material properties, structural steel, high strength low alloy steel

* Nenad Gubeljak, University of Maribor, Faculty of Mechanical Engineering, Smetanova 17, SI-2000 Maribor, Slovenia; e-mail: nenad.gubeljak@uni-mb.si

G. Pluvinage and M.H. Elwany (eds.), Safety, Reliability and Risks Associated with Water, Oil and Gas Pipelines, 23–44.

1. Introduction

The safety of any structure, as well gas pipe with flaw depends on the material properties (tensile mechanical properties and fracture toughness), geometry (size) of component, and loading manner. In spite of geometric imperfections of pipe (e.g., wall thinning, misalignment) and worst loading scenario (overpressure), the safe design required that material should prevent brittle fracture behavior of steel's structure. It is possible, if material meets two main conditions, appropriate fracture toughness and appropriate post-yielding hardening capability.

Therefore, the goal of present study was to find maximum loading capacity of gas pipe with crack which can appear during service made from two different materials. In engineering practice the high strength low alloy (HSLA) steels are used for the manufacturing engineer's structures (e.g., cranes, offshore structures). In same cases the use of HSLA steel has benefit regarding to reduce weight of structure. Usually, for steel pipeline is used structural steel (medium strength) with good weldability. Application of HSLA steels for engineer's structures as pipes and pressure vessels is questionable, because tempered and quenched steel has low hardening, and residual stresses can become significant. Also, the structures are exposed to different environmental influences (e.g., Hydrogen brittleness) and material-ageing process. Parts of the structures are also deformed during installation. However, the mechanical properties of steels change during manufacture and over their service lives. The consequences of these changes can contribute to ductile crack growth resistance of steel. The aim of this study is to estimate maximum internal pressure capacity of pipe regarding to change of the ductile crack growth resistance of HSLA steel and structural steel (S360) in relation to different supply conditions at room temperature and T_{NDT} temperature. In order to compare fracture behavior of structural component made from two different materials, it is possible to use one of structure integrity assessment procedures which has been developed and/or upgrade in last ten years, e.g., EPRI [1], R6 [2], ETM [3], SINTAP [4], FITNET [5]. Although the basic idea for all procedures is the same for the same problems, namely procedure solving. However, different procedures use different solutions for stress intensity factor or limit load solutions, or different failure parameter, what can lead to different results.

2. Application the European Sintap to the Failure

2.1. WHAT IS SINTAP?

From 1996 to 1999 the European Commission sponsored SINTAP ("Structural Integrity Assessment Procedures for European Industry"), an interdisciplinary

Brite–Euram project the aim of which was to unify the fracture mechanics-based flaw assessment approaches available in Europe and to propose a procedure, which should form the basis of a future European standard. Among many other publications a special issue of the journal *Engineering Fracture Mechanics* (67, 2000, 479–668) contains a number of papers, which describe the main features of the SINTAP [6]. The procedure combines element of procedure R6 (which was made by British Energy) and Engineering Treatment Method – ETM (which was proposed by GKSS – Research Centre in Germany). On the base of SINTAP the proof of strength under static loading is possible to perform for components with existing or assumed defects. The components like pipes are assessed deterministically with regard stable crack extension, fracture or plastic collapse under static loading. In a fracture mechanics analysis in contrast of conventional proof of strength (which assumes defect free components), not only the loading and the material but also the existence of defects (size and position) are taken into account.

2.2. DETERMINATION OF CRITICAL CRACK SIZES USING SINTAP

The determination of the critical crack size is illustrated in Figure 1. In the following application of SINTAP to the gas pipe as well as some basic items of the procedure will be addressed following this flowchart. Note that some of the features and analysis steps shown in the flowchart will not be part of the present analysis. Nevertheless they are shown for completeness and will be addressed briefly because they provide important information for many other cases of failure analysis.

In order to determine a critical crack size the following input information is required:

- Geometry and dimensions of the component
- Applied loading including secondary load components such as residual stresses
- Information on crack type and orientation
- The stress–strain curve and fracture toughness of the material

(A) GEOMETRY AND DIMENSIONS OF THE COMPONENT

The geometry of component can be different with many details (e.g., pipe tees). However, in engineering structure integrity assessment, the simplification of geometry is useful because many compendia for stress intensity factor and limit load consists only minimum number of geometric parameters.

In our example the geometry of the pipe is hollow cylinder (internal radius 130 mm and thickness t = 32 mm) under internal pressure.

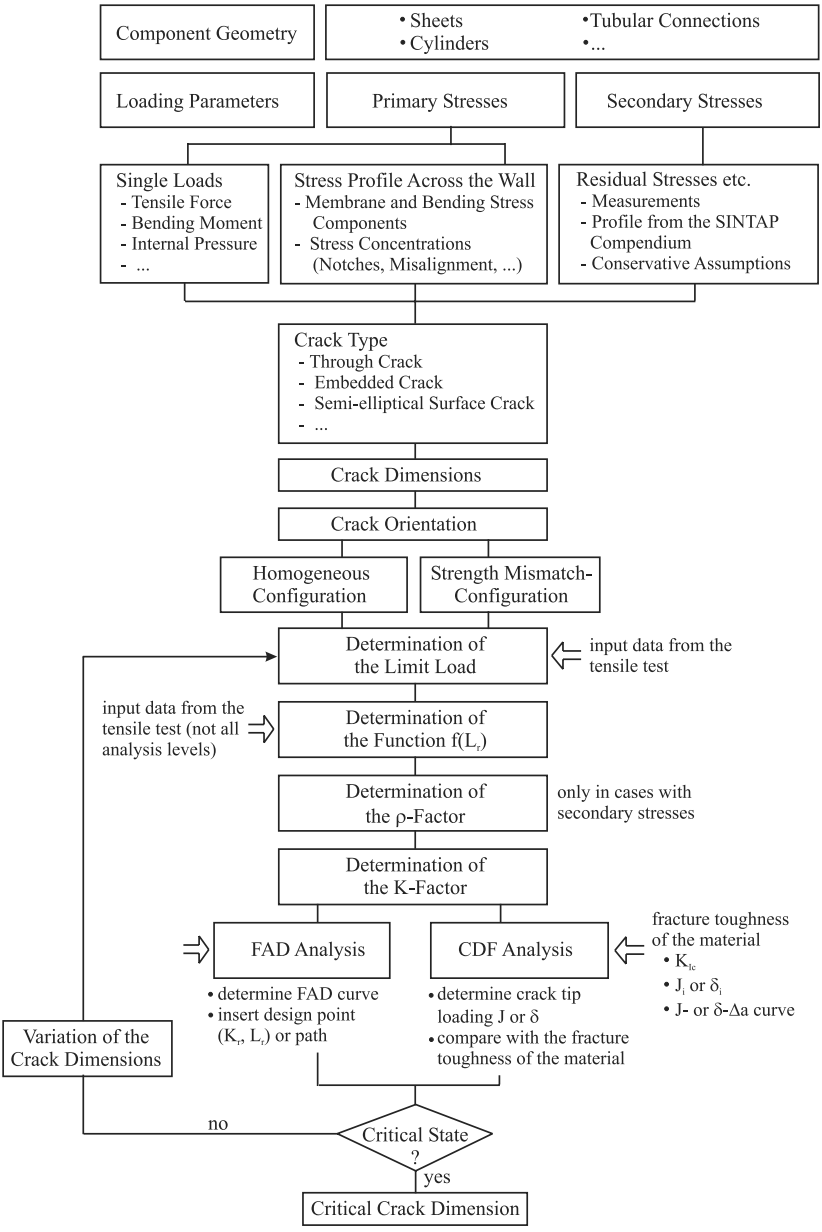

Figure 1. Flowchart for the determination of critical crack sizes using the European flow assessment procedure SINTAP [7].

(B) APPLIED LOADING INCLUDING SECONDARY LOAD COMPONENTS

In the SINTAP the applied load can be introduced as a single load such as a tensile force, a bending moment or an internal pressure in pipe. The consideration as a stress profile, which is, i.e., determined by a finite element analysis is, however, more common. Note that such a stress profile refers to the component without crack. In the present case the loading type was predominant membrane stress. Based on that information a membrane stress component is calculated as hoop stress:

$$\sigma_m = \frac{(R_1 + R_2)}{2 \cdot t} \cdot p \tag{1}$$

In the present case only primary stresses had to be considered. In practice there are, however, many cases – for particular weldments – where these have to be complimented by secondary stresses. In general primary stresses arise from mechanical applied loads including the weight of the structure whereas secondary stresses are due to suspended stresses. Typical examples of secondary stresses are welding residual stresses. The SINTAP gives elaborate guidance on the treatment of secondary stresses. If the residual stresses are not known, recommended normalized residual stress profiles which represent upper envelopes to measured or calculated residual stress profiles over the wall thickness can be used. The stresses in these stress profiles are not self-equilibrating across the wall as in case of individual residual stress profiles. The residual stresses are normalized to the yield strength (lower strength R_{eL} or proof stress $R_{p0,2}$) of the weld metal or the base material at room temperature and given as a function z/t, the depth coordinate z normalized to the wall thickness t. Normalized longitudinal and transversal residual stress profiles for typical pipe seam weld (Figure 2) made of ferritic steel are given in eqs. (2) and (3).

LONGITUDINAL STRESSES FOR FERRITIC STEELS

$$\frac{\sigma_R^L}{R_e} = 0.82 + 2.892 \cdot \left(\frac{z}{t}\right) - 11.316 \cdot \left(\frac{z}{t}\right)^2 + 10.545 \cdot \left(\frac{z}{t}\right)^3 - 1.846 \cdot \left(\frac{z}{t}\right)^4 \tag{2}$$

TRANSVERSE STRESS FOR FERRITIC STEELS

$$\frac{\sigma_R^T}{R_e} = 1 - 0.917\left(\frac{z}{t}\right) - 14.533\left(\frac{z}{t}\right)^2 + 83.15\left(\frac{z}{t}\right)^3 - 215.45\left(\frac{z}{t}\right)^4 + 244.16\left(\frac{z}{t}\right)^5 - 96.36\left(\frac{z}{t}\right)^6 \tag{3}$$

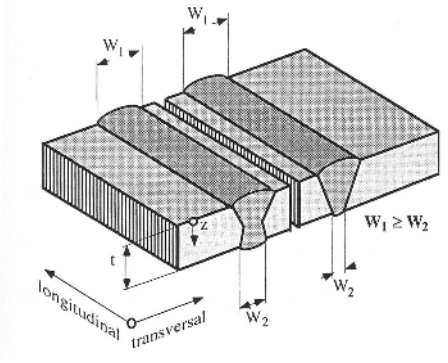

Figure 2. Pipe seem weld.

(C) CRACK TYPE AND ORIENTATION

In a fracture mechanics analysis it is distinguished between through cracks, embedded cracks and surface cracks. Real crack shapes are idealized by substitute geometries such as rectangles ellipses and semiellipses. The idealization has to been done such that the crack tip loading will be overestimated. Sometimes a crack or conglomerations of cracks have to be recharacterized if they interfere one with each other or with a free surface. One example how interactions are taken into account is shown in Figure 3.

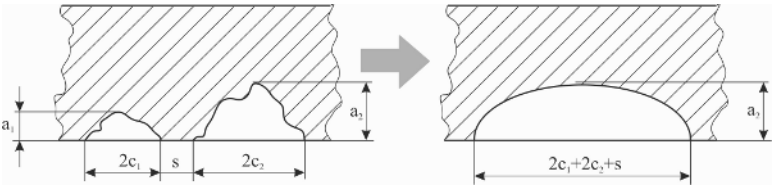

$$c_1 < c_2 \qquad \text{and} \qquad s \le 2 \cdot c_1$$

Figure 3. Crack models for neighbouring surface and embedded defects.

For simplicity the crack was assumed to be of semielliptical surface crack with depth *a* and surface length *2c*, as is shown in Figure 4.

Usually the crack plane is assumed to be perpendicular to the larger of the two principle stresses. There are, however cases, where a real crack will not growth within these plane because of mechanical reasons, i.e., both principal stresses are of a magnitude in the same order, or because of heterogeneity of the material. In such cases a more complicated mixed-mode analysis has to be carried out. In the present case the situation is quite simple because the maximum principle stress direction is identical to hoop stress.

In the flowchart in Figure 1 the crack dimensions are introduced as input information. Actually this refers to a default crack size, which is then varied iteratively. At each iteration step the question has to be answered whether the actual crack size is already critical or not.

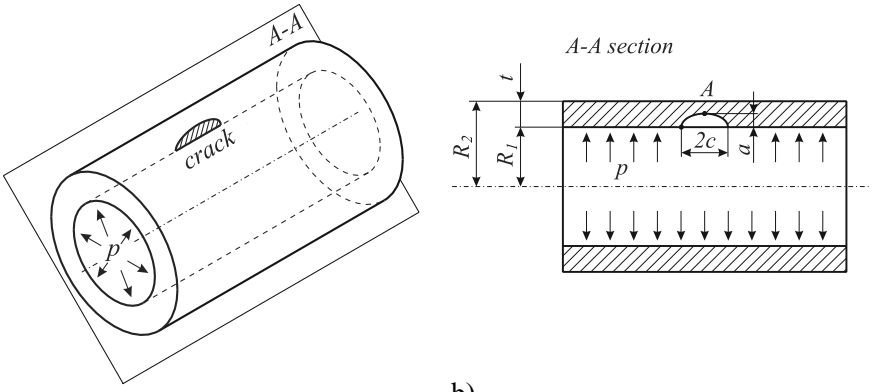

Figure 4. Pipe with internal axial semielliptical surface defect.

(D) HOMOGENOUS OR STRENGTH MISMATCHED CONFIGURATION

Strength mismatch means that, e.g., in a weld, the base plate and the weld material are of different strength with the consequence of local strain concentrations within the softer area. According to the SINTAP, the yield strength of material regions involved in the weld differ more than 10%. For the present example the mismatch does take into account. There are, however, many cases where strength mismatch is of paramount interest. Therefore, the SINTAP offers separate assessment options for the analysis of such cases.

(E) PLASTIC LIMIT LOAD F_Y

The plastic limit load of the component with crack is one of the key parameters of the SINTAP analysis. Here some remarks are due. In solid mechanics the limit load is usually determined for ideally plastic materials. When the limit load is reached the deformation becomes unbounded over the cross section. Real materials, however, work harden with the consequence that the applied force can increase beyond the value given by the nonhardening limit load. Therefore, in the frame of a fracture mechanics analysis it has to be distinguished between a plastic collapse load which is identical to the maximum load which the structure with crack can sustain and a net section yield load which refers roughly to that load at which the still unbroken ligament ahead of the crack is first fully plastic and the local load-deformation curve becomes

nonlinearly. This parameter is what is designated above as the plastic limit load F_Y. In practice it is usually determined under the assumption of an ideally plastic material inserting the yield strength as the maximum sustainable stress. This is supposed to represent the attainment of net section yielding, i.e., each point in the ligament ahead of the crack is supposed to have just reached the yield condition. This is correct for ideally plastic materials, however, for hardening materials there are some points, which are still under elastic deformation condition. Therefore, the thus determined value of F_Y represents a lower bound to the real yield load.

Within the SINTAP a compendium of limit loads is provided. Other compilations are available in the literature, e.g., in BS7910 [8] For cases, which are not covered by this compilation conservative estimates are possible based on substitute geometries. In such cases the stress profiles in the components without crack are taken as input information.

Within the SINTAP a loading parameter L_r is used which is defined as the ratio of the applied load F and the limit load F_Y or applied pressure p and the limit pressure p_Y, respectively as the ratio of an applied net section stress σ_{ref} and the yield strength of the material, σ_Y:

$$L_r = \frac{F}{F_Y} = \frac{\sigma_{ref}}{\sigma_Y} = \frac{p}{p_Y} \tag{4}$$

the later being given as $\sigma_Y = R_{eL}$ for materials with and $\sigma_Y = R_{p0.2}$ for materials without a Lüders plateau.

The plastic limit pressure of the hollow cylinder with axial crack under internal pressure with semielliptical internal surface crack within this paper can easily be determined as p_Y [9]:

$$p_Y = \frac{t}{R_1}\sigma_Y \frac{(t/a-1)}{(t/a-1/M)\cdot(1+a/R_1)} \tag{5}$$

$$M = \sqrt{1+1.255\alpha^2 - 0.0135\alpha^4} \qquad \text{for } \mu < 8$$

$$M = \sqrt{1+0.263\frac{4\cdot c^2}{R_1\cdot t}} \qquad \text{for } \mu \geq 8$$

$$\alpha = \frac{c}{\sqrt{R_1\cdot t}}$$

$$\mu = \frac{c}{\sqrt{R_1\cdot t}}(12\cdot(1-0.3^2))^{0.25}$$

(F) STRESS INTENSITY FACTOR (*K* FACTOR)

As in the case of the limit load numerous solutions for *K*-factors are available in compendia (e.g., [3, 4]). The SINTAP provides an own compilation of such solutions. Stress intensity factors can be determined for single loads such as forces, bending moments, internal pressures etc. as well as for stress profiles. The latter alternative allows to handle geometrically complex components by using substitute structures, i.e., the stress profile is determined for the real structure without crack whereas the determination of the *K*-factor is based on a simpler geometry like a plate, a cylinder etc. According to SINTAP the stress intensity factor $K_{I,a}$ for deepest point is given by:

$$K_{I,a} = F \cdot \sigma \cdot \sqrt{\pi \cdot a} \cdot 0,97 \cdot \left(\frac{r_a^2 + r_i^2}{r_a^2 - r_i^2} + 1 - 0,5\sqrt{\frac{a}{t}} \right) \cdot \frac{t}{r_i} \tag{6}$$

where

$$F = \frac{\left(M_1 + M_2 \cdot \left(\frac{a}{t} \right)^2 + M_3 \cdot \left(\frac{a}{t} \right)^4 \right)}{\sqrt{Q}}$$

$$M_1 = 1,13 - 0,09\frac{a}{c}$$

$$M_2 = -0,54 + \frac{0,89}{0,2 + \frac{a}{c}}$$

$$M_3 = 0,5 - \frac{1}{0,65 + \frac{a}{c}} + 14 \cdot \left(1 - \frac{a}{c} \right)^{24}$$

$$Q = 1 + 1,464 \cdot \left(\frac{a}{c} \right)^{1,65}$$

for surface point

$$K_c = K_a \left(1,1 + 0,35 \left(\frac{a}{t} \right)^2 \right) \cdot \sqrt{\frac{a}{c}} \tag{7}$$

stress $\sigma = \sigma_m$ is membrane stress (normal to the perspective crack plane) in an uncracked cylinder and calculated by eq. (1).

(G) CORRECTION FUNCTION $F(L_R)$

Under conditions of small-scale yielding (roughly up to 0.6 times the limit load) a fracture mechanics analysis can be based on the linear-elastic *K*-factor. This

is, however, not possible for contained and net section yielding where the plastic zone is no more limited to a small region ahead of the crack tip. Under these conditions any application of the *K*-concept would lead to a significant underestimation of the real crack tip loading in terms of the J-integral or CTOD. Irrespective of this general statement the application of a formal *K*-concept becomes possible when the linear-elastic *K*-factor is corrected with respect of the yield effect. This is the essential of the correction function $f(L_r)$. With respect of $f(L_r)$ the SINTAP is structured in a hierarchic manner consisting of various analysis levels constituted by the quality and completeness of the required input information. Higher levels are more advanced than lower levels: they need more complex input information but the user is "rewarded" by less conservative results. An unacceptable result provides a motivation for repeating the analysis at the next higher level rather than claiming the component to be unsafe. The SINTAP standard analysis levels are:

Basic level – Only the toughness and the yield strength and the ultimate tensile strength of the material need to be known. Different sets of equations are offered for materials with and without Lüders plateau.

Mismatch level – This is a modification of the basic level for inhomogeneous configurations such as strength mismatched weldments.

Advanced or stress–strain level – This requires toughness data and the complete stress–strain curve of the material. Both, homogenous and strength mismatched components can be treated.

There are additional levels:

Default level – Only the yield strength of the material is required. The fracture resistance of the material can be conservatively estimated from Charpy data.

Constraint level – Within this level, the effect of loss of constraint in thin sections or predominately tensile loading on fracture resistance is considered.

J-integral analysis level – This level includes a complete numerical analysis of the defect structure.

Within the present paper the basic level is applied. The according equations for $f(L_r)$ for ferritic steels without Lüders plateau are:

- Default level:

$$f\left(L_r\right)=\left[1+\frac{1}{2}\cdot L_r^{\,2}\right]^{-1/2}\times\left[0.3+0.7\exp\left(-0.6L_r^{\,6}\right)\right] \quad \text{for } 1\le L_r\le L_r^{\max} \tag{8}$$

$$L_r^{\max}=1+\left[\frac{150}{R_{p0.2}}\right]^{2.5} \qquad R_{\mathrm{p0,2}} \text{ in [MPa]} \tag{9}$$

The fracture toughness is estimated in a conservative manner from Charpy data by

$$K_{mat}=\left[\left(12\sqrt{KV}-20\right)\cdot\left(\frac{25}{B}\right)^{\frac{1}{4}}\right]+20 \tag{10}$$

on the lower shelf and by

$$K_{mat}=K_{J0.2}=\sqrt{\frac{E\left(0.53\cdot KV^{1,28}\right)\cdot 0.2^{\left(0.133\cdot KV^{0,256}\right)}}{1000\left(1-\nu^2\right)}} \tag{11}$$

on the upper shelf. In addition SINTAP offers a correlation for the ductile to brittle transition based on the Charpy transition temperature for 28 J,

$$K_{mat}=20+\left\{11+77\exp\left[0.019\left(T-T_{28J}-3°C\right)\right]\right\}\cdot\left[\frac{25}{B}\right]^{\frac{1}{4}}\cdot\left[\ln\frac{1}{1-P_f}\right]^{\frac{1}{4}} \tag{12}$$

K_{mat} in $MPa\sqrt{m}$; specimen thickness B in mm; Charpy energy KV in J; P_f probability of Charpy impact energy at service temperature T.

- Basic level:

$$f\left(L_r\right)=\left[1+\frac{1}{2}L_r^2\right]^{-1/2}\cdot\left[0.3+0.7\exp\left(-\mu\cdot L_r^{\,6}\right)\right] \quad \text{for } 0\le \mathrm{L_r}\le \tag{13}$$

$$\text{With } \mu=\min\begin{bmatrix}0.001\ \mathrm{E/R_{p0.2}}\\ 0.6\end{bmatrix} \tag{14}$$

and

$$f\left(L_r\right)=f\left(1\right)\cdot L_r^{\frac{(N-1)}{2N}} \quad \text{for} \quad 1\le L_r\le L_r^{\max} \tag{15}$$

$$N = 0.3\left[1 - \frac{R_{p0,2}}{R_m}\right] \tag{16}$$

$$L_r^{\max} = \frac{1}{2}\left[\frac{R_{p0.2} + R_m}{R_{p0.2}}\right] \tag{17}$$

with $L_r^{\max}$ being the limit against plastic collapse.

- Advanced level:

$$f(L_r) = \left[\frac{E \cdot \varepsilon_{ref}}{\sigma_{ref}} + \frac{1}{2} \cdot \frac{L_r^{\,2}}{\frac{E \cdot \varepsilon_{ref}}{\sigma_{ref}}}\right]^{-1/2} \quad \text{for } 1 \le L_r \le L_r^{\max} \tag{18}$$

$$L_r^{\max} = \frac{\sigma_f}{\sigma_Y} \quad \text{with } \sigma_f = \frac{1}{2}\left[\sigma_Y + R_m\right] \tag{19}$$

Different to the levels above *f(Lr)* is a continuous function, which follows pointwise the true stress–strain curve. Each value of σ_{ref} is assigned to an L_r value by

$$\sigma_{ref} = L_r \cdot \sigma_Y \tag{20}$$

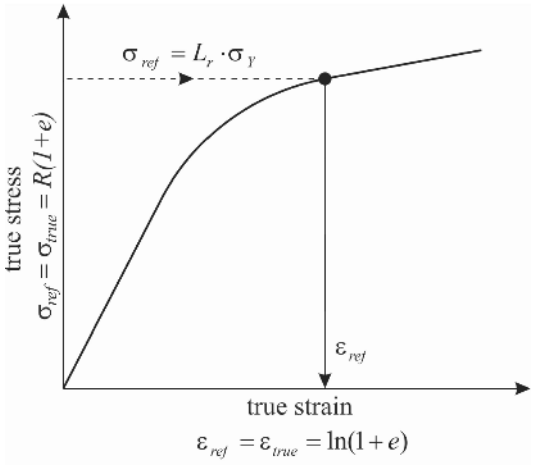

Figure 5. Determination of the reference strain from the true stress–strain curve of ε_{true} for the assessment of the normalized load.

(Note: *R* and *e* designating the engineering stress and engineering strain)

The corresponding reference strain ε_{ref} is obtained from the true stress-strain curve as illustrated in Figure 5. No distinction is necessary between materials with and without a Lüders plateau. On the other hand $\sigma_{ref}/\varepsilon_{ref}$ values have to be available at L_r = 0.7/0.9/0.98/1/1.02/1.1 and other values of L_r.

(H) THE ρ FACTOR

ρ is a correction function for secondary stresses, which takes into account yielding and relaxation effects. Because it is not applied within this paper this parameter will not be discussed here.

(I) CDF VERSUS FAD ANALYSES

SINTAP pursues two different assessment philosophies, which are designated as crack driving force (CDF) and failure assessment diagram (FAD) concepts, as is shown in Figure 6a and 6b. Both are complementary and give identical results. In the CDF route the determination of the crack tip loading in the component and its comparison with the fracture toughness of the material are two separate steps. The CDF curve, which relates the applied load with the crack tip loading in terms of J or CTOD, is a geometry independent function, which depends only on the deformation behavior of the material.

Failure is predicted when the crack tip loading exceeds the fracture toughness. In the FAD route, a geometry independent failure line is constructed by normalizing the crack tip loading by the material's fracture resistance. The assessment of the component is then based on the relative location of a geometry dependent assessment point with respect to this failure line. In the simplest application the component is regarded as safe as long as the assessment point lies within the shaded area below the failure line. It is regarded as potentially unsafe if it is located on the line or outside the shaded area. An increased load or larger crack size will move the assessment point along the loading path towards the failure line.

In Figure 6 the basic CDF and FAD applications are illustrated which consider the fracture toughness as a single value (K_{IC} or J or CTOD at stable crack initiation). Note that CDF and FAD applications also exist for a so-called R-curve behavior of the fracture resistance, which, however, will not be described here.

The basic equations of the CDF philosophy are

$$J = J_e \cdot \left[f\left(L_r\right) \right]^{-2} \tag{21}$$

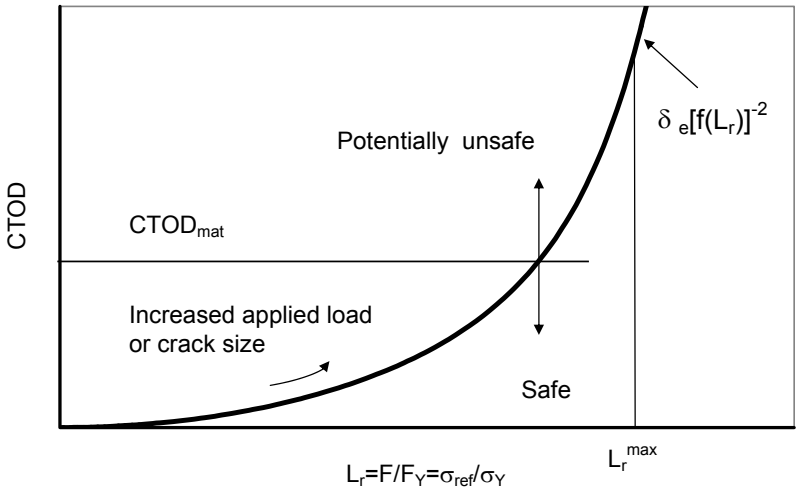

a) CDF philosophy

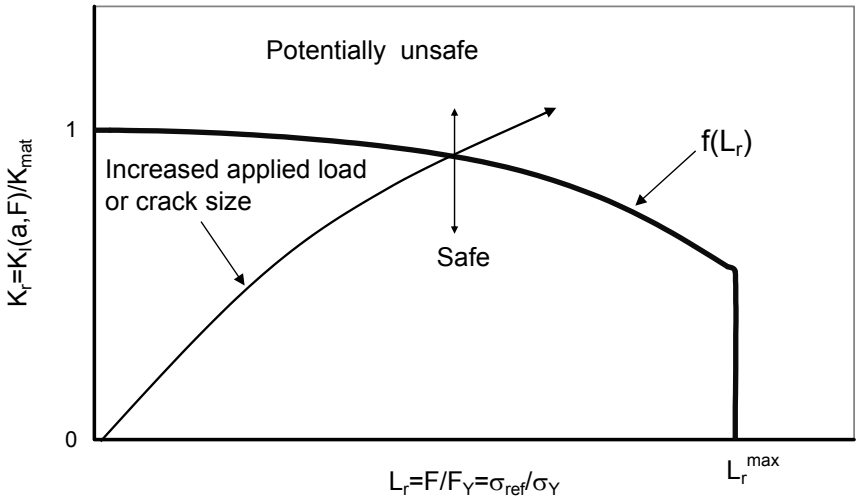

b) FAD philosophy

Figure 6. SINTAP assessment philosophy.
(Note: The function $f(L_r)$ is identical for the FAD and CDF routes)

With

$$J_e = \frac{K^2}{E'} \tag{22}$$

for the J integral and

$$\delta = \delta_e \cdot \left[f\left(L_r\right) \right]^{-2} \tag{23}$$

with

$$\delta_e = \frac{K^2}{E' \cdot \sigma_Y} \tag{24}$$

for CTOD as crack tip parameters. The basic equation of the SINTAP–FAD route is

$$K_r = f\left(L_r\right) \tag{25}$$

with K_r being the linear-elastic K-factor normalized to the fracture toughness which is designated here by the general term K_{mat}

$$K_r = \frac{K_I}{K^{mat}} \tag{26}$$

(J) FRACTURE TOUGHNESS

Fracture mechanics quantities for the characterization of the material resistance under static loading are called fracture toughness. They describe in particular: crack initiation, stable crack extension and unstable fracture. They are expressed in terms of the stress intensity factor K, the crack tip opening displacement δ or the J-integral. They are convertible into each other with restrictions. Fracture toughness parameter can be determined in terms of the crack tip opening displacement CTOD (δ), K_{IC} or J-integral according to the relevant standards [10, 11, 12].

(K) CHARPY ENERGY

Information on the Charpy energy is necessary for the SINTAP Default Level assessment. Charpy energy is used if direct measurements of the fracture toughness are not possible, or if no data, or only unsatisfactory data are available according correlations eqs. (10, 11, 12).

3. Structural Integrity Assessment of Pipe

In present structure integrity assessment two steels are used:

- One HSLA (grade HT60) design »V«
- Structural steel S360 (grade DIN St-52), design »C«

Three different material conditions were observed:

1. HSLA steel in normalized condition (as-delivered), design »A«
2. Aged condition, after 10% cool plastic deformation and heating at 250°C for 30 min., design »B«
3. Deformed condition after a 10% cool plastic deformation, design »C«

By using flowchart in Figure 1, it is possible also for assumed crack size to find maximum loading capacity of component with crack. In present case, the arising questions are:

4. Does use of HSLA steel is benefit for pipe line comparing to structural steel?
5. How degradation of material's properties (ageing and deforming) of HSLA or structural steel affect to structural integrity of pipe with different crack size?
6. What is difference in internal pressure of pipe between integrity assessment at room temperature and temperature of nonductile tearing of both steel?

The mechanical properties were determined at room temperature and at T_{NDT} temperatures (determined by drop weight testing) and by longitudinal testing, as given in Table 1. The increasing strength of the steel, associated with decreasing elongation at the fracture is clearly seen in Table 1. In addition, a further increase of yield strength with decrease of temperatures is obvious.

TABLE 1. Mean values for mechanical properties of both steels (»V« and »C«) at room temperature and T_{NDT} temperatures.

Material condition	Yield strength MPa	Ultimate tensile strength MPa	Elongation at fracture %	T_{NDT} °C	Yield strength at T_{NDT} MPa
HSLA: VA	442	610	13.7	–72	514
VB	647	726	4.7	–104	780
VC	627	684	4.5	–134	757
S360: CA	366	533	24.2	–82	475
CB	586	656	6.7	–114	653
CC	595	624	8.9	–128	675

On the basis of the results obtained (Table 1), it was decided that fracture toughness testing would be carried out at room (+20°C) temperature and T_{NDT} temperatures.

The compact tension (CT) specimens were cut from a 32 mm thickness plate according to the standard ASTM 1820 [12]. Experiments were done on six series of 15 standard CT specimens. On the basis of the F-CMOD (Load versus Crack Mouth Opening Displacement) records, J-R resistance curves were determined, at room temperature and with J_c values at T_{NDT} temperatures (where all specimens were fractured in a brittle manner). The parameters $J_{0.2BL}$ and J_c (determined from brittle fracture tests at T_{NDT}) were used for probabilistic analyses.

The mean values of $J_{0.2BL}$ and J_c are listed in Table 2. Table 2 shows higher toughness of HSLA steel in as-delivered conditions, but it is obvious that HSLA steel does not show significant benefit in aged condition or deformed condition.

TABLE 2. Mean values of measured *J*-integral ($J_{0.2BL}$ and J_c) at room temperature and T_{NDT} temperatures.

Material condition	Toughness $J_{0.2BL}$ N/mm	Toughness J_c N/mm
	Mean value	Mean value
VA	476.5	52.62
VB	231.6	20.44
VC	333.2	25.02
CA	335.5	196.4
CB	262.5	47.62
CC	282.3	65.4

Since the service temperature can significantly change, it is necessary to estimate the effect of temperature decreasing on fracture behavior (from RT (ductile) to T_{NDT} (brittle) temperature) for the same crack length and crack configuration. In present case, a pipe was estimated under unknown critical internal pressure p_c (Figure 2a, with outside diameter $2R_2 = 320$ mm, internal diameter $2R_1 = 260$ mm, wall thickness $t = 32$ mm). Calculation was performed for internal axial semielliptical surface crack, Figure 2b). Three different crack depths were estimated:

with $a = 2.5$ mm and $2c = 25$ mm; $a/t = 0.08$, $2c/a = 10$
$a = 16$ mm and $2c = 80$ mm; $a/t = 0.50$, $2c/a = 5$
$a = 30$ mm and $2c = 150$ mm; $a/t = 0.94$, $2c/a = 5$

All dimensions are possible to detect by conventional nondestructive inspection equipment. In this case the structural integrity assessment is performed in order to find maximum internal pressure for pipe with crack. First comparison

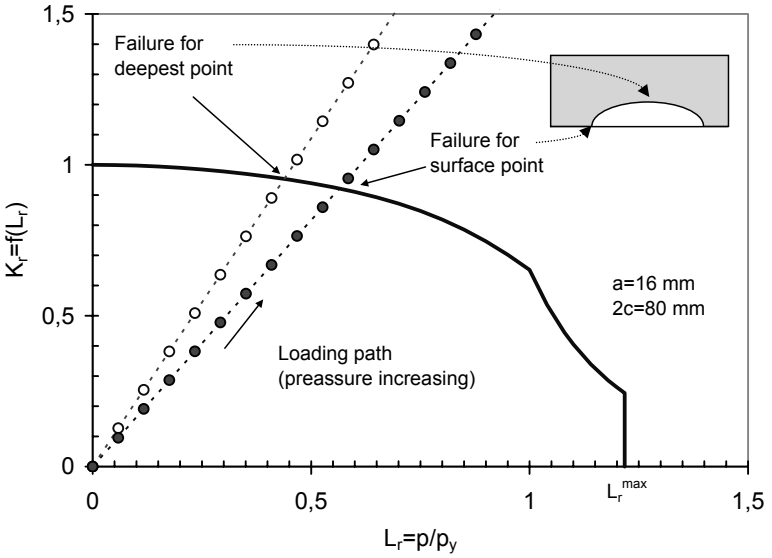

Figure 7. Example of loading paths for deepest point and surface point.

was performed between deepest crack point and surface crack point at wall of cylinder's pipe. The analyses shown in all cases that the most critical is deepest point, as is shown in Figure 7. Since the deepest point of crack shows much higher stress intensity factor than at the surface, the rest of analysis is going to perform only for more critical deepest point.

Comparison among loading paths for different crack size shows that failure is predominantly plastic for deep through thickness crack or close to leak-before-break (a/t = 0.94) and failure becomes more brittle in case of short shallow crack (a/t = 0.08), as is shown in Figure 8a and Figure 8b for HSLA steel and S360 steel, respectively. Comparison between HSLA steel and S360 structural steel is shown in Figure 9 for the same crack's depth a = 30 and crack's width 2c = 150mm and same material's condition. Figure 9 shows nonsignificant difference in internal pressure loading capacity between both steels in case of long crack, but in case of short crack HSLA steel is more brittle than S360 steel. The all results for steels and all material's condition are shown in Figure 10. Figure 10 shows change of critical internal pressure capacity regarding to material degradation and crack depth (a/t). This degradation is caused by material properties change and fracture toughness degradation at both

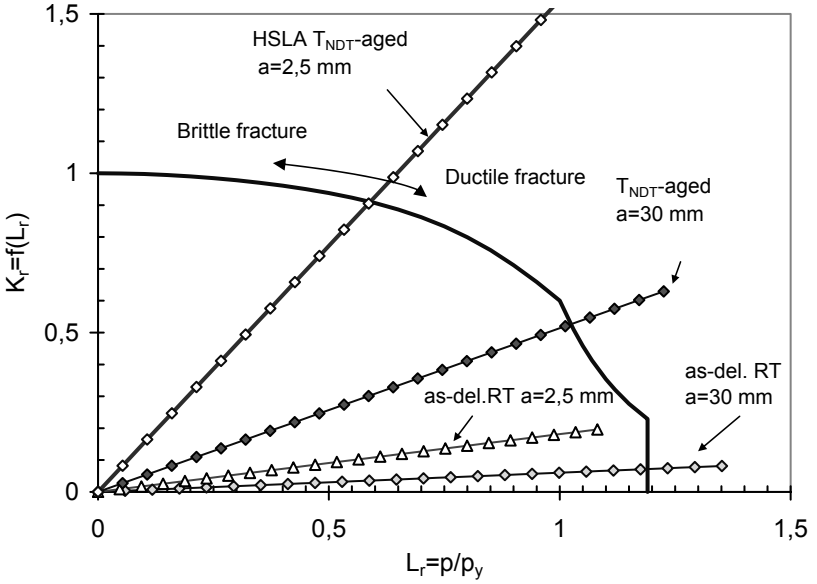

a) HSLA steel

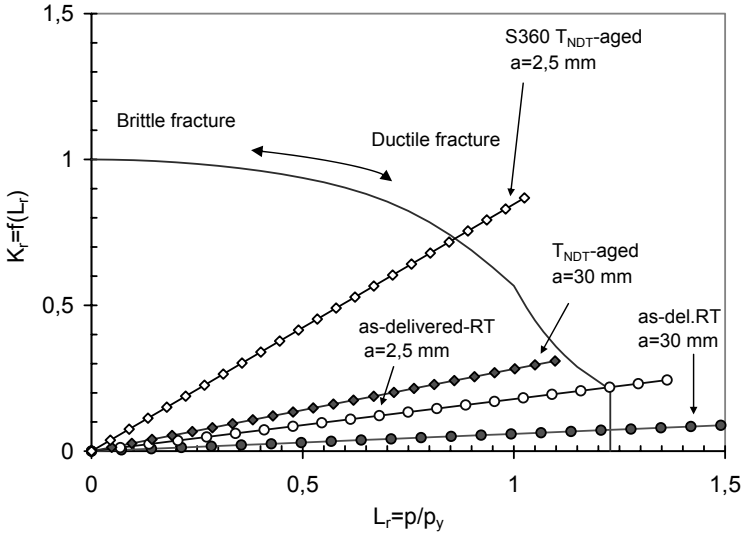

b) S360 steel

Figure 8. Comparison among loading paths for different crack size and material conditions and assessment at RT-room temperature , T_{NDT}-temperature of nonductile tearing.

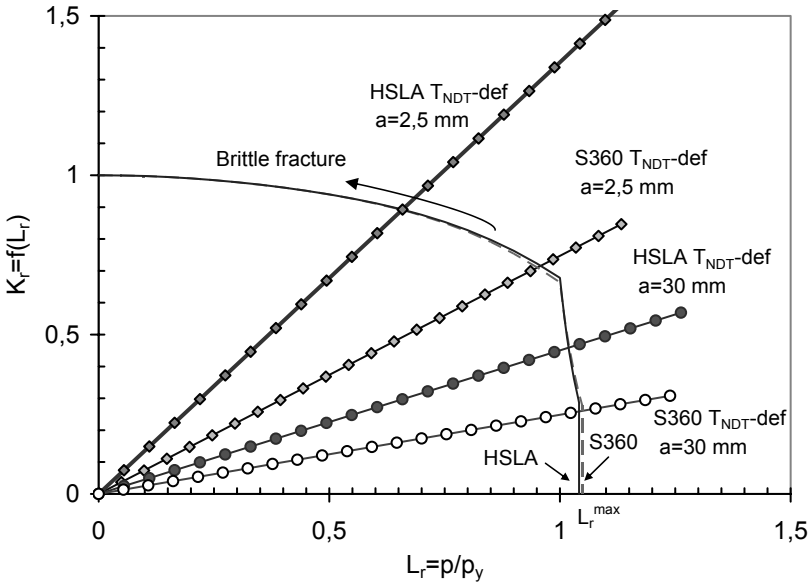

Figure 9. Comparison between HSLA steel and structural steel for same material condition.

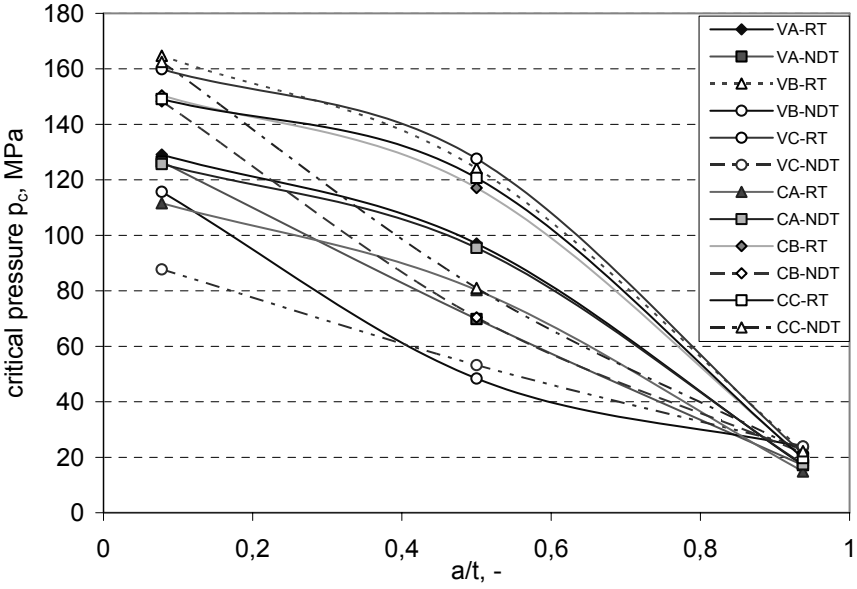

Figure 10. Change of critical internal pressure capacity regarding to material degradation and crack depth (*a/t*).

temperatures. In the case of very short shallow crack, it is obvious difference in maximum critical internal pressure, but with crack extension the differences becomes small. Almost, the difference are negligible at the close the through thickness crack ($a/t = 0.94$).

Figure 10 shows also, that drop of critical internal pressure p_c is higher, as was expected at T_{NDT} temperature for both material, but in case of deepest crack the differences between capacity of both steels at the room temperature and T_{NDT} temperature are nonsignificant. The material properties degradation (ageing or deforming condition) do not have effect on structural integrity of pipe made from HSLA steel or structural steel at deepest crack length. Consequently, the use of HSLA steel or structural steel have not benefit for pipe integrity in case of leak-before-break.

4. Conclusion

This chapter represents the use of SINTAP in order to find maximum internal pressure capacity of gas pipeline. Each issue of structural integrity assessment has been discussed by using flowchart for determination of critical crack size. In the case when crack size is assumed, it is possible to find critical (maximum) internal pressure of pipe by using SINTAP. In order to ensure clear presentation of procedure's application, only few issues of SINTAP on Level 1 are taken into account. However, sensitivity of applied compendia's equations for stress intensity factor and limit loads, and applied route of procedure shows vary in critical internal capacity from shallow crack to deep close leak-before-break crack size. SINTAP is useful for integrity assessment of pipes with different crack size for room temperature and T_{NDT} temperature, as well.

References

1. Kumar V., German M. D. and Shih C. F. (1981), An Engineering Approach for Elastic-Plastic Fracture Analysis, EPRI, Final Report to NP 1931.
2. R6 (1998), Assessment of the integrity of structures containing defects, Nuclear electric procedure R/H/R6, Revision 3.
3. Schwalbe, K.-H. and Cornec, A. (1991), The engineering treatment model (ETM) and its practical application, *Fatigue and Fracture od Engineering Materials and Structures* **14**, pp. 405–412.
4. SINTAP (1999), Structural Integrity Assessment Procedure. Final Revision. EU-Project BE 95–1462. Brite Euram Programme.

5. FITNET (2006), European-Fitness-for-Services Thematic Network, final draft MK7, (Edited by Koçak M., Webster S., Janosch J.J., Ainsworth R. A., and Kores R.) European project GIRT-CT-2001-05071, Amsterdam, May 2006.
6. *Engineering Fracture Mechanic Journal* **67**, (2000), Zerbst, U. (guest editor): pp. 479–668.
7. Gubeljak, N., Zerbst U., Predan J., and Oblak M. (2004), Application of the European SINTAP procedure to the failure analysis of breken forklift, *Engineering Failure Analysis* **11**(1), pp. 33–47.
8. BS 7910 (1999), Guide on methods for assessing the acceptability of flaws in fusion welded Structures, 4th draft.
9. Kiefner J. F., et al. (1973), Failure Stress Levels of Flaws in Pressurized Cylinders, ASTM STP 536, S.461–481.
10. BS 7448 (1997), Fracture mechanics toughness tests; Part 2. Method for determination of K_{IC}, Critical *CTOD* and critical *J* values of welds in metallic materials.
11. ASTM E 399 (2001), Standard Test Method for Plane-Strain Fracture Toughness of Metallic Materials, American Society for Testing and Materials, Philadelphia.
12. ASTM E-1820 (2004), 01 Standard Test Method or Measurement of Fracture Toughness, Volume 03.01, ASTM International, W. Conshohocken, PA.

INTERACTION BETWEEN MATERIAL PROPERTIES, INSPECTION ACCURACY AND DEFECT ACCEPTANCE LEVELS IN STRAIN BASED PIPELINE DESIGN

RUDI DENYS
Laboratorium Soete, Universiteit Gent, St Pietersnieuwstraat, 41 B9000 Gent, Belgium

Abstract: Nowadays, pipelines are being built in regions where ground movements can cause post-yield longitudinal strains. Consequently, established material selection and weld integrity assessment procedures need to be re-assessed. This is because the actual material properties, and not the specified ones, determine the plastic strain capacity. Also, the accuracy with which the material properties and defect parameters are established needs special care. The purpose of this paper is to review the variables affecting the plastic strain capacity and to discuss the associated material and inspection requirements. The information presented has been inferred from studies of the failure characteristics of large-scale Curved Wide Plate (CWP) tests.

Keywords: defect size, strain-based design, weld metal mismatch, remote strain, defect sizing, AUT, uniform elongation, yield to tensile ratio

1. Background

The input parameters to be addressed for a stress-based (applied strain, e < 0.5%) girth weld integrity defect are: toughness of the material containing the defect (minimum specified) yield and tensile strength of the pipe metal, applied stress, defect type and defect dimensions, Figure 1. In contrast, when girth welds have to resists longitudinal plastic strains, additional variables must be considered in the evaluation process.

The supplementary variables to be considered include the level of weld metal strength mismatch, the yield strength and Y/T ratio (strain hardening capacity) of both weld and pipe metal, and the uniform strain capacity of both

G. Pluvinage and M.H. Elwany (eds.), Safety, Reliability and Risks Associated with Water, Oil and Gas Pipelines, 45–64.

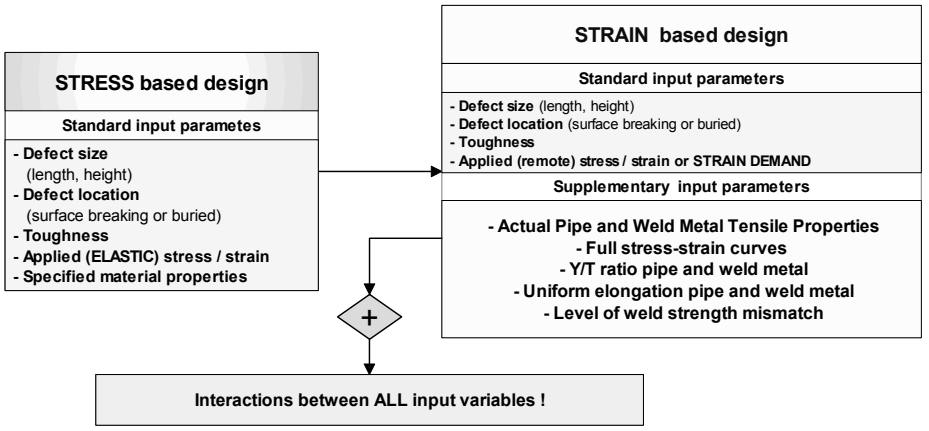

Figure 1. Input parameters for stress-based and strain-based defect acceptance.

weld and pipe metal. Moreover, the interactions between these variables, which are neither fully understood nor adequately documented, cannot be disregarded while the study of the interaction between the plastic strain capacity and the defect dimensions requires knowledge of the *actual* values of the input data. The point is that the minimum specified material properties cannot be used. This also means that the weld acceptance for strain-based designs can no longer be based on the standard material qualification procedures. Also, the accuracy with which the material properties and defect parameters are established needs special care. The other issue is that the established assessment procedures cannot be uncritically used when the remote strains exceed the 0.5% level.

2. Challenges

A tough* girth weld with part-wall defect under tensile loading deforms according to the following sequence of events: blunting, crack initiation, ductile tearing. Ductile tearing occurs essentially in the post-yield loading range. At load instability, CWP testing has demonstrated that four distinct deformation modes can occur, Figure 2. The probable limit conditions, when $e > 0.5\%$, are: failure by necking of the pipe body, pop through followed by a stable leak or complete failure of the net cross section. When the strain hardening capacity of the defective region is insufficient, the remote failure strain will elastic ($e < 0.5\%$). This failure mode corresponds with the standard definition of plastic collapse (or Net Section Yielding, NSY). Apart from the fact that strain-based designs exclude NSY, it is of interest to know that the occurrence of remote yielding depends on the interaction between strain hardening, weld strength mismatch and defect size. However, for the common combinations of materials used in pipeline construction, defect size is a key variable.

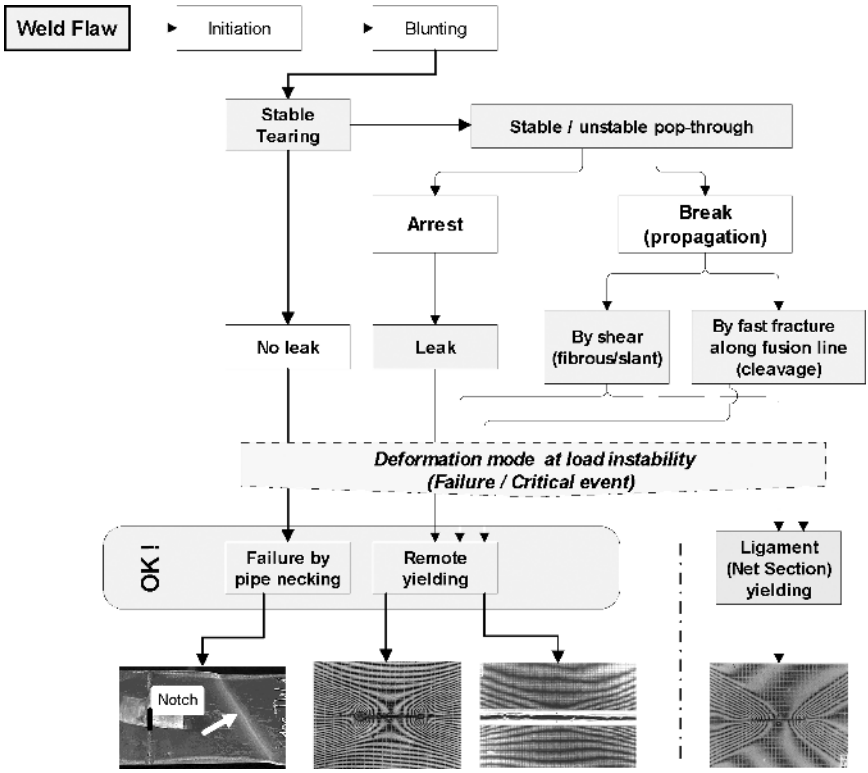

Figure 2. Deformation and failure modes of notch tough material.

Failure by pipe necking occurs for small, but significant, defects located in overmatched welds. Failure by local instability (defect pops through) is avoided since the local damage escalates into a global instability.

The main feature of ductile tearing is that it changes the defect size, leading to a more unfavourable situation in terms of plastic strain capacity. Ductile tearing cannot be excluded, but extensive tearing can be mitigated by a proper material selection. For example, an adequate level of overmatching may be sufficient to offset the adverse effect associated with ductile crack growth. However, this solution does not always prevent poor performance of low tearing resistance in the post-yield loading range. Therefore, blunting capacity is a desired property because it is a consequence of the material's ability to spread deformation away from the defective region. In particular, blunting readily occurs in materials exhibiting Lüders elongation, while materials characterized by a continuous stress–strain curve and low strain hardening capacity (high Y/T ratio) have normally lower resistance to ductile tearing. Thus, materials with a high Y/T ratio could be a concern in a strain-based design.

Finally, Curved Wide Plate (CWP) test results also demonstrate that, amongst others, the comprehension of failure by remote yielding requires an intimate understanding of many interacting variables.

3. Assessment Options

The construction of pipelines in areas prone to earthquakes and discontinuous permafrost involves many new challenges. One of the major challenges is related to the assessment of girth integrity when the welds contains a defect and when the remote axial strain exceeds the 0.5% level. Information published on the ongoing research on girth weld integrity provides three options [1–7], Figure 3.

Option A, or the analytical approach makes use of the failure assessment diagram (FAD), Option B explores the results of (case-specific) numerical modelling (Finite Element Analysis, FEA) while Option C focuses on the study of the failure characteristics of full-scale or CWP test results [8–9]. As is shown in Figure 3, each of the options may produce a predicted (tolerable) defect size while the acceptable defect size is obtained by employing a margin of safety to account for ignorance regarding the variability of input parameters (pipe and weld metal tensile properties, and defect dimensions). The safety factor can vary and depends on the assumption made in the assessment.

Option A uses existing fracture mechanics formulations and case-specific collapse analysis that accounts for post-yield deformations. The rationale behind the Option B approach is that the interaction between the crack tip driving force for failure and the applied strain can be modelled and used to determine the predicted defect dimensions. Anyhow, both the analytical and the numerical procedures assume that toughness is the parameter that governs strain capacity while the critical condition or crack resistance is to be derived from CTOD (or wide plate) tests. So far, the analytical or numerical procedures under development are not designed as predictors of failure. The main feature of Option C is that the *actual limit-strain for failure* can be determined. In addition, Option C allows the effect of all relevant variables and the interaction between them on strain capacity to be studied at the same time.

Option C is normally not the cheapest option, however, CWP tests on girth weld with surface breaking defects reveal that reliance on the correlation between CTOD and strain capacity can produce conservative predictions, particularly if one neglects the fact that the correlation between CTOD, CMOD (or the Crack Mouth Opening Displacement under tensile loading) and strain capacity is far from unique [10]. An associated concern is that Options A and B produce stringent, often unrealistic, CTOD requirements. In other words, the

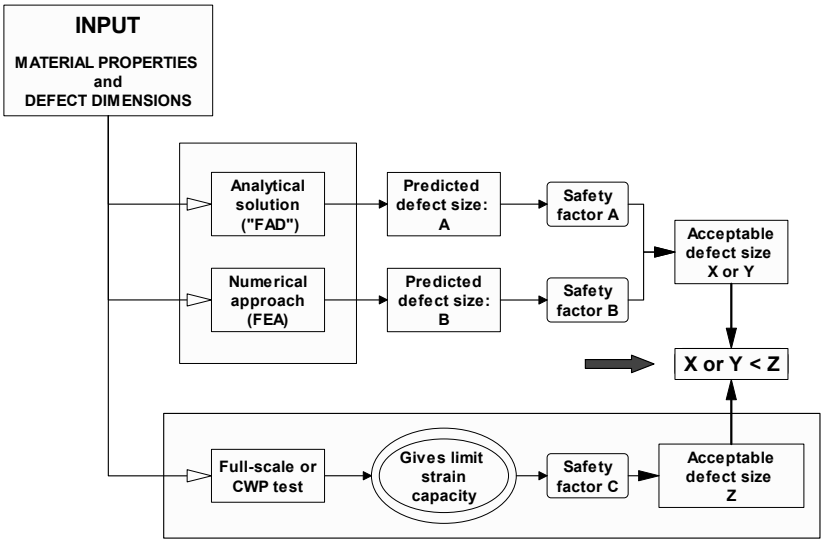

Figure 3. Weld defect acceptance and strain-based design.

engineering significance of CTOD requirements for strain-based designs needs to be clarified. The interaction between defect size, weld reinforcement, weld groove design, and the level of weld strength mismatch on ductile tearing is another aspect for which an answer is needed.

In summary, since Options A and B rely on "idealized" material property models and use conservative assumptions, the predicted defect sizes (A or B) are smaller than the critical or limit defect size (C). In this light, it is worth mentioning that a combination of worst-case assumptions may produce unworkable recommendations. This opinion reflects the often underestimated fact that the stress–strain response of each pipe in the pipeline strength is different, and thus differs from the "idealized" model used in the predictions. In other words, full scale or CWP data large test will always be needed to validate the effectiveness of analytical/numerical predictions.

4. Toughness

The toughness ensuring remote plastic strain depends on the contribution of, and trade-off between, many variables including defect size. An assessment of the results of 600 CWP tests has demonstrated that the minimum and average EPRG-Tier 2 toughness requirements [11] are equally sufficient for strain-based designs, Table 1. In true perspective, these requirements are conservative and safe since nobody will accept, despite the fact that 0.5% remote strain can be ensured, a defect with an area ratio greater than 7%.

TABLE 1. EPRG-Tier 2 toughness requirements* / **

	Min./Ave* / **	Additional requirements
Charpy V impact (CVN)	30/40 J	• Weld metal is matching or overmatching
CTOD	0.10/0.15 mm	• Y/T of pipe and weld metal < 0.90

* : To be achieved at design (wide plate) temperature.
** : Ensures the onset of remote yielding (e = 0.5%) if the defect area ratio within an arc length of 300 mm is less than 7% of the cross-sectional area.

Once the toughness of the region containing the defect meets the EPRG threshold levels of Table 1, a further analysis of the CWP database demonstrated that the strain capacity is controlled by the level of weld strength mismatch, the uniform strain capacity of the pipe metal, the shape of stress–strain curve (strain hardening rate) etc., and the defect related variables (dimensions, location, etc.). More interestingly, the analysis also revealed that for defect area ratios smaller than 7% of the cross-section area, high toughness does not automatically contribute to an increase in remote plastic strain capacity [12]. This suggests that specifying toughness levels greater than the EPRG requirements can exclude welds, which will provide adequate performance.

5. Toughness and Ductile Tearing

Fracture toughness (CTOD) of a ductile material is composed of "real" CTOD (or crack tip blunting) and ductile tearing, Figure 4. Blunting and the process of stable tearing are complicated phenomena [13–14]. The details of how these phenomena occur are dependent on many variables. Ductile tearing also interacts with the failure process in a complex way. This interaction is not yet fully understood.

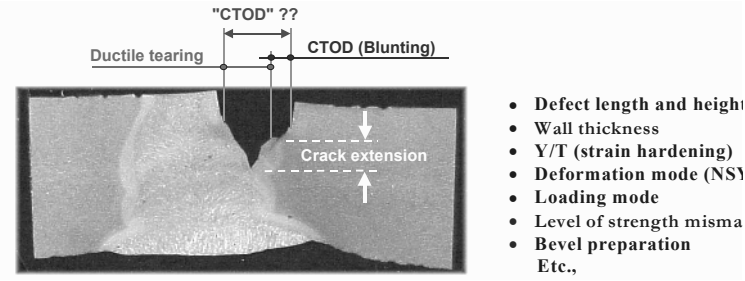

Figure 4. Factors affecting CTOD, blunting and ductile tearing.

An exploratory study of the tearing resistance of CTOD and CWP specimens show that the linear extent of ductile tearing depends on loading mode (bending versus tension), specimen dimensions, flaw size, flaw location (weld metal or HAZ), wall thickness to ligament ratio and the strain hardening characteristics of the material surrounding the defect. Further, the path of ductile tearing in a tension-loaded CWP specimen is not necessarily confined to the plane perpendicular to the applied stress, Figure 5. Ductile tearing is a three-dimensional problem.

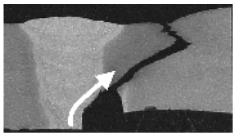

Defect location: FL/HAZ region
Initiation: Blunting and tearing towards pipe metal
Failure location: Pop-though and arrest (leak)

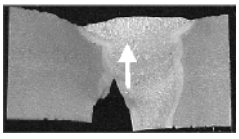

Defect location: FL/HAZ region
Initiation: Blunting and tearing towards weld metal
Failure location: Pipe metal (pipe necking)

Figure 5. Typical fracture paths in overmatched girth welds.

For the reasons discussed above, standard fracture tests cannot be used to quantify the ductile tearing characteristics of tensile loaded girth welds with surface breaking defect. In particular, standard (bend) tests produce conservative information as they are designed to simulate the highest level of structural constraint. An additional problem is translating the information into the assessment procedure. The point is that different defect length to height ratios cause different levels of through-thickness constraint. In addition, the testing of a "narrow" tension-loaded specimen does not directly provide a solution since the lack of lateral constraint (width direction) provides optimistic information.

As shown in Figures 4 and 5, ductile tearing changes the initial height (and length) of the defect. However, contrary to the current opinion, a limited amount of ductile tearing does not, in itself, threaten the structural integrity in the post-yield loading range any more than the initial defect. This observation does not exclude the fact that measures have to be taken to delay its occurrence. Premature ductile tearing can be prevented when the Y/T ratio pipe for weld metals is as low as possible. Another very effective measure consists of maximizing the level of weld metal strength overmatch. When these measures cannot be implemented, the effect of ductile tearing on plastic straining capacity needs to be accounted for in the assessment procedure.

6. Pipe and Weld Metal Tensile Property Requirements

Once the threshold level of toughness is satisfied, the strain capacity is controlled by the tensile properties of both plate and weld metal. However, an axially tensile loaded girth weld with a defect can only fail in the post-yield loading range when (a) the materials involved have adequate strain hardening capabilities and (b) the weld metal tensile properties match, as a minimum, those of the pipe metal [15–19]. The first requirement is necessary to force the applied plastic strain into the pipe metal whilst the second must prevent excessive straining of the girth weld region (weld metal and HAZ). Thus, in selecting welding consumables for strain-based designs, one should avoid undermatched weld metals; undermatching welds in yield strength concentrate plastic strain in the weld region.

These basic requirements involve the knowledge of (a) the stress–strain response in the post-yield loading range of the materials surrounding the defect, (b) the effect of weld strength overmatch and strain hardening rate of the material on the strain limit. The percentage elongation at ultimate tensile strength or the uniform strain capacity, uEL, is another essential variable since the plastic strain capacity is proportional to uEL [7].

6.1. POST-YIELD BEHAVIOUR

The insert in Figure 6a illustrates that the stress limit of an axially (or equi-stress) tension loaded girth weld with defect is determined by the failure stress of the section containing the defect, W, while the intersection of the horizontal line passing through point W and the pipe metal stress–strain response in the post-yield loading range defines the corresponding strain limit, e_i. Thus, the stress–strain response of a strain hardening overmatched girth weld with defect coincides with that of the pipe metal in the longitudinal direction. Note that the stress–strain curves, P, reproduced in Figure 6a, are representative of those, which are observed by testing contemporary pipeline steels in the longitudinal direction.

Figure 6a clearly illustrates that the shape of the post-yield response of the pipe metal has a significant effect on the strain limit. For example, by assuming a fixed defect, pipe steels characterized by a steep slope (high strain hardening rate) in the early post-yield range have a lower plastic strain capacity in their welded form than pipe steels displaying a Lüders plateau or a gradual strain

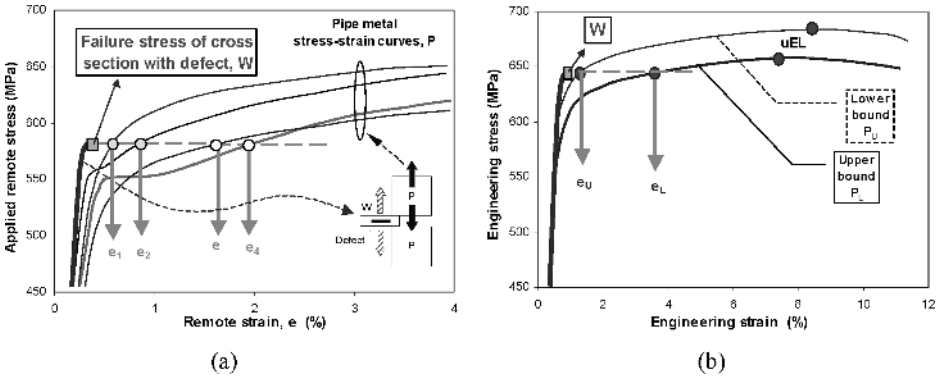

Figure 6. Effect of strain hardening behaviour on remote strain.

hardening behaviour (e_1 or $e_2 < e_3$ or e_4). In addition, Figure 6b shows the effect of the lower and upper bound stress–strain responses on the strain limit. That is, if the actual variation is taken into account, the predicted strain limit can vary from e_L (Reference Pipe P_L) to e_U (Reference P_U). In other words, a too widespread of the pipe metal tensile properties might cause pipe failure of the low strength pipe while the strain occurring in a neighbouring higher strength pipe can be insufficient. To prevent this, the specified pipe metal yield strength range must be kept as small as possible.

6.2. UNIFORM ELONGATION AND Y/T RATIO

The value of the Y/T ratio is normally used to assess failure by plastic collapse. This simplification is acceptable for stress-based designs. For strain-based designs, the Y/T ratio alone could be insufficient to characterize post-yield capacity because pipes with the same Y/T ratio can exhibit different post-yield stress–strain behaviours.

Associated challenges, not covered by codes or technical literature, are related to the determination of uEL and the effects of yield strength or Y/T ratio on uEL. With regard to the first issue, the first appearance of the maximum load plateau should be used, since further straining beyond this point goes entirely into ductile tearing (failure occurs in the defective section) or pipe necking (failure occurs in the pipe). However, this point cannot always be determined in a straightforward way. With respect to the second issue, our present understanding regarding the relationship between uniform elongation and Y/T ratio is summarized in Figure 7.

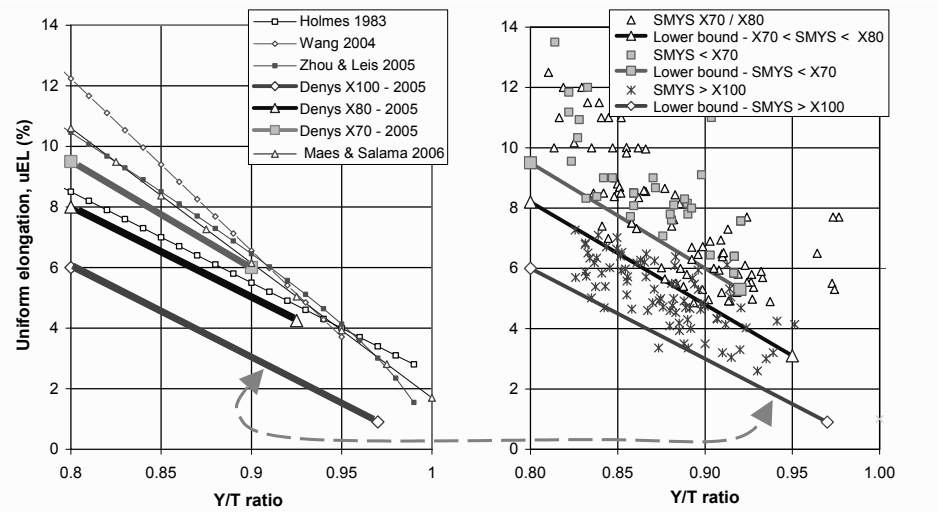

(a) Published correlations (b) Experimental correlations

Figure 7. Relationship between Y/T ratio and percentage uniform elongation.

The dotted lines in Figure 7a compare the relationship between Y/T ratio and uEL proposed by Holmes, Wang, Zhou and Maes ("published" predictions). These predictions were developed for assessing pipeline steels [20–23]. Figure 8b, shows experimental correlations obtained from the results of tensile tests on longitudinal full section 25 mm wide strap specimens extracted from pipe grades in the range from X65 to X100 of 14 mm to 25 mm wall [14]. The grades are identified in the key to the plot. The uniform elongations were determined at the onset of the maximum load plateau. The straight lines represent lower bound (solid lines) or "Denys" lower bound fits to the relevant experimental data. For example, the thick line annotated with open squares represents the lower bound fit to the X70 data. These lines are also reproduced in Figure 7a.

The comparison of the published and the Denys predictions indicates that that the former can be conservative in some cases, and unconservative in others. More importantly, the Denys correlations reveal that the derivation of uEL from tensile data should take the effect of yield strength into account. That is, the assumption that uEL is uniquely proportional to the Y/T can render non-conservative predictions. Figure 7a illustrates that uniform strain capacity decreases with increasing yield strength. The plots also show that a pipeline steel of comparable Y/T ratio can exhibit significantly different uELs. For example, at a Y/T ratio of 0.90, the uniform strain varies between 5.0% (lower bound X80) and 7.0%.

As will be discussed in Section 6.3, steels of the same nominal strength supplied by different manufacturers have a different mechanical stress–strain response. In addition, pipe of the same supplier can exhibit different tensile properties around the pipe circumference. Therefore, it is recommended to measure the actual uEL data, or in the absence of such information it is suggested to use one of the lower bound correlations shown in Figure 7b. In addition, since pipes in the coating-aged condition can also exhibit higher Y/T ratios and lower uniform elongations than pipes in "as-received" condition, the possible effects of strain ageing induced by coating should be determined. The tensile properties should be derived from test coupons which have undergone a thermal cycle representative of the plant and/or field coating.

6.3. WELD STRENGTH MISMATCH

It is standard practice to define the weld strength mismatch in terms of yield strength. The percentage yield strength mismatch, OM_{YS}, or the corresponding mismatch factor, M_{YS}, as defined in Figure 7, ignores the strain hardening effects of both pipe and weld metal on the post-yield strain capacity. Note that, because of their definition, OM_{YS} and M_{YS} have a similar significance.

Since strain hardening is an essential variable when the applied strain is beyond yield, the combined effects of yield strength mismatch and strain hardening should be quantified by a weld mismatch factor which accounts for this. The flow strength mismatch factor, $M_{FS,}$ defined in Figure 8, combines these effects into a single parameter. M_{FS} also partly incorporates the effects of differing post-yield strain behaviours of the pipe and weld metal on strain partioning between the weld and remote regions.

Figure 8 shows that yield strength overmatch ($M_{YS} > 1$) does not automatically ensure that strength overmatching occurs in the entire post-yielding loading range. The reverse reasoning also applies for yield strength undermatch. Note that, for easier illustration, the materials are assumed to have a linear strain hardening behaviour.

On the other hand, specifying that both mismatch factors M_{YS} and M_{FS} are greater than 1, 0 ensures that the girth weld is effectively overmatched. This requirement may seem to be conservative, but it excludes situations judged as overmatched in terms of yield strength are effectively undermatched in the post-yield loading range. However, considering the natural variability of the pipe and weld metal tensile properties, it is a challenge to determine the minimum values of M_{YS} and/or M_{FS}. Further, it must also be accepted that, because of the variability of material's tensile properties, each pipe and each girth weld in a pipeline string will respond differently to the applied tensile load in the post-yield loading range.

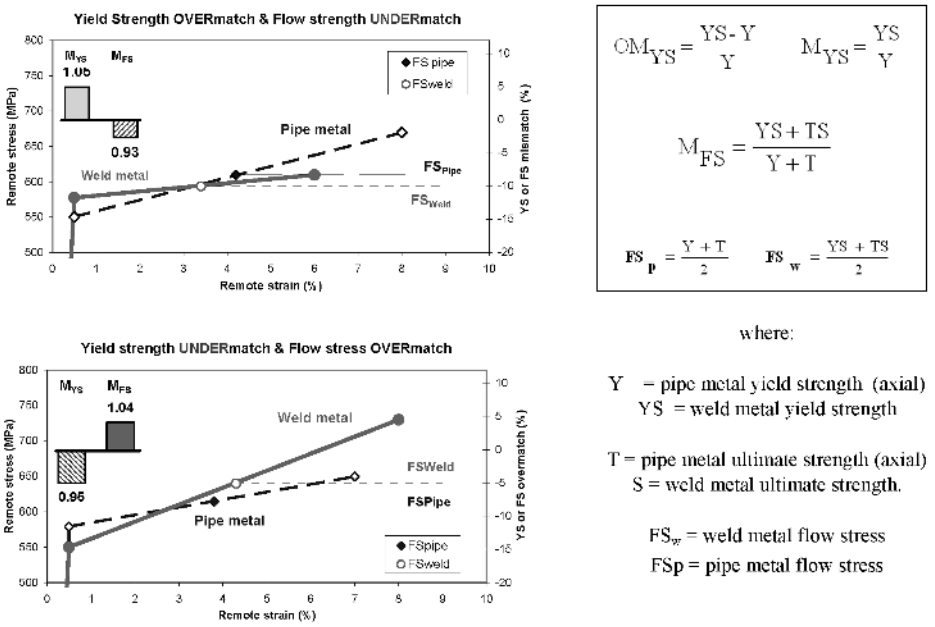

Figure 8. Effect of post-yield stress–strain behaviour on strength mismatch.

6.4. TESTING REQUIREMENTS

Currently, the pipe metal tensile properties controlled by the pipe suppliers include minimum yield strength, ultimate tensile strength and elongation at failure. The full stress–strain curve is not needed to determine these properties. Consequently, full stress–strain curves are not recorded. Moreover, the longitudinal tensile properties are not measured. Further, there is very little published statistical data to judge the natural variation of the stress–strain response and the uniform strain capacity at different locations within an individual pipe. In summary, tensile tests are performed to demonstrate that the materials comply with the minimum specified requirements.

As outlined above, the actual material properties determine the strain limit. In other words, when the testing is limited to a single all-weld metal and a few pipe metal tensile tests, significant errors can be made in the correct determination of the relevant material properties. This concern is based on the observation that [24–25]:

- The actual pipe metal yield strength in the longitudinal direction can exceed the specified minimum yield strength (SMYS) by a significant margin (>100/120 MPa). For thin wall pipes, yield strength variability tends to be higher than for thick wall pipe.
- The all-weld metal tensile properties (round bar specimens) are sensitive to the sampling location. The 6 o'clock position gives lower values than the 12 o'clock position [13]. For SMAW welds, the difference between the highest and lowest values can amount to 70 MPa. This difference is explained by the variation in weld bead shape around the circumference. For mechanized GMAW welds, the spread of the tensile properties is usually less prominent. Additionally, it is easier to obtain strength overmatch in mechanized GMAW welds than for SMAW welds.

Figure 9 shows that the actual level of strength mismatch depends on many interdependent variables. Although a detail discussion of Figure 9 is beyond the scope of this paper, one should note that:

- Different proprietary TMCP-processing routes produce different distributions ranges
- Forming of the plate into pipe causes not only differences in the longitudinal and transverse tensile properties, but also local variations around the pipe circumference
- Round-bar (RB) and full-wall strap (FT) tensile specimens produce different results. This is because the amount of material sampled with a FT specimen is greater than for a RB specimen, and the material under test in a RB specimen is taken from the mid-wall thickness location so that the inner and outer pipe surfaces are not tested
- Variation in weld metal tensile properties can differ for each welding consumable/procedure combination
- Etc.

Thus, Figure 9 illustrates that the traditional way of tensile testing provides insufficient information. That is, the statistical information needed will require stringent material specifications. In particular, it cannot be overemphasized that for each pipe and all-weld metal tensile test the complete load-elongation curve must be provided. These records must be available in order to provide information on the strain hardening characteristics (shape of the tensile curve) and to determine the uniform elongation and level of weld metal strength mismatch factors M_{YS} and M_{FS}.

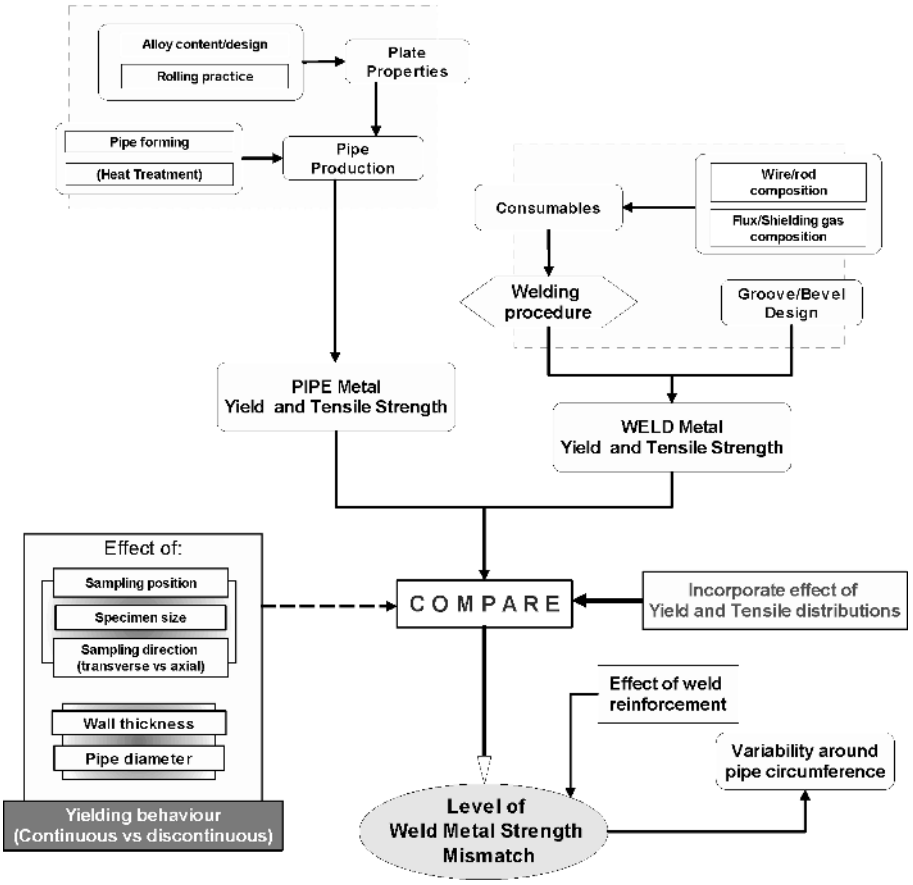

Figure 9. Factors affecting the level of weld metal yield strength mismatch.

7. Defect Sizing Capabilities and Acceptable Defect Dimensions

If the limit strain capacity as a function defect size is known, it remains to determine the acceptable defect size. As will be discussed in the next sections, the capabilities of non-destructive inspection play an important role in this process.

7.1. DEFECT SIZING CAPABILITIES

Automated Ultrasonic Testing (AUT) is a necessity for a girth weld integrity assessment of girth welds subjected to remote plastic strains. In terms of defect

sizing, it is generally accepted that defect height is the important dimension. However, it should be noted that high precision defect length sizing is also needed for strain-based design. However, since weld defects may have complex geometries, Figure 10, it is clear that it is not easy to determine the achievable levels of accuracy in defect sizing.

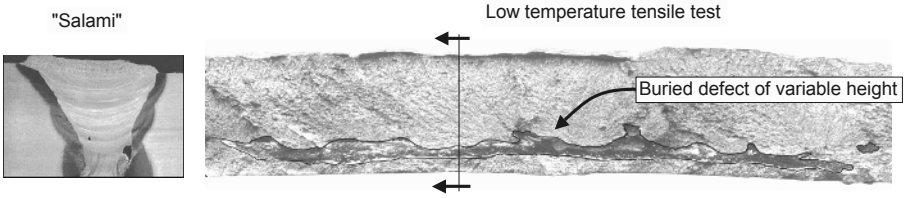

Figure 10. Verification of defect dimensions. Macro sectioning versus low temperature tensile testing.

Different opinions exist about AUT capabilities. The claimed levels of accuracy with which defects can be sized vary widely. Reported height sizing accuracies, derived from laboratory round-robins or preconstruction qualification programmes [26–28], vary from as little as ±0.5 mm to ± 2.0 mm. This information's value cannot be appreciated because the full details of the validation work are, in general, either not available, or not known (databases are proprietary). The reported "discrepancies" in height sizing accuracy can be explained by the (a) inspection procedure used, (b) the design of calibration block(s), (c) the differences in validation methodology used and (d) the type, shape and position of defects inspected. For example, the actual defect size could be underestimated by using the "salami" technique. The "salami" approach establishes the defect dimensions from a series of macro sections, Figure 10a, sampling the portion of the weld that contains the defect. In contrast, low-temperature wide-plate (long defects) or bend (small defects) testing provides direct visual access to the whole defect, and thus, a better quantification of the maximum defect dimensions, Figure 10b. Using the low-temperature technique, the sizing capabilities of AUT and radiographic (x-ray, D6 film) inspection are illustrated in Figure 11.

The charts in Figure 11 compare the actual (measured after destructive testing at low temperature) with the predicted defect sizes of a portion of a girth weld. The comparison reveals that the differences in reported heights can be significant. Note also that length-sizing errors in the circumferential direction cannot be neglected [28]. Thus, AUT reliability studies should not only be focused on improving the defect height sizing accuracy because any uncertainty on measured defect length may have a significant impact on acceptable defect height.

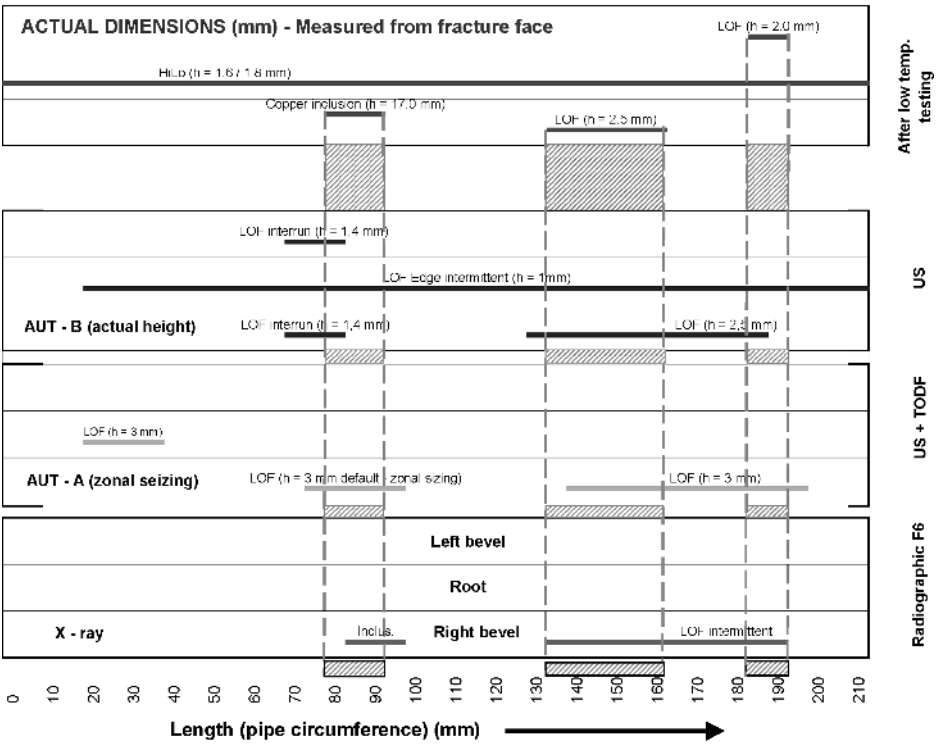

Figure 11. Example of variations in sizing accuracy for lack of fusion defects.

The sizing problem can indirectly be overcome by (a) imposing higher quality standards on construction than are routinely employed for stress-based designed pipelines, (b) maximizing the levels of weld yield strength overmatch in order to maximize the shielding of a weld defect from plastic strains and (c) using the most advanced AUT technique(s) so that all significant defects can be detected.

7.2. ACCEPTABLE DEFECT DIMENSIONS

Since it is unsafe to assume that a weld defect has the dimensions predicted by non-destructive inspection, the acceptable defect dimensions must be smaller than their predicted or limit dimensions. As shown in Figure 12, the acceptable defect size must include two safety factors; the first safety factor covers the effect of material variability on the predicted or (known) limit defect size while

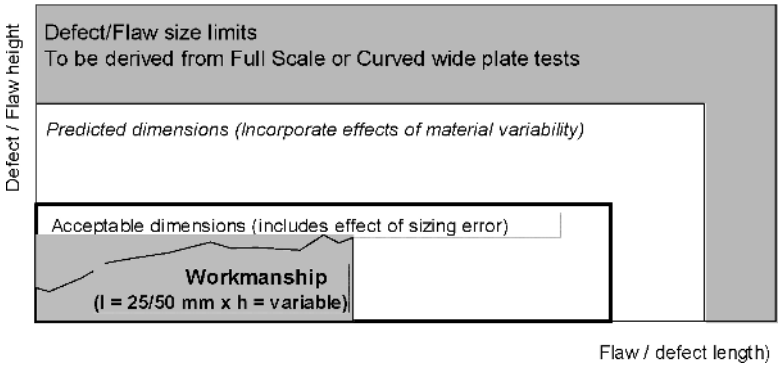

Figure 12. Interaction of critical defect dimensions, safety factors and workmanship.

the second accounts for errors in defect sizing. Additionally, the upper limit of defect size which might be missed during AUT (and/or radiographic) inspection in a production environment must be defined.

The effect of such a correction for matching girth welds subjected a remote strain of 1% is illustrated in Figure 13. The solid thick (upper) line defines the predicted boundary between acceptable defect length–height combinations (below the curve) and unacceptable defect dimensions (above the curve) for surface breaking weld defects in 18 mm wall pipe. The two lines below this line represent the acceptable defect length–height combinations for two levels of inaccuracy in defect height sizing (h = 1.0 mm and h = 2.0 mm). The horizontal dashed line represents the "base line" defect height of 3.0 mm whilst the vertical dashed lines illustrate the effect of height sizing error on the acceptable defect length.

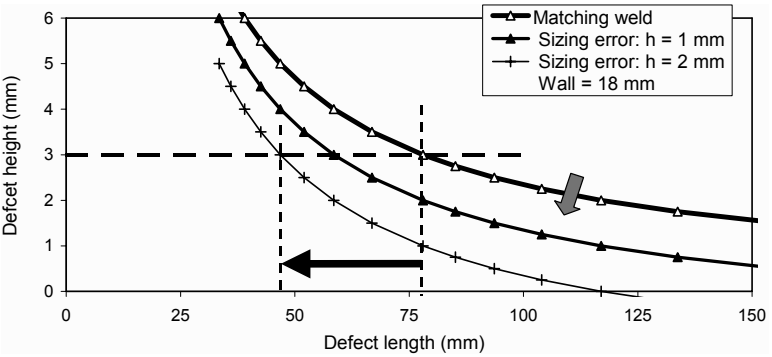

Figure 13. Effect of sizing error on tolerable defect size (strain demand: 1%).

Figure 13 is very instructive in that it demonstrates that the accuracy of defect height and length sizing must be known to establish safe acceptable defect sizes. Reference to Figure 11 shows that there is a pressing need to improve defect length sizing accuracy.

8. Conclusions

The most important conclusions arising from this paper are:

- The assessment of girth weld integrity for designs involving axial plastic strains depends on a complex interrelation of many contributing variables.
- The minimum and average EPRG-Tier 2 toughness requirements can be used as threshold values for strain-based designs. When the toughness of the weld metal or HAZ regions exceeds this threshold level, plastic strain capacity solely depends on the tensile properties of both the region (weld metal/HAZ) containing the defect and the pipe metal.
- Because of the many variables involved, many possible solutions exist to achieve remote strains exceeding the 0.5% level. High levels of remote plastic strain can be ensured by selecting:
  - Weld metals that gives a high degree of strength overmatch
  - Pipe with a Y/T ratio as low as possible and uniform strain capacity as high as possible
  - Pipes which do not exhibit high strain hardening in the early part of their post-yield stress-strain response
- The actual and not the minimum specified material properties determine the strain limit. Moreover, statistical information on the stress–strain response of the pipe and weld metals in the post-yield loading range has to be gathered if appropriate strain capacities are to be determined. The direct consequence of this observation is that traditional qualification procedures provide insufficient information.
- High precision defect height and defect length sizing capability is a must for strain-based girth weld defect inspection.

Finally, experimental data allow concluding that the above toughness and tensile property requirements can be fulfilled for contemporary pipeline steels and welding consumables. However, these requirements could be a challenge to the industry if (very) high steel grades are to be employed in regions where post-yield longitudinal strains are expected. In particular, this means that continued efforts are needed to improve the consistency of properties in pipe and welding consumables. Additionally, efforts must be directed towards a further improvement of defect sizing accuracy.

References

1. B. Graville and A. Dinovitzer, Strain-based failure criteria for part-wall defects in pipes, *ASME PVP Conference*, Montreal, July 1996.
2. A. Nogueira, G. A. Lanan, T. M. Even, and B. A. Hormberg, Experimental validation of limit strain criteria for the BPXA Northstar Project, *Proceedings of Pipeline Welding and Technology*. ICAWT '99, David Yapp, Ed., Galveston, Texas.
3. BS 7910:2000, Guide on methods for assessing the acceptability of flaws in metallic structures.
4. Y. Y. Wang, R. Denys, D. Rudland, and D. Horseley, A preliminary strain-based design criterion for pipeline girth welds, *Proceedings of IPC2002, 4th Int. Pipeline Conference*, Calgary, Canada, 2002, Paper 02-27169.
5. W. C. Mohr, Strain-based design of pipelines, Report #45892GTH to MMS, October 2003. http://primis.phmsa.dot.gov.
6. Y. Y. Wang, W. Cheng, D. Horsley, A. Glover, D. J. Zoe, and M. McLamb, Tensile strain limits of girth welds with surface-breaking defects – Part I an analytical framework and Part II experimental correlation and validation, *Proceedings of the Fourth International Pipeline Technology Conference* Volume I, Oostende, Belgium, 2004.
7. R. Denys, W. Dewaele, A. Lefevre, and P. De Baets, An engineering approach to the prediction of the tolerable defect size for strain based design *Proceedings of the Fourth International Pipeline Technology Conference*, Volume I, Oostende, Belgium, 9–13 May 2004.
8. R. Denys, Wide Plate Testing of Weldments, Part I, II and III, Fatigue and fracture testing of weldments, ASTM STP 1058, pp. 157–228, ASTM Philadelpia, 1990.
9. R. Denys, Universiteit Gent CWP-database.
10. R. Denys, Significance of CTOD in cross welded loaded joints with weld metal overmatching in strength, ASTM, STP 945, USA, June, 88, pp. 686–698.
11. G. Knauf and P. Hopkins, The EPRG guidelines on the assessment of defects in transmission pipeline girth welds, 3 R Intern, Jahrgang 35, Heft 10-11/1996, S. 620–624.
12. R. Denys, A. Lefevre, C. De Jaeger, and S. Claessens, Failure characteristics and defect tolerance levels of girth welds in large diameter X65/X70 steel pipelines: experimental verification through wide plate testing and comparison with ECA prediction models. *Proceedings of the Third International Pipeline Technology Conference*, pp. 151–167 Volume I, Brugge, Belgium, Elsevier Science, 2000.
13. R. Denys, A. Lefevre, P. De Baets, and J. Degrieck, Effects of stable ductile crack growth on plastic collapse defect assessments, *Proceedings of the Third International Pipeline Technology Conference*, pp. 169–89, Belgium, Elsevier Science, 2000.
14. R. Denys and A. Lefevre, Material test requirements for strain-based pipeline design, CBMM Conference, Araxa, January 2006, To be published by TMS (The Minerals, Metals & Materials Society).
15. R. Denys, Effect of weld metal matching on girth weld performance, Volume II, AGA Catalog No. L51 851-IN1, p. 137, January 1993.
16. R. Denys, Strength and performance characteristics of welded joints, *International Symposium on Mis-Matching of Welds*, *ESIS* (Ed. Schwalbe and Kocak) 1994, Mechanical Engineering Publications London, pp. 59–102.
17. R. Denys and A. A. Lefevre, Weld metal mismatch, challenges and opportunities, *Proceedings of Pipeline Welding and Technology*. ICAWT '99, David Yapp, Ed., Galveston, Texas.
18. R, Denys, A. Lefevre, and A. G. Glover, Weld metal yield strength variability in pipeline girth welds, Elsevier Publication ISB N0. 444 82197, Volume II, pp. 591–598.

19. R. Denys, W. De Waele, and A. Lefevre, Effect of pipe and weld metal post-yield characteristics on plastic straining capacity of axially loaded pipelines, *Proceedings of IPC 2004*, Calgary, Canada, Paper # IPC04-0768.
20. B. Holmes, Prediction of linepipe fracture behaviour from laboratory tests, *International Journal Pres. & Piping*, 12 (1983), pp. 1–27.
21. X. K. Zhu and B. Leis, The influence of the Y/T ratio on the failure assessment of corroded pipelines, *The Journal of Pipeline Integrity*, **4**(3), pp. 141–154.
22. Y. Y. Wang, W. Cheng, and D. Horsley, Tensile strain limits of buried defects in pipeline girth welds, *Proceedings of the Fifth International Pipeline Conference 2004*, Paper IPC04-0524, Calgary, Alberta, Canada.
23. M. A. Maes and M. Salama, Impact of yield to ultimate ratio on the relaiability of burst limit states, *Proceedings of the Sixth International Pipeline Conference 2006*, Paper IPC2006-10323, Calgary, Alberta, Canada.
24. R. Denys, A. Lefevre, and P. De Baets, Significance of the tension test in relation to plastic pipeline design, *Proceedings of the International Conference on Application and Evaluation of High-Grade Linepipes in Hostile Environments*, 2002, Yokohma, Japan.
25. R. Denys and Glover, A. G., Experimental investigation of the fracture behaviour of over- and undermatched pipeline girth welds*, Mis-Matching of Welds, ESIS 17, MEP*, 1994.
26. R. Denys, A. Lefevre, C. De Jaeger, and S. Claessens, *Weld Defect Acceptance Criteria*, June 2000 http://www.iploca.com.
27. M. Moles, Defect sizing in pipeline welds – What can we really achieve? *ASME PVP Conference Proceedings*, San Diego, 2004.
28. T. Bouma and R. Denys, Automated ultrasonic testing and high-performance pipelines: bridging the gap between science and practice, *Proceedings of the Fourth International Pipeline Technology Conference*, Volume I, Oostende, Belgium, 2004.

FAILURE OF CYLINDRICAL SHELLS: NUMERICAL AND EXPERIMENTAL STUDY

A. ELHAKIMI[1], H. MOUSTABCHIR[2], S. HARIRI[1], Z. AZARI[2]

[1]*Ecole des Mines de Douai – Département technologie des polymères et composites & ingénierie mécanique, 941 rue Charles Bourseul, BP1038, 59508 Douai cedex;*
[2]*Laboratoire de Fiabilité Mécanique, ENIM, 57045 Metz, France*

Abstract: In industrial structures, the presence of cracks under critical loads leads to complete ruin. Fracture mechanics allows the study of macroscopic defect damage. This requires the knowledge of the stress fields and the deformations near the crack. Our work is an application of fracture mechanics into the domain of the pressurized structures with defects. Design of this type of structures is subjected to standards, codes and regulations driven by the potential risks which they represent. The knowledge of the pressure limit in these structures allows respecting the safety domain. We present in this paper the numerical solutions and experimental results for stress distribution at defect tip. The structure's elastic and elasto-plastic modelling will be treated by the finite element simulation. In the elastic case, we study the influence of the geometrical parameters for axial and circumferential cracks and determine the elastic integral *J*. Measures of strains near defects in the studied model have been made by strain gauges. The experimental results validate the numerical simulations. In addition, acoustic emission is used to define sensitive zones and to control defect evolution during the test until failure in the structure.

Keywords: fracture mechanics, pressure vessels, numerical solutions, experiments

1. Methods for *J* Estimation

1.1. THE ELECTRIC POWER RESEARCH INSTITUTE (EPRI) METHOD

The EPRI method for a given material and geometry estimates the *J*-integral value and the maximal load applied to structures [1, 2].

G. Pluvinage and M.H. Elwany (eds.), Safety, Reliability and Risks Associated with Water, Oil and Gas Pipelines, 65–77.

For instance, in the case of a cylindrical shell submitted to an axial load P, the elastic J_e-integral is given by:

$$J_e = \frac{K_I^2}{E} = f_b^2\left(\frac{\theta}{\pi}\right)\left(\frac{(P)^2}{E(Rb)^2}\right) \tag{1}$$

where b is the ligament size and R is the pipe radius.

The stress–strain behaviour is given by the Ramberg-Osgood's law [1, 3]:

$$\frac{\varepsilon}{\varepsilon_e} = \frac{\sigma}{\sigma_e} + \alpha\left(\frac{\sigma}{\sigma_e}\right)^n \tag{2}$$

where n is the strain hardening coefficient and α a material constant.

For this type of material, the J_p-plastic integral is given by the following expression [10]:

$$J_P = \alpha.\varepsilon_e.\sigma_e.c.h\left(\frac{a}{t}, n, \frac{R}{t}\right)\left[\frac{P}{P_0}\right]^{n+1} \tag{3}$$

where a is the crack length, t the pipe thickness and R its mean radius. c is a characteristic length like the ligament size, P the applied load and P_0 the reference load. h is a function which depends on the material and the geometry. To limit errors due to the Ramberg-Osgood's model, Ainsworth's behaviour law [4] proposes a "real" material behaviour law:

$$\sigma_{ref} = \frac{P}{P_L}.\sigma_e \tag{4}$$

where P_L is the load limit, σ_{ef} the reference stress [10] and σ_e the yield stress.

In this case, J is given by a simplified relationship [11–12]:

$$J = J_e\left(\frac{E\varepsilon_{ref}}{\sigma_{ref}} + \Phi\right) \tag{5}$$

where ε_{ref} is the reference strain corresponding to the reference stress σ_{ef} on the actual material behaviour law and Φ is the plastic zone at bottom crack tip i. Ainsworth overestimates the plastic zone diameter by the following expression:

$$\Phi = \tfrac{1}{2}.\frac{\sigma_{ref}^2}{\sigma_{ref}^2 + \sigma_e^2} \tag{6}$$

1.2. A16 RCC-MR METHOD

CEA engineers have developed a simplified estimation method called JA_{16} based on Ainsworth's works. They propose to calculate J_p from J_e multiplied by a K_{A16} factor which takes into account the plasticity correction [5, 6, 8 and 9]:

$$J_p = K_{A16} * J_e \tag{7}$$

The K_{A16} factor is a correction coefficient, which quantified the plastification level at crack tip. It is a function of the reference stress σ_{ref} and strain ε_{ref}:

$$K_{A16} = K_{1A16} * K_{2A16} \tag{8}$$

The stress correction coefficient can be written as:

$$K_{1A16} = \left(\frac{\sigma_{nor}}{\sigma_n} \right)^2 \tag{9}$$

The net stress σ_n and the real net stress σ_{nor} are determined from the real material behaviour law.

The strain correction coefficient can be written as:

$$K_{2A16} = \Psi_{A16} + \frac{E\varepsilon_{ref}}{\sigma_{ref}} \tag{10}$$

Ψ_{A16} is the plastic zone correction:

$$\Psi_{A16} = \frac{1}{2} \frac{\sigma_{ref}^2}{\sigma_{ref}^2 + \sigma_e} \tag{11}$$

The Von Mises's stress in the case of an axisymetric loading is written as:

$$\sigma_{eq} = \left[\left(\sigma_{1m}^2 + \sigma_{2m}^2 - \sigma_{1m}\sigma_{2m} \right) + \frac{2}{2\sqrt{3}} \left| \sigma_{1m}\sigma_{1b} + \sigma_{2m}\sigma_{2b} - \frac{\sigma_{1m}\sigma_{2b} + \sigma_{2m}\sigma_{1b}}{2} \right| \right.$$
$$\left. + \left(\frac{2}{3} \right)^2 \left(\sigma_{1b}^2 + \sigma_{2b}^2 - \sigma_{1b}\sigma_{2b} \right) \right]^{1/2} \tag{12}$$

σ_{1m} : axial membrane stress
σ_{1b} : axial bending stress
σ_{2m}: hoop stress and
σ_{2b}: circumferential bending stress

1.3. R6 METHOD

The R6 Route proposes a different plastic correction from the A16 method [7, 8]

$$J_{R6} = \frac{J_e}{\left(K_r - \rho\right)^2} \tag{13}$$

with

$$K_r = \left(\Psi_{R6} + \frac{\varepsilon_{ref} E}{L_r \sigma_e} \right)$$

The ρ coefficient depends on the L_r parameter.

$$\Psi_{R6} = \frac{L_r^3 \sigma_e}{2E\varepsilon_{ref}} \tag{14}$$

is the plastic zone correction.

2. Experimental Part

The aim of these tests is to measure strain near defect tip in a pipe. At the same time, the evolution of the defects size is followed by an acoustic emission method. The experimental devices and the equipments used in the different tests are as follows:

- Test Parameters: tube geometry, temperature, loading and others parameters according to the test nature.
- Material characterizations: chemical composition and mechanical properties.
- The different devices used to control crack evolution.

2.1. SPECIMEN CHARACTERIZATION

The experimental study is done on a specimen made from a cylinder closed at the end by two toroidal segments of a sphere with large radius. Figure 1 gives the geometrical parameters of the studied structure.

To determine the mechanical properties of the material, tensile tests have been performed at room temperature. Coupons have been cut with their length along the longitudinal direction. Six cylindrical specimens of 7 mm diameter have been machined from these coupons. Geometry and specimen dimensions are given in Figure 2.

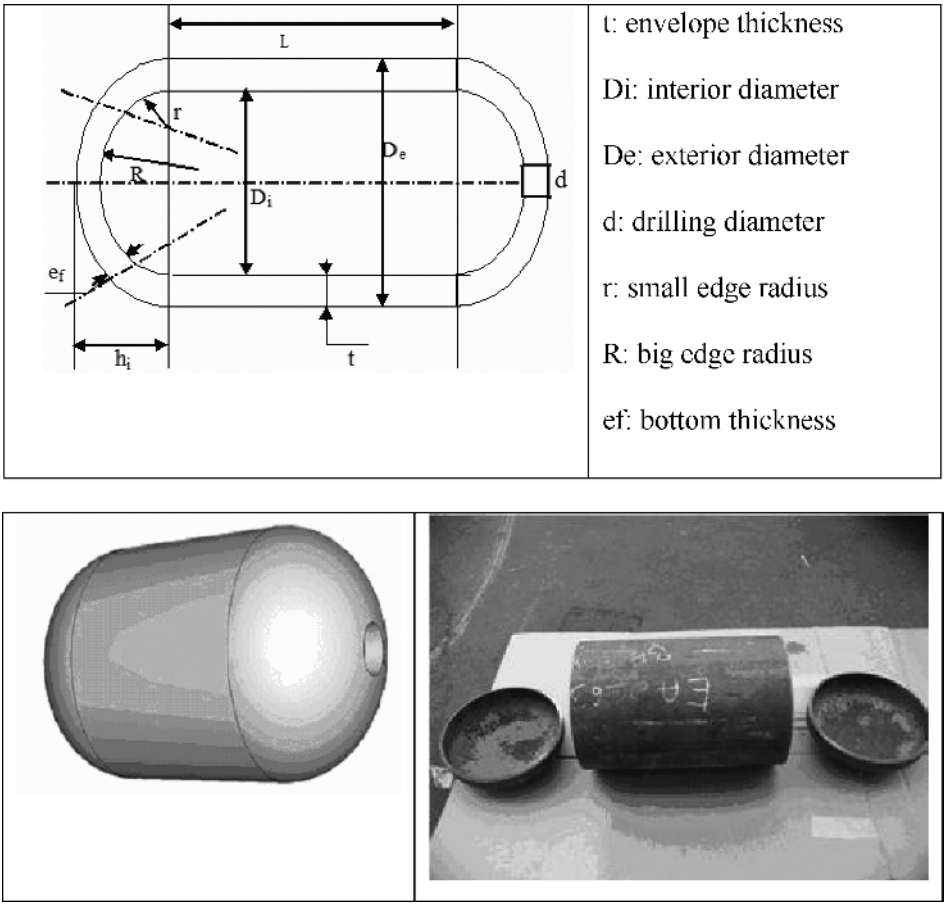

Figure 1. Specimen geometry.

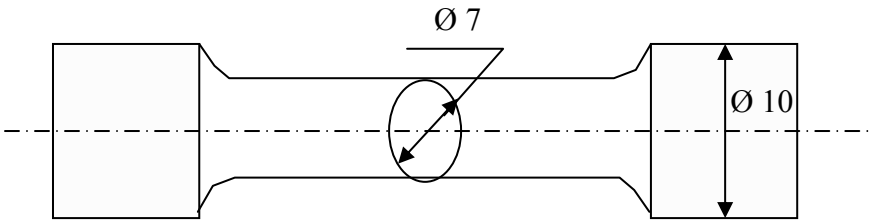

Figure 2. Geometry and dimensions of tensile specimens.

Figure 3 presents the evolution of experimental conventional stress-strain curve and it clearly indicates the ductile behaviour of the material.

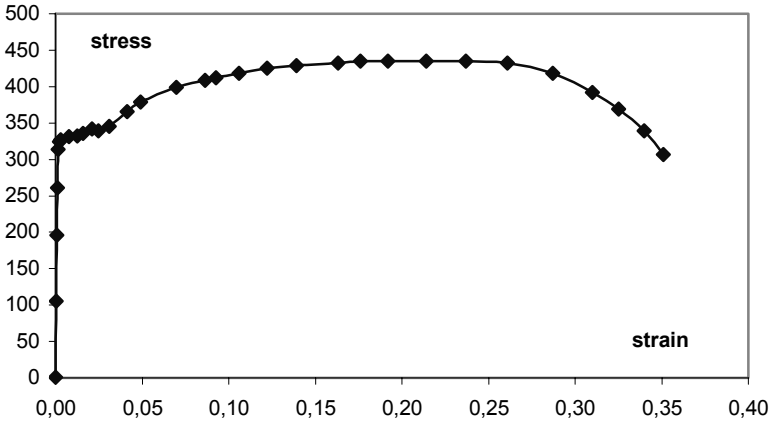

Figure 3. Stress–strain curve of the material.

The mechanical properties extracted from Figure 3 are given in Table 1.

TABLE 1. Mechanical characteristic of the material.

1.1.1.a.1.1 Mechanical characteristic				
Young's modulus (MPa)	Poisson's ratio	Yield stress (MPa)	Ultimate strength (MPa)	Elongation % .1.a.1.2
207,000	0.3	360	440	35

The chemical composition of the material is given in Table 2.

TABLE 2. Chemical compositions (% mass).

%	C	Min	S	Yew	P	Al
Material	0.135	0.665	0.002	0.195	0.013	0.027
Standard (max)	0.18	1	0.015	0.4	0.025	0.02

The pipe is submitted to an internal water pressure, which induces nominal stress σ_N = 147 MPa. Figure 4 gives the pipe dimensions.

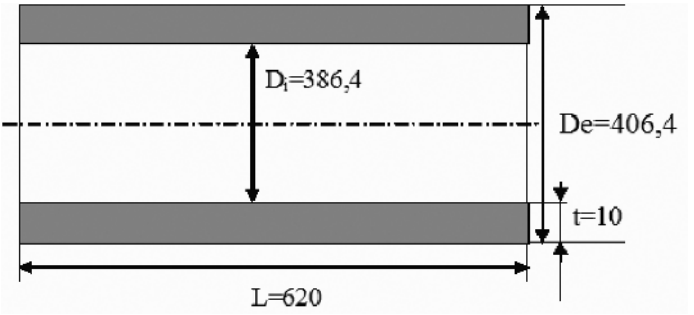

Figure 4. Specimen dimensions.

σ_N : Nominal stress
Test pressure was P = 74 bars

2.2. GEOMETRY OF THE DEFECT

The studied specimens are cylindrical shells with some axisymetrical or elliptical cracks at internal or external surfaces (Figures 3 and 4). The semi-elliptical defects are characterized by two aspects, ratios a/t and a/c, with crack depth measured in radial direction 2. *c* is the crack length. The pipes are characterized by a non-dimensional ratio (t/R) where t is the thickness and R the internal radius, (Figure 5).

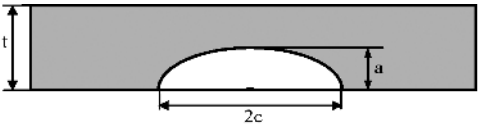

Semi-elliptical cracks

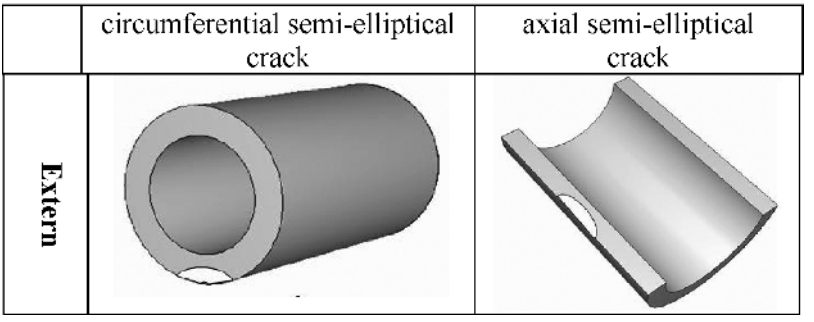

Figure 5. Cylindrical geometries.

Table 3 gives the different dimensions and orientations of the cracks.

TABLE 3. Defect dimensions.

Specimens	Defects	Orientations	Dimensions
M1	**D1**	Axial	a = 8 mm, c = 32 mm
	D2	Axial	a = 2 mm, c = 8 mm
M2	**D3**	Circumferential	a = 8 mm, c = 32 mm
	D4	Circumferential	a = 2 mm, c = 8 mm
M3	**D5**	Axial	a = 4 mm, c = 16 mm
	D6	Circumferential	a = 4 mm, c = 16 mm

2.3. SPECIMEN INSTRUMENTATION

For this study, we have several objectifies:

- To determine the experimental strain distribution near the crack tip (elastic domain), in order to validate our numerical models, the specimens are instrumented by gauges in the defect zone (Figures 6 and 10). For an optimal comparison with numerical computation, a total of 90 gauges were necessary.

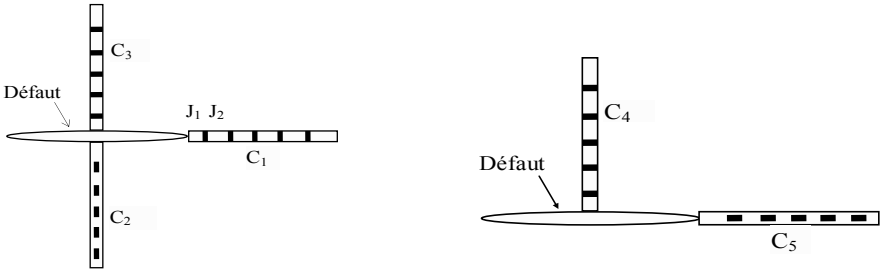

Position and orientation of strain gauges (defect D_1)

Position and orientation of strain gauges (defect D_2)

Figure 6. Position and orientation of strain gauges.

To follow the crack evolution by acoustic emission and by strain gauges, the acoustic emission sensors are set up according to Figure 7.

In each studied specimen, 14 sensors were used (two working at 30 kHz and 12 at 150 kHz), Figure 7.

2.4. D. VERIFICATION OF SENSORS SENSITIVITY

Sensitivity of every sensor was checked with the help of a Hsu-Nielsen source (three at distance 5 cm and 20 cm). For each distance, sensor emission should be about ±3db.

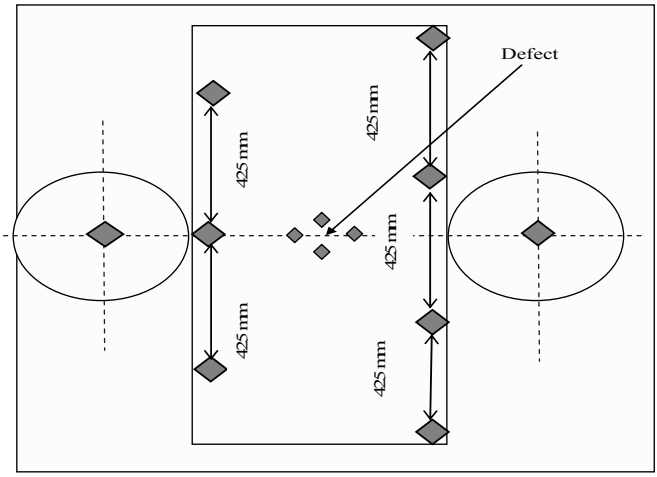

Figure 7. Acoustic sensors positions.

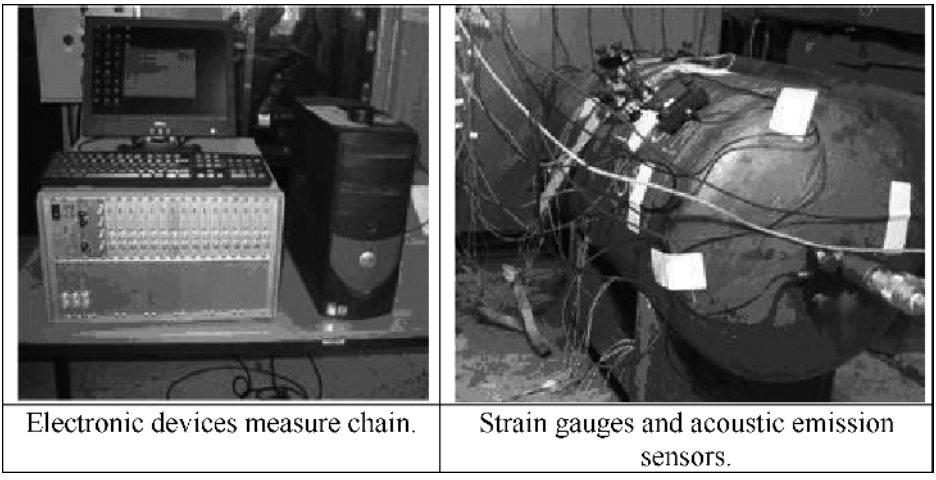

Figure 8. Details of the acoustic emission procedure.

3. Numerical Method

The meshing, as well as all the numerical calculations, is performed with the help of the Castem software. In the case of axisymmetric defects, 2D-axisymmetric modelling is retained, based on the fact that both geometry and loading are axisymmetric. A 3D model is required for more complicated case of semi-elliptic defects.

A specific adjusted crack block is used to mesh the vicinity of the crack front (Figure 10). A plain crack mesh is extruded along the elliptic crack front. A reference volume surrounding the whole crack is obtained, which is completed by transitional volumes in order to finally get a plane and parallel volume. This crack block is then wrapped with the ad hoc curvature radius, before incorporation into the total meshing of the structure (only one quarter is meshed because of symmetry) generated by suitable translations and rotations (Figure 9). For instance, for smaller details the use of quadratic finite elements is made. Meshing in the vicinity of the crack front is particularly small (most of the elements are concentrated in the crack block) in order to ensure a good description of the stress field when it is singular. The developed crack block has been optimized and validated (in the range of crack sizes presented above) in comparison with other numerical results found in the literature. Stresses are directly prescribed onto the crack tips, involving constant, linear, quadratic and cubic distributions. This procedure enables to perform stress intensity factors calculations for arbitrary global loading conditions, according to the super-position principle in linear elasticity.

4. Results

The J calculation is made by finite elements and by simplified rules R6 and A16 routes. The results are presented according to the non-dimensional parameter Pa/Pe.

It is noticed that a constant loading on the crack tip translates a constant global loading due to internal pressure, which is the most current case in industrial practice.

It is observed that for the lower loads (Pa/Pe = 0.6), the simplified R6 and A16 methods estimate correctly the J-integral. This is due to the low plasticity at crack tip. If load increases, the difference between the different methods increases. In any case, J increases with the applied load, Figure 10. It is also noticed that in all cases, the simplified methods overestimate the J-integral and are therefore conservative.

The strain gauges indicate good agreement between experimental and theoretical values, Figure 11.

Semi-elliptic circumferential external crack.	Semi-elliptic axial external crack.
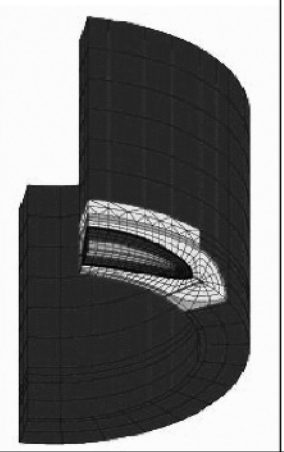	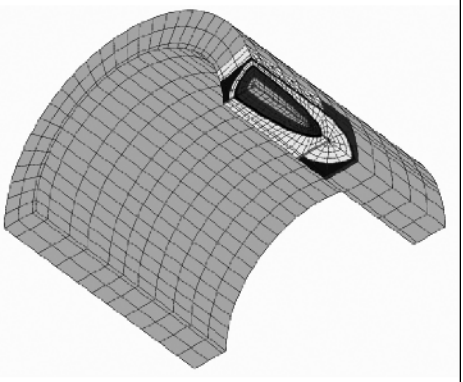
Semi-elliptic circumferential internal crack.	Semi-elliptic axial internal crack.
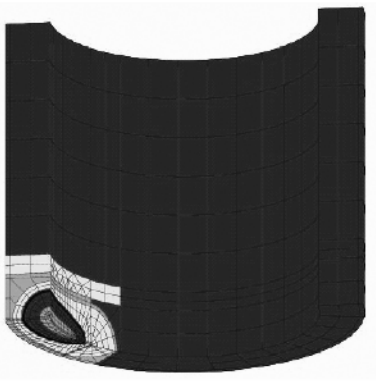	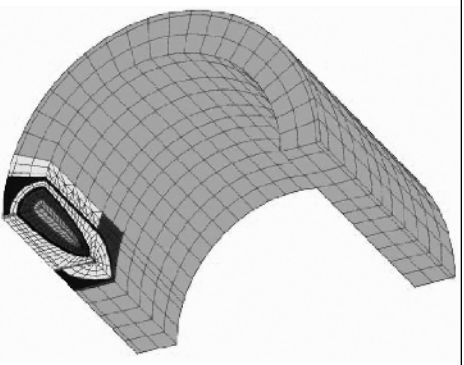

Figure 9. Different studied cases.

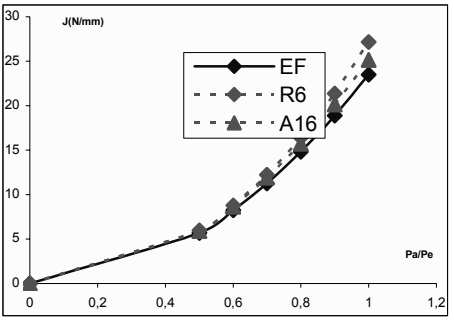

J evolution with load (a/t = 0.8, a/c = 1/4 et t/Ri = 1/10).

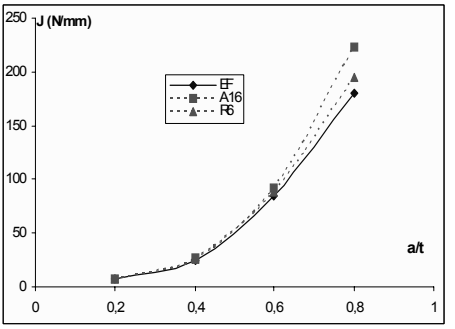

J evolution with load de a/t (a/c = 1/8, Pa/Pe = 0.8 et t/Ri = 1/10).

Figure 10. *J* evolution versus load.

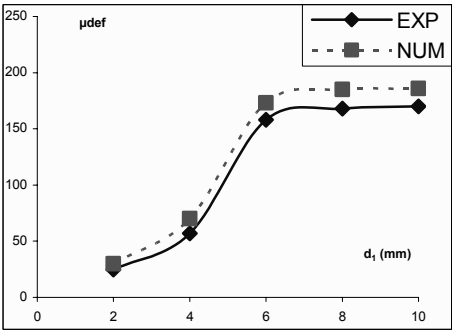

Circumferential strain according to distance (P = 2.5 MPa, M1, C4).

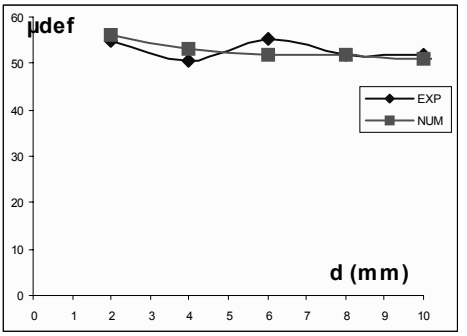

Circumferential strain according to distance (P = 2.5 MPa, M1, C5).

Figure 11. Hoop strains with respect to distance.

5. Conclusion

This work consisted in a numerical and experimental study of the semi-elliptical defects occurring in cylindrical shells. The goal of this investigation is to propose tools and a methodology for the characterization of the harmfulness of such defects usually present in the equipments under pressure, such as gas pipes.

This study has been based on an elastic and elasto-plastic analysis of the shells with defects subjected to pressure. The stress field is decomposed using a polynomial form in the crack plan. The stress intensity factors are determined as a function of the geometrical parameters of the shells and cracks. In the elastic-plastic domain, the *J*-integral is numerically determined; and then by the simplified rules R6 and A16.

An experimental study is carried out on models including orientation cracks with various geometries in order to validate the numerical approach. The strain gauge enabled validation of the related strain results. In the same way, during pressure tests, the defect evolution is controlled by the acoustic emission technique.

References

1. B. Raj, K. Bhanu, S. Roa, T. Jayakuma, and R. K. Dayal, Materiel's ageing and life management, **2** (2000).
2. V. Kumar, M. D. German, and C. F. Shih, An engineering approach of elastic plastic fracture mechanics, NP 1931, Res.Pr.1237-1- EPRI (1981).
3. I. Delvallee, Thèse, "Nocivité d'un défaut semi elliptique complexe dans une coque cylindrique fermée soumise à une pression interne" (September 1999).
4. R. A. Ainsworth, The assessment of defects in structures of strain hardening material, *Engineering Fracture Mechanics*, **19**(4), pp. 633–642 (1984).
5. D. Moulin, B. Drubray, and M. Nedelec, Méthode pratique de calcul de J, in *Annexe du RCC-MR: Méthode* J_s.
6. B. Drubay, Guide pour l'analyse de la nocivité des défauts et la fuite avant rupture, *troisième préliminaire* CEA (December 1995).
7. I. Milne, R. A. Ainsworth, A. R. Dowlind, and A. T. Stewart, Background to and validation of G.EG.B report R/H/R6-Revision 3, *International Journal of Pressure Vessel and Piping*, **32**, pp. 105–196 (1988).
8. R. A. Ainsworth, U. Zerst, and K. H. Schwalbe, Basic principles of flaw assessment methods, *International Journal of Pressure Vessels and Piping*, **77**, pp. 855–867 (2000).
9. A. EL Hakimi, Ph.d Thesis, Étude numérique et expérimentale de la nocivité des défauts dans des coques cylindriques et sphériques sous pression (June 2006).
10. A. Saffih and S. Hariri, Numerical study of elliptic cracks in cylinders with a thickness transition *International Journal of Pressure Vessels and Piping*, pp. 35–41 (January 2006).
11. A. Saffih and S. Hariri, Comparison of semi-elliptic cracks in cylinders with a thickness transition and in a straight cylinders – elastic-plastic behaviour, *Engineering Fracture Mechanics*, **73**(17), pp. 2685–2697 (November 2006).
12. A. El Hakimi, S. Hariri, A. Laksimi, P. Le Grognec, and Z. Azari, Étude numérique et semi-analytique de la nocivité de défauts dans les coques sphériques, *Revue Européenne de Mécanique Numérique*, **16/1**, pp. 79–101 (2007).

LEAK DETECTION BY USING THE IMPEDANCE METHOD

EZZEDDINE HADJ TAIEB*
Departement de mecanique, ENIS
BP W, 3038 SFAX, Tunisia

Abstract: Consideration is given in this paper to the numerical techniques of leakage detection in pipes utilizing transient state heads and discharges. Transient flow, considered herein, is produced by a rapid valve closure at the downstream end of the pipe. A mathematical model of transient flows is presented and resolved by the method of characteristics. The computed results describe the influence of the presence of leaks on the head and discharge time-histories. In the case of steady oscillatory flow, the impedance method and the harmonic analysis is used to develop the transfer function at the closed valve. The impedance diagram of a system with leak is analyzed and compared with the one of a system without leak. To determine the leak location, a numerical tool, based on the values of the normalized harmonic frequencies and represented by the ratio of those producing infinite or zero impedance values, is developed.

Keywords: transient flow, method of characteristics, impedance method, transfer function, leak detection

1. Introduction

In many water distribution systems a significant percentage of water is lost while in transit from treatment plants to consumers. According to an inquiry made in 1991 by the International Water Supply Association (IWSA), the amount of lost or "unaccounted for" water is typically in the range of 20–30% of production [1]. Unaccounted for water is usually attributed to several causes including leakage, metering errors and theft-leakage is the major cause. In

* Ezed.Hadj@enis.rnu.tn

G. Pluvinage and M.H. Elwady (eds.), Safety, Reliability and Risks Associated with Water, Oil and Gas Pipelines, 79–97.

addition to environmental and economic losses caused by leakage, leaky pipes pose a public health risk as leaks are potential entry points for contaminants if a pressure drop occurs in the system.

To develop a policy of maintenance for a water supply network, in order to extend the life duration above the expected date of replacement, one can use a programmed over pressurizing of a selected part of the network. Hence, two situations can arrive: leak or no leak. If no leaks occur, it is possible to know a lower bound of life duration and possible date of replacement by methods using damage evolution and fracture mechanics. If leak occurs, new techniques based on acoustic emission allows knowing its exact position, and methods based on hydraulic and fracture mechanics allows to know the size of the open defects [2].

Experimentally, by using acoustic equipment which detects the sound or the vibration induced by water as it escapes from pipes under pressure, one may obtain information about the location and size of leaks.

Theoretically, different methods for leak detection have been developed. Leak detection methods that are based on time transient analysis ([3], [4], [5], [6], [7], [8]) usually are based on the acquisition and analysis of extensive real-time data. Often, these data are either not available or costly to obtain.

Leak detection and evaluation in pipe systems can also be reached by means of unsteady state tests that minimize both time consuming and costs for water supply companies as well as minimize the risks for the integrity of conduits.

In this paper, two techniques for leak detection, the time transient analysis and the harmonic analysis, are described. Being inspired by Ferrante and Brunone study on leak detection [9], a numerical model based on the impedance method is developed leading to the head spectrum at the downstream end section of a single pipe system, with or without leak, during transients. A diagnostic tool is then proposed to locate the leak and to determine its size.

2. Mathematical Model

2.1. MOTION EQUATIONS

The equations which describe transient 1D flow in a cylindrical pipe of linear elastic behaviour according to the Hooke law can be adapted from the analytical model developed by Wylie et al. [10]. Applying the laws of conservation of mass and momentum yields to the following equations of continuity and motion:

$$\frac{\partial Q}{\partial x}+\frac{gA}{C^2}\frac{\partial H}{\partial t}=0 \tag{1}$$

$$\frac{\partial H}{\partial x}+\frac{1}{gA}\frac{\partial Q}{\partial t}+\frac{\lambda Q|Q|}{2gDA}=0 \tag{2}$$

where Q is the fluid discharge, $H = z + p/\rho g$ is the head, C is the pressure waves celerity, ρ is the fluid density, λ is the coefficient of friction, A is the cross section area of the pipe, D is the circle pipe diameter, t is the time and x is the distance along the pipe.

The classical integration of eqs. (1) and (2) using the method of the characteristics allows explaining the pressure time-history at each computational point as originated by the propagation of positive and negative pressure waves.

2.2. LEAK ANALYSIS IN PIPES USING TRANSIENTS

The method of characteristics [11] is applied to transform the system of partial differential eqs. (1) and (2) into a system of ordinary differential equations that can be integrated numerically without difficulty. One gets:

$$dQ\pm\frac{gA}{C}dH+gAJdt=0 \quad \text{and} \quad dx=\pm Cdt \tag{3}$$

the + is for the waves coming from the upstream while the – is for the waves coming from the downstream. $J=(\lambda/D)Q|Q|/(2gA)$ is the linear head loss by unit of length of the pipe.

Equation (3) determines the evolution of the head pressure and the discharge according to the time and the space. They are much appropriated to be solved numerically on a microcomputer. The obtained numerical solution constitutes a solution to the original system of eqs. (1) and (2).

As an example in a single pipe system (L = 1600 m, D = 0.3048 m, C = 1200 m/s, H_0 = 50 m, Q_0 = 0.02 m^3/s, q_{L0} = 0.002 m^3/s, λ = 0, Figure 1), when the valve is suddenly closed, an abrupt increase in pressure occurs and a pressure wave propagates upstream along the pipe. Such a positive pressure wave is then reflected back by the leak provoking a partial reduction of incoming pressure wave. Then, the wave is reflected by the reservoir, bringing on a negative pressure wave.

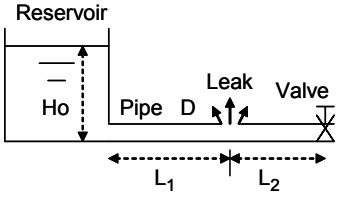

Figure 1. Time history of head for suddenly valve closure.

Analogously, discontinuities in the pipe flow conditions such as leaks, provoke partial reflection of incoming pressure wave (Figure 2). Hence, through correctly interpreting these head and leak discharge-time histories at the valve section, that is $h' = (H - H_0)/H_0$ and $q' = (q_L - q_{L0})/q_{L0}$, it is possible to extract information on leak location $l_r = L_2/(L_1 + L_2) = L_2/L$ [8]:

$$l_r = t_{f1} C / 2L = t_{f1} / T_C \tag{4}$$

where t_{f1} is the time difference between the initial transient wave and the reflected wave at the leak section.

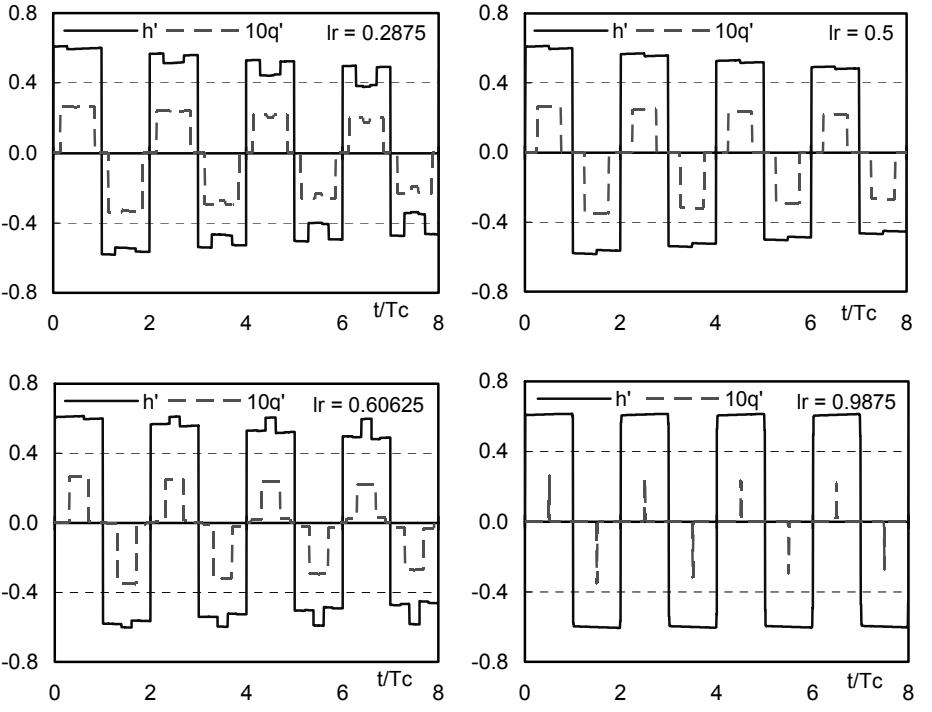

Figure 2. Time-histories of head and leak discharge for suddenly valve closure and different leak locations.

2.3. IMPEDANCE THEORY

2.3.1. *Hydraulic Impedance*

The instantaneous hydraulic grade line elevation H and the discharge Q are divided into two parts, the average magnitudes $\overline{H}$ and $\overline{Q}$ and the oscillatory terms h and q. Thus,

$H = \overline{H} + h$ and $Q = \overline{Q} + q$

In order to substitute these into eqs. (1) and (2) the following relations are needed [10]:

$$\frac{\partial H}{\partial x} = -\frac{\lambda \overline{Q}^2}{\left(2gDA^2\right)} + \frac{\partial h}{\partial x}, \quad \frac{\partial H}{\partial t} = \frac{\partial h}{\partial t}, \quad \frac{\partial Q}{\partial x} = \frac{\partial q}{\partial x}, \quad \frac{\partial Q}{\partial t} = \frac{\partial q}{\partial t}$$

and

$$\frac{\lambda Q^2}{\left(2gDA^2\right)} = \frac{\lambda \overline{Q}^2}{\left(2gDA^2\right)} + Rq, \tag{5}$$

where $R = \lambda \overline{Q} / \left(gDA^2\right)$.
By substituting eq. (5) into eqs. (1) and (2):

$$\frac{\partial h}{\partial x} + \frac{1}{gA}\frac{\partial q}{\partial t} + Rq = 0 \tag{6}$$

$$\frac{\partial q}{\partial x} + \frac{gA}{C^2}\frac{\partial h}{\partial t} = 0 \tag{7}$$

By taking the partial derivatives and combining eqs. (6) and (7), first to eliminate h, then to eliminate q, two equations identical in form are obtained.

$$\frac{\partial^2 q}{\partial x^2} = \frac{1}{C^2}\frac{\partial^2 q}{\partial t^2} + \frac{gA}{C^2}\frac{\partial q}{\partial t} \tag{8}$$

$$\frac{\partial^2 h}{\partial x^2} = \frac{1}{C^2}\frac{\partial^2 h}{\partial t^2} + \frac{gA}{C^2}\frac{\partial h}{\partial t} \tag{9}$$

One solves eqs. (8) and (9) by using the separation-of-variables technique which assumes that $h = \mathrm{H}(x)e^{i\omega t}$ and $q = \Theta(x)e^{i\omega t}$, where ω is the angular frequency.

After substituting and rearranging, eq. (9) yields:

$$\frac{1}{\mathrm{H}}\frac{d^2\mathrm{H}}{dx^2} = \gamma^2 = (\alpha + i\beta)^2 = \frac{Ag\omega}{C^2}\left(-\frac{\omega}{gA} + iR\right) \tag{10}$$

in which $\gamma = \alpha + i\beta$ is commonly referred to as the propagation constant.
The particular solutions for the oscillatory pressure head and discharge are:

$$h = e^{i\omega t}\left(C_1 e^{\gamma x} + C_2 e^{-\gamma x}\right)$$

$$q = \frac{\omega g A}{iC^2\gamma} e^{i\omega t}\left(C_1 e^{\gamma x} - C_2 e^{-\gamma x}\right)$$

where C_1 and C_2 are the integration constants.

The hydraulic impedance $Z(x)$ is defined as the ratio of the head fluctuation h to the discharge fluctuation q. Thus,

$$Z(x) = \frac{h}{q} = \frac{\mathrm{H}(x)}{\Theta(x)} = \frac{i\gamma C^2}{\omega g A}\frac{C_1 e^{\gamma x} + C_2 e^{-\gamma x}}{C_1 e^{\gamma x} - C_2 e^{-\gamma x}} = -Z_c \frac{C_1 e^{\gamma x} + C_2 e^{-\gamma x}}{C_1 e^{\gamma x} - C_2 e^{-\gamma x}} \qquad (11)$$

The characteristic impedance Z_c is defined by:

$$Z_c = \frac{\gamma C^2}{i\omega g A} = \frac{C^2}{\omega g A}(\beta - i\alpha)$$

Specific boundary conditions of the pipe must be introduced to evaluate the integration constants C_1 and C_2.

The boundary conditions at $x = 0$, are (Figure 3):

$$\mathrm{H}(0)e^{i\omega t} = H_R \text{ and } \Theta(0)e^{i\omega t} = Q_R$$

and the boundary conditions at $x = \mathrm{L}$, are:

$$\mathrm{H}(L)e^{i\omega t} = H_S \text{ and } \Theta(L)e^{i\omega t} = Q_S$$

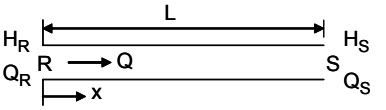

Figure 3. Simple pipeline.

where the subscript R stands for the receiving end of the pipeline and S refers to the sending end.

By introducing the hyperbolic functions, one expresses the impedance at one point in terms of conditions at another location, usually a terminal condition. At $x = 0$, $Z_R = H_R/Q_R$ and at $x = L$, $Z_S = H_S/Q_S$. For known conditions at the upstream or receiving end of the pipe,

$$Z(x) = \frac{\mathrm{H}(x)e^{i\omega t}}{\Theta(x)e^{i\omega t}} = \frac{Z_R - Z_c \mathrm{th}\gamma x}{1 - (Z_R/Z_c)\mathrm{th}\gamma x} \qquad (12)$$

For known conditions at the downstream or sending end of the pipe, let $x = L\text{-}x_1$; then

$$Z(x) = \frac{Z_S + Z_c \text{th}\gamma x_1}{1 + (Z_S / Z_c)\text{th}\gamma x_1} \tag{13}$$

Expressions relating impedance at the downstream end in terms of impedance at the upstream end, or vice versa, are particularly useful:

$$Z_S = \frac{Z_R - Z_c \text{th}\gamma L}{1 - (Z_R / Z_c)\text{th}\gamma L} \text{ or } Z_R = \frac{Z_S + Z_c \text{th}\gamma L}{1 + (Z_S / Z_c)\text{th}\gamma L} \tag{14}$$

Equation (14) represents the transfer functions of the pipe.

2.3.2. *Boundary Conditions*

In order to apply the impedance solution of the previous section to hydraulic systems, one must represent the boundary conditions as terminal impedances. Some of the cases common to hydraulic installations are presented.
Constant-head reservoir $H_R = 0$.

$$Z_R = H_R / Q_R = 0 \tag{15}$$

In these conditions, the hydraulic impedance at S in the system shown in Figure 1, when there is no leak, is:

$$Z_S = -Z_c \text{th}\gamma L \tag{16}$$

Dead end or closed end $Q_R = 0$.

$$Z_R = H_R / Q_R = \infty \tag{17}$$

Matched line

A pipeline terminated in its characteristic impedance Z_c is a matched line. No reflections are returned to the excitation point in this case. Thus,

$$Z_R = Z_c \tag{18}$$

Oscillating valve

An oscillating valve producing small pressure variations can be analyzed as a terminal condition. The orifice equation, relating total head and discharge, $Q = C_D A_G \sqrt{2gH}$, can be linearized if $h << \overline{H}$. Thus:

$$Z_R = \frac{2\overline{H}}{\overline{Q}} \frac{\tau_0 H(0)}{H(0)\tau_0 + 2\overline{H}e^{i\phi_A}} \text{ or } Z_R = \frac{2\overline{H}}{\overline{Q}} - \frac{2\overline{H}e^{i\phi_A}}{Q(0)\tau_0} \tag{19}$$

where $\tau_0 = C_D A_G / (C_D A_G)_0$ and ϕ_A is the phase angle of the valve motion with respect to the head fluctuation.

Fixed orifice

If the magnitude of the valve-opening oscillation is set to zero in eq. (19), the terminal impedance at a fixed orifice having an oscillatory flow superimposed upon a mean flow is seen to be:

$$Z_R = 2\overline{H}/\overline{Q}$$

This is a real number indicating no phase difference between head and discharge at the orifice.

The leak impedance is defined by the same relation as for the orifice that is:

$$Z_L = \frac{2\overline{H}_L}{\overline{Q}_L} \tag{20}$$

In the following, attention is focused on transients occurring in a single pipe system with a constant level reservoir upstream and a manoeuvre valve at the downstream end.

3. Detection of Leaks by Using the Impedance Method

3.1. THE RESPONSE OF FLOW VARIATION AT THE VALVE FOR A PIPE WITHOUT LEAK

The transfer function, or the impedance, for a single pipe system without a leak is given by eq. (16). The transfer function plays a crucial role in detecting water leaks in pipes. It can be used to evaluate the head time-history at the end section during transients. In fact, using the well known property of the Fourier transform and the time convolution theorem, the Fourier transform of the head variation, $\Delta h_S = h_S / \overline{H}_S$, can be obtained as the product of the Fourier transform of the discharge variation, $\Delta q_S = q_S / \overline{Q}_S$, and the transfer function Z_S.

$$\Delta\hat{h}_S(\omega) = Z_S \Delta\hat{q}_S(\omega) \tag{21}$$

where the $"\wedge"$ denotes the Fourier transform of the function.

As an example, in Figure 4a the numerical simulation of Δh_S for instantaneous closure maneuver is given, while in Figure 4b the Fourier transform of Δh_S is shown. In Figure 4c and d, the transfer function and the Fourier

transform of Δq_S are depicted, respectively. In the plots $t_r = t/T_C$, with $T_C = 2L/C$ being the pipe characteristic time, and $\omega_r = \omega 2T_C/2\pi$ is the normalized angular frequency. According to eq. (21), the product of the Figures 4c and d gives the Figure 4b. As pointed by Ferrante and Brunone [9], this finding is very important as it gives the cipher-key for understanding the dependence of the head spectrum on the maneuver and on the characteristics of the system. As a matter of fact; since leaks significantly change the characteristics of the system, differences will originate in head spectrum for systems with and without leaks. As a consequence, if the effect of the maneuver is separated, impedance method can be used as a diagnostic tool to detect the presence of a leak.

For fast linear closure maneuver of different durations $t_{m,r} = 0,0.1,0.2,0.5,1.0$ where $t_{m,r} = t_c/T_C$ and t_c is the time valve closure, Figure 5a shows the variation in time of the flow rate while Figure 5b shows the corresponding Fourier transform which are:

$$\Delta\hat{q}_S(\omega) = \frac{-\overline{Q}_S}{t_c\omega^2}\left(e^{-i\omega t_c} - 1\right) \quad if \quad tc \neq 0 \tag{22}$$

$$\Delta\hat{q}_S(\omega) = \frac{\overline{Q}_S i}{\omega} \; if \; tc = 0 \tag{23}$$

The absolute value of the Fourier transform of Δq_S, is

$$\left|\Delta\hat{q}_S(\omega_r)\right| = \frac{\overline{Q}_S T_C}{\pi\omega_r}\frac{\sqrt{2-2cos(\pi t_{m,r}\omega_r)}}{\pi t_{m,r}\omega_r} \; if \; t_{mr} \neq 0 \tag{24}$$

$$\left|\Delta\hat{q}_S(\omega_r)\right| = \frac{\overline{Q}_S T_C}{\pi\omega_r} \; if \; t_{mr} = 0 \tag{25}$$

Ferrante and Brunone [9] established that for fast maneuvers ($t_{m,r} < 1$) when $\omega_r < 2/t_{mr}$, $\left|\Delta\hat{q}_S(\omega_r)\right|$ is almost coincident with the one for an instantaneous maneuver. Basing on this result, in the range $0 < \omega_r < 2/t_{mr}$, he concluded that for fast linear maneuvers, the maneuver can be considered as instantaneous and its effects on the head spectrum at the end section are given by eq. (23).

However, as it can be seen in Figure 5, coincidence between instantaneous maneuver and fast linear maneuvers is obtained only for small value of ω_r. Hence, leak can only be detected by instantaneous closing maneuver.

The response function is a characteristic of the pipe system end does not depend on the maneuver. For an intact single pipe system, if friction effects can be neglected ($\lambda = 0$), the transfer function (16) becomes:

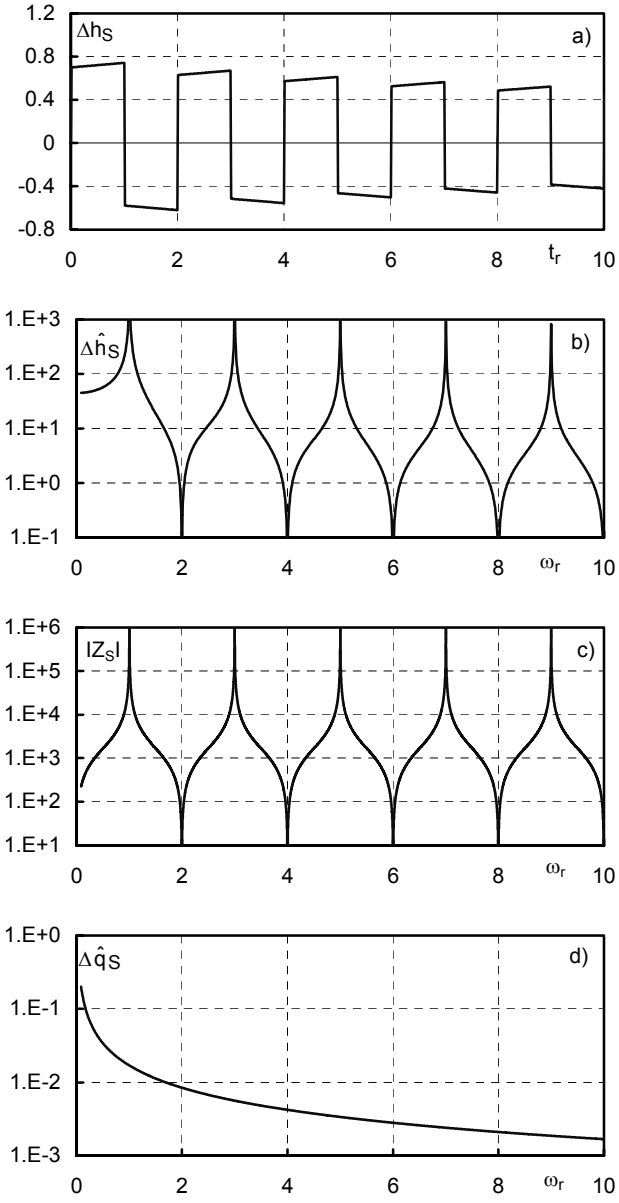

Figure 4. Time-history (a) and Fourier transform (b) of the head for an instantaneous closing maneuver in a single pipe system; the Fourier transform of the head can be obtained as the product of the end system impedance (c) and the Fourier transform of the discharge at the valve (d).

$$|Z_s| = Z_c tg\left(\frac{\omega L}{C}\right) = Z_c tg\left(\frac{\pi}{2}\omega_r\right) \tag{26}$$

$|Z_S|$ goes to infinity for odd values of ω_r, that is:

$$\omega_r = T\,\omega/2\pi = 2n-1 \quad n = 1,2,\cdots \tag{27}$$

which correspond to the resonance frequencies, and it is equal to zero for even values ω_r that is:

$$\omega_r = T\,\omega/2\pi = 2n \quad n = 1,2,\cdots \tag{28}$$

which correspond to the anti-resonance frequencies.

As an effect of considering friction the function $|Z_S(\omega_r)|$ has finite values for odd frequencies and values different from zero for even frequencies.

In Figure 6, function $|Z_S(\omega_r)|$ is plotted referring to the single pipe system of Figure 1 without leak. The differences in $|Z_S(\omega_r)|$ maxima and minima are evident.

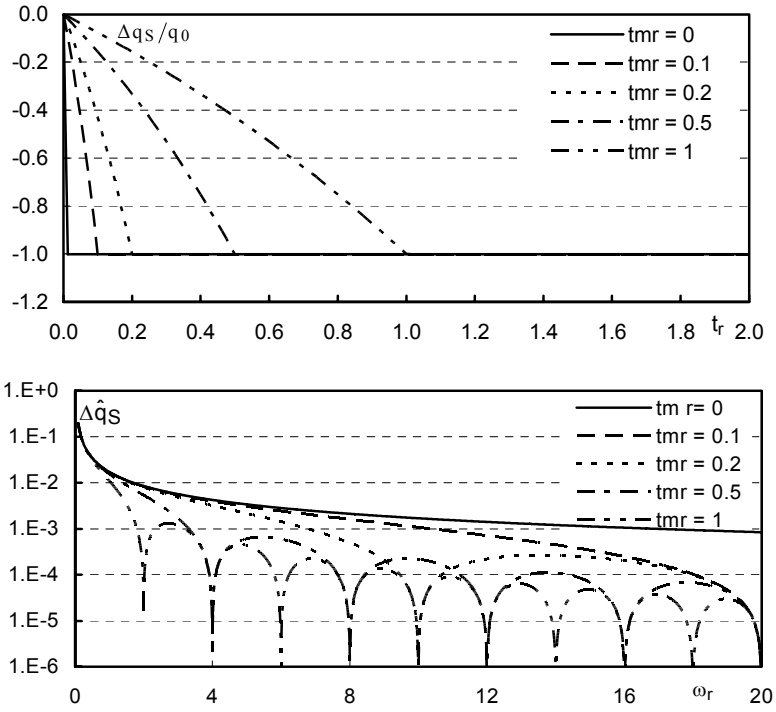

Figure 5. Time-history and Fourier transform of the discharge for closing maneuver of different duration, with a linear variation of the discharge.

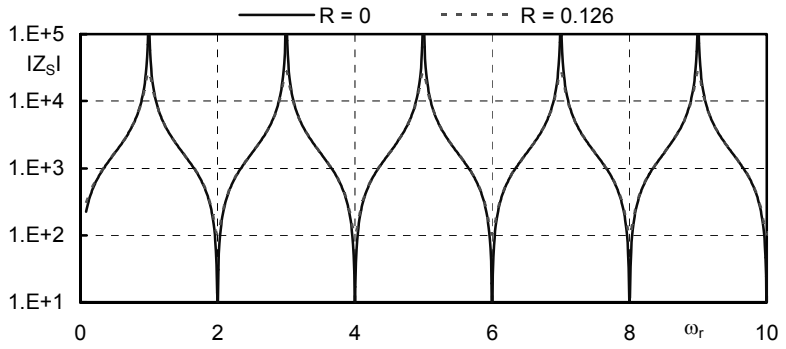

Figure 6. Analytic values of $\left|Z_S(\omega_r)\right|$.

3.2. THE RESPONSE OF FLOW VARIATION AT THE VALVE FOR A PIPE WITH A LEAK

The single pipe system with a leak at the distance L_2 from the valve, can be divided in two pipes (Figure 1), with leak is located at the junction. The impedances for the system may be written:

$$Z_{S1} = -Z_c \text{th}\gamma L_1\,,\; Z_L = \frac{2\bar{H}_L}{\bar{Q}_L}\,,\; Z_{R2} = \frac{Z_{S1}Z_L}{Z_L - Z_{S1}}\,,\; Z_{S2} = \frac{Z_{R2} - Z_c \text{th}\gamma L_2}{1 - \left(Z_{R2}/Z_c\right)\text{th}\gamma\, L_2}$$

By combining these relations, the impedance at the valve is

$$Z_{S2} = -\left(\frac{Z_L Z_c \text{th}\gamma L_1}{Z_L + Z_c \text{th}\gamma L_1} + Z_c \text{th}\gamma L_2\right) \Bigg/ \left(1 + \frac{Z_L \text{th}\gamma L_1}{Z_L + Z_c \text{th}\gamma L_1}\,\text{th}\gamma L_2\right) \tag{29}$$

Neglecting friction effects, that is $\gamma = \dfrac{i\omega}{C}$, the impedance at the valve becomes:

$$\left|Z_{S2}\right| = \left\{ Z_c \Bigg/ \left(\left[1 + tg^2\left(\pi\omega_r l_r/2\right)\right]^2 + \frac{Z_c^2}{Z_L^2}\left[tg\left(\pi\omega_r l_r/2\right) - tg\left(\pi\omega_r/2\right)\right]^2 \right) \right\} *$$

$$\left\{ \left[-\frac{Z_c}{Z_L}\left[1 + tg^2\left(\pi\omega_r l_r/2\right)\right]\left[tg\left(\pi\omega_r/2\right) - tg\left(\pi\omega_r l_r/2\right)\right]^2 \right]^2 + \right. \tag{30}$$

$$\left. \left[\frac{Z_c^2}{Z_L^2} tg\left(\pi\omega_r l_r/2\right)\left[tg\left(\pi\omega_r l_r/2\right) - tg\left(\pi\omega_r/2\right)\right]^2 + tg\left(\pi\omega_r/2\right)\left[1 + tg^2\left(\pi\omega_r l_r/2\right)\right]^2 \right]^2 \right\}^{1/2}$$

where $l_r = L_2/(L_1 + L_2)$ is the normalized distance of the leak from the valve.

From eq. (30), the terms depending on Z_L are equal to zero for frequencies ω_r^L defined by:

$$tg\left(\pi\omega_r^L l_r/2\right) - tg\left(\pi\omega_r^L/2\right) = 0$$

In this case eq. (30) becomes:

$$\left|Z_S\left(\omega_r^L\right)\right| = Z_c tg\left(\frac{\pi}{2}\omega_r^L\right) \tag{31}$$

and values of $|Z_S|$ for a single pipe system with and without a leak, as defined by eqs. (30) and (23), respectively, are equal. Moreover, as the value of Z_L changes in eq (30), the value of $\left|Z_S\left(\omega_r^L\right)\right|$ does not change, as expressed by eq. (31).

For $\omega_r = 2n-1$, the values of $|Z_S|$ are defined as

$$|Z_{S2}| = Z_c \left\{ \frac{\left[1 + tg^2\left(\pi\omega_r l_r/2\right)\right]^2}{Z_c^2/Z_L^2} + \left[tg\left(\pi\omega_r l_r/2\right)\right]^2 \right\}^{1/2} \tag{32}$$

Hence, although friction has been neglected, function $|Z_{S2}|$ does not approach infinity unless

$$\omega_r \frac{\pi}{2} l_r = (2n-1)\frac{\pi}{2} l_r = (2n'-1)\frac{\pi}{2} \quad (n, n' = 1, 2, \cdots \quad n > n') \tag{33}$$

and

$$l_r = \frac{(2n'-1)}{(2n-1)} \quad (n, n' = 1, 2, \cdots \quad n > n') \tag{34}$$

As an example, for $n = 2$, $|Z_{S2}|$ goes to infinity if the leak is located at $lr = 1/3$ (n' must be equal to 1).

Figure 7 shows the impedance diagram, or the transfer function, of a single pipe with leak at $L_2 = L/3$. The number series corresponding to the values of $|Z_{S2}|$ approaching infinity are:

$$\frac{(2*1-1)}{(2*2-1)}=\frac{1}{3},\ \frac{(2*2-1)}{(2*5-1)}=\frac{3}{9},\ \frac{(2*3-1)}{(2*8-1)}=\frac{5}{15},\ \frac{(2*4-1)}{(2*11-1)}=\frac{7}{21},\ \frac{(2*5-1)}{(2*14-1)}=\frac{9}{7}$$
$$\frac{(2*6-1)}{(2*17-1)}=\frac{11}{33}$$

For $\omega_r = 2n$, the values of $|Z_S|$ are defined as:

$$|Z_{S2}| = Z_c tg^2(\pi\omega_r l_r/2) \Bigg/ \left\{ \frac{\left[1+tg^2(\pi\omega_r l_r/2)\right]^2}{Z_c^2/Z_L^2} + tg^2(\pi\omega_r l_r/2) \right\}^{1/2} \tag{35}$$

and they differ from zero, unless

$$\omega_r \frac{\pi}{2} l_r = n\pi l_r = n'\pi \ \ (n,n' = 1,2,\cdots\ n > n') \tag{36}$$

and

$$l_r = \frac{n'}{n} \ \ (n,n' = 1,2,\cdots\ n > n') \tag{37}$$

As an example, for $n = 3$, $|Z_{S2}|$ goes to zero if the leak is located at $lr = 1/3$ when $n' = 1$. The number series corresponding to the values of $|Z_{S2}|$ approaching zero are:

$$\frac{2*1}{2*3}=\frac{1}{3},\ \frac{2*2}{2*6}=\frac{2}{6},\ \frac{2*3}{2*9}=\frac{3}{9},\ \frac{2*4}{2*12}=\frac{4}{12},\ \frac{2*5}{2*15}=\frac{5}{15}.$$

As it can be noted, the ratio is always $l_r = 1/3$ for the two series.

In Figure 8, $|Z_{S2}|$ is plotted for the same system of Figure 1 but with a leak ($Z_c/Z_L = 0.0343$) at different locations ($lr = 0.2875$ $lr = 0.5$ $lr = 0.60625$ $lr = 0.9875$) that is ($L_2 = 460m$ $L_2 = 800m$ $L_2 = 970m$ $L_2 = 1580m$). The values of the corresponding series are respectively:

lr = 1/5, 3/11, 21/73, 109/379, 151/525, 187/637, 225/783, 355/1235 = 0.287449

lr = 1/2, 5/9, 13/25, 21/41, 29/57, 37/73, 45/89, 53/105, 61/121, 69/137 = 0.503649

lr = 1, 3/5, 15/25, 25/41, 83/137, 191/315, 357/589, 465/767, 739/1,219 = 0.6062346

lr = 1, 151/153, 311/315, 629/637, 789/799, 949/961, 1,109/1,123, 1,251/1,267, 1,267/1,283 = 0.987529

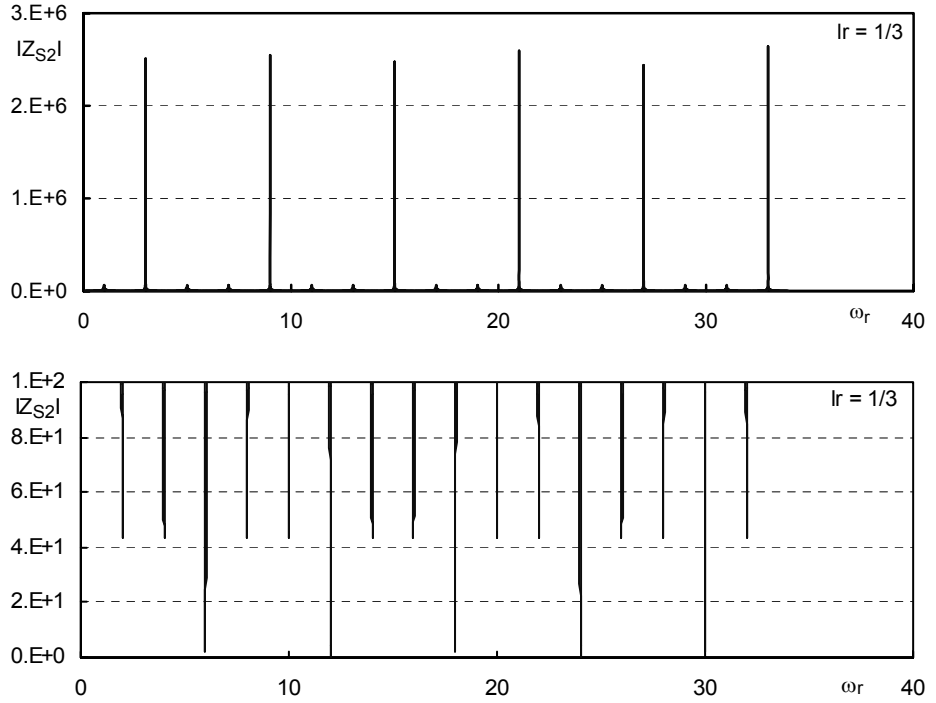

Figure 7. The transfer function for a leak location $lr = 1/3$.

One can demonstrate that for $\omega_r = (2n-1)/(l_r/2)$, function (30) becomes

And the comparison between this expression and the impedance of the system without a leak, eq. (26), allows evaluating the difference:

$$\frac{\Delta|Z_{S2}|}{Z_c tg(\omega_r \pi/2)} = \frac{1}{2}\frac{Z_c^2}{Z_L^2}\frac{1}{tg^2(\omega_r \pi/2)} - \frac{1}{8}\frac{Z_c^4}{Z_L^4}\frac{1}{tg^4(\omega_r \pi/2)} + \cdots \tag{38}$$

which depends on the term

In Figure 9, $|Z_{S2}|$ is plotted for the same system of the Figure 1 but with a leak $(Z_c/Z_L = 0.5)$ at different locations $(l_r = 0.25\ \ l_r = 0.5\ \ l_r = 0.75)$.

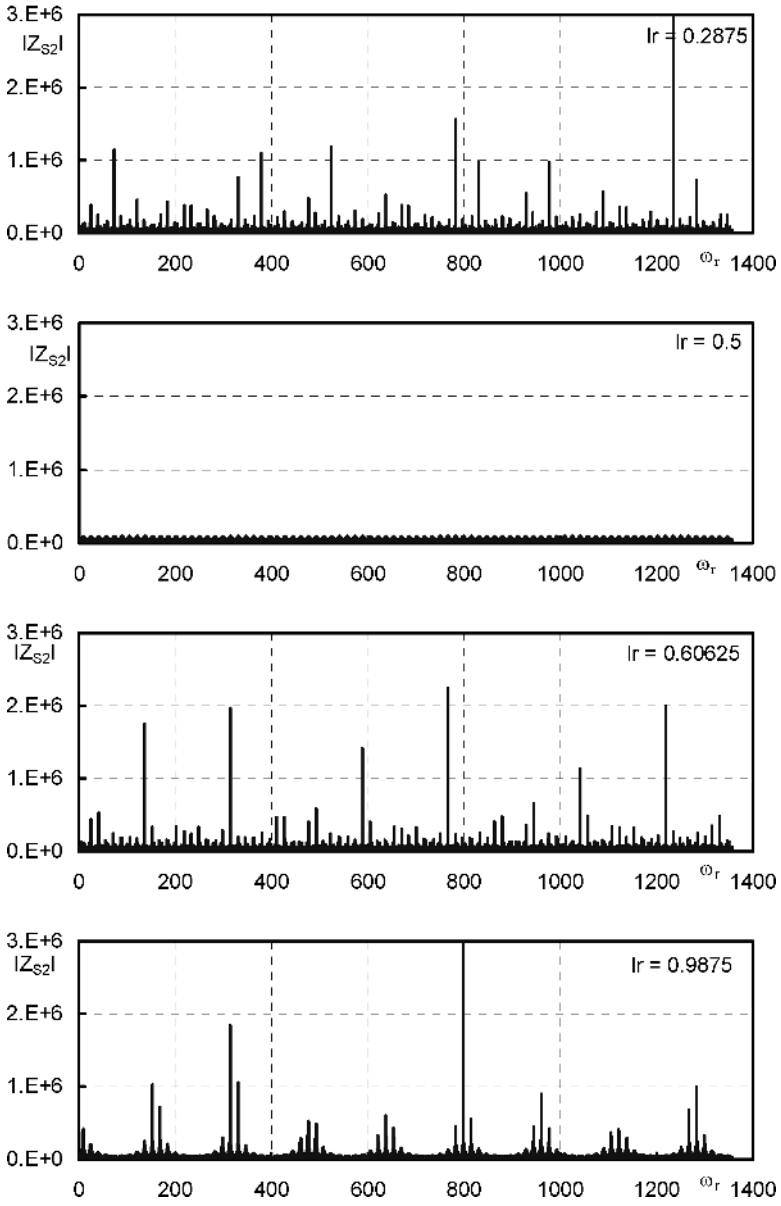

Figure 8. Impedance diagrams for different values of the normalized leak location *lr*.

$$\frac{Z_c^2}{Z_L^2}=\left(\frac{C}{gA}\frac{\overline{Q}_L}{2\overline{H}_L}\right)^2=\left(\frac{1}{2}\frac{\Delta H_{max}}{\overline{H}_L}\frac{\overline{Q}_L}{\overline{Q}_2}\right)^2$$

where $\overline{Q}_2$ is the steady state discharge at the valve and $\Delta H_{max}=C\overline{Q}_2/gA$ is the maximum frictionless overpressure that can be generated by the fast total valve closure. $\Delta|Z_{S2}|$ depends also on the leak location by the term $tg^{-2}(\omega_r\,\pi/2)=tg^{-2}\left[(2n-1)\frac{\pi}{2l_r}\right]$.

To obtain $\overline{Q}_L$, one can resolve eq. (38) for given values of ω_r, l_r and $\Delta|Z_{S2}|$.

Figure 10 shows the impedance diagrams for different values of q_L/Q_0 with a leak ($Z_c/Z_L=0.0343$).

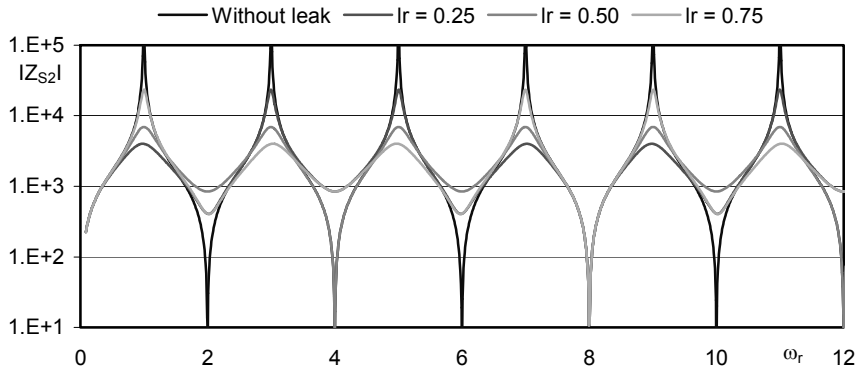

Figure 9. Impedance diagrams for different value of the normalized leak location *lr*.

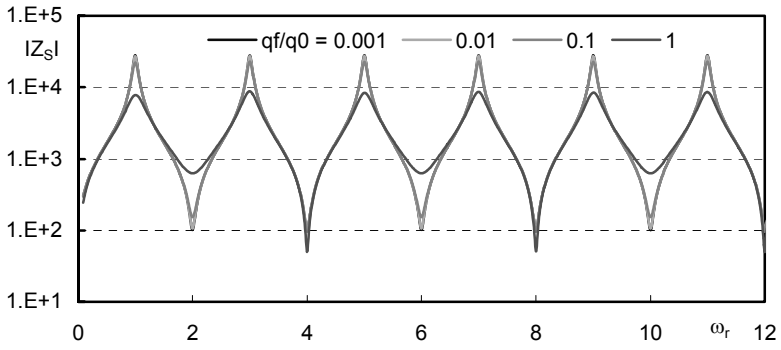

Figure 10. Impedance diagrams for different value of the normalized leak discharge.

4. Conclusion

The numerical solution of the leak detection in pipes has been presented in this paper. The study of the leak detection is necessary to avoid economic losses, ensure safety and control environmental and health problems. This problem is based on two coupled linear partial differential equations describing transient flows in pipes. The two numerical methods employed are the method of characteristics and the impedance method.

Of the two methods employed, the former seems to be the superior one. There is less computer cost involved with this method. The characteristics method allows detecting and locating the leak. Supplementary equations are however necessary in computing the leak magnitudes. Hence, this method can be directly used to determine the magnitude of leaks in pipe systems by developing relations between the location and the amplitude of the reflected wave at the leak section.

The impedance method is more practical and simulates correctly the leak location by analyzing the transfer function. In effect, the series of the ratio of normalized harmonics that give infinite or zero impedance value will converge to the leak location. The Newton-Raphson iterative method is used to determine the leak magnitude by resolving the difference between the transfer functions for systems with and without leak.

References

1. Gerhard G. (1999) Leak detection and locating – AZ Survey, PSIG 0301, Pipeline Simulation Interest Group.
2. Schmitt C., Pluvinage G., Hadj-Taïeb E., and Akid R. (2006) Water pipeline failure due to water hammer effects, *Fatigue and Fracture of Engineering Materials and Structures*, **29**, p. 1075 (December 2006), doi:10.1111/j.1460-2695.2006.01071.x, **29**(12).
3. Covas Q., Ramos H., and Almeida A. B. (2005) Standing wave difference method for leak detection in pipeline systems', *Journal of Hydraulic Engineering*, **131**(12), pp. 1106–1116.
4. Brunone B. and Ferrante M. (1999) On leak detection in single pipes using unsteady-state tests, in M. H. Hamza (Ed.): Modeling and simulation, IASTED ACTA PRESS, Anheim, California, pp. 268–272.
5. Chilekwa V., Sharp D. B., and Hill T. J. W. (2003) Leak detection in musical wind instruments using acoustic pulse reflectometry, Proceedings of the Stokholm Music Acoustics Conference, , Norway, 6–9 August , Stokholm, Sweden.
6. Ferrante M. and Brunone B. (2003) Pipe system diagnosis and leak detection by unsteady-state tests. 2 Wavelet analysis, *Advances in Water Resources*, **26**, pp. 107–116.
7. Mpesha W., Chaudry M. H., and Gassman S. L. (2000) Leak detection in pipes by frequency responce method using a step excitation, *Journal of Hydraulic Research*, **40**(1), pp. 55–62.

8. Al-Khomairi A. M. (2005) Use of the steady state orifice equation in the computation of transient flow through pipe leaks, *The Arabian Journal for science and Engineering*, **30**, 1B, pp. 33–45.
9. Ferrante M. and Brunone B. (2003) Pipe system diagnosis and leak detection by unsteady-state tests. 1 Harmonic analysis, *Advances in Water Resources*, **26**, pp. 93–105.
10. Wylie E. B., Streeter V. L., and Suo L. (1993) Fluid transients in systems, Prentice Hall, Englewood Cliffs, NJ.
11. Fox J. A. (1977) Hydraulic analysis of unsteady flow in pipe networks, The Macmillan, London.

CORROSION FATIGUE CRACKING AND FAILURE RISK ASSESSMENT OF PIPELINES

IHOR DMYTRAKH*
Karpenko Physico-Mechanical Institute of National Academy of Sciences of Ukraine, 5 Naukova Street, 79601, Lviv, Ukraine

Abstract: Problem of corrosion and corrosion fatigue damaging of feeding pipelines of heat-and-power generating units under long-term operating conditions is considered. The two main factors were taken into account: degradation of metals properties and purity of operating aqueous environment that causes by ecological pollution of natural water scoop. Corrosion fracture mechanics approach for assessment of workability and fracture risk of pipelines with crack-like defects is proposed, which is based on conception of threshold and critical cracks depth and also corrosion fatigue crack growth parameters.

Keywords: power-generating unit, feeding pipelines, exploited metal, operating environments, corrosion damaging, defects, corrosion fatigue crack, crack growth rate, threshold and critical crack depth, diagram of fracture risk assessment.

1. Introduction

Nowadays the pipelines, used for supplying water and oil or other liquids and gases, may be considered as important objects within the social and industrial infrastructure [1–3]. It has become increasingly paramount to ensure their safe utilisation in order to prevent economical, social and ecological losses.

From an engineering point of view, pipelines are complicated 3D structures that include straight pipes, pipe-bends, dissimilar welded joints, etc. In addition, their operating conditions can be quite severe, that is, internal pressure and cyclic loading (pulsation) combined with the influence of internal and external

* To whom correspondence should be addressed. Ihor Dmytrakh, Karpenko Physico-Mechanical Institute of National Academy of Sciences of Ukraine, Naukova 5, 79601, Lviv, Ukraine, e-mail: dmtr@ipm.lviv.ua

G. Pluvinage and M.H. Elwany (eds.), Safety, Reliability and Risks Associated with Water, Oil and Gas Pipelines, 99–113.

corrosive environments. The potential synergy of such parameters can lead to an increase in the risk of damage and unexpected fracture of these structures during their long-term exploitation [4–6].

Therefore the key challenge for this and similar engineering problems is the development of a reliability and fracture risk assessment tool based upon a scientific understanding of the failure mechanisms occurring in structures subject to corrosion and corrosion fatigue damaging.

This paper contains the data of corrosion and corrosion fatigue damaging of the feeding pipelines of heat-and-power generating units and also proposes some approaches to expert assessment of their workability and reliability in cases of crack-like defects presence.

2. Problem of Damaging of Feeding Pipelines of Heat-and-Power Generating Units Under Operating Conditions

In general, reliability and safety of heat-and-power engineering equipment is actual problem for Ukraine as well as other industrial countries, because for prevailing number of heat power plants the planned life of exploitation will be expired at nearest future. As typical example, the statistic data on exploitation history of two Ukrainian power plants is given in Table 1. Further extension of their work needs the detailed inspection and expert conclusions for all critical components of heat-and-power generating units and also revision of their operating regimes.

TABLE 1. Statistic data on the exploitation regimes of power plant units.[1]

Heat-and-power generating units	Time of exploitation in thousand hours	Number of start-and-stop	Number of loading cycles
Power plant V	120–150	170–350	850–1750
Power plant L	135–145	360–455	1800–2275

From this point of view, the feeding pipelines are critical structures, which have the length of several hundred metres for each heat-and-power generating unit and different dimension-types of tubes: external diameter exceeds 500 mm and maximal wall thickness is about 50 mm.

From modern engineering practice [7, 8] it has been shown that service life extension of such structures should be based on taking into account of two main factors:

- Degradation of metals properties and ageing pipelines components that causes by long-term exploitation
- Purity of operating aqueous environment that causes by ecological pollution of natural water scoop

The joint action of these factors leads to accelerated corrosion and corrosion fatigue under early stage of damage of pipelines components [9]. Under early stage of damaging the corrosion factor is dominated (Figure 1). This process can be classified as sequence: general corrosion of surface – initiating of localised corrosion – corrosion furrows and corrosion pits nucleation.

These corrosion defects serve as effective stress concentrators and during exploitation time, some number of corrosion defects is transformed into corrosion fatigue cracks (Figure 2). Depending on combination of corrosion/fatigue factors these cracks can be sharp or blunted by corrosion and also branched.[1]

Thus, exploited pipeline contains simultaneously the different types of defects and such structural element should be assessed from position of its workability and potential risk of failure.

For solution of this problem the corrosion fracture mechanics methods are applicable together with the special laboratory tests of metal from pipelines, which were exploited under assigned operating conditions.

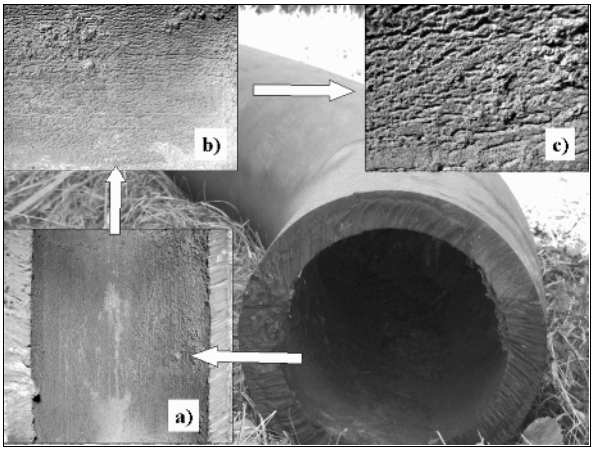

Figure 1. Corrosion damaging of feeding pipelines of heat-and-power-generating units under operating conditions: general corrosion of surface (a); initiating of localised corrosion (b); corrosion furrows and corrosion pits nucleation (c).

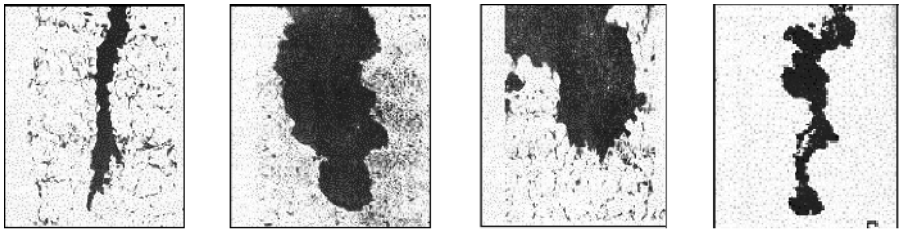

Figure 2. Typical corrosion fatigue defects in the wall of feeding pipelines: sharp crack (a); blunted cracks (b, c); cracks branching (d).

3. Fracture Mechanics Approach for Assessment of Workability and Fracture Risk of Pipelines With Crack-Like Defects

3.1. CRACK-LIKE DEFECTS MODELLING

The most characteristic types of corrosion and crack-like defects were considered, which detected by non-destructive methods and visual observation of exploited tubes: corrosion furrow, corrosion pit and corrosion fatigue crack [1, 10].

All types of defects were modelled by semi-elliptical cracks (see Figure 3) with different ratio of their half-axis a and c: $(c/a) = 0{,}01 - 0{,}8$.

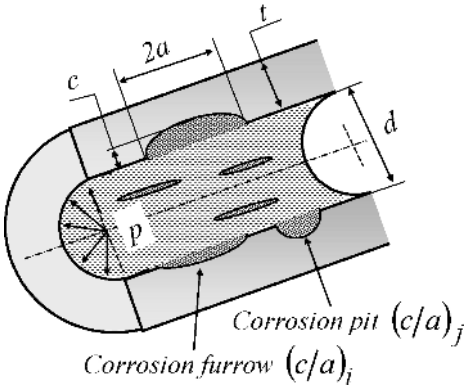

Figure 3. Model presentation of corrosion and corrosion fatigue defects in pipelines wall.

3.2. STRESS INTENSITY FACTOR FOR TUBE WITH SEMI-ELLIPTICAL CRACK UNDER INTERNAL PRESSURE

For calculation a stress intensity factor for longitudinal semi-elliptical crack in tube wall under internal pressure p (Figure 3), the following expression was used [1, 4]:

$$\Delta K_I = \Delta\sigma \cdot \sqrt{\pi c} \cdot \left\{ \frac{1}{\sqrt{\pi}} \cdot \frac{1.12 - 0.48\beta + 0.13\left(\frac{2\theta}{\pi}\right)^2 \cdot \beta(3\beta - 2 - \alpha)}{1 - \alpha(1 - 0.75\beta)} + \right.$$
$$\left. + \frac{1.13}{k_f}\left[\beta\left(\frac{2\theta}{\pi}\right)^2 \cdot (\alpha - 0.4 + 0.6\beta) + \beta(1 - 1.4\alpha) + 0.62\lambda(1 - \beta)\cdot\psi(\alpha) \right] \right\}; \qquad (1)$$

where $\Delta\sigma$ is a tensile stress range per loading cycle: $\Delta\sigma = (\Delta p \cdot d)/2t$; Δp is pulsation of a pressure p in pipeline; d is an internal diameter of tube; t is a thickness of tube wall; c is a depth of crack $\beta = c/a$ under $(0 \le \beta \le 1)$; a is a

crack half length; $\alpha = c/t$; θ is an angle from small axis of semi-elliptical crack; k_f is a coefficient, which takes into account the tube cross section form;

$$\lambda = \begin{cases} 1, \alpha \geq 1/20 \\ 1.15 - 60(\alpha)^2;\ 0 \leq \alpha \leq 1/20 \end{cases} \qquad \psi(\alpha) = (\alpha)^{-1/2} \cdot \sqrt{(1-\alpha)^{-3} - (1-\alpha)^3}$$

3.3. CORROSION FATIGUE CRACK GROWTH RESISTANCE

For corrosion fatigue crack growth behaviour it was assumed that propagating crack saves its semi-elliptical shape, but the ratio of half-axis (c/a) is a variable value:

$$c/a = f(C_m, N); \tag{2}$$

where C_m are the constants, which depend on "material- environment" system; N is number of loading cycles.

Here was also supposed that crack growth rate diagrams [4] fully define of resistance of defects to propagation in pipelines wall in direction of both axis c and a. They have been presented analytically using well known Paris equation:

$$dc/dN = da/dN = C(\Delta K)^n; \tag{3}$$

where C and n are the constants of "material- environment" system.

These diagrams are located between two characteristic values of stress intensity factor range ΔK_I, [4]: ΔK_{th} – threshold stress intensity factor range and ΔK_{fc} – cyclic fracture toughness. The parameter ΔK_{th} defines of limit load, below which the detected defects can be considered as non-propagated and cyclic fracture toughness ΔK_{fc} indicates the critical loading level, above which the detected defects are potentially able to catastrophic (spontaneous) growth.

The above-mentioned parameters were chosen as base for further development of expert assessment of workability and fracture risk of the feeding pipelines with crack-like defects. Here needed data were received with using the special experimental technique [4] and with taken into account both the real metal state of exploited pipelines and actual composition of operating aqueous environment.

3.4. THRESHOLD DEFECTS DEPTH c_{th} CRITERION

This criterion is based on relationship between the depths of semi-elliptical crack in tube wall and value of threshold stress intensity factor ΔK_{th} [4]. Here the

threshold defect depth c_{th} defines as the semi-elliptical crack depth of given shape (c/a), for which at point $\theta = 0$ stress intensity factor is equal of the threshold value: $K_I = K_{th}$.

Thus the criterion of the "safe" crack-like defects will be condition:

$$c \le c_{th}(\Delta K_{th}) \text{ under } (c/a) = const. \tag{4}$$

Therefore, all detected crack-like defects in the pipelines by depth $c \le c_{th}$ can be accepted as "safe", inasmuch as they do not have the potential ability to further development in wall depth.

3.5. CRITERION OF LIMITATION OF CORROSION FATIGUE CRACK GROWTH RATE

This criterion can be applicable for cases when the detected cracks in pipeline wall slightly exceed the threshold depth: $c > c_{th}$.

Here, the assessment of the admissible crack depths in pipeline walls may be realised on the base of limitation of corrosion fatigue crack growth rate [10,11], i.e.,:

$$dc/dN \le (dc/dN)_* . \tag{5}$$

where $(dc/dN)_*$ is the maximum crack growth rate that may be admitted in the wall of pipeline during planned service term between two inspection.

The admissible crack depth c_* in the given pipeline under assigned operating conditions, can be determined as

$$c_* = \Phi(c/a) \quad under \quad (dc/dN)_* = const. \tag{6}$$

For any considered cases the calculation (6) may be done with using eq. (3) for determining of the value $K_I = K_*$, which correspond $dc/dN = (dc/dN)_*$ and then on the basis eq. (1) the parameter c_* may be found as $c_* = F(K_*)$.

3.6. CRITICAL DEFECTS DEPTH c_{fc} CRITERION

In this case the assessment is realised according to well known criterion of brittle fracture mechanics:

$$\Delta K_I \le \Delta K_{fc} ; \tag{7}$$

where ΔK_{fc} is a cyclic fracture toughness.

On this ground, the critical defect depth c_{fc} defines as the semi-elliptical crack depth of given shape (c/a), for which at point $\theta = 0$ stress intensity factor

is equal of the critical value: $K_I = K_{fc}$ and the criterion of the "critical" crack-like defects will be condition:

$$c \le c_{fc}\left(\Delta K_{fc}\right) \text{ under } \left(c/a\right) = const. \tag{8}$$

Thus, all detected crack-like defects in the pipelines by depth about $c \approx c_{fc}$ can be considered as critically dangerous, because exist high probability to their spontaneous growth that will lead to catastrophic failure of pipeline.

3.7. DIAGRAM FOR ASSESSMENT OF WORKABILITY AND FRACTURE RISK OF PIPELINE WITH CRACK-LIKE DEFECTS

Grounding on considered above criteria, the diagram [12] for assessment of workability and fracture risk of pipeline of the given dimension-type with crack-like defects of different shape can be built (Figure 4).

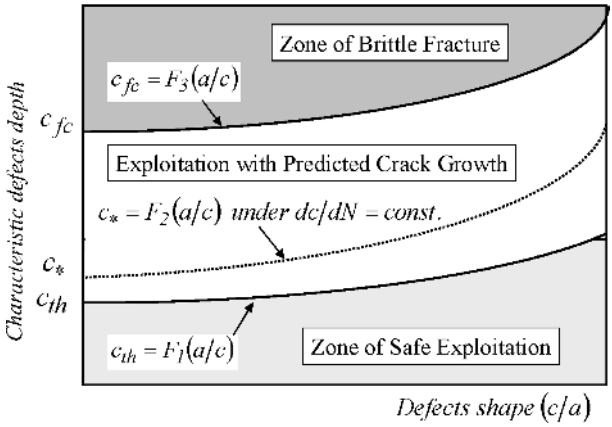

Figure 4. Schematic view of diagram for assessment of workability and fracture risk of pipeline with crack-like defects.

This diagram consists of three zones. The area below curve $c_{th} = F_1(c/a)$ determines the conditions of safe exploitation and area above curve $c_{fc} = F_3(c/a)$ indicates of brittle fracture zone. The area between curves $c_{th} = F_1(c/a)$ and $c_{fc} = F_3(c/a)$ is zone of subcritical crack-like defects growth. Here, for assigned operating conditions of pipeline, the appropriate limiting curve $c_* = F_2(c/a)$ may be built. Below this curve growth rate of all existed defects will not exceed the admitted maximum rate during planned operation term to next inspection of pipeline.

Thus, all detected defects by NDT methods under inspection can be compared with described above diagram and expert assessment of workability and fracture risk of the given pipeline can be done.

4. Determination of Corrosion Fatigue Crack Growth Resistance of Feeding Pipelines Metal

4.1. EXPERIMENTAL PROCEDURE

The power engineering steel 16HS ($\sigma_{YS} = 250MPa$ and $\sigma_{UTS} = 480MPa$) was investigated. Steel chemical composition (in weight%): C = 0.12–0.18; Si = 0.4–0.7; Mn = 0.9–1.2; Cr < 0.3; Ni < 0.3; Cu < 0.3; S < 0.04; P < 0.03; As < 0.08; remainder Fe.

The standard beam specimens by thickness of 10 mm and with V-shape notches were machined from metal of tubes. Three different materials were used: metal from new tube, metal from pipe-lines of power plant "V" and metal from pipe-lines of power plant "L".

Two types of the environments were used. First – an environment of nominal composition according to rules of power plants exploitation. It was the high purity water under $pH = 7 \pm 0.5$ and conductivity $\chi \le 3mS/m$. Second – the same environment but with organic additions: the formic acid (C = 3,000 μg/kg) and 2, 4-dinitrophenyl (C = 400 μg/kg). It should be noted that these additions were chosen on the base of the preliminary investigations. These electrochemical studies showed that formic acid and 2, 4-dinitrophenyl are the most corrosion aggressive additions with respect to pipes metal among others, which were detected in natural reservoir for the given power plants [1,7].

Corrosion fatigue crack growth tests were carried out under frequency of cyclic loading $f = 1.0Hz$ and stress ratio $R = 0.7$ that imitates the real pulsation of operating pressure in feeding pipelines of heat-and-power generating units. The tests were carried out with using the specially developed technique [4], where the constant environment composition in the crack tip area was provided by circulation of the environment through crack cavity.

4.2. CORROSION FATIGUE CRACK GROWTH RESISTANCE DIAGRAMS OF FEEDING PIPELINES METAL

The corresponding series of the corrosion fatigue crack growth tests were conducted both for different metals and environment composition. The received experimental data were initially presented as scatter plots of crack growth rate versus stress intensity factor range, from which the following basic parameters were determined: constants C and n in eq. (3); threshold intensity factor range ΔK_{th} and critical intensity factor range ΔK_{fc} (see Table 2). Corrosion fatigue crack growth diagrams for considered cases are given in Figure 5.

The main observation to be made from these results is the decrease of the corrosion fatigue crack growth resistance characteristics of exploited metal with

comparison to new that shows on degradation of materials properties under given operating conditions. Especially it can be seen for metal from power plant L, for which crack growth rate curve have the highest steep slope (see Figure 5, curves 3). It is inauspicious for providing of the pipelines workability, because any negligible operating overload may lead to significant increasing of corrosion fatigue crack growth rate [1,7].

TABLE 2. Corrosion fatigue crack growth resistance data for metal of feeding.

No.	System "material – environment"	n	C	$K_{th}, MPa\cdot\sqrt{m}$	$K_{fc}, MPa\cdot\sqrt{m}$
1	New metal – nominal environment	11.21	$8.71\cdot10^{-16}$	6.32	22.05
2	New metal – with organic admixtures	10.55	$3.02\cdot10^{-15}$	6.36	23.79
3	Exploited metal from Power plant L - nominal environment	32.87	$1.66\cdot10^{-33}$	6.83	9.94
4	Exploited metal from Power plant L - with organic admixtures	18.36	$4.36\cdot10^{-22}$	6.86	14.57
5	Exploited metal from Power plant V - nominal environment	14.07	$1.66\cdot10^{-18}$	6.89	18.35
6	Exploited metal from Power plant V - with organic admixtures	10.66	$3.24\cdot10^{-15}$	6.11	22.87

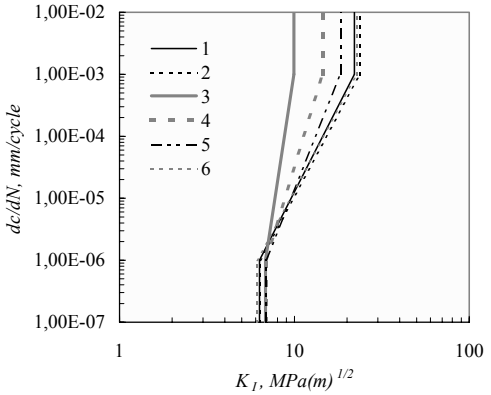

Figure 5. Corrosion fatigue crack growth diagrams for metal of feeding pipelines. Number of curve corresponds of the number of "material-environment" system given in Table 2.

These data were used for forecasting of workability and fracture risk of feeding pipelines of different dimension-types with crack-like defects.

5. Forecasting of Workability and Fracture Risk of Feeding Pipelines With Crack-Like Defects from Different Power Plants

5.1. TUBES SIZE AND OPERATING CONDITIONS

The four dimension-types of tubes are used for feeding pipelines of heat-and-power generating units (see Table 3). High purity water at maximal pressure $p_{max} = 35MPa$ serves as operating environment. The possible operating pulsation of pressure is $\Delta p = 10.5MPa$.

TABLE 3. Tubes size for feeding pipelines.

Nominal external diameter *D*, *mm*	Nominal thickness of wall *t*, *mm*	Material
526	50	Steel 16HS
467	45	
405	40	
165	16	

5.2. INFLUENCE OF EXPLOITATION TERM

Based on proposed fracture mechanics approach and corrosion fatigue crack growth resistance data, the diagrams of workability and fracture risk assessment for feeding pipelines with crack-like defects have been built both for different operating conditions and dimension-types of pipes.

The diagrams, which are shown in Figure 6, demonstrate the influence of exploitation term. It can be seen that degraded metal from power plant L possesses the very low corrosion fatigue crack growth resistance and as result the characteristic crack depths c_{th}, c_* and c_{fc} are lower than for new pipes. Besides that, a difference between curves $c_{th}(c/a)$ and $c_{fc}(c/a)$ is significantly smaller for exploited pipes than new one.

These facts show on the low reliability of exploited pipes where even relatively small defects have potential ability to propagation and difference between threshold and critical crack depth is only few millimetres.

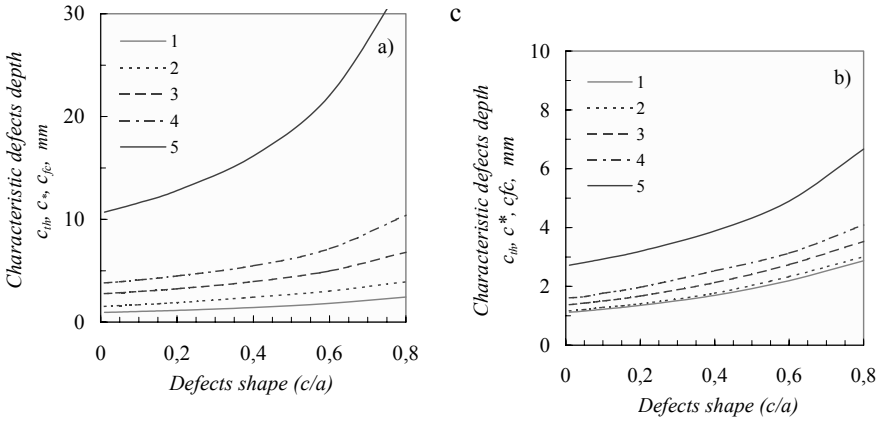

Figure 6. {*SEQ Figure* ARABIC*}. Diagrams of workability and fracture risk assessment for new (a) and exploited on Power plant L: (b) pipes with crack-like defects for nominal environment: 1 – c_{th}; 2 – $c_*\left(dc/dN = 10^{-5}\ mm/cycle\right)$; 3 – $c_*\left(dc/dN = 10^{-4}\ mm/cycle\right)$; 4 – $c_*\left(dc/dN = 10^{-3}\ mm/cycle\right)$; 5 – c_{fc} (pipes size: D = 526 mm; t = 50 mm).

5.3. INFLUENCE OF LOCATION OF DEFECTS AND THEIR SHAPE

From engineering practice it is know that pipelines bends are subjected more intensive damaging than straight parts from the reason of higher stress level. This factor takes into account by coefficient k_f in eq. (1) for stress intensity factor of semi-elliptical crack in pipe wall. It is accepted that k_f changing range is $0.8 \le k_f \le 1$, where $k_f = 0.8$ for elbow bend and $k_f = 1$ for straight pipe.

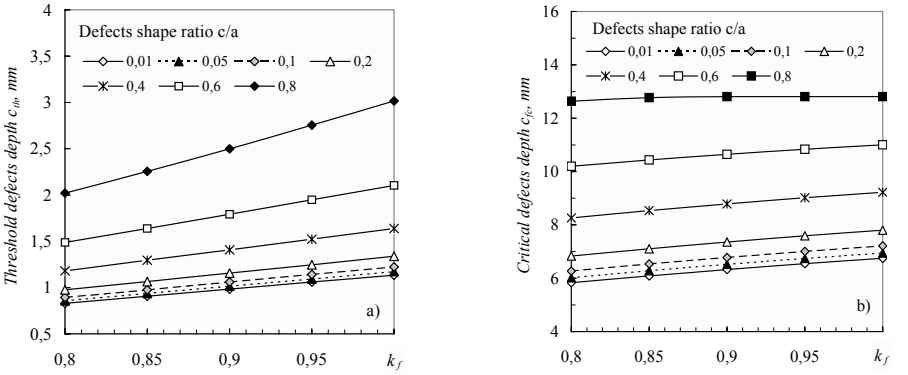

Figure 7. Influence of cross section form of pipe (k_f) on threshold c_{th} (a) and critical c_{fc} (b) defects depth of different shapes (new pipes: D = 165 mm; t = 16 mm; nominal environment).

The diagrams in Figure 7 reflect the influence of location of different defects (c/a) on their threshold c_{th} and critical c_{fc} depth. For all crack shapes the parameter c_{th} is more sensitive to the k_f changing with comparison of the c_{fc}. Although, the variables rate dc/dk_f of these parameters versus crack shape are principally different (Figure 8).

Thus, for realistic assessment of the existed defects in pipelines, it is mandatory to know their actual location and shape.

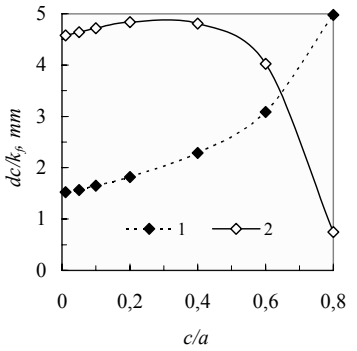

Figure 8. Variables rate dc/dk_f of threshold c_{th} (1) and critical c_{fc} (2) defects depth versus crack shape (c/a) for new pipes by size: D = 165 mm: t = 16 mm (nominal environment).

5.4. INFLUENCE OF ENVIRONMENTAL COMPOSITION AND PIPES SIZE

The factor of operating environment is important for the given considerations, because it defines the corrosion fatigue crack growth behaviour in pipelines wall.

This statement is confirmed by results, which are shown in Figures 9 and 10. The presence of organic admixtures in operating environment increases the risk of failure, because in this case the threshold defects depths c_{th} are decreasing (Figure 9). Although, at the same time, these admixtures can positive affected (in some degree) on the critical defects depth c_{fc} (Figure 10). Last circumstance may be explained by the specificity of material/environmental interaction at high level of stress intensity factors [4].

Finally it should be noted that actual size of threshold and critical defects depths are depending on the given pipe size, that is clear from the analysis of the structure of relations (eqs. 1, 4 and 8).

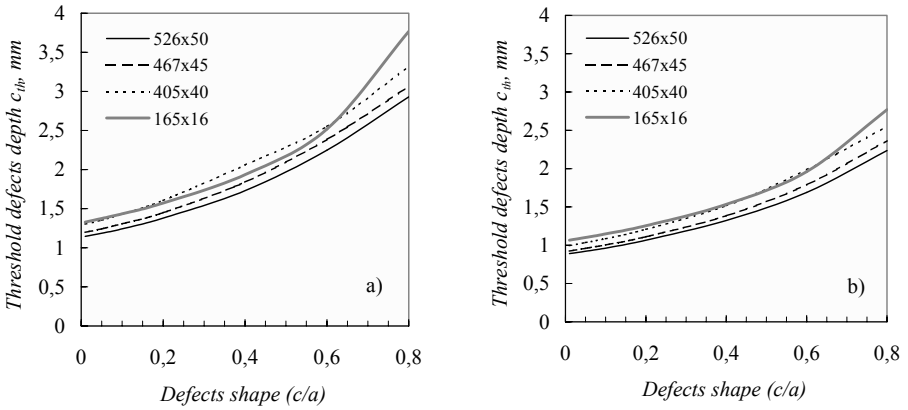

Figure 9. Threshold defects depth c_{th} versus defects shape c/a for different size of pipes from power plant V: a – operating environment of nominal composition, b – with organic admixtures.

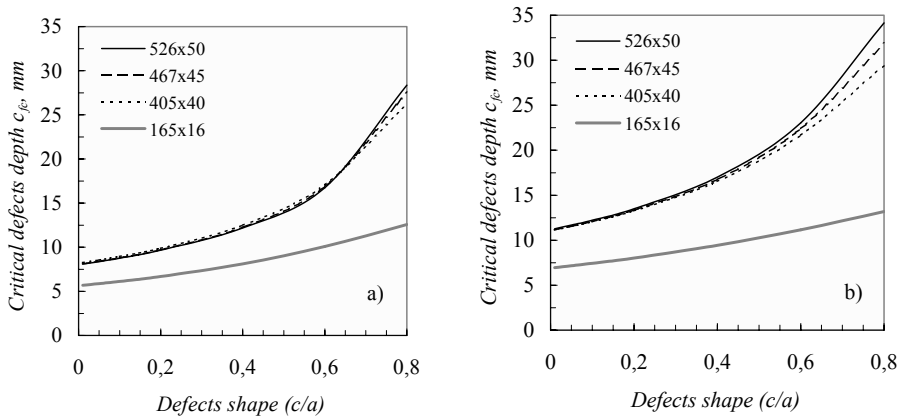

Figure 10. Critical defects depth c_{fc} versus defects shape for different size of pipes from power plant V: a – operating environment of nominal composition, b – with organic admixtures.

6. Conclusions

Problem of corrosion and corrosion fatigue damaging of feeding pipelines of heat-and-power generating units under long-term operating conditions was considered with taken into account of metal degradation and real composition purity of operating aqueous environment.

Corrosion fracture mechanics approach for assessment of workability and fracture risk of pipelines with crack-like defects is proposed, which is based on conception of threshold and critical cracks depth and also corrosion fatigue crack growth parameters.

For assessment of the detected defects in pipelines, the special diagrams are developed, which contain three zones: safe exploitation, brittle fracture risk and zone of exploitation with predicted growth of existed defects. Here, the importance of factors of exploitation term, location and shape of defects and composition of operating environment has been shown.

Acknowledgements

This study has been conducted within the project 2.6/284 “Development of advanced methods for technical diagnostics of workability of water-steam circuit systems of heat power plant units” of the Targeted Research and Engineering Programme “RESURS” of National Academy of Sciences of Ukraine.

References

1. I. M. Dmytrakh, A. B. Vainman, M. H. Stashchuk and L. Toth, *Reliability and durability of structural elements for heat-and-power engineering equipment*. Reference manual/Eds. I. M. Dmytrakh (Publishing House of National Academy of Sciences of Ukraine “Academperiodyka”, Kiev, 2005) (in Ukrainian).
2. I. M. Dmytrakh and V. V. Panasyuk, Problems of lifetime assessment of water-steam circuit elements of power units, Bay Zoltan Institute for Logistics and Production Systems Miskolc, Hungary (11–12 April 2006); http:part.bzlogi.hu.
3. I. M. Dmytrakh and V. V. Panasyuk, in: *Mechanical Fatigue of Metals*, Edited by V. T. Troshchenko (Ternopil State Technical University, Ukraine, 2006), pp. 23–28.
4. I. M. Dmytrakh and V.V. Panasyuk, *An influence of the corrosive environments on local fracture of the metals near the stress concentrators* (National Academy of Sciences of Ukraine Karpenko Physico-Mechanical Institute, Lviv, 1999) (in Ukrainian).
5. I. M. Dmytrakh, R. Akid, and K. J. Miller, Electrochemistry of deformed smooth surfaces and short corrosion fatigue crack growth behaviour. *British Corrosion Journal*, **32**(2), pp. 138–144 (1997).
6. R. Akid, I. M. Dmytrakh, and J. Gonzalez-Sanchez, Fatigue damage accumulation: the role of corrosion on the early stages of crack growth. *Corrosion Engineering, Science and Technology*, **41**(4), pp. 328–335 (2006).
7. I. M. Dmytrakh, A. B. Vainman, and R. I. Vovk, in: *Fracture from Defects*, Edited by M. W. Brown, E. R. de los Rios, and K. J. Miller (EMAS Publishing, UK, 1998), pp. 1145–1150.
8. I. M. Dmytrakh, in: *Notch Effects in Fatigue and Fracture – NATO Science Series: II. Mathematics, Physics and Chemistry*, Edited by G. Pluvinage and M. Gjonaj (Kluwer , Dordrecht/Boston/London, 2001), pp. 331–346.
9. I. Dmytrakh, A. Syrotyuk, and R. Leshchak, Assessment of surface corrosion fatigue damaging of pipeline steels. *Physicochemical Mechanics of Materials*, Special Issue No. 4, pp. 67–72 (2004) (in Ukrainian).

10. I. M. Dmytrakh, A. M. Syrotyuk, and R. S. Hrabovskyi, On admissible depth assessment of crack-like defects in pipelines of power-generating units. *Physicochemical Mechanics of Materials*, **37**(5), pp. 69–74 (2001) (in Ukrainian).
11. I. M. Dmytrakh and A. M. Syrotyuk, in: *Fracture Mechanics of Materials and Structural Integrity*, Edited by V. V. Panasyuk (Karpenko Physico-Mechanical Institute of the NASU, Lviv, 2004), pp. 465–470 (in Ukrainian).
12. I. M. Dmytrakh, A. M. Syrotyuk, B. P. Rusyn, and Yu. V. Lysak, in: *Problems of Service Life and Safe Exploitation of Structures, Facilities and Machines*, Edited by B. Ye. Paton (National Academy of Sciences of Ukraine, Kyiv, 2006), pp. 221–225 (in Ukrainian).

INITIATION OF STRESS CORROSION CRACKING AND HYDROGEN-INDUCED CRACKING IN OIL AND GAS LINE-PIPE STEELS

MAHMOUD T. SHEHATA, MIMOUN ELBOUJDAINI
AND R. WINSTON REVIE
CANMET Materials Technology Laboratory
Natural Resources Canada, 568 Booth St.
Ottawa, Ontario, Canada K1A OG1
mshehata@nrcan.gc.ca

Abstract: Environmentally assisted cracks in line-pipe steels are initiated either as a result of stresses in combination with environmental effects, as in stress corrosion cracking (SCC), or as a result of trapped hydrogen in the steel, as in hydrogen-induced cracking (HIC). To understand better the mechanism of the crack initiation process, key metallurgical and environmental elements that can affect the cracking phenomena were investigated and are reviewed in this paper. The complexity of both cracking phenomena results from the dependence of SCC and HIC on multiple metallurgical, mechanical, and environmental parameters that may all influence both crack initiation and propagation; e.g., composition, microstructure, and nonmetallic inclusions in the steel, applied stress, water chemistry in the field, and ionic concentrations in the groundwater near the pipe surface to name a few for SCC. In addition, for HIC phenomena, one can add the concentration of hydrogen sulfide (H_2S) in the fluids transported in the pipe as well as concentration of CO_2, pH, etc. In this paper, cracking of line-pipe steels is analyzed critically, with particular attention to the crack initiation process. The paper is divided into two parts: The first part covers SCC and the second covers HIC.

Keywords: stress corrosion cracking, hydrogen-induced cracking, environmentally assisted cracking, oil and gas line-pipe steels

G. Pluvinage and M.H. Elwany (eds.), Safety, Reliability and Risks Associated with Water, Oil and Gas Pipelines, 115–129.

1. Stress Corrosion Cracking (SCC) Phenomena

1.1. CANADIAN NATIONAL ENERGY BOARD INQUIRY

SCC is a form of environmentally assisted cracking (EAC) that is of great significance to Canadian oil and gas pipelines. In these pipelines when ground water penetrates under the pipe coating, cracks may develop and grow through the pipe wall. Over the past decades, thousands of colonies of such cracks have been found in pipelines in Canada (see Figure 1). These cracks frequently go dormant at depths of about 1 mm. Occasionally, for reasons as yet not understood, the cracks continue to propagate and this can lead to pipe rupture. This phenomenon led to several serious ruptures within the Canadian pipeline system between 1985 and 1995 and the phenomenon was the subject of two National Energy Board (NEB) inquiries in the 1990s.[1]

Figure 1. Small "SCC" cracks, that are widespread in tape-coated pipeline.

1.2. SCC MECHANISM

SCC has been observed on the soil side of buried, natural gas pipelines since the early 1960s. Transgranular SCC has caused service as well as hydrotest failures, and cracks have been found associated with gouges and dents. Transgranular cracking occurs in environments with pH about 6.5, and is referred to as near-neutral pH cracking, as opposed to high pH cracking, which is intergranular in nature.

The SCC results from multiple metallurgical, mechanical, and environmental factors. Chemical composition of the steel, residual stress in the steel as well as applied stress, water chemistry in the field, including CO_2, oxygen, and

ionic concentrations in the groundwater near the pipe surface, may all have an effect on crack initiation and propagation [2–6].

SCC in pipelines involves several steps:

1. The coating applied to the pipeline during installation becomes degraded, an electrolyte comes into contact with the surface, and the environment that causes SCC to develop
2. The initiation and growth of multiple cracks that form colonies
3. These cracks may continue to grow and coalesce
4. In the final step, a dominant crack reaches a critical size for rapid growth to failure, producing either a leak or a rupture

The time to failure depends on a number of factors, including the pipe material, stress history, environment, and crack distribution. Nevertheless, most colonies do not result in failure as the cracks become dormant.

Nearly all studies of SCC have been carried out without distinguishing the characteristics of initiation from those of propagation. Many of the studies on propagation have focused on growth of long cracks in precracked specimens. Initiation of SCC is, however, studied using specimens that are not precracked. The definition of an initiated crack is not well defined, and there is no clear mechanistic interpretation of the events that lead to initiation.

SCC has been observed to initiate from the base of localized corrosion sites (i.e., pits, crevices) for a variety of metal–environment combinations [7–10]. There remains debate on whether the stress intensification at the base of the pit or the enhanced electrochemical conditions within the pit is the controlling factor in SCC [11–14]. Several investigators believe it is the localized environment that plays the biggest role in crack initiation and not necessarily the stress concentration provided by the localized corrosion site [15–16], whereas others believe that crack initiation in smooth samples requires the presence of a stress raiser [17]. The most common way to establish such a stress raiser is either through corrosion or mechanical damage.

1.3. COMPLEXITIES IN SCC PHENOMENA

SCC in steels for oil and gas pipelines is a very complex and challenging phenomenon. The complexity of SCC is reflected in the changes, with time, of the diverse parameters influencing the cracking phenomena, whereas the biggest challenge is in obtaining field-relevant reproducible laboratory data. SCC encompasses major effects from metallurgical, mechanical, and environmental parameters, all of which can be dominant under specific conditions. Adding to

the complexity are the loading conditions in operating pipelines that define the mode of failure as SCC or corrosion fatigue (CF). While SCC and CF are sometimes regarded as different modes of failure, the distinctions between them in mechanistic or engineering terms are becoming less sharply defined. Thus, to consider SCC and CF as involving static and cyclic loads, respectively, appears increasingly arbitrary, since in many cases SCC is found in operating pipelines where the loads are not static.

1.4. INITIATION OF SCC

There are generally three stages for the cracking process: (i) generation of an environment that causes cracks to initiate; (ii) Initiation of cracks; and (iii) propagation of cracks until failure occurs. The present study is focused on crack initiation, types of cracks, crack behavior, role of crack initiation sites, inclusions, factors governing crack growth, and the crack coalescence process in the context of low-pH SCC in line-pipe steel. For the current research, the validation of the results under accelerated test conditions is based on the assumption that the microprocesses, microstructural features, and specific sites associated with initiation of cracks in laboratory tests are those associated with the initiation of SCC in operating pipelines. In this context, the following aspects were studied for SCC initiation:

1. The sites where cracks are initiated in relation to metallurgical factors, such as nonmetallic inclusions (see Figure 2), grain boundaries, specific phases, or other forms of surface discontinuity or surface defect
2. The role of applied mechanical loading conditions, including: the effects of stress level (for static and cyclic loading), strain rate (for dynamic loading), stress ratio, R, and loading frequency, f
3. The time dependence of crack development, including: (i) existence of an incubation time, (ii) changes in crack number density, crack size with time, dormancy, and (iii) the crack growth rate. The cracks are found to become dormant and hence are innocuous. Significantly, they are always found near the site of ruptures (see Figure 3), so it is felt that these cracks are sometimes precursors to rupture [18]
4. The spatial distribution of cracks. Spacing affects crack interaction and coalescence and significantly influence the overall cracking behavior and hence, the lifetime of a pipeline. The linking or coalescence process for neighboring growing cracks (see Figure 4) that was proposed [19, 20] as a means to encourage growth, but which was shown by measurements to be more likely associated with crack tip dormancy [21].

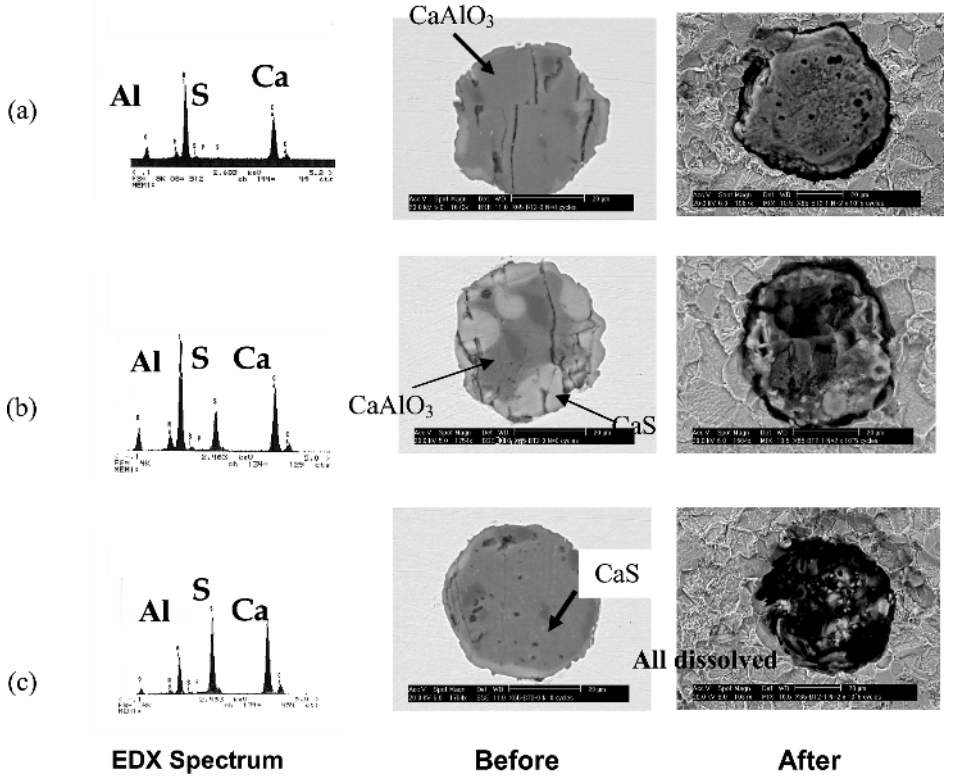

Figure 2. EDS spectra indicating chemical composition of three different inclusions as associated with the initiation of pits in X-65 steel sample (before and after test at smax = 90%YS, R = 0.6 and, f = 0.1Hz in NS-4 solution saturated with N2/5% CO_2). Note the rapid dissolution of CaS inclusions and the formation of corrosion pits around the inclusions.

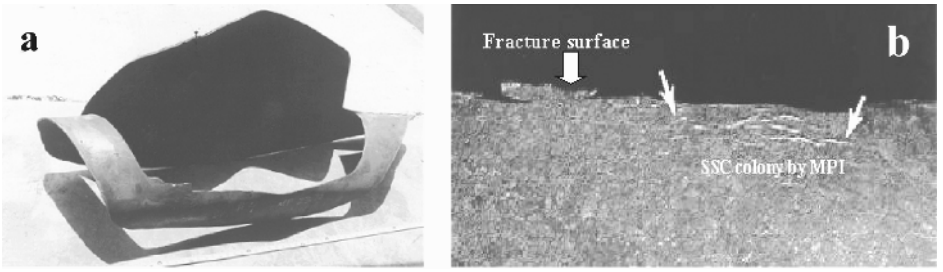

Figure 3. (a) Failure in hydrostatic testing, SCC as root cause; (b) Magnetic Particle Inspection (MPI) picture of SCC colony found next to a pressure failure. The outside pipe surface shows additional, longitudinal cracks adjacent to the fracture origin.

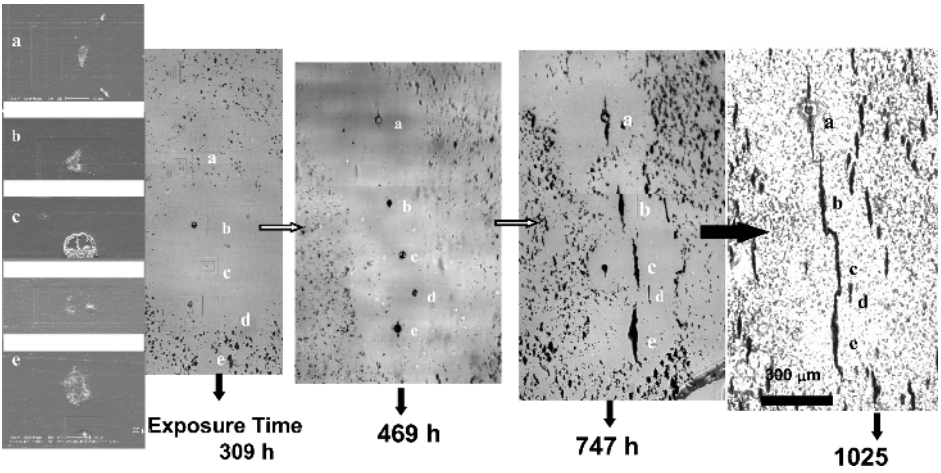

Figure 4. Development of five cracks a, b, c, d, and e after total exposure time show, in a X65 specimen at Smax = 70% YS, R = 0.6, and f = 0.1 Hz in NS4 solution saturated with CO_2, showing the correlation of crack initiation at pits from nonmetallic inclusions and the interaction and coalescence of cracks (observations were made on replicas) Ref. 7.

1.5. IMPLICATIONS ON THE OPERATION OF PIPELINE

There are several implications of the above factors on the operation of a pipeline. The cause of stresses that are exerted on the pipe during its operation must be considered. For example, the operating pressures in the pipeline and more importantly the pressure variation during operation. Other implications are concerned with the type of soil surrounding the pipe and expectations of soil movements and permafrost that could exert pressure and external stresses on the pipe. The type of soil and how it could affect the acidity around the pipe is also important. Metallurgical factors relate to nonmetallic inclusions in the steel from which the pipe is made and what steel making practices were used in its production. Other metallurgical factors relates to the various welds in the pipe and what kind of problems that could be expected from welds. It is hoped that this work provided some valuable insights on the initiation process of SCC and some understanding of the competing processes in the development of SCC in steels for oil and gas pipelines.

2. Hydrogen-Induced Cracking (HIC) Phenomena

2.1. HIC MECHANISM

HIC of pipeline steels and oil country tubular goods (OCTG) is a very important problem in sour oil and sour gas environments. Cracks were caused by hydrogen embrittlement of metal during corrosion reaction in environments containing H_2S. Such factors as metal microstructure, type of heat treatment, grain size, type, and shape of nonmetallic inclusions (oxides, sulfide, etc.) and alloying additions exert a great effect on HIC susceptibility [22, 23].

Some common features of HIC are now known: HIC occurs when hydrogen concentration (C_o) in the steel matrix exceeds the threshold hydrogen concentration (C_{th}). The C_{th} might be considered as a parameter unique to a given material [24]. With increased material strength, C_{th} tends to decrease, and threshold stress-intensity factor becomes dependent on C_o irrespective of material. Hydrogen content in the steel is known to be dependent on alloy composition, H_2S partial pressure, and pH, whereas C_{th} depends on inclusions and segregation in the matrix [25, 26, 27]. The atomic hydrogen formed at the reacting surface can diffuse into the steel where it may cause embrittlement and/or accumulate at the inclusion/matrix interface, building up pressure that leads to cracking. Two typical types of HIC cracks are shown in Figures 5 and 6: blister cracks and centerline cracks. Blister cracks are those hydrogen-induced cracks that are formed near the surface so that the hydrogen pressure is able to lift the material and form blisters that are observable on the surface (Figure 5). The formation of blister cracks is directly related to the type and distribution of nonmetallic inclusions in the steel [28].

H_2S is known to poison the hydrogen recombination reaction, thereby increasing hydrogen diffusion into and its absorption in steel. As a consequence, H_2S accelerates HIC in carbon steel and low-alloy steel in sour environments.

The most probable mechanism of the accelerating effect of H_2S involves the formation of a molecular surface complex (Fe H-S-H)$_{ads}$, which on cathodic polarization leads to formation of hydrogen atoms. Some of the hydrogen atoms may recombine while others diffuse into the metal.

$$\begin{aligned} Fe + HS^- &\rightarrow Fe\,(HS^-)_{ads} \\ Fe(HS^-)_{ads} + H_3O^+ &\rightarrow Fe\,(H\text{-}S\text{-}H)_{ads} + H_2O \\ Fe\,(H\text{-}S\text{-}H)_{ads} + e^- &\rightarrow Fe(HS^-)_{ads} + H_{ads} \end{aligned}$$

2.2. THRESHOLD HYDROGEN CONCENTRATION, C_{TH}

The use of C_{th} of a steel as a measure of its resistance to HIC would be a rational alternative to that used in the present NACE standard test [28]. There would be less difficulty in ranking steels in their susceptibility to HIC; also, the C_{th} value of steel can be related directly to the performance of that line-pipe steel containing a corrosive sour environment. In such pipe, permeation methods can be used in the field to determine the maximum concentration of dissolved hydrogen in the wall C_0; HIC should only occur when $C_0 > C_{th}$.

Data on C_{th} and pH_{th} values for line-pipe steels in Table 1, are summarized in Table 2. Also reported in Table 2 is the occurrence of cracking as indicated

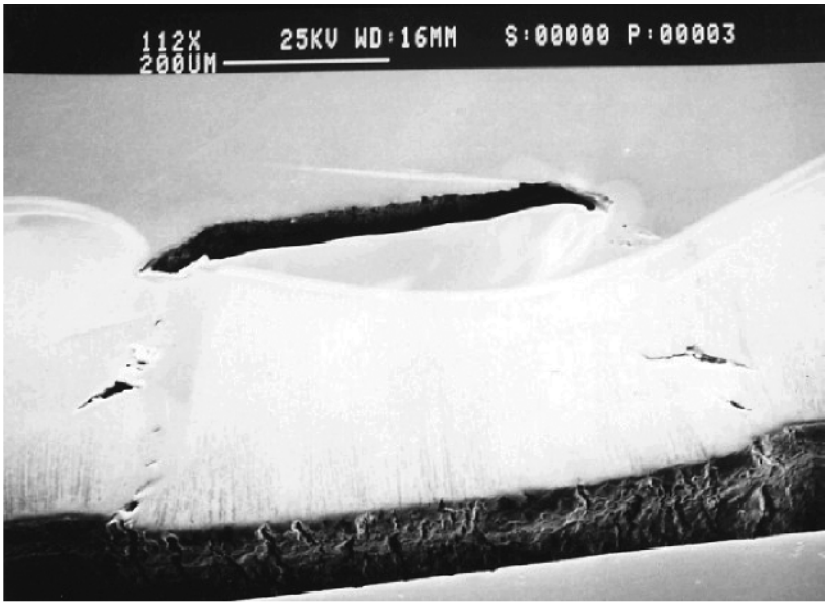

Figure 5. Hydrogen-induced cracking – blister crack.

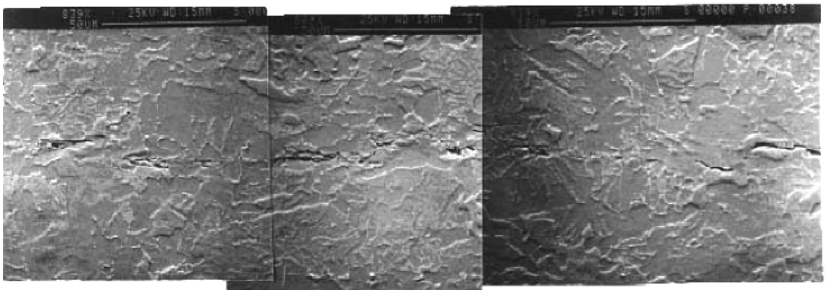

Figure 6. Hydrogen-induc ed cracking – centerline cracks.

by ultrasonic C-scans (Figure 7). For each steel, the C_{th} and pH_{th} are arrived at from the data presented in the corresponding table for that steel. It may be noted here that cracking was observed below pH 5 in all but two of the steels. These two steels CTR-2 and AM-2, did not crack even at pH 1, whereas the other steels showed cracking below pH 5.

TABLE 1. Chemical analysis (weight%).

Steel code	C	Mn	P	S	Si	Cu	Ni	Cr	Yield strength, MPa (ksi)
WC-1	0.105	1.03	0.010	0.0270	0.075	0.20	0.08	0.05	518(75)
G-2	0.130	1.09	0.012	0.0084	0.165	0.22	0.07	0.06	646(93)
AM-1	0.120	0.69	0.006	0.0031	0.008	0.33	0.095	0.17	597(86)
PC-1	0.090	0.73	0.013	0.0036	0.200	0.23	0.08	0.06	538(78)
CTR-2	0.100	0.84	0.018	0.0013	0.175	0.005	0.25	0.03	526(76)
AM-2	0.120	0.80	0.003	0.0016	0.410	0.011	0.015	0.027	572(85)

2.3. ROLE OF INCLUSIONS IN HIC

The EDX microanalysis revealed that the inclusions in cracks are manganese sulphide (MnS). The present investigation shows that MnS inclusions are the dominant initiation sites for cracking. In fact, microvoids around MnS and other inclusions provided sites for hydrogen to accumulate, leading to higher HIC susceptibility.

TABLE 2. Data on threshold pH and C_0.

	Steel	Threshold pH	Threshold hydrogen concentration mL (STP)/100 g steel	Ca/S ratio	Cracking
Three samples were tested in each pH	WC-1	5.3	0.3 ± 0.1	0.15	Yes
	G-2	5.0	0.6 ± 0.3	0.50	Yes
	PC-1	5.1	0.4 ± 0.3	0.96	Yes
	AM-1	5.2	1.2 ± 0.4	1.31	Yes
Six samples were tested in each pH	CTR-2	<1.1	>1.5 ± 0.2	2.62	No
	AM-2	<1.1	> 2.0 ± 0.2	2.50	No

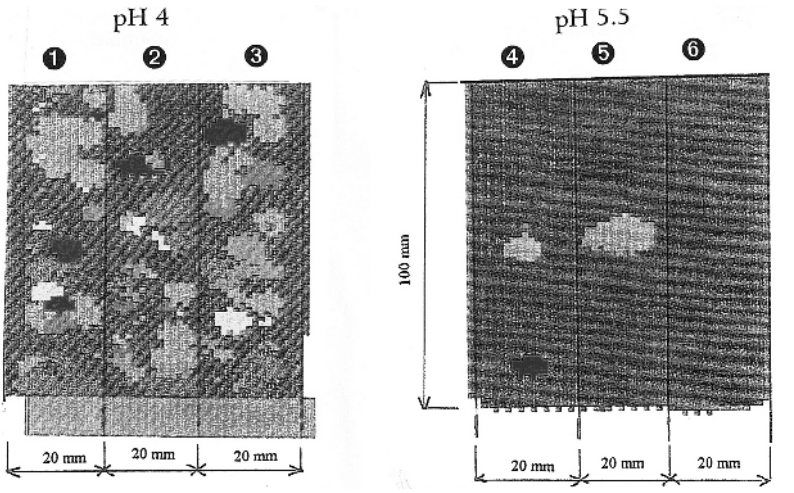

Figure 7. Ultrasonic C-scan images of six coupons tested in TM-0284 solution: coupons#1, 2, and 3 tested at pH 4 show significant cracks. However, coupons #4, 5, and 6 tested at pH 5.5 have no crack detected.

Figure 8a shows a montage of SEM micrographs following a long string of fragmented inclusions on a polished metallographic section. In order to assess the relationship between HIC and nonmetallic inclusions and in particular

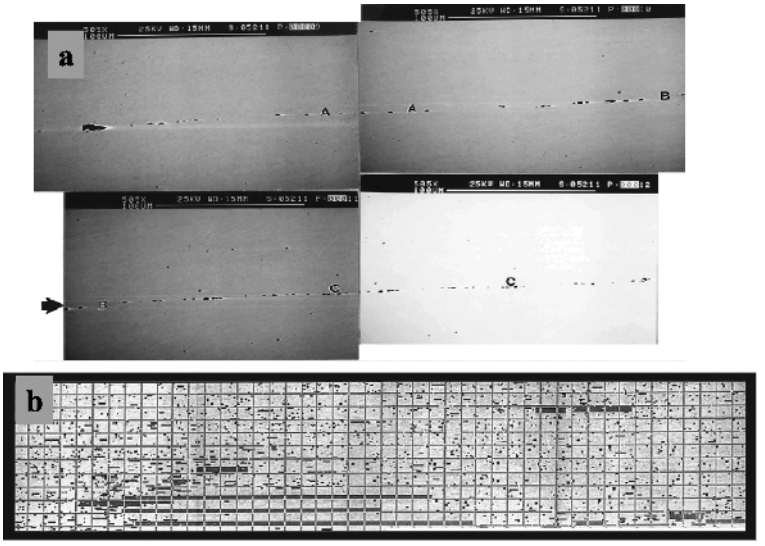

Figure 8. (a) Montage of SEM photomicrographs showing a long string of fragmented inclusions on a polished metallographic section. (b) The image analysis methodology where maps are constructed and used to measure long microscopic features that run through more than one microscopic field. Measurements of nonmetallic inclusions in line-pipe steels.

planar arrays of aligned inclusions, it was desired to obtain quantitative metallographic information for the inclusion population in a number of line-pipe steels that were assessed for HIC (see, Table 1). This was achieved by image analysis where two types of inclusion geometry were identified and measured separately: long strings of fragmented inclusions and other dispersed inclusions. The end map shown in Figure 8b illustrates this. The end map is basically a low magnification assembly for the metallographic information observed at high magnification, which indicates the overall picture of the inclusion population through the wall thickness of the line-pipe steel. The sample covers by 12 microscopic fields through the wall thickness (6 mm) by 46 fields in the longitudinal direction (each field is 400 × 400 mm). The end map shown in Figure 9b identifies susceptible areas for HIC on the sample as indicated by the thick solid lines (representing long strings of fragmented inclusions) and blister crack in Figure 5.

Data on volume percent, average size, and length of inclusions were investigated by image analysis and are reported in Table 3(29). The results are correlated with C_{th} and plotted in Figures 9 and 10. Both volume fraction and total length per unit area have a relationship with the C_{th}. It is clear from these figures that the steel with minimum inclusions has the highest C_{th} and vice versa.

The size and shape of the inclusions were considered to depend on the Ca/S ratio in steel. The Ca/S ratio [28] in Table 2 showed that a greater ratio of Ca/S decreases the hydrogen damage susceptibility (i.e., steels CTR-2 and AM-2). According to the results, steel susceptibility to SSC and HIC depends on the stress localization around large and hard inclusion particles. This localized stress could exceed the yield strength.

The metallurgical aspects of HIC can be summarized as follow: (i) the formation of internal blister cracks by the accumulation of hydrogen at inclusion microvoids, (ii) the extension of these cracks parallel to the rolling plane by the internal hydrogen-pressure, and (iii) the linking of nearby cracks along directions inclined to the rolling plane by plastic deformation and fracture. The formation of blister cracks seems to be directly related to the type and distribution of nonmetallic inclusions in the steel. Extension of blister cracks takes place along paths of low-fracture resistance parallel to the rolling plane. The exact nature of these fracture paths is not known, but it has been suggested that they are bands of certain transformation products in the steel. The linking of nearby cracks takes place along bands of localized shear, which result from the internal hydrogen pressure acting on elongated blister cracks.

TABLE 3. Line-pipe steels data on inclusions.

Sample	Vol. %	Av. size (:m)	#/mm^2	Length/mm^2	Threshold hydrogen concentration mL (STP)/100 g
WC-1	0.387	1.73	16963	29.3	0.3
G-2	0.338	2.45	5729	14.1	0.6
AM-1	0.209	3.71	1774	6.5	1.2
PC-1	0.205	4.96	1382	6.9	1.3
CTR-2	0.042	3.25	278	0.9	>1.5
AM-2	0.034	1.41	1614	2.2	>2.0

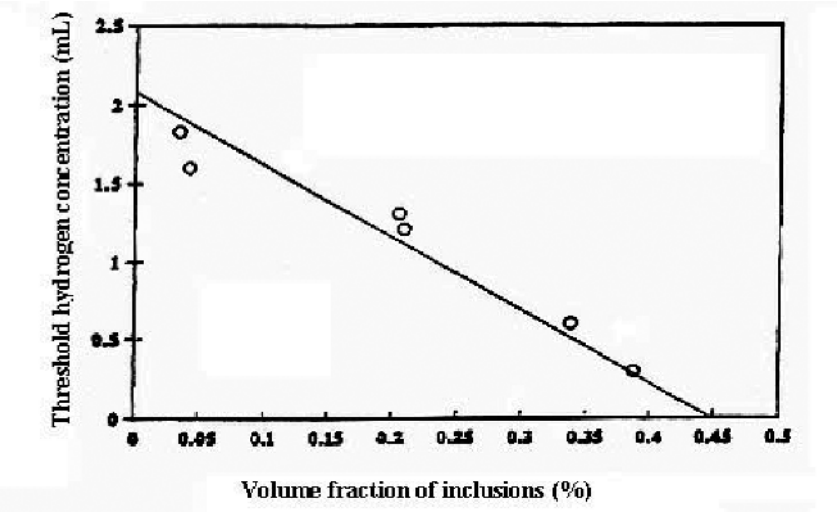

Figure 9. Effect of the volume fractions (%) on C_{th} for cracking.

Hydrogen, as an embrittling element in steels, is still a significant problem. The mechanism of hydrogen in steels is not completely understood, especially since no one theory in particular is able to describe all of the hydrogen-metal interaction phenomena observed. From the various damage theories proposed, in the de-cohesion theory both the adsorbed and absorbed hydrogen may be accepted.

According to the reduced atomic cohesion/model for hydrogen embrittlement proposed by Oriani [30], hydrogen embrittlement might be interpreted as being due to reduced atomic cohesion at the location of stress concentration by the accumulation of hydrogen atoms. The higher the C_o value, the greater the extent of reduction in atomic cohesion at the stress concentration location.

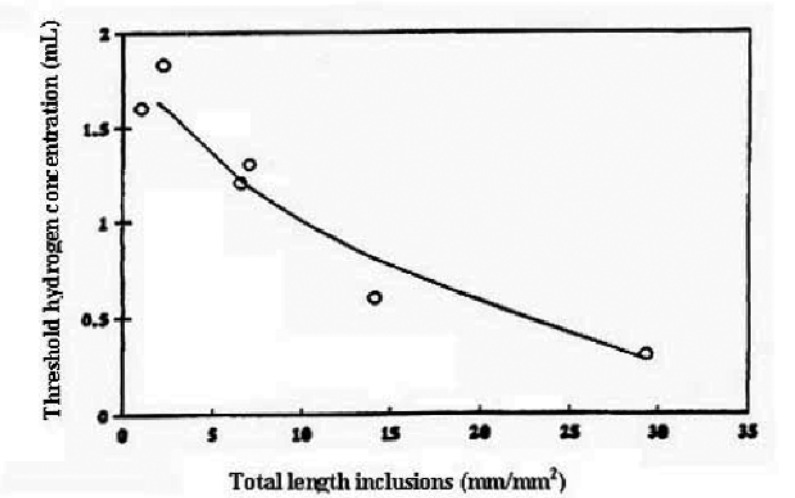

Figure 10. Effect of the total length inclusions on C_{th} for cracking.

3. Conclusions

- Multiple types of crack initiation sites exist for SCC of pipeline steel in low-pH solutions.
- Stress corrosion crack initiation is a competitive process, cracks initiate at the most favorable sites first, then at other sites.
- The correlation between pits and nonmetallic inclusions indicates that pitting results from effects associated with inclusion composition.
- There is a good correlation between inclusion measurements and HIC.
- The elongated MnS and planar array of other inclusions are primarily responsible for HIC.
- Lower volume fractions of inclusions corresponded to higher resistance to HIC.
- However, the microstructure may also plays a role in HIC, in particular, heavily banded microstructures could enhance HIC by providing low fracture resistance paths for cracks to propagate more easily. The balance of C and Mn has an overriding effect on resistance to HIC.
- HIC depends on both material composition and C_0. The HIC susceptibility would increase due to increased C_0 as the consequence of decreased D.

Acknowledgments

The authors acknowledge helpful discussions with colleagues at the CANMET Materials Technology Laboratory.

References

1. National Energy Board, Calgary, Alberta, Stress Corrosion Cracking on Canadian Oil and Gas Pipelines, Report No. MH-2-95 (1996).
2. Sutcliffe, J. M., Fessler, R. R., Boyd, W. K., and Parkins, R. N., Stress Corrosion Cracking of Carbon Steel in Carbonate Solutions, *Corrosion*, **28**, 313 (1972).
3. Beavers, J. A. and Harle, B.A., Mechanisms of High-pH and Near-Neutral-pH SCC of Underground Pipelines, ASME International Pipeline Conference, Calgary, Alberta (June 1996).
4. Charles, E. A. and Parkins, R. N., Generation of Stress Corrosion Cracking Environments at Pipeline Surfaces, *Corrosion*, **51**, 518–527 (1995).
5. Parkins, R. N., Blanchard, W. K., and Delanty, B. S., Transgranular Stress Corrosion Cracking of High-Pressure Pipelines in Contact with Solutions of Near-Neutral-pH, *Corrosion*, **50**, 394–408 (1994).
6. Delanty, B. S. and Beirne, J. O., Major Field Study Compares Pipeline SCC with Coatings, *Oil and Gas Journal*, June 15, 39–42 (1992).
7. Wang, Y.-Z., Revie, R. W., Shehata, M. T. and Parkins, R. N., Early Stages of Stress Corrosion Crack Development of X-65 pipeline Steel in Near-Neutral pH Solution, Materials for Resource Recovery and Transport, The Metallurgical Society of CIM 1998, 71–94 (1998).
8. Beavers, J. A. and Johnson, J. T., 1998 Annual Report on Effects of Pressure Fluctuations on SCC Propagation, Prepared for Line Pipe Research Supervisory Committee of PRC International, CC Technologies, Dublin, Ohio (May 1999).
9. Parkins, R. N., Metals Science and Engineering, A103 (1988), p. 143.
10. Christman, T. K., *Corrosion*, **46**, 6 (1990), p. 450.
11. Silcock, J. M., *Corrosion*, **38**, 3 (1982), p. 144.
12. Brown, B. F. and Beachem, C. D., *Corrosion Science*, **5** (1965), p. 745.
13. Yasuda, M., Weinberg, F., and Tromans, D., *Journal of the Electrochemical Society*, **137**, 12 (1990).
14. Issacs, H. S. and Newman, R. C., Local Electrochmistry of Pitting Corrosion in Stainless Steels, Corrosion Chemistry within Pits, Crevices, and Cracks, London: HMSO (1987).
15. Dolphin, A. S. and Turnbull, A., Experimental Determination of the Electrochemistry in Corrosion-Fatigue Cracks in Structural Steel in Marine Environments, Corrosion Chemistry within Pits, Crevices, and Cracks, London: HMSO (1987).
16. Jonas, O., Molecular Modeling of Corrosive Environments in Cracks, Effects of the Environment on the Initiation of Crack Growth: ASTM STP 1298, (Philadelphia: ASTM) (1997).
17. Parkins, R. N., *Metals Technology*, **9** (1984), p. 122.
18. Parkins, R. N., *Materials Science and Technology*, **1** (1985), p. 480.
19. Elboujdaini, M., Wang, Y.-Z., Revie, R. W., Shehata, M., de Sliveira, G., and Parkins, R. N., Initiation of Stress Corrosion Cracking in Pipeline Steel, prepared for GRI, MTL report no. MTL 2001-38(CF) (August 2001).
20. Elboujdaini, M., Li, J., Gertsman, V., Gu, G., Revie, W., Ming Gao, and David C. Katz, Stress Corrosion Cracking: Microstructural and Material Properties for Crack Initiation of 16 X-52 Line Pipe Steel - Corrosion 2004, NACE Conference Paper 04553 (2004).
21. Parkins, R. N. and Delanty, B. S., The Initiation and Early Stages of Growth of Stress Corrosion Cracks in Pipeline Steels Exposed to a Dilute, Near Neutral pH Solution, Ninth Symposium on Pipeline Research, AGA Catalog No. L 51746 (1996), pp. 19-1–9-14.

22. Elboujdaini, M., Wang, Y. Z., Revie, R. W., Parkins, R. N., and Shehata, M. T., Stress Corrosion Crack Initiation Processes: Pitting and Microcrack Coalescence, Corrosion 2000, Paper 00379, NACE, Houston, TX (2000).
23. Chen, W., King, F., and Vokes, E., Characteristics of Near-Neutral pH Stress Corrosion Cracks in an X-65 Pipeline, *Corrosion*, **58** (2002), pp. 267–275.
24. Ikeda A. and Kowada M., Stress Cracking in Low and High-strength Steels in Wet Hydrogen Sulfide Environment, *Chem. Economy Engineering Rev*, **10**(5) (1978) 12.
25. Asahi H., Sogo Y., Ueno M., and Higashiyama H., Metallurgical Factors Controlling SSC Resistance of High-strength Steels, *Corrosion*, **45**(6) (1989), p. 519.
26. Ikeda A., Morita Y., Terasaki F., and Takeyama M., *Proceedings of the 2nd International Congress on Hydrogen in Metals*, Paris (1977), 4A-7.
27. Tau L., Chan S. L. I, and Shin C. S., Effects of Anisotropy on the Hydrogen Diffusivity and Fatigue Crack Propagation of a Banded Ferrite/pearlite Steel, *Proc. of the 5th International Conference on Hydrogen Effect in Materials*, Edited by A. W. Thompson and N. R. Moody, The Minerals, Metals and Materials Society(1996), pp. 475.
28. Standard Test Method TM-0284 – Test Method Evaluation of Pipeline Steels for Resistance to Stepwise Cracking – NACE International, Houston, TX (1996).
29. M. Elboujdaini, M. T. Shehata, V. S. Sastri, R. W. Revie, and R. R. Ramsingh, Hydrogen Induced Cracking and Effects of Non-Metallic Inclusions in Line-pipe Steel, *Corrosion* **98** Paper No.784, pp. 1–17.
30. Oriani R. A and Josephic P. H., *Metallurgical Transaction*, **11A** (1980), p. 1809.

FAILURE ANALYSIS OF POLYETHYLENE GAS PIPES

KAMEL CHAOUI[*1], RABIA KHELIF[2], NASSEREDDINE ZEGHIB[3] AND ALAA CHATEAUNEUF[4]

[1]*LR3MI, Mechanical Engineering Dept., Badji Mokhtar University, BP 12, Annaba, 23000, Algeria;* [2]*LaMI – IFMA, Université Blaise Pascal, Campus de Clermont-Ferrand, BP 265, 63175 Aubière Cedex, France;* [3]*LR3MI, Mechanical Engineering Dept., Badji Mokhtar University, BP 12, Annaba, 23000, Algeria;* [4]*LGC – UBP, Complexe Universitaire des Cézeaux, Université Blaise Pascal, BP 206, 63174 Aubière Cedex, France*

Abstract: Natural gas transmission and distribution industry is using pipes of different origins to transport hydrocarbons under pressure. The use of polymeric material such as polyethylene (PE) made it possible to achieve significant profits in construction times and installation costs. However, some catastrophic failures took place for various reasons. The objective of this study is to highlight the various mechanisms of rupture of PE pipes in service and in laboratory conditions. It is clear that at least two mechanisms control PE pipe failures based on results cumulated in operating conditions. They are nominally ductile and brittle mechanisms respectively characterizing short and long-term failures. Several laboratory tests are used to extract design data for long-term failure-type prediction based on stress and time to failure relationship. It remains difficult to assess the relation between creep and fatigue loadings on the one side. On the other side, the manufacturing process of the test specimens (extruded pipes and compression molded sheets) influences considerably the obtained performance for viscoelastic materials subjected to working conditions. When analyzing different results, it is found that there is a certain correlation between failure times under both constant and fluctuating loading patterns and moreover, fatigue can be used as an accelerating agent of brittle fracture which normally occurs in the long-term span and under low load levels. Brittle-to-ductile transition is studied under fatigue crack propagation mode using an energy criterion. It is found that the approach leads to critical energy rates of 211 and 695 J/m² for brittle and ductile regimes respectively. The brittle fracture damage zone is characterized by a single craze made up by locally drawn fibers and dispersed

[*] To whom correspondence should be addressed; e-mails: chaoui@univ-annaba.org and chaoui_k@yahoo.fr

G. Pluvinage and M.H. Elwany (eds.), Safety, Reliability and Risks Associated with Water, Oil and Gas Pipelines, 131–163.

voids whereas ductile rupture is rather dominated by highly yielded material and significantly transformed matter as observed under polarized-light microscopy. PE mechanical behavior is affected by several factors including the state of residual stresses and the morphological variances induced by the extrusion process and subsequent cooling. As a result, there is a crystallinity increase from inner to outer layers of the pipe. The assessment of PE pipe failure mechanisms is to contribute to a better understanding of effects of other external chemical agents such as solvents in degrading the pipe overall resistance.

Keywords: polyethylene pipe, failure, fatigue, creep, damage zone, brittle, ductile

1. Introduction

Polyethylene (PE) resins are processed into pipes and fittings on a large scale to construct water and natural gas transmission and distribution networks. As shown in recent statistics [1], more than 22,000 km of PE pipes constitute the Algerian medium pressure gas network and all newly installed gas distribution systems around the country are exclusively made of PE because of its relatively low cost, ease of installation and maintenance, and long-term durability against environmental degradation; these properties made it a real alternative to metallic systems. Despite the large acceptance of PE pipes as an economic alternative, safety and reliability remain basic issues, especially for long-term brittle-like failure and accelerated stress corrosion cracking in both water and gas mains. Many studies have been carried out to highlight various behavioral aspects of both medium density polyethylene pipes (MDPE) and high density polyethylene pipes (HDPE) in terms of service lifetime [2], mechanical characterization [3], structure relationship [4], failure mechanisms [5], pipe joining [6], and environmental effects [7].

To a certain extent, it is possible to control the mechanical properties of semicrystalline polymers by morphology management [8] during processing operations. Substantially improved Young's moduli and tensile strengths have been obtained in shear-controlled orientation in injection-molded and high-pressure injection-molded HDPE because of the appearance of highly oriented structures. Quasi-static mechanical testing of HDPE processed by shear-controlled orientation in injection molding exhibited an improvement of 59% in the flexural modulus in comparison with the mechanical performance of conventional injection-molded specimens. The search for homogeneous geometrical dimensions in terms of the diameter and wall thickness, which are represented by the Standard Dimension Ratio (SDR is the ratio between the outside pipe

diameter and the minimum pipe wall thickness), imposes rapid cooling. As a result, compressive stresses in the extrusion process are generated on external pipe layers, whereas the internal layers develop positive stresses. The resistance to crack propagation is amply influenced by the state and magnitude of these residual stresses. Moreover, it has been shown that the propagation of cracks is slower in the external layers when they are subjected to compressive residual stresses.

Slow crack growth (SCG) is additional critical issue because PE pipe materials exhibit stress-lifetime curves [9] that have at least two separate rates corresponding to both ductile and brittle fracture mechanisms. The long-term behavior associated with brittle-like failure is most feared as it takes place without any presaging signs. At the same time, the long-term strength is substantially reduced, and so linear predictions from short-term behavior are no longer applicable. As a result, appropriate test designs have been developed to study crack propagation in real pipe materials under creep and fatigue modes [10–12] and to establish correlations between various mechanisms. Using a fatigue crack propagation mode at a maximum stress intensity factor of 13 MPa$\sqrt{m}$, researchers have identified basic differences [13] in the damage zone between HDPE and MDPE pipe resins with scanning electron microscopy examinations. Those observations are critical because the damage zone represents sites at which most hierarchical events happen and automatically controls the crack growth rate. Subsequently, this control defines the ultimate resistance to long-term fracture. Knowing that most of the pipe lifetime [13] is controlled by the initiation period and having identified the notch root damage zone, researchers become interested in single and epsilon-shaped crazes in PE pipe materials. The corresponding morphologies reveal drastic differences in the organization of the highly drawn material. Although a single HDPE craze accommodates uniaxially drawn fibrils, the multiple MDPE craze is solely made of voids and biaxially stretched planes. At this stage, we need to correlate the usual mechanical properties, measured macroscopically, with the associated structure of pipe resins. In other words, there is a need to explain the physical properties of pipe materials with respect to the molecular architecture and viscoelastic behavior. This resistance is deeply affected by the processing and service temperatures during the transmission of pressurized gas and consequently, both the vitreous transition and fusion temperature become significant parameters that condition the employment and working opportunities of PE pipes.

This work is aimed to investigate mechanisms of failure in PE pipes and fittings under service and laboratory conditions. The understanding of those mechanisms needs to study some associated phenomena such as damage evolution, residual stress distribution, morphology layout, and the various changes in

mechanical properties caused the extrusion process. Also, it is necessary to comprehend the possible transition between mechanisms and the effects of environment on the long-term pipe behavior.

2. Polyethylene (PE) Applications

2.1. PE PRODUCTION

PE is a generic name employed to describe polyolefins resulting from the polymerization process of gaseous ethylene that is a subproduct in natural gas and crude oil. Its molecular structure consists of two carbon and four hydrogen atoms in the basic repeating unit called a monomer. Usually, the polymerization conditions of low temperature, low pressure and appropriate catalysts and co-monomers result in a linear PE indicating that there are limited branches in the polymer chains. Mainly, three great families are defined according to their density: (i) low (LDPE), (ii) medium (MDPE) and, (iii) high (HDPE) density PEs. In 2003, among the 44 millions of tons of PE produced worldwide [14], approximately 40% was HDPE. More than 90% of the PE production is consumed by six principal applications, including 50% for films and sheets, approximately 25% for the moulded products and just 6% for pipes. These data inform us about the development undertaken by PE as a potential substitute of metals and similar materials for specific technical applications in manufacturing spare parts, machine elements and coatings as illustrated in Figure 1. Pipe applications are very much diversified as it is possible to use them for the construction of networks to convey fluids under pressure such as drinkable water and natural gas or for agricultural irrigation and in the petrochemical industry. The main uses of PE pipes are compared for both USA (Figure 2a) and EU (Figure 2b) during 2003, and it is observed that natural gas and drinkable water networks come well behind drainage applications. The part reserved for natural gas distribution is important and is in constant increase. In a developing country such as Algeria, the use of plastic pipes is expanding [1] at a dramatic rate while both steel and cast iron pipes are becoming costly and difficult to maintain (Figure 3). HDPE is one type of linear PE with a density range from 0.941 to 0.965 g/cm^3 as stated in ASTM D-883.

2.2. PE PIPE INTERACTIONS

As shown in Figure 4, in real conditions, plastic pipe is in constant interaction with the other underground networks (sewers, drinking water, cables, etc.), which are not necessary made out of polymers. So its vulnerability increases as

the risks of being deteriorated might become significant. The protection measures are reexamined by including different means of protections and suitable pipe backfills. Physical indications of are placed with gas networks upon pipe burial to facilitate spotting and to reduce the probability of damage by third parties. It should be emphasized that most significant applications of PE pipes remain related to fluid conveyance.

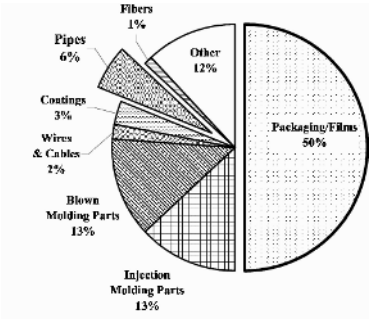

Figure 1. Percent distribution of worldwide PE applications.

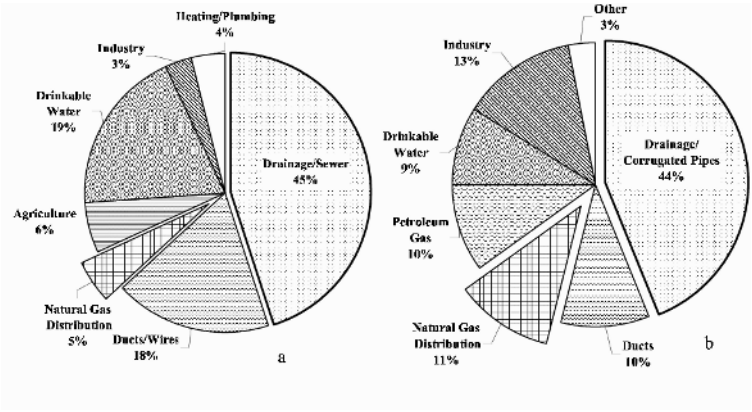

Figure 2. Main applications of PE in (a) USA and (b) EU.

2.2.1. *Fuel Pipes*

HDPE is the reference material used for gas transport under pressure. As a pipe, it has the advantages of being smooth-walled and with small SDR. SDR is related to the allowable pipe pressure through the following equation shown in French Standard NF EN 921 for pressurized plastic pipe:

$$\sigma_{hoop} = P\frac{OD - h}{2h} \tag{1}$$

Using SDR definition, eq. (1) becomes:

$$\sigma_{hoop} = P\frac{SDR-1}{2} \tag{2}$$

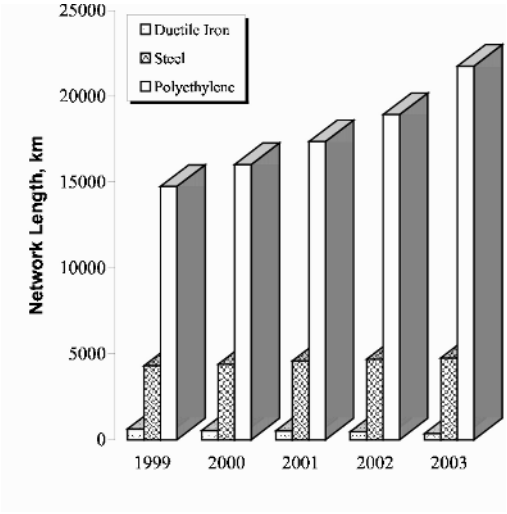

Figure 3. Evolution of PE pipes installation in the Algerian gas industry.

Figure 4. HDPE gas pipe with protective duct being installed close to a drinkable water main and a sewer line.

where, σ_{hoop} = hoop stress, P = gas pressure, OD = average outside diameter, and h = minimum wall thickness. ASTM D-2837 defines the pressure rating of the pipe as the estimated maximum pressure that the medium in the pipe can exert continuously with a high degree of certainty that failure of the pipe will not occur. Safety factors impose a working pressure in the pipe lower than this upper limit.

2.2.2. *Water Pipes*

Today in Algeria, HDPE water pipes are laid in the northern part of the country with diameters reaching up to 300 mm. The introduction of plastic pipes enabled eliminating corrosion and water loss problems. More than 50% of input water in the Algerian steel-cast iron network is lost by uncontrolled leakages and lack of maintenance. As much as 19% of PE pipes are chosen for drinkable water systems in EU countries (Figure 2a) whereas in Algeria, this figure is yet much less. When exposed to hot water, long-term HDPE pipe failure occurs by precipitation and diffusion-controlled migration of antioxidants combined to thermal oxidation [9] of the polymer.

2.2.3. *Drainage Pipes*

Most gravity water flow systems are constructed using corrugated HDPE pipes. They basically comprise mostly sewers, drains, under-drains, and sanitary sewers. In drainage systems, underground pipe diameters may be as large as 1,524 mm and they are calculated to support both soil and live loads. HDPE pipe flexibility is used to transfer a portion of the overload onto the surrounding soil. The risk of pipe buckling exists as a result of excessive deformation. Corrugation is incorporated into the pipe profile to increase the structural stiffness of the structure and according to AASHTO M294 standard; three types of HDPE pipe profiles [15] are used:

- *Type C:* Full circular cross section with an annular corrugated surface both inside and outside.
- *Type S:* Full circular dual-wall cross section with an outer corrugated pipe wall and a smooth inner liner.
- *Type D:* Circular cross section consisting of a smooth inner wall joined to a smooth outer wall with annular or spiral connecting elements.
- Observed field problems [16] included: (i) Deflection resulting from the lack of control of construction procedures and the use of poor backfill materials, (ii) Erosion at outlet ends which often resulted in significant loss of material and longitudinal bending and cracking of the corrugated HDPE pipe and, (iii) Erosion as a result of joint leakage.

2.2.4. *Protection Ducts*

In this case, HDPE pipes are used as external shields to isolate cables or pipes from external aggressive environments. Usually, the protection is aimed to reduce significantly the presence of both moisture and oxygen. In the gas industry, HDPE ducts are commonly used to protect steel pipelines crossing swampy and marine environments.

3. Pepipe Testing

3.1. SUSTAINED PRESSURE

In 1962, the Plastic Pipe Institute (PPI) selected stress rupture testing as the most suitable test method for rating plastic piping materials. The design of is achieved through the "Rate Process Method for Projecting Performance of Polyethylene Piping Components" which is standardized in ASTM D-2837, ISO 9080, and D-2513. It well established that PE creep rupture curve may be divided into three regions as illustrated in Figure 5 and the same testing procedure allows differentiating between various PE resins and manufacturing processes (Figure 6).

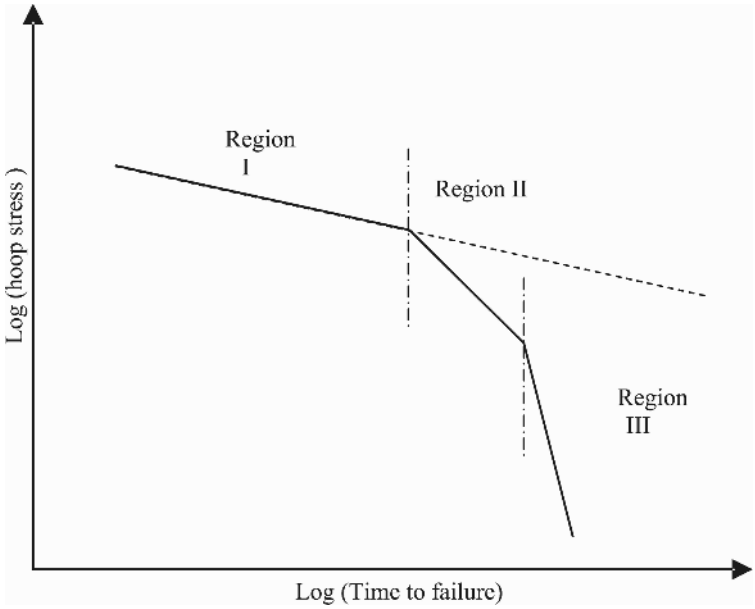

Figure 5. Schematic of a creep rupture curve for PE pipes at high temperature.

Today, the calculation is based on two or three coefficients equations [2, 17–19], which link lifetime (time to failure), hoop stress, and testing temperature:

$$Logt = A + BLog\sigma \tag{3}$$

and

$$Logt = A + \frac{B}{T} + \frac{BLog\sigma}{T} \tag{4}$$

where A, B, C = constants, t = failure time (hours), σ = hoop stress (Pa), T = temperature (°K). Either ASTM D-2837 based on hydrostatic design basis (HDB) or ISO 9080 based on minimum required strength (MRS) use data from sustained hydrostatic pressure tests of pipe specimens, but the extrapolation protocols are different [2]. It is understood that the actual long-term performance under internal pressure and temperature will be the same regardless of the method. Normally, HDB and MRS are used to obtain allowable pressure ratings considering pipe diameter, thickness, and a safety factor.

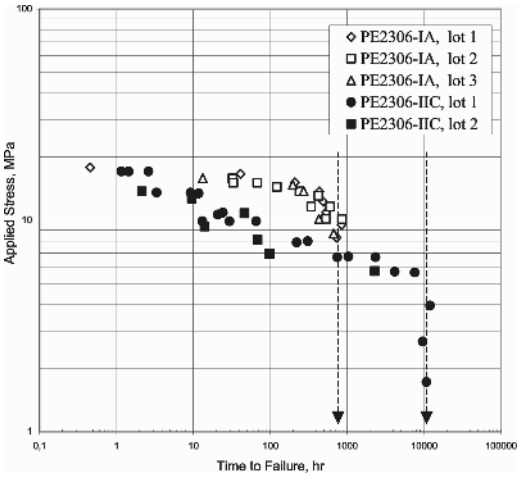

Figure 6. Stress versus time to failure under sustained pressure for 50 mm OD pipes (ethylene/hexane copolymer; PE2306-IIC: two lots) and (ethylene/butene copolymer; PE2306-IA: three lots).

3.2. CREEP

Under conditions of constant low stress and room temperature, it is established that PE resins fracture by slow crack growth. This mode of failure limits pipe

lifetime but constant tensile load (CTL) test was devised to extract long-term information from accelerated testing [11, 20, 21]. Available data from such a test is able to differentiate between similar products coming from different manufacturers or using different copolymers in the extrusion process. CTL is a good quality assurance test to evaluate new pipe lots and to set a minimum required resistance [22].

3.3. FATIGUE

In general, fatigue can be defined as a phenomenon that takes place in components and structures subjected to time-varying external loading and that manifests itself in the deterioration of the material ability to carry an applied load that is well below the elastic limit. Testing under fatigue has been used in different studies as an accelerating agent to deduce PE lifetime under specific conditions. As gas consumption is fluctuating throughout the day, so will do operating pressure. This indicates that fatigue is a possible loading mode of PE pipes and if temperature fluctuations are added, cycling will occur but the amplitude is of a random form. In fact, such conditions complicate the real situation since it is necessary to load a pipe in conformity with service operating conditions. Laboratory studies use basically periodic loading functions and have to limit frequency to avoid hysteric heating in the tested specimen [11, 12, 23]. In order to describe the fatigue strength, Wöhler curves are the most common model for practical use and design. The log-scale leads to a straight line between the stress amplitude and the number of cycles to failure. When crack is initiated, the analysis of crack growth history shows that there is a log–linear relationship between the apparent crack size and the lifetime. Also, there is a linear relationship between the crack growth rate and the crack length or the stress intensity factor range in mode I(ΔK_I) when plotted in a log–log scale as stated by Paris-Erdogan [11, 12, 23–25] law.

Statistical analysis of PE compression molded sheets has shown that fatigue lifetime cannot be suitably modeled by lognormal distribution as usually adopted in the literature. Two- and three-parameter Weibull distribution, as well as three-parameter lognormal, can be adequately applied for probabilistic lifetime characterization (Figure 7) and an expression in the power type form has led to more appropriate representation of fatigue data [25] compared to linear fitting in the log-scale.

3.4. BRIDGING BETWEEN FATIGUE AND CREEP

The correlation between creep and fatigue strengths, undertaken by Parsons et al. [12], showed that MDPE was much more creep resistant than HDPE, but

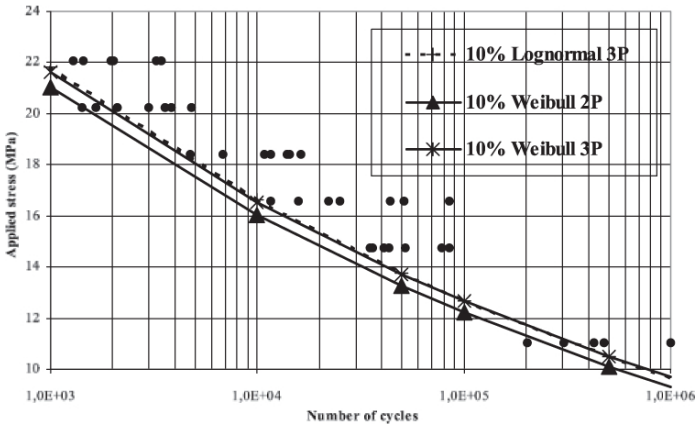

Figure 7. Fatigue lifetime quantiles at 10% for three multiparameter models.

MDPE pipes was much more sensitive to strain rate in fatigue. In the same approach, Zhou and Brown [11] concluded that a higher resistance to fatigue does not necessarily correlate with a higher resistance to failure under creep. Since ASTM tests are based on creep data, it is interesting to compare it with fatigue data. Figure 8 illustrates such relation between failure times from both creep and fatigue modes. The data were gathered from literature and a proportional relation is found to characterize both modes (Figure 8). This is an important result which states that fatigue tests can also be used to draw conclusion on pipe life under acting pressure.

These results suggested an article to Chudnovsky et al. [27] about a mathematical model to bridge creep and fatigue lifetimes with crystallization behavior. The model relates two morphology parameters (z_1 = onset of temperature of crystallization and z_2 = rate of crystallization) with crystallization kinetics and rate constants of degradation (a_0, a_{ij}, and c_j) through a function φ in the form:

$$Ln\varphi\left(Z_1 - Z_2\right) = a_0 + \sum_{i,j=1}^{2} a\left(Z_i - c_i\right)\left(Z_j - c_j\right) \tag{5}$$

The 2D normal distribution density of z_1 and z_2 is used to approximate the fatigue-creep correspondence function φ. Just in these areas of investigation, numerous testing methods have been proposed and some were adopted as new standards.

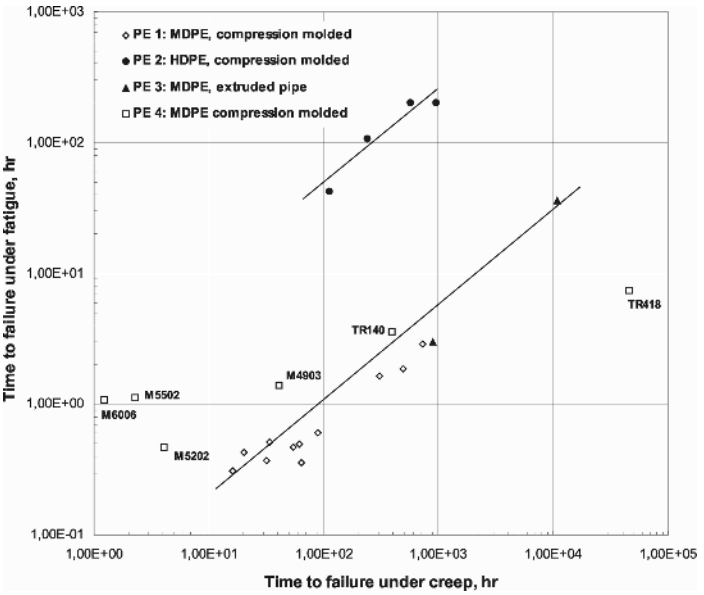

Figure 8. Relationship between failure times under creep and fatigue modes for different resins [26].

It should be noted that there is some aspects of complementary information between different tests depending on test type, specimen source, test condition, and the purpose sought as summarized in Table 1 [15, 27].

Laboratory work has well established that extruded plastic pipes fail in a ductile manner as applied loads are sufficiently high and failure zone is characterized by large deformations around the damaged area. Despite such favorable important ductility, PE piping and fitting materials are also found to undergo brittle-like fracture under service conditions when they are subjected to low stresses for long service periods or to temperatures above the ambient one. Such conditions usually favor SCG fracture mode in PE pipes. As a result, constant load tests (Figure 6) exhibit two general crack propagation mechanisms: (i) ductile failure which is dominated by large-scale homogeneous deformations in the bulk and (ii) brittle failure that starts at stress concentration points and propagates slowly preceded by a craze zone containing transformed material. Figure 9 shows failure modes that could occur in PE pipe cracking depending on the loading spectrum and the environmental conditions.

It is clear that stress cracking (SC) is critical as it leads to brittle failure under either creep or fatigue-related working parameters. The mechanisms of fatigue failure of externally notched sections of PE pipe under pressure have been investigated by Reynolds et al. [10], who confirmed that the origin of

TABLE 1. Comparison of PE test methods and specimen shapes according to some standards.

Test Method	Standard	Specimen source	Specimen shape	Notch	Test condition	Note
Bent strip	ASTM D1693	Molded plate	Rectangular bar	yes	10% Igepal solution, T=50°C	Simple, less accurate
Stress rupture test	ASTM D1598	Pipe	Pipe	no	Water, various temperatures and pressures	Most representative of working condition extremely time-consuming
Notched pipe test	ISO 13479	Pipe	Pipe	yes	Water, 80°C, single stress	Representative of working pipe, very time-consuming
PENT on pipe specimens	ASTM D1473	Pipe	Pipe section for D < 25 mm, rectangular bar for others	yes	Air, 80°C, single stress	Less representative, less time-consuming
PENT on plaque specimens	ASTM D1473	Molded plaque	Rectangular bar	yes	Air, 80°C, single stress	Not representative, less time-consuming
FNCT	ISO 16770	Molded plaque	Square bar	yes	Liquid, 80°C, single stress	Not representative, less time-consuming
NCLS	ASTM F2136	Pipe	Dumbbell U-shaped	yes	10% Igepal solution, 50°C, single stress	Not representative, not time-consuming
Fatigue tests	—	Pipe and molded plate	Rectangular bar and C-shaped	yes	Room air or controlled environment	Depends on particular tests and testing conditions

branching fracture features lies in the localized shear deformation. Basically, ductile and brittle failure modes dominate the damage mechanisms of PE pipe fracture as studied through microscopy.

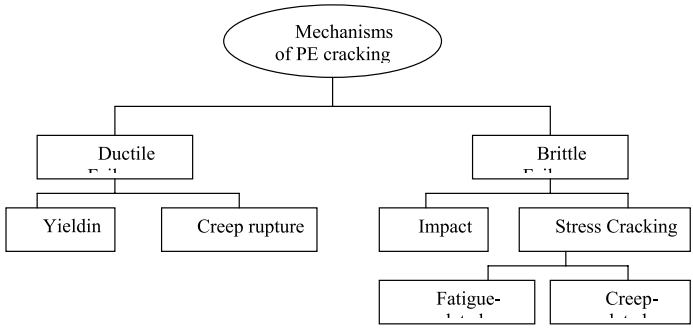

Figure 9. Failure mechanisms occurring during PE cracking under different loadings.

4. Failure Mechanisms of PE Pipes

4.1. DUCTILE FAILURE

Ductile failures are characterized by large-scale material yielding adjacent to the failure location. For instance, a flow phenomenon takes place represented by cold drawing during in typical tensile tests of semicrystalline polymer samples. Ductility is more expressed as applied stresses are higher and usually

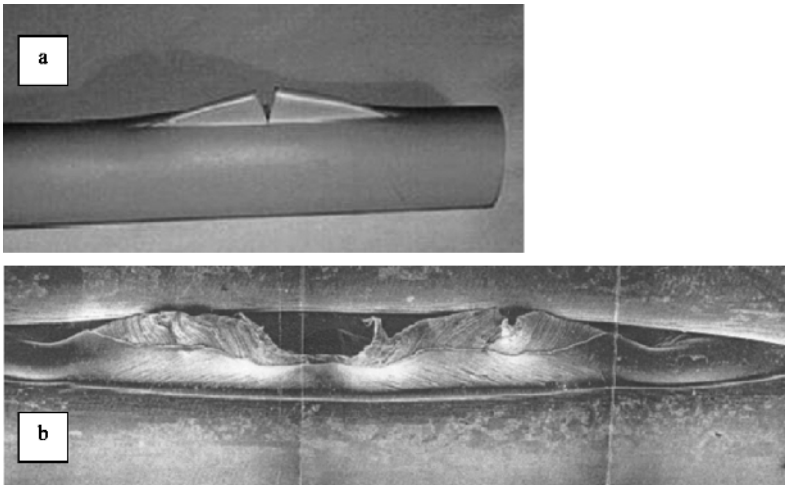

Figure 10. Ductile failure in HDPE pipes (a) wall thinning and tearing in circumferential direction, (b) large-scale deformation and tearing in the longitudinal direction.

rupture occurs in a relatively short time. This mechanism is related to the viscoelastic behavior of PE materials and specifically refers to the creep rupture. The resulting failure shows large deformation accumulating in during this process as indicated in Figure 10.

4.2. BRITTLE FAILURE

Typical brittle failures in HDPE pipes are exhibited in Figure 11. Less deformation characterizes the fracture process, which is a long-term mechanism. Temperature [22, 26] is known to accelerate brittleness from sustained pressure tests. Brittle failure in semicrystalline polymers has been claimed to originate from chain disentanglement in fibrils, and recently other studies have also concluded that chain breaking due to applied stress during crack propagation involves fibrillation within the damage zone [9, 19–21, 24, 26]

A level of complexity lies in the intramolecular heterogeneity of co-unit distribution that should be as efficient as intermolecular heterogeneity for producing tie molecules and random chain folding at the expense of regular chain folding. Crystalline domains within semicrystalline polymers strongly influence such low-strain-rate properties as the elastic modulus, yield stress, SCG, and environmentalSC, whereas high-strain-rate properties such as impact, tear, and rapid crack propagation are basically controlled by amorphous regions [28]. In many cases, complementary techniques have been adopted to assess

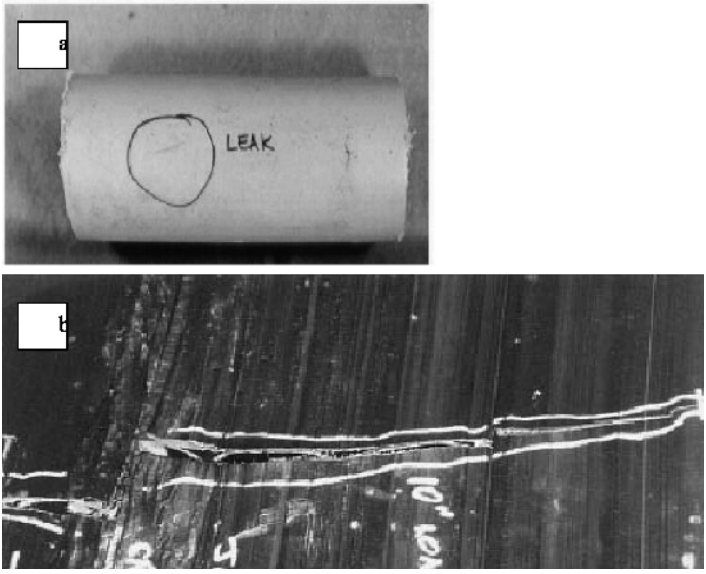

Figure 11. Brittle failure in HDPE pipes (a) typical region II and (b) typical region III [9] (Figure 5).

from physical property measurements molecular information. For instance, brittle fracture toughness, crazing, and SCG measurements have been used to determine the tie-molecule concentration and to infer valuable structural information. In simpler cases, tie-molecule concentrations have been evaluated from the modulus of a mechanically oriented material. Post-yield experiments assume that tie molecules and entangled chains behave like rubbery networks in the drawing and strain-hardening regions; these molecules are steadily pulled out from fragmented lamellae to become part of an oriented amorphous domain.

5. Brittle to Ductile Transition

Ductile failure is mostly associated with macroscopic shear flow of the ligament while brittleness is linked to SCG of a permanent craze. It is known that brittle fracture in PE pipes refers to slit-like cracks (Figure 11a) that are obtained under long-term hydrostatic laboratory testing. In the example given in Figure 12a, a hoop stress of 9.85 MPa was continuously applied for a period of 14,528 h (>20 months); and the failure occurred at the end cup starting from the inner side at a stress concentration point. To reveal fracture surface, crack length and crack opening, the pipe and the welded end cup were sectioned in the radial direction and then separated into two parts. It is evident that propagation under constant load started from a stress concentration point and

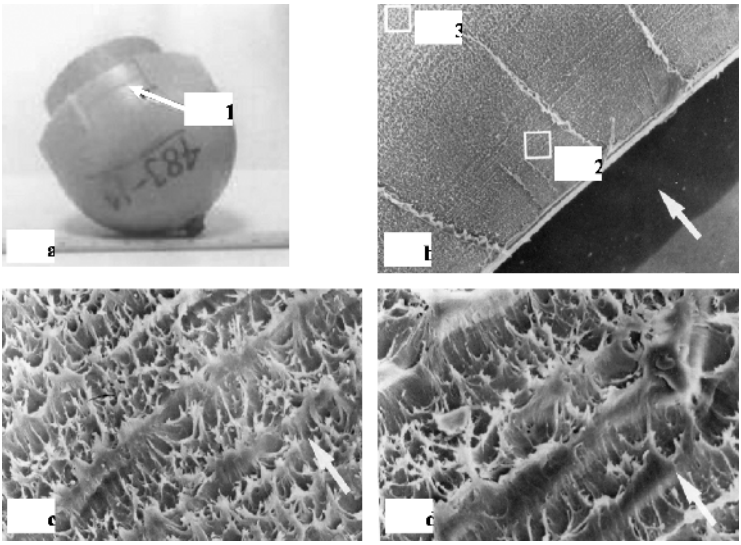

Figure 12. End cup brittle failure, (a) end cup, (b) fracture surface after sectioning, (c) higher magnification of region “2” (d) higher magnification of region “3”.

went from the cup bore through the wall on a distance of almost 26 mm at the leaking slit. The mirror-like flat fracture surface appearance is a typical long-term brittle failure (Figure 12b) and the final ligament failed by ductile tearing (point 3). Closer SEM examinations, however, revealed that progressively increased ductile contributions are noted as crack length increased (Figures 12c and d). In fact, these findings ought to guide our attempts for brittle crack acceleration under fatigue mode.

5.1. DUCTILE VERSUS BRITTLE FAILURE

It is accepted that ductile failure in PE pipes is associated with macroscopic yielding. The time to failure of ductile failure is determined by creep rate. On the other hand, brittle failure is associated with crack growth. It is suggested that the two processes occur simultaneously; and the final failure depends on which process is faster under given stress, temperature, and notch depth. As a general rule, the long-term fracture resistance of a given material can be expressed in terms of its stress and time dependent yielding as the following relationship [29, 30]:

$$t_f = C\sigma^{-n} \tag{6}$$

where C is the load capacity parameter, a positive constant representing stress level at which the material fails at unit time. The exponent n is a damage evolution index. Typical values of n for ductile and brittle failures are in the ranges 20–27 and 2.5–4.5 respectively. The transition stress is roughly equal to one half the yield points at a given temperature. Ductile failure is characterized by microscopic shear flow while brittle fracture occurs by slow crack growth.

5.2. BRITTLE TO DUCTILE TRANSITION

Other workers [31–33] concentrated their studies on the phenomenon of brittle to ductile transition in PE in an effort to understand the underlying mechanics-causing component's life termination catastrophically. It is found that at a given temperature brittle-like behavior has been observed at high and low speeds while ductile failure characterized intermediate speeds. An increase in temperature shifted brittle–ductile–brittle transitions to higher speeds because of a competition between three rival mechanisms: (i) brittle failure by disentanglement, (ii) ductile shear yielding and, (iii) brittle failure by chain scission. Using Charpy impact test, brittle–ductile transition temperatures (BDTT) of PE were investigated with different degrees of crystallinity. A rise in the cooling plate temperature for MDPE and HDPE brought out a fall in BDTT and an increase

in impact energy. With decreasing degrees of entanglement density, PE exhibited a slightly decreasing BDTT. Using rapid crack propagation in pressurized PE pipes, the brittle–tough transition temperature was assessed and shear lips controlled the failure process. Short-term failure in PE is accomplished through fibril breakdown within the central part of the craze because of overall yielding whereas long-term failure occurred by an accumulation brittle damage as microvoids at fibril roots and film joints.

In view of the unacceptable length of time required to observe brittle fracture particularly in newer tough resins, it became urgent to develop an alternative testing procedure based on fatigue crack propagation acceleration. A C-shaped specimen [24] is introduced to study accelerated fatigue crack propagation in resistant PE materials (Figure 13). Some studies [10–13, 23, 27] converged in someway toward the conclusion that fatigue might simulate the stepwise fracture mechanisms observed in real pipe.

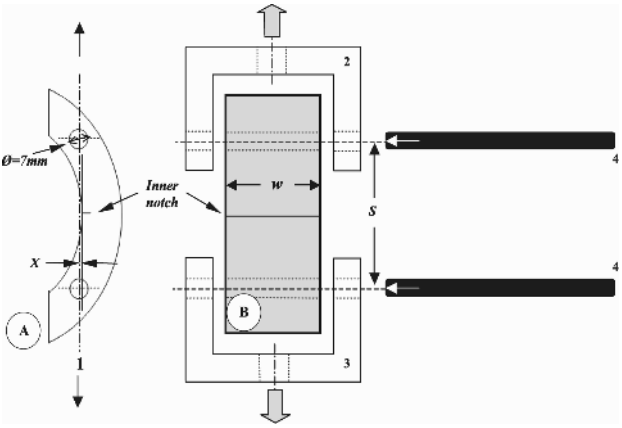

Figure 13. Schematics of side (A) and front (B) views of PE C-shaped specimen with its gripping metallic fixtures (2 and 3) and loading pins (4).

5.3. FATIGUE BRITTLE TO DUCTILE TRANSITION

The fracture surface of a failed C-shaped specimen is shown in Figure 14. Crack propagation initiated from a manufactured notch and clearly exhibits both brittle and ductile mechanisms. Microscopy is used to identify the plastic zone ahead of the crack tip. Thin sections were obtained from interrupted fatigue crack propagation tests and observed using microscopy. The results are illustrated in Figure 15. In the brittle regime, the plastic zone is very small and is associated with a main craze. The latter is made of yielded material and structural voids. Under polarized light, the extent of damaged material is confined to a narrow zone next to the crack plane. For the ductile regime, the

damaged zone is much important and the craze are longer compared the brittle stage. The SEM examination illustrates the multiple crazes and the highly deformed material at the crack tip. Around the damage zone, another part of the transformed material is highly affected plastically as its limits extend many folds until the specimen edge. Figure 16 illustrates higher magnifications of the hierarchical events inside the craze zone that appears to be constituted of highly yield local matter and important voids.

In order to study the FBDT, it is interesting to use an energetic approach proposed by N. W. Klingbeil [34] for ductile solids failed under fatigue. This study is concerned with a new theory of fatigue crack growth (FCG) in ductile

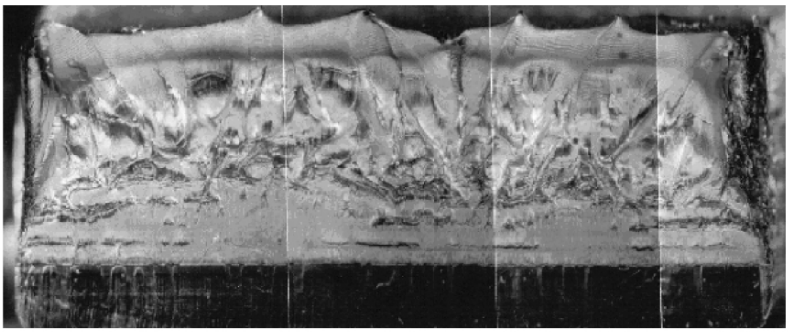

Figure 14. Fracture surface illustrating combined brittle and ductile failure under fatigue.

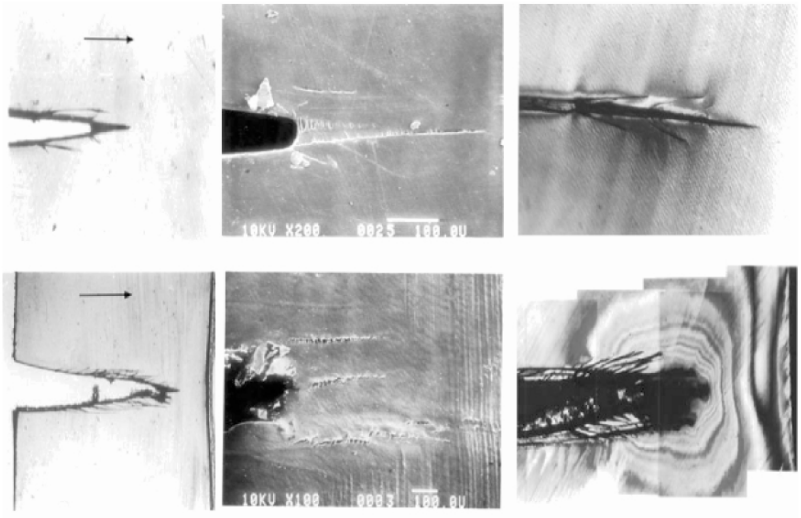

Figure 15. Optical, SEM and polarized light photomicrographs of plastic zone shape ahead of the crack tip in both brittle and ductile regimes under fatigue mode.

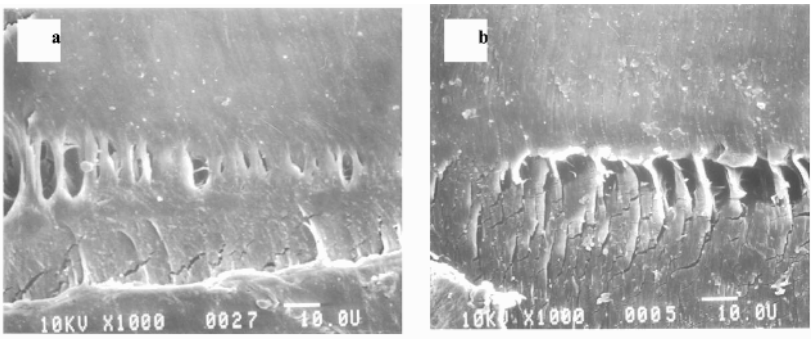

Figure 16. SEM observation of the inner part of the craze zone at higher magnification; (a) brittle and (b) ductile.

solids based on the total plastic energy dissipation per cycle ahead of the crack tip. The FCG is explicitly given in terms of the total plastic dissipation par cycle and the plane strain fracture toughness of the material from the equation:

$$\frac{1}{t_0}\frac{da}{dN} = \frac{1}{G_C}\frac{dW}{dN} \tag{7}$$

where G_c is the critical energy release rate. In this instance, typical plots of the rate of irreversible plastic work as a function the crack propagation rate are constructed. These plots for 20%, 25%, 30%, and 35% of yield stress are shown in Figure 17. It is observed that both damage mechanisms are well separated and each slope would represent an independent resistance to fatigue crack propagation. The equivalent load levels are well below the failure loads indicated in Figure 6 since it is the same PE being tested under fatigue. The computed values of toughness are summarized in Table 2.

It is found that the brittle regime critical energy release rate so calculated lies between 97.7 J/m² and 264 J/m² and these values are quite small compared to the measured energy rates from potential energy evolution [26]. The ductile regime energy is important as it considers a lot of energy spent on damage and high deformation. There is a consistent evolution of calculated G_c as this value is much higher when ductility becomes important. This approach is interesting as it allows separating brittle from ductile contributions in a given FCP test. The use of microscopy enables to confirm the extents of each mechanism from fracture surface analysis and damage dissemination within PE. Compared to long-term hydrostatic strength (LTHS), FCP may be considered as a more efficient approach since it helps produce BDT in much shorter times. A recent study [32] showed that under creep testing, ductile failure is primarily driven by the yield stress of PE. The examination of ductile failure data at different temperatures also indicated that a systematic improvement in performance is

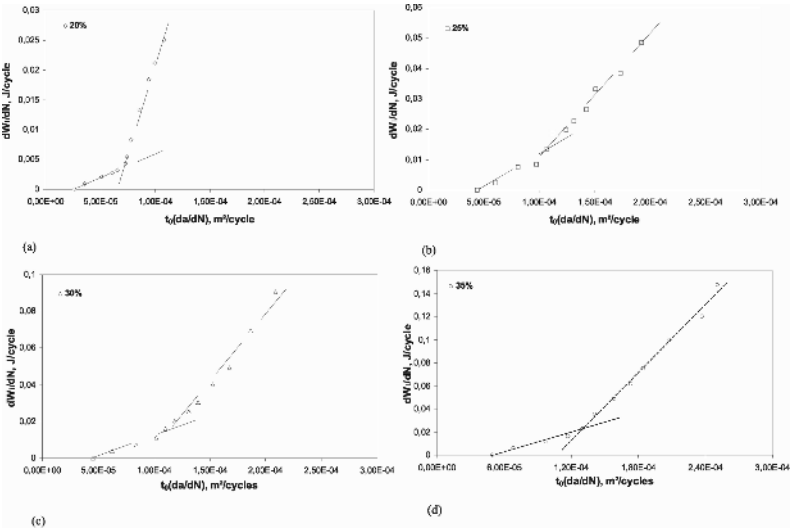

Figure 17. Rate of irreversible work spend on deformations as a function of corresponding fatigue crack growth (FCG) rate at (a) 20%, (b) 25%, (c) 30%, and (d) 35% of applied stress.

observed with increasing temperature, and this might be related to the progressive relaxation of internal stresses.

TABLE 2. Calculated fracture toughness from brittle to ductile transitions under fatigue testing with determination coefficients (R^2).

Stress level (% σ_y)	G_c brittle (J/m²)	R^2 (Brittle)	G_c ductile (J/m²)	R^2 (Ductile)
0.20	97.7	0.937	589.5	0.997
0.25	256.5	0.928	411.6	0.976
0.30	226.2	0.971	790.1	0.982
0.35	264.0	0.980	987.8	0.988

6. Residual Strain Relaxation

For extruded pipes, the residual stresses and morphology variations are primarily due to the fabrication process, which does not allow progressive heat dissipation.

6.1. RESIDUAL STRESS

Residual stress can also be a factor causing SC. It is known that all plastic pipes contain residual stress introduced during the manufacture processes. The extent

and distribution of residual stress vary significantly depending on manufacturing process. One of the main factors causing residual stresses is differential shrinkage through the pipe wall during the cooling process. If cooling takes place from only one side of the pipe wall, the cooled side will shrink rapidly. The newly solidified section constrains the adjacent part from shrinking freely. As a result, compressive residual stresses are created in the cool side and tensile residual stress is formed in the opposite side. However, if both sides are cooled simultaneously, compressive stress will be created near the two surfaces and tensile stress in the center [15].

High residual stress in the pipe could have significant impact on the SC property of the pipe. Therefore, quantifying the residual stresses in the pipe is essential in predicting the long-term behavior of the pipes.

6.2. STRAIN RELAXATION

Elasticity manifests itself by the tendency to oppose deformation to which a material is subjected. Generally either (i) instantaneous or (ii) delayed elasticity are considered and are explained using the very different microscopic origins. Considering both first and second laws of thermodynamics, two particular cases can arise: The first case corresponds to a state where the material entropy would not be modified by the deformation and thus, this state will characterize crystalline structure. Such behavior is solely caused by an increase in internal energy and is termed as instantaneous elasticity. Indeed, the crystal lattice reacts instantaneously to any stress by the modification of the interatomic distances and angles of the structure. In the second case, the internal energy of the matter remains constant during the deformation. This is the typical state of an amorphous polymer constituted by independent macromolecular chains. The internal energy is roughly constant whatever their configuration looks like and in the absence of stresses; the macromolecular chains accumulate maximum disorder corresponding to maximum entropy. After application of an external load, the state of final balance becomes characterized by a higher order and thus corresponding to lower entropy caused by orientation effects. The new configuration is not instantaneously reached and, indeed it takes a certain time to establish equilibrium. The lower the thermal energy of agitation and the temperature the longer the duration. Such state is referred to as delayed or differed elasticity and usually it is necessarily accompanied with heat release even in the case of an infinitely slow deformation. However, PE as a semicrystalline material, presents simultaneously the two types of elastic strains when it is subjected to a constant load as a function of time (creep case). In fact, such load can be internal stresses due to material processing effects.

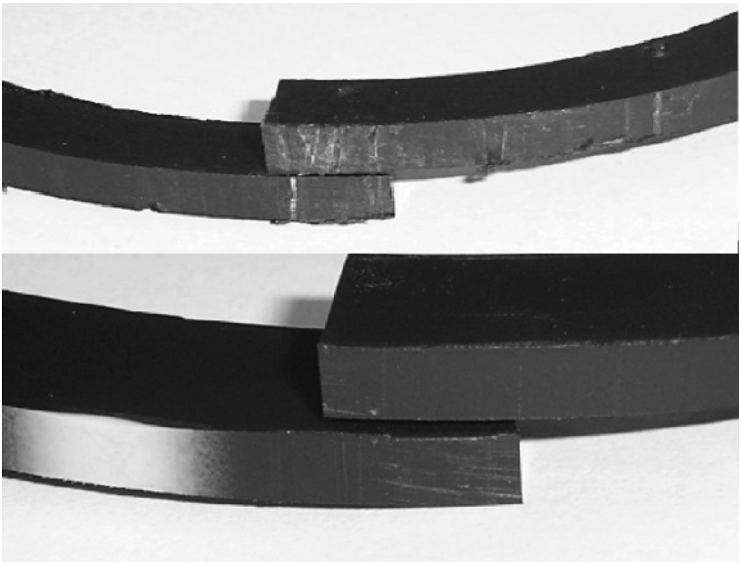

Figure 18. HDPE pipe ring under residual deformation for PE 80 (Gas) and PE 100 (Water).

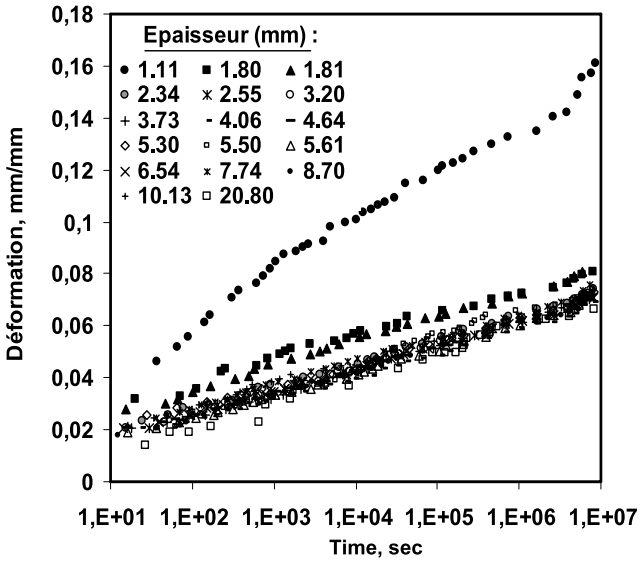

Figure 19. Deformation as a function of time and ring width.

In order to materialize such an idea [35], rings were machined out of a HDPE pipe, sliced longitudinally and set to deform in the circumferential direction as shown in Figure 18. The deformations (ε) are measured and plotted

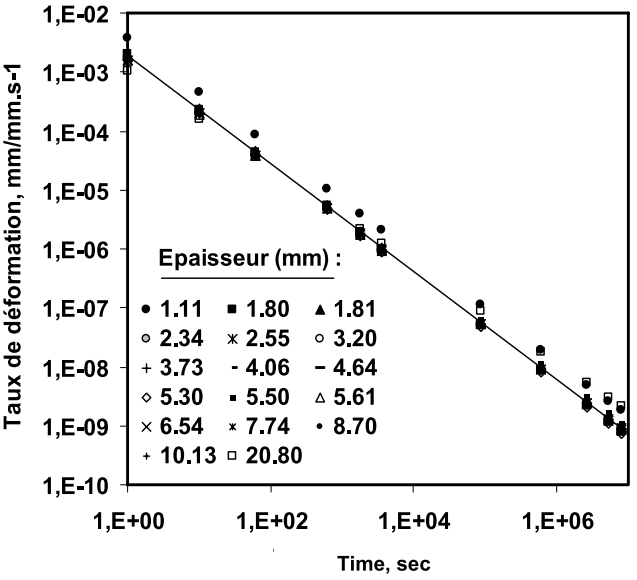

Figure 20. Rate of deformation as a function of time and ring width.

against elapsed time (t). The results are presented in Figures 19 and 20. It is found that deformation-time curves are similar to those of creep of semicrystalline viscoelastic materials.

The results are well described by the following mathematical models that are commonly used in describing creep studies:

$$\varepsilon = A \cdot t^{n} \tag{8}$$

and

$$\varepsilon = B + C \cdot Ln(t) \tag{9}$$

where A, B, C, and n are parameters specific to the material PE obtained by treatment of the measured deformations. In this case, the applied load is represented by the residual stress already present in the tube. The variation of the deformation as a function of ring width can be explained by the effect of the stress state. The rate of deformation ($d\varepsilon/dt$) was defined as being the first derivative of the deformation-time curve. This rate is inversely proportional to time, which corresponds at the first stage of creep where the rate of deformation continues to decrease. As the measured deformation is due to modifications and

rearrangements within the bulk of a finite number of macromolecular chains, the rate of deformation must decrease with time and will tend to vanish. The values of constants A, B, C, and exponent n are tabulated in literature [35].

7. Mechanical Properties Evolution

Figure 21 illustrates a typical set of stress–strain curves of specimens obtained from a filament machined throughout a HDPE pipe. Three distinctive zones characterized the behavior [28]: (i) a linear elastic region, (ii) a cold-drawing region, and (iii) an ultimate material tearing coupled with failure. This curve intrinsically identifies the mechanical behavior of semicrystalline polymers, which are normally more ductile, especially between the glass-transition temperature and the melting temperature, and undergo cold drawing before ultimate failure. Additionally, a trend is being followed as the measurements moved from the inner layer toward the outer one. For the elastic modulus (Figure 22) and stress at yield there were clear increase from the inner pipe layers toward the outer layers, and within the region between 30% and 70% of the pipe thickness, a plateau was observed; it probably indicated a zone that was not readily affected by transient heat transfer during extrusion, especially for pipes obtained from the melt and rapidly water cooled from the external surface. On the other hand, the inner surface had enough time to cool down by free convection. Alternatively, in other cases, the onset of drawing was characterized by multiple necking locations independently evolving and then merging together. Although plastic flow took place, the crystallites became deformed plastically and underwent plastic shearing localized in slip planes. The plastic hardening was ascribed not only to a weak share of crystalline plasticity consolidation but also to the strong entropic effects of the molecular orientation in the amorphous phase and then in the crystallites themselves.

For large plastic deformations, the chains also underwent a progressive orientation, and so their later distortion became increasingly difficult. This required an increase in the strain-hardening stress, and the crystallites finally split into a strongly anisotropic fibrous texture oriented in the direction of traction. Final fiber rupture occurred by large-scale deformations and locally cracked fibers. Using Statistica software (version 5.1), the goodness of fit was tested with the Fisher–Snedecor test for a preset probabilistic error level of $p \leq 0.05$. The accepted correlations are shown with an asterisk in Table 3.

To confirm the usefulness of the approach with statistical analysis, we observed that stress and strain at the yield point presented an acceptable correlation

(Figure 23) while both E and σ_y correlated very well with increasing pipe wall thickness. Consequently, a plot of yield stress as a function of E was constructed and compared with data from the literature (Figure 24). We concluded that the linear relationship between these two mechanical properties was preserved in this approach. The correlation governing this relationship for PE 80 is:

$$\sigma_y = 0,0152E + 4,2367 \tag{10}$$

TABLE 3. Determination coefficients and <p> values for selected variables.

	Position inside pipe wall	Young's modulus	Yield stress _0.2%	Stress Max	Sigma CD	Stress failure	Strain yield	Strain failure	ΔStrain CD
Young's modulus	0.772* p = 0.0001	–							
Yield stress _0.2%	0.725* p = 0.0005	0.881* p = 0.0000	–						
Stress max	0.784* p = 0.0004	0.878* p = 0.0007	0.972* p = 0.0000	–					
Sigma CD	0.861* p = 0.0000	0.886* p = 0.0005	0.929* p = 0.0000	0.967* p = 0.0000	–				
Stress failure	0.343* p = 0.0223	0.334* p = 0.0273	0.151 p = 0.3271	0.199 p = 0.1968	0.249 p = 0.1029	–			
Strain yield	–0.358* p = 0.0177	–0.453* p = 0.0022	–0.718* p = 0.0008	–0.669* p = 0.0009	–0.589* p = 0.0009	0.190 p = 0.2170	–		
Strain failure	–0.284 p = 0.0624	–0.224 p = 0.1444	–0.253 p = 0.0982	–0.232 p = 0.1301	–0.281 p = 0.0651	0.565* p = 0.0004	0.200 p = 0.1930	–	
ΔStrain CD	0.503* p = 0.0003	0.538* p = 0.0008	0.623* p = 0.0003	0.645* p = 0.0005	0.632* p = 0.0002	–0.206 p = 0.1796	–0.511* p = 0.0001	–0.349* p = 0.0208	–
Cristallinity	0.923* p = 0.0000	0.633* p = 0.0003	0.596* p = 0.0005	0.643* p = 0.0003	0.710* p = 0.0009	0.382* p = 0.010	–0.270 p = 0.0760	–0.250 p = 0.1020	0.306* p = 0.0436

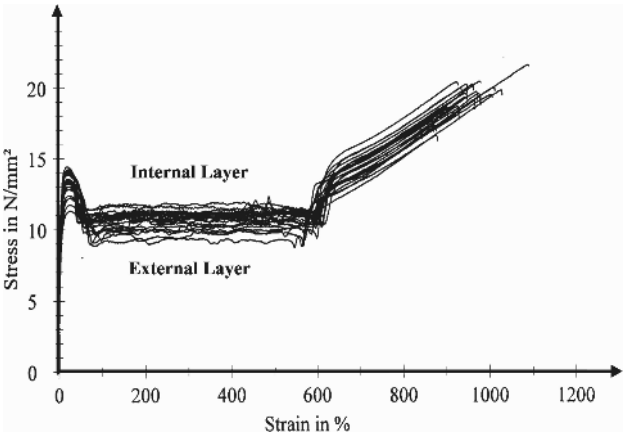

Figure 21. Comparison of stress–strain curves from inner to outer HDPE pipe layers.

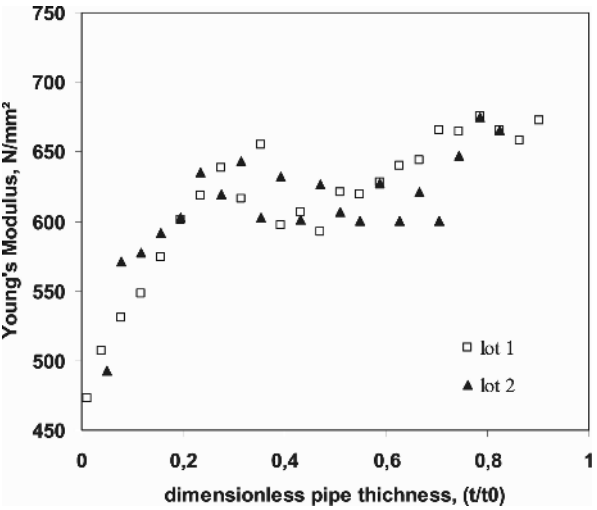

Figure 22. Young's modulus evolution as a function of pipe thickness in air.

For the testing conditions adopted here and recent measurement of crystallinity across pipe wall, it is found that a good correlation exists with thickness [36] (Table 3). This result should be integrated as new evidence in the assessment of long-term strength and is to be closely correlated with internal stresses.

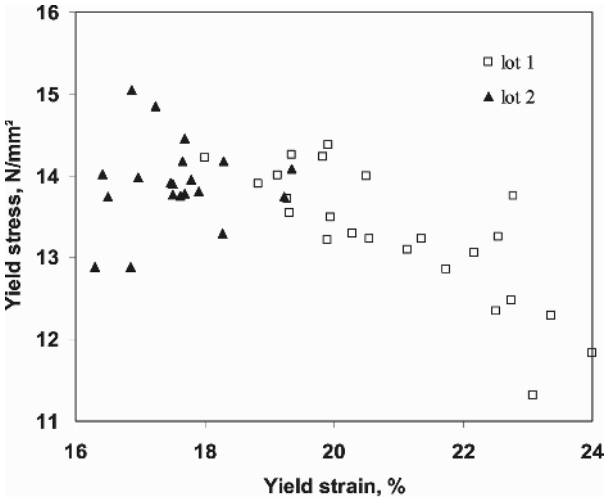

Figure 23. Relationship between stress and strain at yield in air.

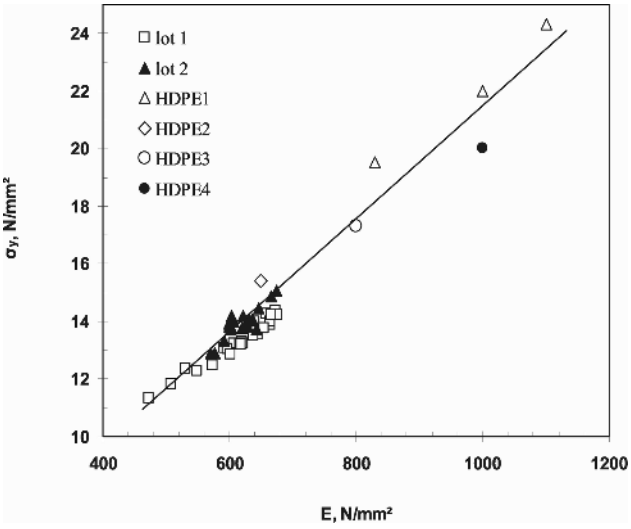

Figure 24. Linear correlation between young's modulus and stress at yield in air.

8. Environmental Stress Cracking (ESC)

Perhaps this topic is the most complicated when considering mechanisms of failure in PE pipes. It is a mixture of aspects in connection with material integrity, environment parameters and the stress–strain relationship (Figure 25). Environmental stress cracking (ESC) occurs when PE is subjected to a combination of a stress field and an environmental agent (chemical). Although, fundamental molecular mechanism of ESC in PE is still discussed; nevertheless, both ESC and SCG share many similarities, such as load and temperature dependence of failure time, and brittle-like failure surface. Therefore, it is thought that they probably have a common microscopic deformation mechanism that governs failure. If so, it would be valuable to use ESC as a tool to evaluate the long-term behavior of PE material, since the ESC times are much shorter compared to other tests [7, 9, 15, 20]. The acceleration process is supposed to be due to the pressure of aggressive agents and to diffusion and/or absorption within crystallites.

Again, machined filaments are exposed to both ambient air and to some organic solvents in order to study the effect of SC. From stress–strain analysis, typical curves as in Figure 21 are obtained. Part of results analysis is shown in Figure 26 based on young's modulus calculations.

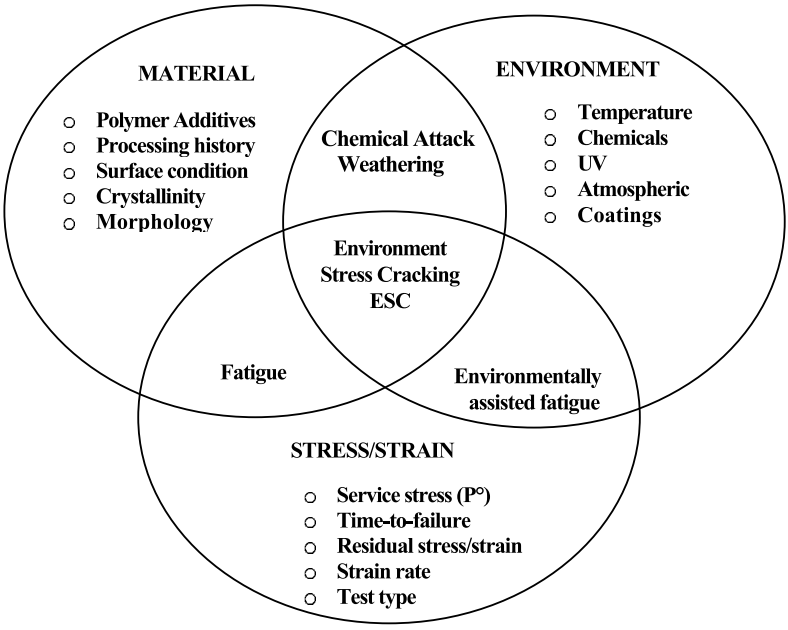

Figure 25. Interaction between material integrity, environmental parameters, and the stress–strain relationship in ESC of PE pipes.

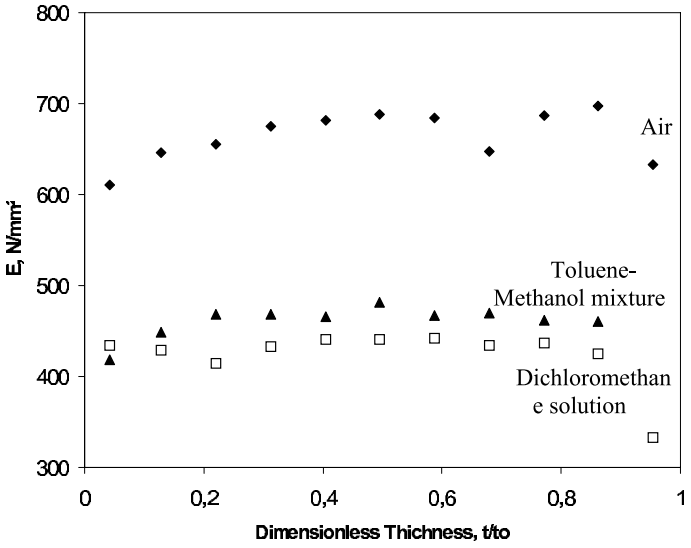

Figure 26. Comparison of Young's modulus evolution in air and in controlled aggressive environments as a function of pipe thickness.

Figure 27. Electrofusion join deformation upon cutting in longitudinal direction.

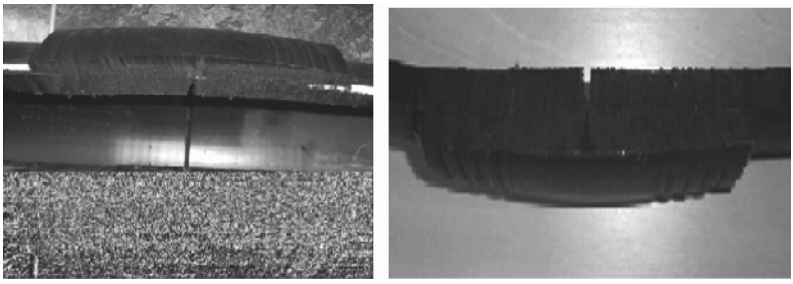

Figure 28. Gap in an electrofusion join.

It is concluded that both solvents (mixture of toluene-benzene and dichloromethane solution) are very aggressive to PE pipe materials as E dropped by almost one half of its value in air after an [37]. The problem is that those solvents could be present in natural gas streams and might degrade irreversibly the pipe. Another issue that needs attention is PE pipe weldability since different polymeric phases are brought together in the melt state (Figures 27 and 28). Here, we may obtain residual stresses and morphology variations which will complicate further the behavior for long term. The evolution of crystallinity should also be studied and how it is redistributed after welding; many aspects have to be considered such as the knowledge of thermal history, the degree of molecular interpenetration from both melts and the role of pigments and some additives [38].

9. Concluding Remarks

PE pipes in the gas and water industries have open wide many fields of research. World production of PE is an important indication on how this material became part of our life and our industries. Technical developments are found in long-term performance evaluation and how research is trying to bridge between different approaches such as fatigue and creep. Mechanisms of failure of PE pipes are basically driven toward the understanding of brittleness, as it is the most dangerous for the integrity of a PE underground structure. The study of brittle to ductile transition is a potential way to establish PE toughness from short-term fatigue tests. The assessment of residual stresses and morphology variances is relevant to model and to predict lifetime under creep or fatigue. Finally, ESC of PE remains the most critical issue to settle since many questions remain unanswered if not clearly asked.

References

1. Sonelgaz National Company, Algiers (December 2006); http://www.sonelgaz.dz.
2. The Plastic Pipe Institute, Nature of Hydrostatic Stress Rupture Curves, Technical Note TN-7/2000, p. 11.
3. W. G. Perkins, Polymer Toughness and Impact Resistance, *Polym. Eng. Sci.* 39(12), 2445–2460 (1999).
4. R. Seguela, Critical Review of the Molecular Topology of Semicrystalline Polymers: The Origin and Assessment of Intercristalline Tie Molecules and Chain Entanglements, *J. Polym. Sci. Part B: Polym. Phys.* 43, 1729–1748 (2004).
5. C. J. G. Plummer, A. Goldberg, and A. Ghanem, Micromechanisms of SCG in PE under Constant Tensile Loading, *Polymer* 42, 9551–9564 (2001).

6. M. Fujikake, M. Fukumura, and K. Kitao, Analysis of the Electrofusion Joining Process in PE Gas Piping System, *Comput. & Struct.* 64(5/6) 939–948 (1997).
7. B-H. Choi, Z. Zhou, A. Chudnovsky, S. S. Stivala, K. Sehanobish, and C. P. Bosnyak, Facture Initiation Associated with Chemical Degradation: Observation and Modeling, *Int. J. Solid. And Struct.* 42, 681–695 (2005).
8. J. F. Mano, R. A. Sousa, R. L. Reis, A. M. Cunha, and M. J. Bevis, Viscoelastic Behaviour and Time-temperature Correspondence of HDPE with Varying Levels of Process-induced Orientation, *Polymer* 42, 6187–6198 (2001).
9. U. W. Gedde, J. Viebke, H. Leijstrom, and M. Ifwarson, Long-term Properties of Hot-water Polyolefin Pipes: A Review, *Polym. Eng. Sci.* 34(24), 1773–1787 (1994).
10. P. T. Reynolds and C. C. Lawrence, Deformation and Failure in Polyethylene: Correlation Between Mechanisms of Creep and Fatigue, *J. Mater. Sci.* 26, 6197–6202 (1991).
11. Y. Zhou and N. Brown, Anomalous Fracture Behaviour in Polyethylenes under Fatigue and Constant Load, *J. Mater. Sci.* 30, 6065–6069 (1995).
12. M. Parsons, E. V. Stepanov, A. Hiltner, and E. Baer, Correlation of Fatigue and Creep SCG in MDPE Pipe Material, *J. Mater. Sci.* 35, 2659–2674 (2000).
13. M. Parsons, E. V. Stepanov, A. Hiltner, and E. Baer, The Damage Zone Ahead of the Arrested Crack in PE Resins, *J. Mater. Sci.* 36, 5747–5755 (2001).
14. Société Française de Chimie, Paris (December 2006); http://Erreur ! Référence de lien hypertexte non valide.
15. J. Zhang, Experimental Study of Stress Cracking in High Density Polyethylene Pipes, Ph.D. thesis, Drexel University, (Philadelphia, PA, 2005).
16. Y. G. Hsuan and T. J. McGrath, HDPE Pipe: Recommended Material Specifications and Design Requirements, Report 429, NCHRP, (1999).
17. E. F. Palermo and I. K. DeBlieu, Rate process concepts applied to hydrostatically rating PE pipes, 9th Plastic Fuel Gas Pipe Symposium, (AGA, New Orleans, 1985), pp. 215–240.
18. K. G. Toll, E. F. Palermo, and G. T. Appleton, Using laboratory tests on PE piping systems to solve gas distribution engineering problems, 11th Plastic Fuel Gas Pipe Symposium, (AGA, New Orleans, 1987), pp. 143–161.
19. T. Trankner, M. Hedenqvist, and U. W. Gedde, Structure and Crack Growth in Gas Pipes of Medium and High Density PE, *Polym. Eng. Sci.* 36(16), 2069–2076 (1996).
20. A. L. Ward, X. Lu, and N. Brown, Accelerated Test for Evaluating Slow Crack Growth of Polyethylene Copolymers in Igepal and Air, *Polym. Eng. Sci.* 30(18), 1175–1179 (1996).
21. H. B. H. Hamouda, M. Somoes-betbeder, F. Grillon, P. Blouet, N. Billon, and R. Piques, *Polymer* 42, 5425–5437 (2001).
22. D. T. Raske, Analysis and application the CTL test for polyethylene gas pipe materials, 11th Plastic Fuel Gas Pipe Symposium, (AGA, New Orleans, 1987), pp. 102–116.
23. J. J. Strebel and A. Moet, Accelerated Fatigue Fracture of PE Pipe Material: Crack Layer Analysis, *Int. J. Fract.* 54, 21–34 (1992).
24. K. Chaoui and A. Moet, A Fatigue Accelerated Test Method to Rank Plastic Piping Materials, in: Recent *Advances in Experimental Mechanics*, *Proc. 10th Inter. Conf. on Experimental Mechanics*, Silva Gomes et al., Editors, (Lisbon, Portugal, 1994), pp. 1271–1275.
25. R. Khelif, A. Chateauneuf, and K. Chaoui, Statistical Analysis of HDPE Fatigue Lifetime, *Polym. Test.*, (2006).
26. R. Khelif, N. Zeghib, K. Chaoui, and M. Naït-Abdelaziz, Critical Energy Analysis of Fatigue Brittle to Ductile Transition in PE Gas Pipe Materials, *J. Eng. & Appl. Sci.* 1(4), 462–467 (2006).
27. K. Kadota, S. Chum, and A. Chudnovsky, Bridging the PE Lifetime under Fatigue and Creep Conditions with its Crystallisation Behavior, J. *Appl. Polym. Sci*. 49, 863–875 (1993).

28. N. Kiass, R. Khelif, L. Boulanouar, and K. Chaoui, An Experimental Approach to Mechanical Properties Variability Through HDPE Pipe Wall, *J. Appl. Polym. Sci.* 97, 272–281 (2005).
29. D.-M. Duan and J. G. Williams, Craze Testing for Tough Polyethylene, *J. Mater. Sci.* 33, 625–638 (1998).
30. X. Lu and N. Brown, Abnormal Slow Crack Growth in PE, *Polymer* 38(23), 5749–5753 (1997).
31. K. Kitao, A Study of Brittle-ductile Transition in Polyethylene, *Polym. Eng. Sci.* 37(5), 777–788 (1997).
32. R. K. Krishnaswany, Analysis of Ductile and Brittle Failures from Creep Rupture Testing of HDPE Pipes, *Polymer* 46, 11664–11672 (2005).
33. P. A. O'connell, R. A. Dukett, and I. M. Ward, Brittle-ductile Transition in Polyethylene, *Polym. Eng. Sci.* 42(7), 1493–1508 (2002).
34. N. W. Klingbeil, A Total Dissipated Energy Theory of Fatigue Crack Growth in Ductile Solids, *Int. J. Fatigue*, 25, 117–128 (2003).
35. N. Kiass et K. Chaoui, Étude des déformations résiduelles dans les tubes en HDPE, *Revue Sciences et Technologie B*, *Université de Constantine* 22, 79–85 (2004).
36. N. Kiass, R. Khelif, B. Bounamous, A. Amirat, and K. Chaoui, Etude expérimentale des propriétés mécaniques et morphologiques dans un tube de gaz en HDPE-80, *Mécanique & Industries* article mi0041-2004, under press.
37. S. Rehab and K. Chaoui, Environmental stress cracking of HDPE grade 80 and 100 in chemical solvents, to be published.
38. K. Leskovics, M. Kollár, and P. Bárczy, A Study of Structure and Mechanical Properties of Welded Joints in Polyethylene Pipes, *Materials Science and Engineering* A 419, 138–143 (2006).

STABLE AND UNSTABLE CRACK GROWTH IN PIPES

V.T. SAPUNOV
Moscow Engineers and Physicians Institute
31, Kachirskoe Chosse. 115409, Moscow, Russia

Abstract: For pipe containing surface cracks, the possibility to build in subcritical and critical fracture diagrams is realized by calculation. Fracture and leak conditions for a pipe are presented as generalized fracture diagram which makes possible to determine the admissible dimensions of surface cracks for service regime.

Keywords: pipe, surface crack, subcritical growth of a crack, diagrams of fracture, generalized diagram of fracture

Pipes defects occur at different stages of production, construction, or repair, as well as those obtained in service. Development of crack from surface or through walls results in pipe fracture or leak. It is possible to assert, that presence of pipe defects (cracks) is the first of principal causes of fracture and the second one is the insufficient ductility of steel and its ability to resist to emerging and development of defects (cracks).

From the point of view of maintenance for safe operation of the pipe, the greatest interest is represented by the stage of the subcritical development of a crack associated with fracture initiation (the beginning of unstable development of a crack). Accordingly, it is important to obtain answers to the following questions:

- What are the critical dimensions of a crack?
- What way subcritical growth of a crack from initial size (found out or prospective) up to critical (inadmissible) size?
- How to determine the crack size for leak or fracture?

Some answers to these questions are presented in this paper.

G. Pluvinage and M.H. Elwany (eds.), Safety, Reliability and Risks Associated with Water, Oil and Gas Pipelines, 165–182.

1. Build-in of Subcritical and Critical Fracture Diagrams for a Cracked Body

Criteria of linear and nonlinear fracture mechanics describe the critical state of equilibrium (limiting state) of a body containing a macroscopical crack. In other words, if in a body there is a crack with length l_0 the chosen criterion gives value of critical load p_{cr} for this crack. Note that the initial crack length is considered to be a critical crack and starting one when the crack is unstable. Such case is relative to brittle fracture of a cracked body with.

Let us note that it is necessary to distinguish the stress state of the material (elastic or elastic-plastic) and the fracture criterion. Criteria such as $K_{\text{I}} = K_{\text{Ic}}$, $J_{\text{I}} = J_{\text{Ic}}$ are related to different stress states, but they use the same crack propagation model of brittle fracture described above.

For real materials being in overwhelming majority of cases elastic-plastic, the steady subcritical crack growth increases from of its initial length l_0 up to its critical one l_{cr}.

Introduction of subcritical crack growth concept needs two criteria: criterion for crack initiations that determine the initial condition of subcritical growth of a crack, and fracture criterion as condition of transition from stable to unstable crack growth. Different initial conditions of crack development (according to the first criterion) are shown in Figure 1: curve 1 corresponds to the case of crack starting at load $p_{\text{st}} \neq 0$, curve 2 corresponds to the case of $p_{\text{st}} = 0$.

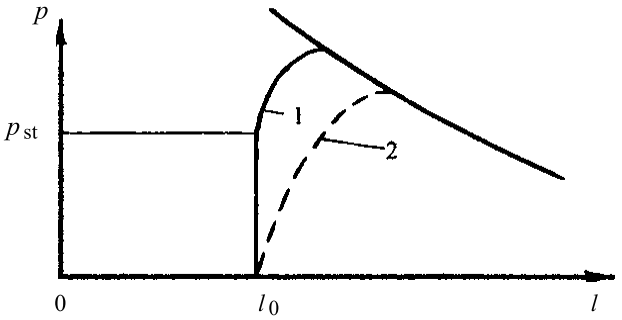

Figure 1. Subcritical growth of a crack at different initial conditions.

The representation of the mathematical relationship between external load *p* and macro crack length *l* (subcritical growth crack curves of types 1 and 2 in Figure 1) is named the subcritical fracture diagram. The limit states curve is as the critical fracture diagram.

Fracture diagrams indicates material resistance to crack development and can be used serve, on the one hand, as estimate characteristic for the choice of

the material, and on the other hand as the basis for design of a structural element exhibited a crack since it makes possible to estimate fracture kinetics. Fracture diagrams are obtained experimentally by the means of equipment recording crack extension. They can also be determined by means of calculations.

Possibility of computing subcritical crack growth and fracture diagrams is obtained using an energetic fracture criterion in integrated form [1] as is shown in [2, 3] where the above mentioned criterion is written as follows:

$$\delta \int_0^l \left(2\gamma - \sigma_y v \right) dx = 0 \tag{1}$$

Here δ is the variation operator; $\sigma_y = \sigma_y(x)$ is the applied stress from external loading in an un cracked body acting on the crack sides (the x axis coincides with the direction of the crack) and opens this crack; $v = v(x, l)$ is the displacement of points of the crack; 2γ is the fracture surface energy. The resulted equation approximately takes into account the existence of a thin plastic zone area ahead of the crack tip, we assumes that the following crack opening displacement COD $v = v(l, l)$ is not equal to zero.

Eq. (1) can be used for calculation of the subcritical diagram with $\delta = \left(\frac{\partial}{\partial l} + \frac{\partial}{\partial p} \cdot \frac{dp}{dl} \right) \delta l$ and the critical one with at $\delta = \frac{\partial}{\partial l} \delta l$, where p is the external load parameter: $\sigma_y(x) = p\, f(x)$.

The use of eq. (1) for construction of fracture diagrams required the preliminary definition of COD function $v(x, l)$ for given body, geometrical, configuration and given loading which is in many cases, complicate. Introduction into eq. (1) of stress intensity factor (SIF) K_{I} allows us to simplify substantially the problem since, on the one hand, it takes into account the geometrical body and loading configurations and, on the other hand, for many structure components and modes of loading K_{I} is either known or easily calculated with the use of numerical methods, for example, the Finite Elements method (FEM). Omitting intermediate transformations and accepting $2\gamma = G_c$ we have:

- For the critical fracture diagram

$$G_c \left[1 - \frac{\sigma_y^2(l)}{\sigma_0^2} \right] - \frac{K_{\mathrm{I}}^2}{E} = 0 \tag{2}$$

- For the fracture subcritical diagram

$$\frac{dp}{dl} = \frac{G_c\left[1 - \dfrac{\sigma_y^2(l)}{\sigma_0^2}\right] - \dfrac{K_1^2}{E}}{\dfrac{2}{E}\int K_1 \dfrac{\partial K_1}{\partial p}\,dl + \dfrac{2G_c}{\sigma_0^2}\int \sigma_y(l)\dfrac{\partial \sigma_y(l)}{\partial p}\,dl} \tag{3}$$

Here σ_0 is flow stress of the material, a mean value of the yield stress σ_Y and ultimate strength σ_{ul} of the material $\sigma_Y \le \sigma_0 \le \sigma_{ul}$. Experience on fracture diagram construction shows better agreement between calculated and experimental results when $\sigma_0 = \sigma_{ul}$. Since eq. (2) derives from eq. (3) for $dp/dl = 0$, the critical fracture diagram can be built as the geometrical location of maxima of subcritical fracture diagrams.

The use of eq. (3) for construction of fracture diagrams by computing needs the SIF formula for the considered cracked body for a given loading, the stress distribution $\sigma_y(x)$ and the material mechanical characteristics $\sigma_{ul}(\sigma_Y)$, E, G_c (K_{Ic}). It is easy to see that the main difficulty here is the preliminary derivation of the formula for the SIF.

The initial condition for solution of eq. (3) for construction of fracture diagrams can be presented as:

$$l(0) = l_0,\ p(l_0) = p_{st} \tag{4}$$

Determination of starting load is a separate problem. As a variant of its solution, we can consider a similar equation to fracture diagram (2), but written newly with $\sigma_0 = \sigma_Y$,

$$1 - \frac{\sigma_y^2(l_0)}{\sigma_Y^2} - \frac{K_1^2(l_0)}{K_{Ic}^2} = 0 \tag{5}$$

where $K_{Ic}^2 = EG_c$. The analogy is pertinent from physical reasons. If fracture as a critical state is defined by ultimate strength $\sigma_0 = \sigma_{ul}$, then condition of crack initiation (being also critical) could be defined by the yield stress limit $\sigma_0 = \sigma_Y$.

The obtained eqs. (3)–(5) are easily transformed into dimensionless form by introduction of the following dimensionless parameters:

$$\lambda = p/\sigma_0,\ \zeta = l/\bar{c},\ \bar{c} = \pi K_{Ic}^2/8\sigma_{ul}^2,\ K_0 = K_I/K_{Ic} \tag{6}$$

Thus, for construction of subcritical fracture diagrams by calculation it is necessary to solve the integro-differential eq. (3) for a zero starting load or for a starting load p_{st} determined by initial condition (5).

2. Calculations of Pipes of Nuclear Energy Installations

Experiences in service conditions on pipes of small, as well as big diameters on nuclear power plants shows, that service failure with formation of cracks leading to leak-or-break are not hypothetic events.

Study of fracture and leak conditions has been carried out with on a ∅500 pipe of the nuclear power plant VVER-440 (Russia) exhibiting superficial cracks at different operational regimes. The material of the pipeline is OX18H12T steel having the following characteristics:

- At $T = 20°C$: the yield stress limit is equal to $\sigma_Y = 270$ MPa (with deviations up to 18%); the ultimate strength equal $\sigma_{\text{ul}} = 550$ MPa (with deviations up to 12%); the Young's equals $E = 2 \cdot 10^5$ MPa; the Poisson ratio equals $\nu = 0{,}3$; the fracture toughness $K_{Ic} = 93\ \text{MPa}\sqrt{\text{m}}$
- At $T = 130°C$: $\sigma_Y = 186$ MPa; $\sigma_{\text{ul}} = 436$ MPa; $E = 1.97 \cdot 10^5$ MPa; $\nu = 0.3$
- At $T = 300°C$: $\sigma_Y = 172$ MPa; $\sigma_{\text{ul}} = 377$ MPa; $E = 1.84 \cdot 10^5$ MPa; $\nu = 0.3$

For stress analysis and calculation of fracture mechanics parameters of the FEM is used. FEM is done with original developments such as an envelope special final element, the weight functions method, the crack rod model and corresponding complex program [4].

For analysis of the subcritical growth and estimation of critical states in a cracked pipe ∅500 the Irwin criterion and the energetic fracture criterion as eqs. (3)–(5) are used.

2.1. PIPE CONTAINING A SEMI-ELLIPTIC LONGITUDINAL SURFACE CRACK

Study of fracture and leak conditions for of different parts of a pipe under static loading was performed for the following three service regimes:

- Normal operational conditions characterized by internal pressure $p = 12.5$ MPa and uniform temperature field $T = 300°C$
- Proof tests characterized by pressure $p = 17.5$ MPa and uniform temperature field $T = 130°C$
- Emergency regime for triggering the pipeline protection at pressure $p = 12.5$ MPa and temperatures on external and internal surfaces respectively 300°C and 290°C (temperature gradient across the wall thickness $\Delta T = 10°C$).

2.1.1. *FEM SIFs Calculation for Straight and Curved Parts of the Pipeline with Surface Longitudinal Cracks*

Straight part of the pipe. A straight part of a ∅500 pipe is represented by a cylindrical envelope with internal radius R_{int} = 248 mm and wall thickness t = 32 mm. Envelope length is equal to 1,600 mm. Surface semi-elliptic longitudinal cracks located on the internal surface of the pipe were examined. Three series of cracks with the following dimensions c.=.64, 128, and 192 mm (c is the greater semi-axis of the ellipse) and relative crack depth $a/t = 0.1$; 0.25; 0.5, and 0.75 were analyzed.

Preliminary calculations have shown, that temperature gradient drop $\Delta T = 10°\text{C}$ across the wall thickness practically does not influence the SIF, so only the internal pressure loading is considered.

It is convenient to present the calculated values of SIF in the following dimensionless form:

$$\overline{K}_{\text{I}} = K_{\text{I}} / \left(\frac{pR_{\text{int}}}{t} \sqrt{\pi a} / \Phi \right) \tag{7}$$

where Φ is the second species full elliptic integral.

As an example values $\overline{K}_{\text{I}}$ are presented in Table 1 as function of dimensionless coordinate x/c, started from the deepest point of the crack front along the greater semi-axis and for different values of the relative depth a/t (c = 192 mm).

TABLE 1. SIFs for an internal longitudinal surface crack (c = 192 mm) in a straight part of a pipe.

a/t	$\overline{K}_I$							
	x/c							
	0	0.125	0.250	0.375	0.500	0.625	0.750	0.875
0.10	1.24	1.22	1.20	1.16	1.12	1.05	0.96	0.80
0.25	1.47	1.41	1.37	1.33	1.25	1.16	1.04	0.88
0.50	1.98	1.93	1.88	1.81	1.71	1.57	1.43	1.21
0.75	2.42	2.41	2.39	2.32	2.22	2.05	1.81	1.49

Let us note, that the greatest value of SIF for a surface crack with semi-axis c = 192 mm and relative depth a/t = 0.75 at pressure p = 17.5 MPa equals 89 MPa$\sqrt{\text{m}}$, that is equivalent to the SIF value for a through longitudinal crack with length l = 58 mm.

Curved part of the pipe. It should be noted that calculation of formulas for the SIF for cracks in the curved part of the pipe with circular cross section is carried out using relationships for determining stress state of a toroidal envelope, i.e., the curved part of the pipe is considered as a part of a tore. Here the greatest stresses under at loading by internal pressure occur on the tore internal contour. But operational practice of curved pipes shows that surface damages (cracks) appear usually on the external surface of the tore external contour. That emphasizes the necessity to consider a curved part as a part of the entire pipe and introduction of the corresponding boundary conditions. The schematic of half of the curved part ($-\pi/4 \le \theta \le \pi/4$) and the imposed boundary conditions are presented in Figure 2.

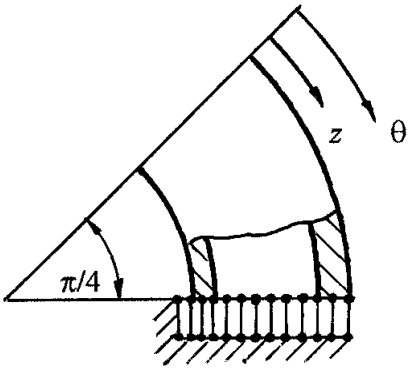

Figure 2. Schematic of half of the curved part and the imposed boundary conditions.

The calculation model of the curved pipe part of diameter ∅500 includes a radius of curvature R_0 = 650 mm. The internal radius of the envelope is equal to R_{int} = 248 mm, the wall thickness equals to t = 50 mm. The semi-elliptic cracks located on the external surface of the external contour of the curved part, were considered as the most dangerous. They have the following parameters: dimensions of the greater semi-axis c = 75, 125, and 175 mm and the relative depth a/t = 0.1; 0.25; 0.4; 0.5; 0.6, and 0.7.

For example, in Figure 3 the SIF $\overline{K}_{\text{I}}$ (7) versus the dimensionless coordinate z/c, which starts from the deepest point of the crack front along the greater semi-axis on external contour of the curved part here c = 75 mm and values of the relative depth are taken as above a/t (curve 1 – a/t = 0.1; curve 2 – 0.25; etc.).

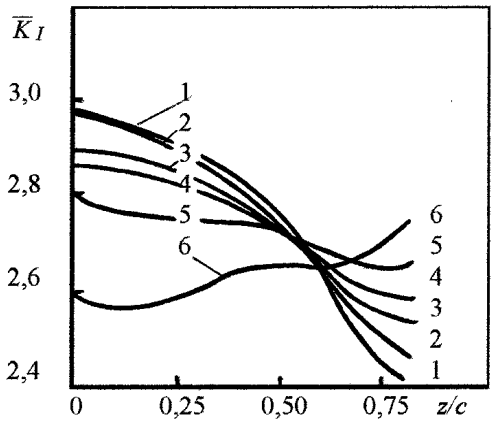

Figure 3. SIFs for a longitudinal internal surface crack (c = 75 mm) in the curved part of the pipe.

From Figure 3 it is clear, that over the coordinate variation interval $0 \le z/c \le 0.4-0.5$ $\overline{K}_{\mathrm{I}}$ values decrease with crack depth growth. That SIF behavior is typical rather for short cracks. It could be explained by the distribution law of hoop stress across the wall thickness of the curved part. On the external side of the curved part tensile stresses are observed where as on the internal one compression stresses are present. In case of short cracks; the contribution of tensile stresses is comparable to the influence of compression stresses. For long cracks (in our case c = 125 and 175 mm), the influence of tensile stresses is prevailing and the SIFs increases with crack depth. Note, that the greatest SIF value, for surface crack with semi-axis c = 175 mm and relative depth a/t = 0.7 for a pressure p = 12.5 and 17.5 MPa are equal to 73.7 and 103.2 MPa$\sqrt{\mathrm{m}}$ respectively.

The surface crack of growth in a curved part can be drawn by the way of Irwin criterion $K_{\mathrm{I}} = K_{\mathrm{I}c}$ and increase of K_{I} with crack growth is presented in Figure 3. At beginning, crack increases in depth. After achievement of some depth, the maximum value of K_{I} (as can be seen from Figure 3), is displaced from the deepest point of the crack front to its surface, and the crack starts to grow in length. After achievement of some length the crack is growing in depth again, etc. This process explains the existence of the long superficial cracks in the curved part which are observed in practice.

By comparison of SIF values for surface cracks in the curved part and linear part of the pipe ∅500 with loading by internal pressure, it is possible to turn into conclusion, that the curved part has smaller brittle fracture resistance than the linear one.

2.1.2. *Construction of Fracture Diagrams for Pipe Parts Based on Calculation*

Complete comprehension of the fracture process kinetic for static loading is based on the subcritical fracture diagram. For a cracked cylindrical envelope loaded by internal pressure, the subcritical crack growth eq. (3) can be rewritten as

$$\frac{d\sigma_\theta}{dl} = \frac{1}{2} \cdot \frac{1 - \dfrac{\sigma_\theta^2}{\sigma_0^2} - \dfrac{K_I^2}{K_{Ic}^2}}{\dfrac{\sigma_\theta}{\sigma_0^2} \cdot l + \displaystyle\int_0^l \frac{K_I}{K_{Ic}^2} \cdot \frac{\partial K_I}{\partial \sigma_\theta}\, dl} \tag{8}$$

Here σ_θ is the hoop stress of a noncracked envelope and, acting on facets located along crack line and perpendicular to this line. The critical fracture diagram is obtained from (8) for $d\sigma_\theta / dl = 0$. Note that on the internal surface of a cylindrical envelope, the hoop stress σ_θ can be determined by formula $\sigma_\theta = pR_{av} / t$ with 0.3% error.

Constructions of subcritical and critical fracture diagrams based on calculation are made by taking $\sigma_0 = \sigma_{ul}$ in the eq. (8) and using two different starting conditions for subcritical cracks. In one case, the starting stress $p_{st} = \sigma_{st}$ is assumed to be equal zero, and in the other one is determined from the condition

$$1 - \frac{\sigma_{st}^2}{\sigma_Y^2} - \frac{K_I^2\left(\sigma_{st}, l_0\right)}{K_{Ic}^2} = 0 \tag{9}$$

2.1.3. *Fracture and Leak Conditions for a Surface Longitudinal Crack under Static Loading*

MFE-calculations of SIF for longitudinal semi-elliptic surface cracks in a straight part of a pipe ∅500 gave a discrete set of SIF values that is to be expressed as an analytical function for its use fracture diagrams construction. For the case of a straight part of a pipe, the following known relation [5] would be used

$$K_1 = \frac{pR_{\text{int}}}{t}\sqrt{\frac{\pi a}{Q}} \cdot F\left(\frac{a}{c}, \frac{a}{t}\right), \; Q = 1 + 1,464\left(a/c\right)^{1,65} \tag{10}$$

The correction function F valid for $a/t < 1$ and $0.2 \le a/c \le \infty$ is determined by the formula

$$F = 0,97 f_c \left[M_1 + M_2 \left(a/t\right)^2 + M_3 \left(a/t\right)^4 \right]$$

where

$$f_c = 1,152 - 0,05\sqrt{a/t}$$

$$M_1 = 1,13 + 0.09\left(a/c\right)$$

$$M_2 = -0,54 + 0,89/\left[0,2 + \left(a/c\right)\right]$$

$$M_3 = -0,5 - 1/\left[0,65 + \left(a/c\right)\right] + 14\left[1 - \left(a/c\right)\right]^{24}$$

Comparison of SIF values obtained with relation (10) and with the numerical solution shows that the relation (10) yields some overestimated results. However, the maximal error does not exceed 10%. It should be noted, that formula (10) takes into account the pressure on crack surfaces, whereas MFE-calculation does not take it into account.

The determination of the critical dimensions of a surface crack for straight part of a pipe will be performed according to the following scheme. Specifying the calculated pressure and one parameter (one of semi-axis) of the examined semi-elliptic crack (supposing it is critical) and using Irwin criterion $K_{\text{I}} = K_{\text{I}c}$, we shall determine the critical value of the second semi-axis. Results of this procedure are presented in Figure 4, where dependence of critical semi-axis c_{cr} versus ratio a_{cr}/t for pressure p = 12.5 MPa (curve 1) and pressure p = 17.5 MPa (curve 2) is shown by solid curves. Each curve determines an interval of the safe dimensions of the crack for the given calculation pressure.

The dotted line in Figure 4 presents the same dependence $c_{\text{cr}} = f\left(a_{\text{cr}}/t\right)$, obtained from the equation determining the critical fracture diagram for the straight part of the pipe at the same pressure values. Note that the obtained diagrams do not take into account subcritical crack growth.

Construction of subcritical fracture diagrams for a crack with c = 200 mm (the regime of proof tests) under starting condition $p_{\text{st}} = \sigma_{\text{st}} = 0$ is shown in Figure 5.

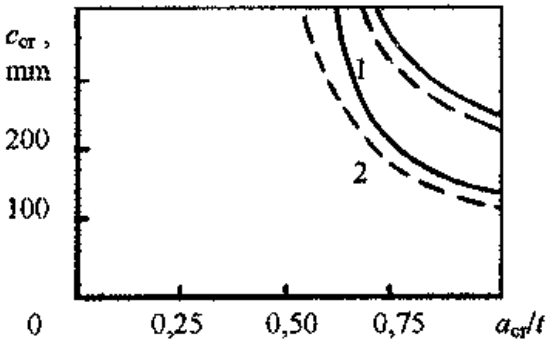

Figure 4. Dependence of critical length versus critical depth for a longitudinal internal surface crack in a straight part of a pipe.

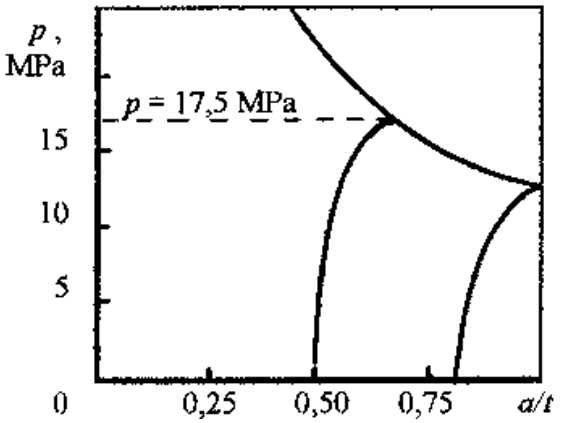

Figure 5. Fracture diagrams of a straight part of a pipe with a longitudinal internal surface crack (c = 200 mm).

The dotted line in Figure 5 shows results for pressure p = 17.5 MPa. It is obvious that for this crack and for this pressure it is possible to determine the interval evolution of a/t, taking into consideration that value $a/t = 1$ is related to the through crack:

$a/t < 0{,}5$ – the crack does not reach the critical state (there is no fracture, there is no leak);

$0{,}5 \le a/t \le 0{,}8$ – the crack reaches the critical state but not yet through (fracture, leak);

$a/t > 0{,}8$ – the crack cuts the pipe wall and becomes a through crack but does not reach the critical state as through one (there is no

fracture, but there is leak), however for some values of c the transition into the critical state is possible (leak with fracture).

Carrying out similar calculations at various values of semi-axis c, it is possible to construct the generalized fracture diagram which makes possible to determine the admissible dimensions of the surface cracks for the given calculation pressure p = 17.5 MPa (Figure 6). The solid line shows the generalized fracture diagrams from subcritical diagrams build up constructed for zero stress starting condition whereas the dotted line corresponds to the starting condition like (9).

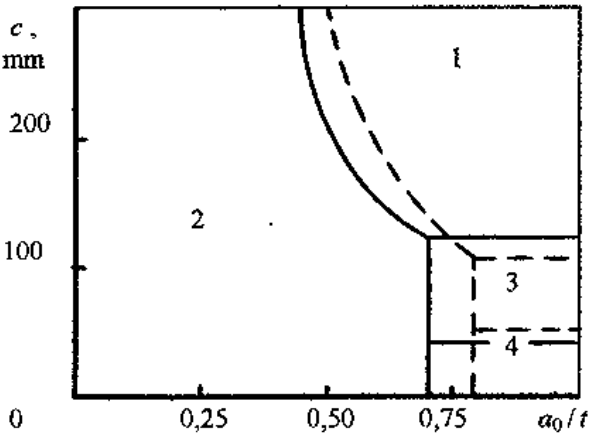

Figure 6. The generalized fracture diagram for the straight part of the pipeline at calculation pressure p = 17.5 MPa (1 – fracture; 2 – there is no fracture, there is no leak; 3 leak with fracture; 4 there is no fracture, but there is leak).

The generalized fracture diagram completely defines conditions of fracture and leak for the considered straight part of the pipe with an internal surface longitudinal crack and can serve as characteristic behavior of this part at static loading.

2.2. PIPE CONTAINING SURFACE CIRCULAR SEMI-ELLIPTIC CRACK

2.2.1. *SIF FEM Calculation for Straight and Curved Parts of the Pipe with Surface Circular Cracks*

Straight part of the pipe. Conditions for fracture and leak of various parts of the pipe were carried out for the following three operational regimes:

- Normal operational conditions characterized by the gross tensile stretching stress σ^{st} = 57 MPa, the gross bending stress σ^{fl} = 31.6 MPa, and the uniform temperature field T = 300°C
- The proof tests characterized by σ^{st} = 89 MPa, σ^{fl} = 31.6 MPa, and uniform temperature field T = 130°C
- The emergency operational regime characterized by σ^{st} = 64 MPa and σ^{fl} = 31.6 MPa. The temperatures on the external and internal surfaces of the pipe are equal to 300°C and 290°C. Temperature gradient ΔT over the wall thickness in this case is equal to 10°C.

By calculations it is shown that a gradient temperature ΔT = 10°C over the wall thickness of the pipe in the emergency regime (regime 3) leads to determines considerably smaller values of the SIF, than loading by internal pressure, and thus can be neglected.

On the straight part of the pipe (internal radius R_{int} = 248 mm, thickness of the wall t = 32 mm) circular semi-elliptic cracks located on the internal surface (as more dangerous), with greater semi-axis length c = 64, 96, 128, 160, and 192 mm and relative depth a/t = 0.1; 0.25; 0.5, and 0.75 are considered.

It is convenient to present the SIF, calculated in points located along the front of the surface semi-elliptic crack in dimensionless form:

$$\overline{K}_{\mathrm{I}} = K_{\mathrm{I}} / \sigma_0 \sqrt{\pi a / Q} \tag{11}$$

where σ_0 is the greatest values of tensile stress or bending stress; a is the depth of the crack; $Q = 1 + 1{,}464(a/c)^{1{,}65}$.

Calculation values of the SIF for external surface semi-elliptic cracks on the straight part of a pipe ∅500 (c = 128 mm) in dimensionless form for tension (numerator of fraction) and bending (denominator) are presented in Table 2. The coordinate x is counted along circular direction, starting from the deepest point of the crack front.

TABLE 2. SIFs for a circular surface crack on the straight part of the pipe subjected to tension and bending.

a/t	$\overline{K}_I$ (c = 128 мм)				
	x/c				
	0	0.2	0.4	0.6	0.8
0.10	1.22/1.22	1.20/1.20	1.16/1.13	1.08/1.03	0.91/0.86
0.25	1.39/1.38	1.36/1.33	1.26/1.16	1.18/1.13	0.98/0.90
0.50	1.79/1.74	1.75/1.70	1.65/1.60	1.46/1.40	1.21/1.13
0.75	2.16/2.06	2.13/2.04	2.06/1.95	1.89/1.78	1.56/1.46

For the estimation of FEM results, comparison was carried out on the obtained maximal values of the SIF for the straight part of the pipe with external semi-elliptic surface crack. This crack is submitted to axial tension and bending with similar values [6] for a strip width $2\pi R_{\text{ext}}$ without crack. This comparison is a relative one, however it shows good enough accordance of results: the maximal error of the axial tension loading exhibits a scatter from –5% up to +7%. Comparison of results related to bending of the straight part of the envelope and the strip with surface cracks shows greater divergence: the maximal error here has a scatter from –13% up to +7%.

Curved part of the pipe. By calculation, SIF for the three loading regimes were considered similarly to the case of straight part but with other stress values in Table 3.

TABLE 3. Loading of the curved bent part of a pipe ∅500.

Stress, MPa	Regime		
	1	2	3
σ^{st}	37	58	42
σ^{fl}	15	15	15

For the curved part of the pipe (radius R_0 = 650 mm, internal radius R_{int} = 248 mm, thickness of the wall t = 50 mm) the external circular surface cracks is located symmetrically with respect to the external contour. It has a semi-axis length c = 64, 96, 128, 160, and 192 mm and a relative depth a/t = 0.1; 0.25; 0.5, and 0.75.

Calculated values of the dimensionless SIF for the external semi-elliptic surface crack in the curved part of a pipe ∅500 (c = 128 mm) for tension (fraction numerator) and flexion (denominator) are presented in Table 4.

TABLE 4. SIFs for a circular surface crack in curved part of a pipe for tension and flexion.

a/t	$\overline{K}_I$ (c = 128 mm)				
	x/c				
	0	0,2	0,4	0,6	0,8
0.10	1.16/1.16	1.15/1.15	1.08/1.12	0.98/1.04	0.81/0.84
0.25	1.32/1.32	1.28/1.28	1.22/1.25	1.08/1.14	0.84/0.96
0.50	1.66/1.67	1.61/1.64	1.59/1.57	1.36/1.42	1.11/1.19
0.75	2.00/–	1.96/2.0	1.90/1.94	1.73/1.80	1.45/1.53

Maximal values of the SIF obtained with FEM calculation for a discrete set of cracks characterized by parameters $\eta = a/t$ and $\xi = a/c$, can be approximated by the following relationship:

$$K_{\mathrm{I}} = \sqrt{\pi a / Q}\left(\sigma^{\mathrm{st}} F_m + \sigma^{\mathrm{fl}} F_b\right) \tag{12}$$

where σ^{st} and σ^{fl} are the tensile and bending stresses in the longitudinal direction. Functions $F_m(\xi, \eta)$ and $F_b(\xi, \eta)$ for a straight part of a pipe have the following form:

$$\begin{aligned} F_m = {} & 1,2 + \left(0,06647 + 0,75711\xi - 9,914\xi^2\right)\eta + \\ & + \left(3,6204 - 18,836\xi + 66,654\xi^2 - 43,998\xi^3\right)\eta^2 + \\ & + \left(0,1031 - 0,73286\xi - 22,205\xi^2 + 23,609\xi^3\right)\eta^3, \end{aligned}$$

$$\begin{aligned} F_b = {} & 1,2 + \left(0,18827 - 2,7038\xi + 2,6732\xi^2\right)\eta + \\ & + \left(3,1958 - 6,2549\xi + 6,1189\xi^2 - 4,2318\xi^3\right)\eta^2 + \\ & + \left(-0,56394 - 2,4077\xi + 8,2732\xi^2 - 4,5605\xi^3\right)\eta^3. \end{aligned}$$

The maximal error for the strip approximation does not exceed 2.5% for all range of crack parameters variation. Relation (12) is used as analytical presentation of the SIF for the investigated surface crack in the straight part of the pipe.

2.2.2. *Conditions Fracture and Leak for Pipe from Circular Surface Crack under Static Loading*

Let us carry out the estimation of critical dimensions of an external surface circular crack by varying the stress for the considered loading regime and assuming the size of one crack semi-axis as critical. The critical length of the second semi-axis is determined from the Irwin criterion $K_{\mathrm{I}} = K_{\mathrm{I}c}$. Results of such a calculation for the straight part of a pipe at different operational regimes are shown in Figure 7. Dotted lines represents the relationships $c_{\mathrm{cr}}/t = f\left(a_{\mathrm{cr}}/t\right)$. In the same figure, continuous lines are related to similar results emanating from the critical fracture diagram.

Carrying out the same calculations for the curved part of a pipe for the same operational regimes and comparison with results for the straight part shows, that existence of the external surface circular cracks on the straight part is more dangerous. Calculations which take into account subcritical crack growth are performed only for the pipe straight part.

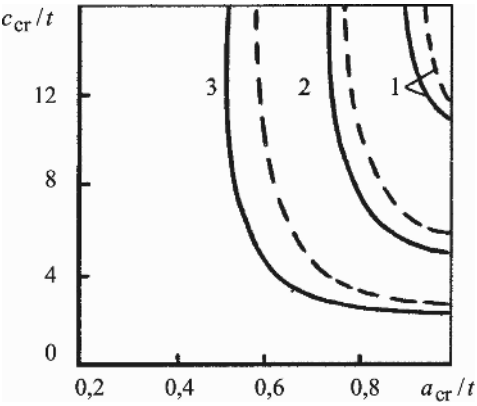

Figure 7. Critical dimensions of external circular semi-elliptic crack in straight part of the pipe (1 – normal operational conditions (NOC); 2 – proof test; 3 – NOC +9 score earthquake).

2.2.3. *Construction of Fracture Diagrams for Pipe with Surface Circular Crack by Calculations*

The equation of subcritical growth of a crack can be presented as:

$$\frac{dp}{dl} = \frac{1}{2} \cdot \frac{1 - \left(\sigma^2 / \sigma_{ul}^2\right) - \left(K_I^2 / K_{Ic}^2\right)}{\int_0^l \left(\frac{\sigma}{\sigma_{ul}^2} \cdot \frac{\partial \sigma}{\partial p} + \frac{K_I}{K_{Ic}^2} \cdot \frac{\partial K_I}{\partial p} \right) dl} \tag{13}$$

where p is the parameter of external loading; σ is the stress on the crack line in a body without crack, which is caused by the external loading p, and opens the crack. The SIF K_I is determined by relation (12).

The initial condition for solution of eq. (13) is the starting condition (the beginning of crack growth) of the subcritical crack $\sigma\left(l_0\right) = \sigma_{st}$.

The peculiarity of the subcritical fracture diagrams construction for a circular surface cracks in a pipe consists in presence of two stress components opening the crack: the gross tensile stress σ^{st} and the gross bending stress σ^{fl}. In the following, the bending stress component σ^{fl} is chosen as variable and the following algorithm would be used for diagram construction:

1. *Bending*. The component σ^{fl} acts as loading. Stresses in the body without crack is determined by the relationship $\sigma = \sigma^{fl} \cos\left(l/R\right)$. The initial crack half-length is l_0. Solving eq. (13), for example, under zero starting condition, the crack growth increment Δl^{fl} is determined for the loading change from zero up to the corresponding fixed value defined by characteristics of the considered regime (up to $\sigma^{fl} = 31.6$ MPa, 89 MPa, etc.);

2. *Tension with bending*. The longitudinal stress component σ^{st} acts here as loading. The stress in a body without crack is $\sigma = \sigma^{st} + \sigma^{fl}\cos(l/R)$. The initial crack length is $l_1 = l_0 + \Delta l^{fl}$. By solving eq. (13) under the same initial condition, it is possible to find the critical value of loading σ_{cr}^{st} and corresponding crack growth increment Δl^{st}. The total crack growth is determined as $\Delta l = \Delta l^{fl} + \Delta l^{st}$.

Subcritical fracture diagrams would be constructed for different values of the semi-axis length c and initial crack depth a/t. The length of crack semi-axis c (this parameter is assumed to be critical) and stresses σ^{st} and σ^{fl}, determined by the chosen operational pipe regime, then, are known. The analysis of subcritical crack growth diagrams constructed as described above makes it possible to obtain the generalized fracture diagrams (see Figure 6) for the straight part of a pipe with an external circular semi-elliptic crack for the considered operational regime.

The analysis of generalized fracture diagrams for various operational regimes of pipe shows that critical conditions (for fracture as well as for leak) can be realized only for rather long (in circular direction) and deep circular surface cracks, that, in general, is improbable.

3. Conclusion

The study of the behavior of a body containing a macroscopical crack allows computing of subcritical crack growth and subcritical and critical fracture diagrams as characteristics of the fracture process.

The method is applied to realize a pipe containing surface (longitudinal or circular) cracks submitted to static and temperature loading.

Study of fracture and leak conditions for different parts (straight or curved) of a cracked pipe with are presented as generalized fracture diagram which makes possible to determine the admissible dimensions of surface cracks under the operational regime.

References

1. Parton V. Z. and Morozov, E. M. Elastic-plastic fracture mechanics. M.: Nauka. 1974, 1985 (in Russian).
2. Morozov E. M. and Sapunov V. T. About calculation of diagrams of fracture//PMTF. 1973. No. 2. P. 172–176 (in Russian).
3. Pluvinage G. and Sapunov V. T. Fuite et rupture des tubes endommagés. Toulouse – France. Cépaduès-Éditions. 2004.

4. Morozov E. M., Nikishkov G. P., et al. The Program complex for the solution of problems of linear and nonlinear mechanics of fracture: Messages 1, 2//Probl. prochnosti. 1987. No. 4, No. 8 (in Russian).
5. Newman J. C. and Raju I. S. Stress-intensity factors for internal surface cracks in cylindrical pressure vessels/Trans. ASME. J. Press. Vessel Techn.1980. V. 102. No. 4. P. 342–346.
6. Newman J. C. et al. Stress intensity factor equations for cracks in three-dimensional finite bodies subjected to tension and bending. NASA-TM-85793, No. 84-23925, 1984.

SOME INSIGHTS INTO THE FATIGUE CRACK PROPAGATION IN TUBES UNDER INTERNAL PRESSURE – PROPOSITION OF PREDICTING MODELS

TAOUFIK BOUKHAROUBA[*1], KRIMO AZOUAOUI[1], JOSEPH GILGERT[2], ZITOUNI AZARI[3] AND GUY PLUVINAGE[3]

[1] *Laboratoire de Mécanique Avancée (LMA), FGMGP de l'USTHB, B.P. 32 El-Alia, 16111, Bab-Ezzouar, Alger –Algérie;*
[2] *Ecole Nationale d'Ingénieur de Metz (ENIM), Ile du Saulcy, 57045 Metz – France;*
[3] *Laboratoire de Fiabilité Mécanique de l'Université de Metz, Ile du Saulcy, 57045 Metz – France*

Abstract: This study is a summary of works performed on fatigue crack propagation, that it is by carrying out experimental tests, or numerical simulations, or those using empirical models, relating principally to thick plates in three points bending, in tension and to thick tubes under internal pressure. The objective is to give the broadest possible comparison of various results allowing the follow-up of the shape evolution of semi-elliptic surface defect during its propagation in fatigue. This review work enabled us to conclude that the form variation of a semi-elliptic defect propagating by fatigue in a cylinder under internal pressure, can be obtained by tests on thick plate in tension, or by the use of model proposed by Mahmoud [36, 37] obtained on plate in tension, and model proposed by Boukharouba et al. [31] obtained and validated by the experimental results on tube under internal pressure.

Keywords: fatigue, crack propagation, thick plates, pressure tubes, experimental

[*] E-mail : atboukha@yahoo.fr

G. Pluvinage and M.H. Elwany (eds.), Safety, Reliability and Risks Associated with Water, Oil and Gas Pipelines, 183–204.

1. Introduction

Various statistical studies [1] carried out over the last 100 years of exploitation of installations under internal pressure, show that 89% of rupture are due to the presence of surface defects and particularly those of angle shape (semicircular or semi-elliptic).

Several organizations or international associations activate in the field of monitoring the various pressure apparatuses park in the world. Among them we note three organizations:

- The American National Board of Pressure Vessel Inspectors [2]
- The association of owners of vapour and electric apparatuses "APAVE", which supervises at days a park of approximately 33,000 overheated water vapour generators and 10,000 boilers [3]
- The Institute of reactor monitoring in Germany, Technischer Ûberwachungs Verein "TÛV" [4]

The question of the knowledge of the form taken by a semi-elliptic or semi-circular defect propagating by fatigue inside a cylinder aroused, and arouse until now, a great interest on behalf of the designer engineers of apparatuses under pressure.

For rather constraining technical considerations related to the performing of fatigue tests under internal pressure on cylinders with quasi-real conditions, led the researchers to circumvent this difficulty by carrying out fatigue cracking tests on thick plates in three points bending (Figure 1a) [5–13] or tension [6, 7, 14–23] (Figure 1b). The results of these tests are then transposed on tubes.

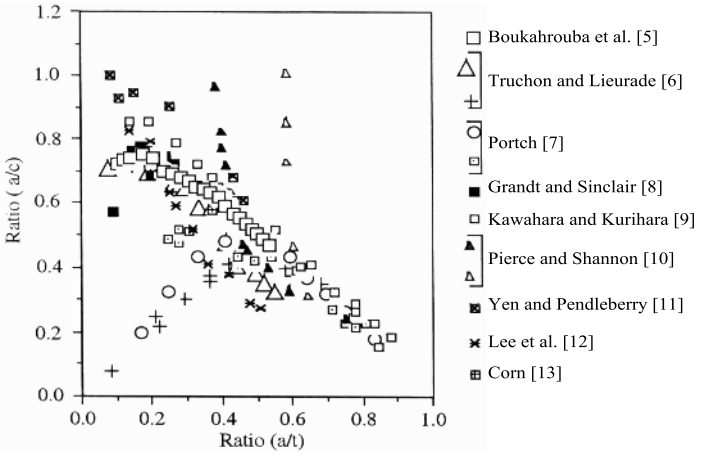

Figure 1a. Development of crack aspect a/c versus normalized crack depth a/t under tension plates.

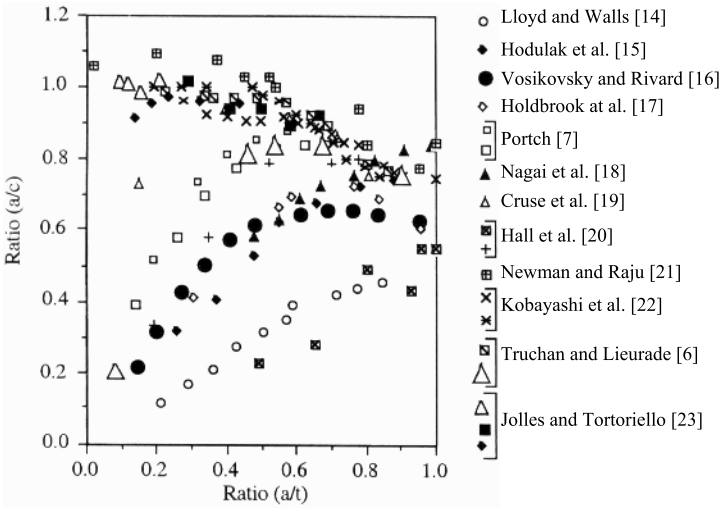

Figure 1b. Development of crack aspect a/c versus normalized crack depth a/t under tension plates.

This problem arises to the engineer at the steps of design, fabrication and start-up of this type of apparatus. For considering only the start-up, and as one cannot prevent these defects to evolve to critical form much more dangerous, one must supervise them.

Therefore, in order to study this type of problem, it is necessary:

1. To carry out cracking tests
2. To perform 3D simulations
3. To use prediction models giving the defect form

2. Experimental Methods

Few results of fatigue cracking were published on tubes under pressure. The totality of the results listed in the literature relates to plates in traction or three points bending.

Boukharouba et al. [5, 24] published experimental results carried out on tubes under internal pressure [24] and on plates under three points bending [5] containing the same type of surface defect of semi-elliptical form. The plates were machined in the wall of forged steel tubes, initially of 80 mm thickness. Several fatigue cracking tests were carried out on tubes as on plates, whose an example of result is given in the Figure (2a and b) below.

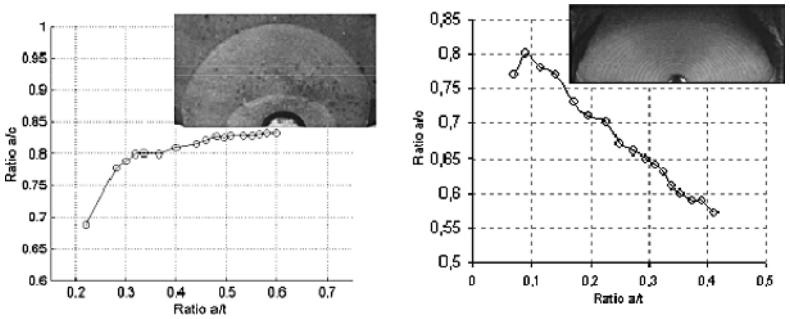

(a): tube under internal pressure [24] (b): plate in three points bending [5]

Figure 2. Experimental results of fatigue evolution of semi-elliptic crack.

In the case of a tube under internal pressure, the curves of shape evolution of the initially semi-elliptic crack converge towards a quasi-horizontal asymptote. The authors conclude that the propagation occurs according to two phases, the first short corresponding to the in-depth propagation is carried out in a dominating way compared to the on-surface propagation. The second phase longer corresponds to a homothetic in-depth and on-surface propagation of the crack. Hence, the crack tends to take a semicircular form at the end of the first phase. The beginning of the second phase (and thus end of the first) depends mainly on the initial dimension of the defect $(a/c)_i$.

Nevertheless, in the case of a plate subjected to three points bending, the curves of shape evolution of the initially semi-elliptic crack show two distinct phases. During the shortly first phase (as in the tube case) in-depth propagation is carried out in a dominating way compared to the on-surface propagation. During the second phase, longer than the first one, the crack is propagated more on surface than in-depth. Therefore, the crack tends to take an increasingly lengthened semi-elliptic form on surface, at the end of the second phase. The beginning of the second phase (and thus end of first) corresponding to a peak on the curve depends mainly, as in the case on tube, of the initial dimension of the defect $(a/c)_i$.

Yoo and Ando [25] carried out tests on tubes of various geometrical dimensions containing circumferential semi-elliptic cracks of different sizes, loaded in four points bending. Both authors noticed, for all the studied configurations that the a/c ratio tends towards a slightly tilted asymptote, stabilized around 0.7 and 0.9 values (Figure 3).

Summon and Ratwani [26] carried out two tests of fatigue crack growth, the first on a 16.5 mm thickness plate, the second on a semi-cylinder of same thickness

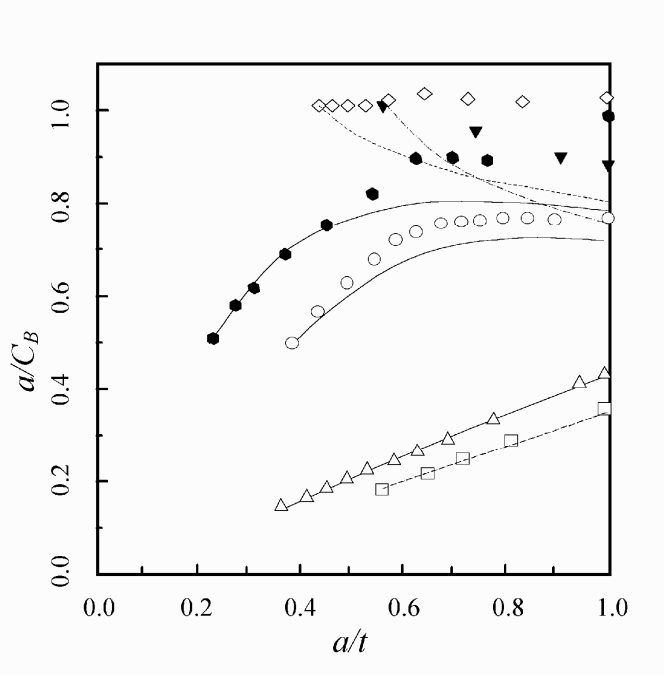

Figure 3. Evolution of semi-elliptic cracks contained.

with interior radius of 40.25 mm. The two specimens containing semi-elliptic cracks of same dimensions and same form were subjected to an alternate tension. So, the two authors conclude that (Figure 4):

- At the beginning of the growth, the crack depth increases definitely more quickly than length
- Beyond the ratio of a/t = 0.5 in the case of the semi-tube, it is hazardous to seek to interpret the results
- The curve corresponding to the semi-cylinder is very close to a line whose slope is very slightly lower than one.

3. Numerical Simulation

The majority of the works we consulted concerns finite elements calculation of the local stress intensity factor. It was noted that a little of researchers were interested to describe the form which a defect takes during its propagation by fatigue.

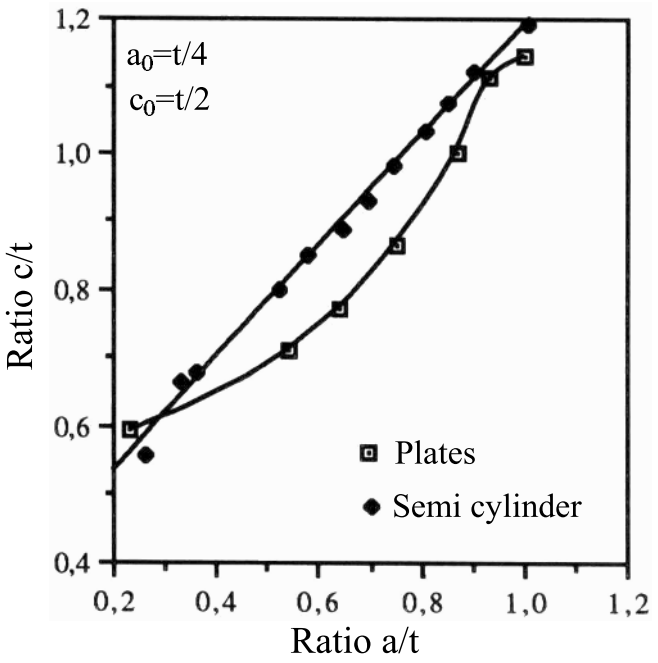

Figure 4. Experimental results of the crack growth in tension fatigue [26].

Shlyannikov, Tchadaev and Kalatchev [27], performed a numerical study on the progression of semi-elliptic cracks contained in a cylinder. Various geometrical dimensions of cylinder and defect were used. These authors used an approach based on the detection of the damaged zone and the calculus of stress intensity factor by the analytical expression of Newman and Raju [28]. They conclude that the a/c ellipse two semi-axes ratio tends towards an asymptotic value ranging between 0.46 and 0.52.

However, Lin and Smith [29] proposed a general method which allows to follow, in three dimensions, the change which occur to the crack shapes during their propagation by fatigue. The authors affirm that their method can be applied to any surface defect and in particular the defects of semi-elliptic forms contained in any type of structures. The two authors used the local stress

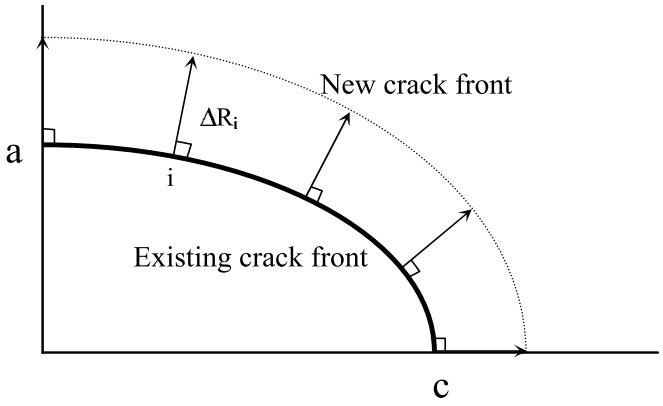

Figure 5. Crack growth prediction using local approach [29].

intensity factor and a propagation law-like Paris-Erdogan one [30] to follow the progression of a certain number of crack front points (Figure 5). The new positions of these points allow to draw the new cracking front.

Boukharouba et al. [31] start from the principle that a semi-elliptic crack of (a_0, c_0) initial size propagating of dA increment tends towards a final form of (a_1, c_1) dimension. This selected final form minimizes the potential energy of the cracked structure. By applying this principle, the authors set up a procedure of follow-up in 3D of the changes occurring to the crack shape during its propagation, without having recourse to a propagation law.

For each new cracking front, the authors calculate the potential energy Π (case of plate and tube) for fictitious increments having the same increment ΔA (Figure 6a) compared to the initial defect. The various values obtained characterize a variation of potential energy which can be represented by a parabola with a minimum (Figure 6b).

The interpolation of these points designates a curve whose minimum represents the new crack front (a_1, c_1). By this way, the authors recreate increment by increment the evolution of the cracking front until the critical dimension. They validate then their results on the real cracking front obtained by tests [5, 24].

An example of computation results compared to experimental data is represented in the Figure (7a and b). We notice in both cases that the precision is a very appreciable degree.

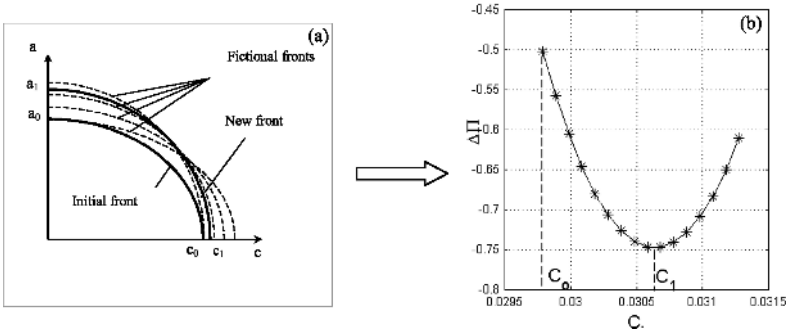

Figure 6. The global method principle; (a) Fictional and real progressions of the crack; (b) Potential energy related to fictional and real progressions of the crack.

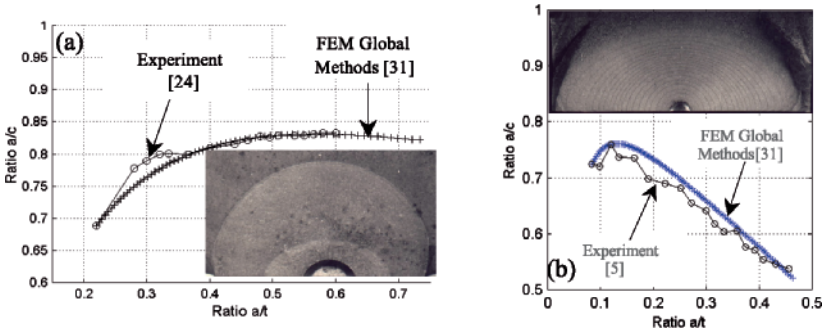

Figure 7. Between the experimental results and those obtained by numerical simulation; (a) case of a tube under internal pressure; (b) case of a plate in three points bending.

4. Empirical Relationships

The empirical equations require only the knowledge of the size of defect propagating by fatigue at a moment (t_i) corresponding to (a_i, c_i), in order to seek the form which this defect adopts after propagation at a moment (t_{i+1}), corresponding to a new size of defect (a_{i+1}, c_{i+1}). This successive determination of various fronts is done until the critical size. We find in the literature various models allowing the prediction of the form which adopts a semi-elliptic or semicircular defect during its propagation by fatigue.

4.1. CASE OF PLATES IN TENSION

PORTCH [7]

$$\left(\frac{a}{c}\right)_{i+1} = \left(1.1 - 0.35\left(\frac{a}{t}\right)_{i+1}\right) - \left[1 - \left(\frac{a}{t}\right)_{i+1}\right]^4 (1.1 - \lambda_P) \tag{1}$$

relation (1) valid to $\left(\frac{a}{t}\right)_{i+1} \geq T$

$$\text{with: } \left(\frac{a}{c}\right)_{i+1} = I\left(\frac{a}{t}\right)_{i+1} \text{ for } \left(\frac{a}{c}\right)_{i+1} < T \tag{1a}$$

$$I = \frac{(a/c)_i}{(a/t)_i} \quad \text{and} \quad T = \frac{4.05 - I}{3(I + 0.35)} \tag{1b}$$

GORNER [32]

$$\left(\frac{a}{c}\right)_i = \left[0.98\left(\frac{a}{t}\right)_i - 0.06\left(\frac{a}{t}\right)_i^2\right]\left\{\left(\frac{a}{t}\right)_i^2 + \lambda_G\left[0.06\left(\frac{a}{t}\right)\right]^{-0.5}\right\} \tag{2}$$

where λ_G calculated starting of a_0 and c_0.

IIDA [33]

$$\left(\frac{a}{c}\right)_i = \left[0.78 - 0.07\left(\frac{a}{t}\right)_i\right] \pm 0.0834\left[\left(\frac{a}{t}\right)_i - \lambda_i\right]^{-2.6} \tag{3}$$

λ_I is a constant calculated from the initial values of *a* and *c*, the sign (+) is for the case $\left(\frac{a}{c}\right) > (0.78 \div 0.07)\left(\frac{a}{t}\right)$ and the sign (–) is for $\left(\frac{a}{c}\right) < (0.78 \div 0.07)\left(\frac{a}{t}\right)$.

CARPINTERI [34 ET 35]

$$\left(\frac{a}{c}\right) = a_0 + a_1\left(\frac{a}{t}\right) + a_2\left(\frac{a}{t}\right)^2 + a_3\left(\frac{a}{t}\right)^3 + a_4\left(\frac{a}{t}\right)^4 \tag{4}$$

a_i depends on crack shape and *m* values.

4.2. CASE OF THE BENDING PLATES

PORTCH [7]

$$\left(\frac{a}{c}\right)_i = \left(1.05 - 0.35\left(\frac{a}{t}\right)_i\right) - \left[1 - \left(\frac{a}{t}\right)_i\right]^4 (1.05 - \lambda_P) \tag{5}$$

relation (6a) valid to $\left(\frac{a}{t}\right)_i \geq D$

$$\text{with : } \left(\frac{a}{c}\right)_i = I\left(\frac{a}{t}\right)_i \text{ for } \left(\frac{a}{c}\right)_i < D \tag{5a}$$

$$I = \frac{(a/c)_i}{(a/t)_i} \text{ and } D = \frac{3.2 - I}{3(I + 1.0)} \tag{5b}$$

GORNER [32]

$$\left(\frac{a}{c}\right)_i = \left[1.05\left(\frac{a}{t}\right)_i - \left(\frac{a}{t}\right)_i^2\right]\left\{\left(\frac{a}{t}\right)_i^2 + \lambda_G\left[1.05 - \left(\frac{a}{t}\right)\right]_i^2\right\}^{-0.5} \tag{6}$$

where λ_G calculated starting of a_0 and c_0.

IIDA [33]

$$\left(\frac{a}{c}\right)_i = \left[0.85 - 0.75\left(\frac{a}{t}\right)_i\right] \pm 0.0063\left[\left(\frac{a}{t}\right)_i - \lambda_I\right]^{-3.8} \tag{7}$$

λ_I is a constant calculated from the initial values of *a* and *c*, the sign (+) is for the case $\left(\frac{a}{c}\right) > (0.85 \div 0.75)\left(\frac{a}{t}\right)$ and the sign (–) is for $\left(\frac{a}{c}\right) < (0.85 \div 0.75)\left(\frac{a}{t}\right)$.

MAHMOUD [36 ET 37]

for: $C_c = (0.9)^m . C_a$ [38]

$$\Delta a/\Delta c = \left[0.9\,(a/c)^{0.5}\left(1.1 + 0.35\,(a/t)^2\right)\right]^{-m} \tag{8a}$$

with: $a/c \leq 0.1$

$$\Delta a/\Delta c = \left[0.9\,(a/c)^{0.5}\left(1.1 + 0.35\,(a/t)^2\,(a/c)\right)\right]^{-m} \tag{8b}$$

with: $a/c > 1.0$

for: $C_c = C_a$ [38]

$$\Delta a/\Delta c = \left[\,(a/c)^{0.5}\left(1.1 + 0.35\,(a/t)^2\right)\right]^{-m} \tag{9a}$$

with: $a/c \leq 0.1$

$$\Delta a/\Delta c = \left[\,(a/c)^{0.5}\left(1.1 + 0.35\,(a/t)^2\,(a/c)\right)\right]^{-m} \tag{9b}$$

with: $a/c > 1.0$

BOUKHAROUBA ET AL. (FIGURE 8)

$$\left(\frac{a}{c}\right)_i = 0.915 - 0.85\left(\frac{a}{t}\right)_i + \lambda_{Bp}\left(\frac{a}{t}\right)_i^{-2} \tag{10}$$

with:

$$\lambda_{Bp} = \left(\frac{a_0}{c_0} + 0.85\left(\frac{a_0}{t}\right) - 0.915\right)\cdot\left(\frac{a_0}{t}\right)^2 \tag{10a}$$

4.3. TUBE UNDER INTERNAL PRESSURE

BOUKHAROUBA ET AL. [31] (FIGURE 9)

$$\left(\frac{a}{c}\right)_i = 0.9 - 0.075\left(\frac{a}{t}\right)_i + \lambda_{Bt}\left(\frac{a}{t}\right)_i^{-2} \tag{11}$$

with:

$$\lambda_{Bt} = \left(\frac{a_0}{c_0} + 0.075\left(\frac{a_0}{t}\right) - 0.9\right)\cdot\left(\frac{a_0}{t}\right)^2 \tag{11a}$$

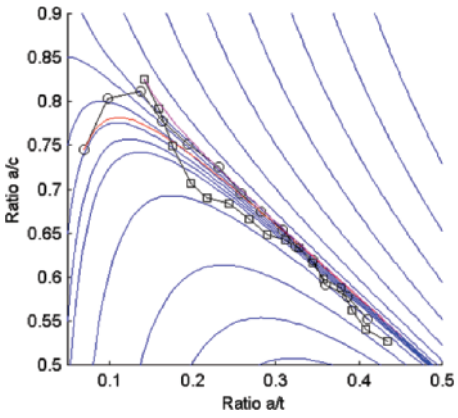

Figure 8. Comparison of the model proposed by Boukharouba et al. with their experimental results, case of a plate in three points bending.

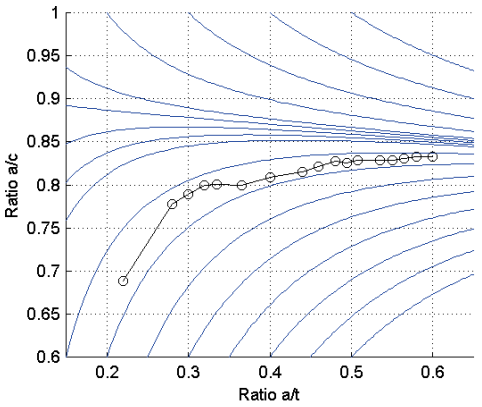

Figure 9. Comparison of the model proposed by Boukharouba et al. with their experimental results, case of a tube under internal pressure [31].

5. Use of a Propagation Law

From the assumption that the crack propagation is sensitive to the stress gradient, therefore governed by the local stress intensity factor (obtained by numerical simulation [5, 24]), even semi-local (obtained by empirical relationship of Cruse and Besuner [39]), and by using a cracking law-like that of Paris [30], the authors calculate the propagation velocity at the deepest point (A) and on surface (C). The stress intensity factor was calculated using the cracking results obtained by tests on tubes [24] and plates [5] for a load ratio R = 0.1, 0.3 and 0.5.

At the deepest point	On surface
$\frac{da}{dN}=C_A\left(\Delta K_{I,A}\right)^{mA}$	$\frac{dc}{dN}=C_C\left(\Delta K_{I,C}\right)^{mC}$
$\frac{\overline{da}}{dN}=\overline{C}_A\left(\overline{\Delta K}_{I,A}\right)^{\overline{m}A}$	$\frac{\overline{dc}}{dN}=\overline{C}_C\left(\overline{\Delta K}_{I,C}\right)^{\overline{m}C}$

(12)

The question is to know if the cracking parameters of Paris law m_i and C_i defined in the system of equation (12) are the same ones.

An example of their results is shown in the Figures (10, 11, 12 et 13), obtained on plates subjected to three points bending and on tubes under internal pressure for a load ratio R = 0.3. The line in continuous feature represents the cracking curve determined on a CT specimen (same material) taken as reference curve.

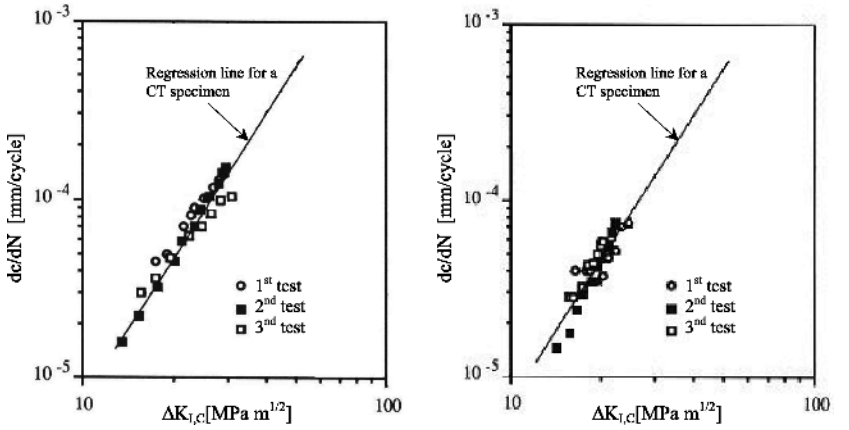

Figure 10. Crack growth rate on surface and at the deepest point against the local value of SIF range, case of three points bending plates, stress ratio R = 0.3 [5].

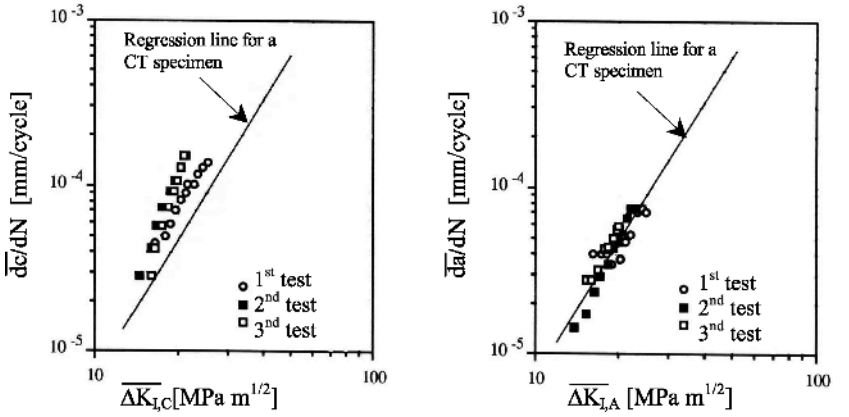

Figure 11. Crack growth rate on surface and at the deepest point against the average value of SIF range, case of three points bending plates, stress ratio R = 0.3 [5].

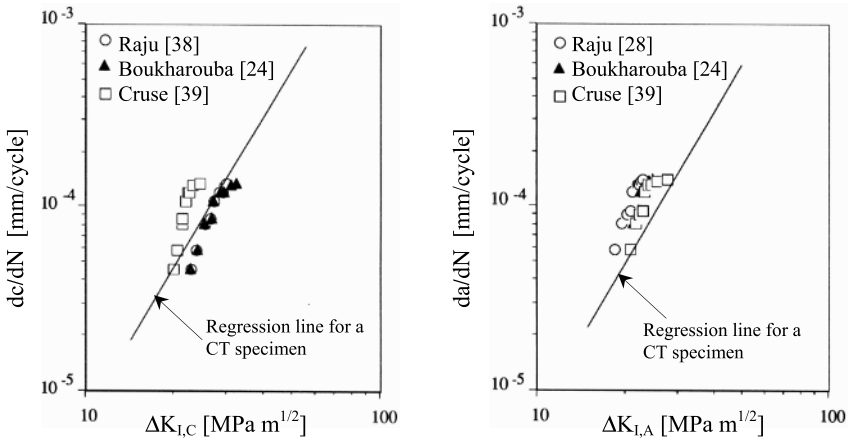

Figure 12. Crack growth rate on surface (dc/dN) and at the deepest point (da/dN) against the local or average value of SIF range, case of tubes under internal pressure [24].

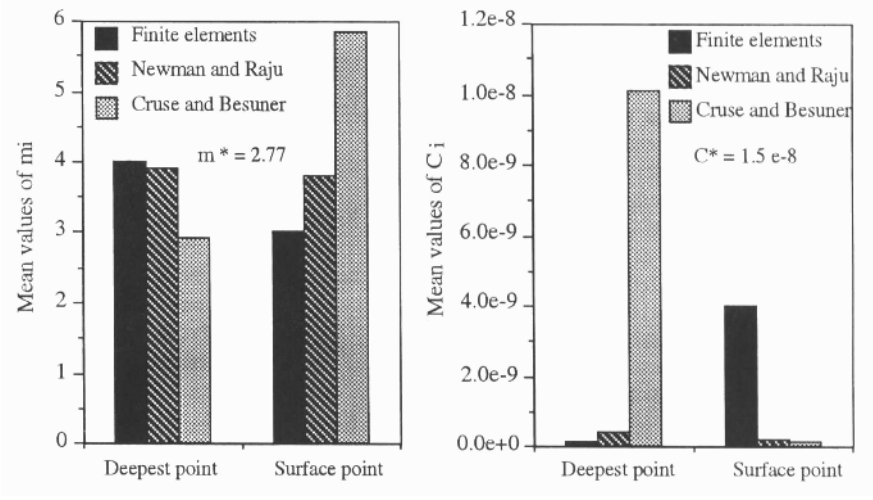

Figure 13. Experimental determination of the mean value of crack propagation C_i and m_i of Paris law [24].

Varfolomeyev et al. [40] performed five tests of fatigue crack propagation. These tests were carried out on standard specimens containing semi-elliptic defect, under four points bending with a load ratio equal to 0.32. A marking of

the cracking front was carried out. From the measurements taken on the crack front, the authors determine the variation of the stress intensity factor:

- Local ΔK_I , using the formulation given by Newman and Raju [38]
- Semi-local ΔK_I, using the formulation given by Cruse and Besuner [39]
- Effective $\Delta K_{I,e}$ (not to confuse with $\Delta K_{I,eff}$), given by the formula: $\Delta K_{I,e} = \gamma \Delta K_{I,local}$, with γ is a coefficient determined by experiments [40]

On the basis of the possibility to use the stress intensity factor-like fatigue crack propagation criterion and basing on the analysis of Letunov et al. [41], the authors estimate that $\Delta K_{I,A}$ (at the deepest point) = $\Delta K_{I,C}$ (on surface). The use of Paris law gives the following:

$$\frac{da}{dN} = C_A \left(\Delta K_{I,A}\right)^m = C\left(\gamma_A \cdot \Delta K_{I,e}\right)^m \qquad \frac{dc}{dN} = C_C \left(\Delta K_{I,C}\right)^m = C\left(\gamma_C \cdot \Delta K_{I,,e}\right)^m \quad (13)$$

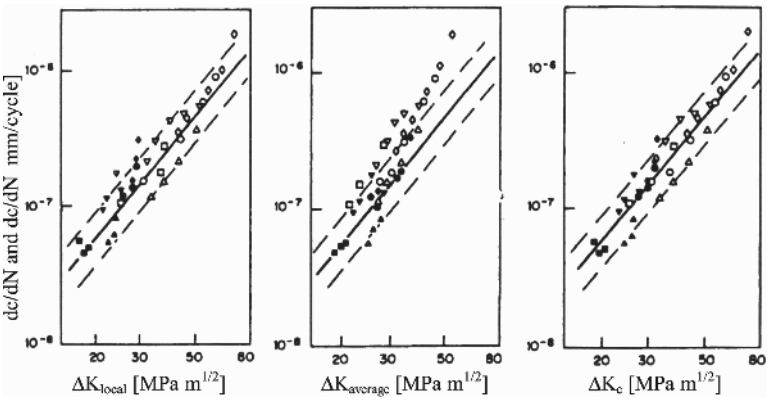

Figure 14. Crack growth rate on surface (dc/dN) and at the deepest point (da/dN) against the local, average and effective value of SIF range, case of four points bending plates [40].

The *m* parameter is independent of the position of the crack front point corresponding to the value found by tests. For a propagation governed by the relationships (13) (Figure 14), the authors conclude that the effective stress intensity factor $\Delta K_{I,e}$ assemble the experimental points better and that all points are inside the dispersion band.

Mahmoud [36] has studied data from literature for crack propagation of a semi-elliptical surface crack under tension loading. The experimental data used in our analysis are taken from the following references [6, 7, 9, 13 to 20, 22, 23, 26, 42 to 44]. Results have been analyzed using the local and the average crack

propagation laws and particular local values of parameters $C_{i,j}$ and $m_{i,j}$ given in Table (1). Experimental and predictive results have been compared using a parameter R_i called residu defined as:

$$R_i = \left(\frac{a}{c}\right)_{i,\,prediction} - \left(\frac{a}{c}\right)_{i,\,experiment} \tag{14}$$

The standard deviation d_s is given by the following relationship:

$$d_s = \frac{\sum R_i^2}{(n-1)^{0.5}} \tag{15}$$

where n is the number of experimental data.

All results have been divided into four groups and are presented in Figure (15). The choice of the most accurate law and the determination of the best-fit coefficient are given by statistical criterion based on the combination of lowest value of residual R_i and the standard deviation d_s. The author in question [36] has found that the best solution for the crack propagation law is obtained by using the local SIF and the particular following values: $m_A = m_C = 4$ and $C_A \neq C_C$ (Table 1).

TABLE 1. Particular values of C_i and m_i given by Mahmoud [36].

Criterion	Point	$C_{i,j}$	$m_{i,j}$
$\Delta K_{I,A}$ / $\Delta K_{I,C}$	A / C	$C_A = C_C$	$m_A = m_C = m$
		$C_C = (0.9)^m \cdot C_A$	
$\overline{\Delta K}_{I,A}$ / $\overline{\Delta K}_{I,C}$	A / C	$\overline{C}_A = \overline{C}_C$	$\overline{m}_A = \overline{m}_C = \overline{m}$
		$\overline{C}_C = (0.9)^m \cdot \overline{C}_A$	

6. Discussion

Since nearly one-half century, several researchers tried to predict the surface cracks evolution during their propagation in fatigue, especially those of semi-elliptic shape. The quasi-totality of this works concerned defects contained in plates and in tubes loaded cyclically in three and four points bending or in tension. A summary of the results reported in the literature relating to plates under bend or tension loading and cylinders loaded in bending and under internal pressure give us already a suspicion of an answer, relatively to:

- The shape evolution of the defect during its propagation
- The criterion or approach to use for the data reduction of test results
- The validity degree of such or such empirical relation established in order to predict the shape evolution of this type of defects during their propagation in fatigue

From the use of empirical models (Figures 15 and 16), one noticed a very great dispersion in the results and even by times contradictions. We can estimate that predictions given by the formulas of Iida [33] and those of Mahmoud [36, 37] with $C_c = 0.9^m.C_a$ are very far away from experimental results obtained by Boukharouba et al. [5, 24], and this, in both two cases. Nevertheless, the relations of Groner et al. [32] underestimate the crack in-depth progression in the case of a tube, on the other hand that proposed by Mahmoud [36, 37] while using $C_c = C_a$ and that given by Boukharouba et al. [31] give a good prediction of the crack shape evolution in both cases, in spite of the fact that Mahmoud relation tends towards an inclined asymptote at the end, in the case of tube (Figure 17).

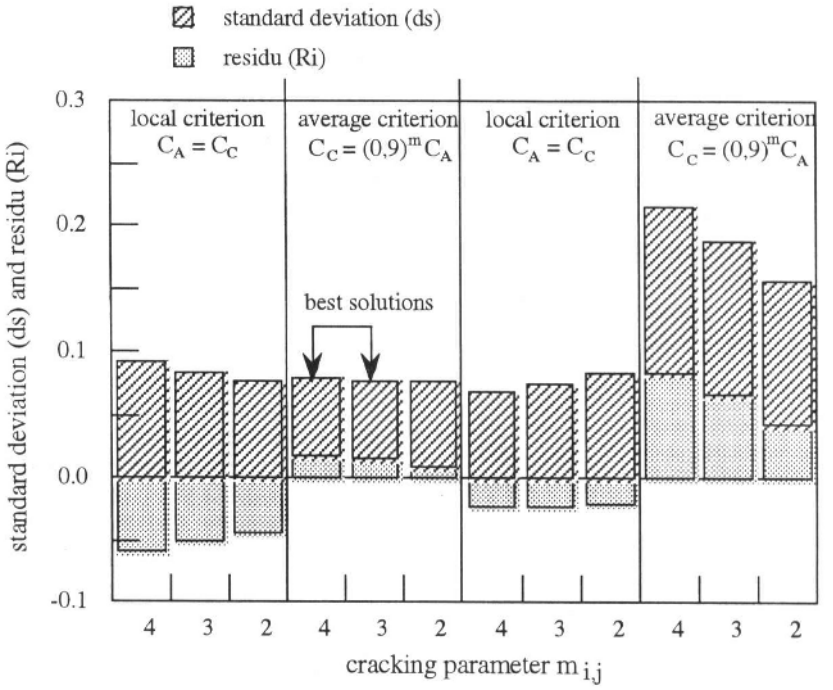

Figure 15. Values of standard deviation and residue for the different crack propagation law for points A and C. Tension case [36].

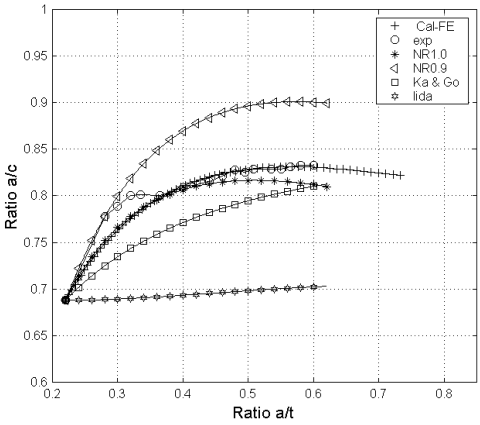

Figure 16. Comparison of the various models, case of a tube under internal pressure and a plate in tension.

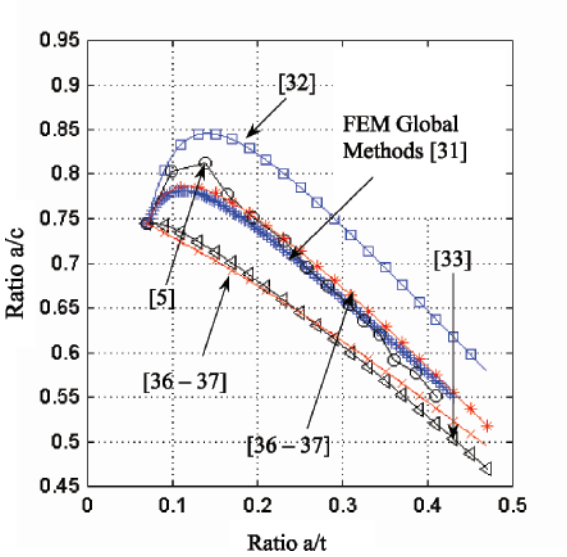

Figure 17. Comparison of the various models, case of a plate in three points bending.

This can be explained by the deficiency of physical justifications and the practical insufficiencies in the use of empirical models (see 4th paragraph) in order to predict the changes in geometrical forms of surface defects during their

propagation in fatigue. This justifies the results dispersion and by time even their contradictions.

However, the results obtained by different researchers using local, semi-local and effective approaches, give propagation law coefficients (m_i and C_i) at the deepest point (A) and at surface (C), and even for intermediate points (see 5th paragraph), completely different.

7. Conclusion

This review paper allows us to note that from a simple numerical simulation or by the use of existing empirical models, one can easily predict the evolution of an elliptic defect propagating in a tube wall or a plate. This method offers some advantages:

- The non-recourse to onerous experimental tests, as in the case of tests under internal pressure, in order to determine the relation between the crack size and the number of cycles in fatigue propagation
- The non recourse to a propagation law which allow to deduce the profile adopted by the crack after or during the propagation. Generally, these propagation laws are inadequately adapted or their validities are not really checked for the 3D cases

This review paper enables us to affirm, that in the case of a plate in three points bending, the evolution of the (a/c) two semi-axes ratio according to the (a/t) ratio is much more complex than in the case of a tube under internal pressure.

- In the case of a plate subjected to three points bending, the a/c ratio passes by a maximum (a evolves more quickly than c) then decreases thereafter linearly (c evolves more quickly than a). During the propagation, the crack thus remains semi-elliptic but no homothetic.
- In the case of a pressurized tube, the a/c ratio passes also by a maximum (a evolves more quickly than c) then remains constant following a horizontal asymptote. The cracking front shows in a first stage a no homothetic semi-elliptic shape, followed by an evolution with a tendency to take a homothetic semi-elliptic form, or straightforwardly semicircular one. This stabilized form adopted by the crack during its propagation strongly depends on the initial ratio of the two semi-axes a and c.

One can conclude that:

- The variation of the same type of defect contained in a thick plate in tension or a thick tube under pressure would give the same type of evolution, see Figure (15)

- From this first remark rises the second one; the evolution of this type of defect depends only on the initial size of the defect and the loading nature
- During its propagation, the initially elliptic defect remains elliptic but no homothetic in the case of bend loading. On the other hand, it tends towards a stabilized form in the case of tension loading or in the case of the internal pressure.

References

1. C. A. G. Philps and R. C. Warwick, A survey on defects in pressure vessels built to high standards of construction. UKAEA Unclassified report, AHSB(b)R162, HM Stationery office, London (1968).
2. National Board of Pressure Vessel Inspectors, USA (1996).
3. C. H. Heron, incidents de chaudières de petites et moyennes puissances, pp. 399–436 (1982).
4. O. Kellerman, Present view on recurving inspection of reactor pressure vessels in the federal republic of germany, Agence Internationale de l'Energie Atomique, rapports techniques, série no. 4 (1981).
5. T. Boukharouba, C. Chehimi, J. Gilgert, and G. Pluvinage, In: Carpinteri, A. (Ed.), Behaviour of semi-elliptical cracks in finite plates subjected to cyclic bending, Handbook of fatigue crack propagation in metallic structures, vol. 1, pp. 707–731 (1994).
6. M. Turchon and H. Lieurade, In: François, D. (Ed.), Experimental study of surface crack propagation, Advances in fracture mechanics, Proceeding of the Fifth International Conference on Fracture, vol. 1, Cannes, France, pp. 33–39 (1981).
7. D. J. Portch, An investigation into the change of shape of fatigue cracks initiated at surface flaws, Central Electricity Generating Board, report RD/B/N-4645, Great Britain (1979).
8. A. Grandt and G. Sinclair, Stress intensity factors for cracks in bending, stress analysis and growth of cracks, ASTM STP 513, pp. 37–58 (1972).
9. M. Kawahara and M. Kurihara, In: Taplin, D. (Ed.), Fatigue crack growth form a surface flaw, Fourth International Conference Fracture, vol. 2, Waterloo, Canada, pp. 1361–1373 (1977).
10. W. Pierce and J. Shannon, Surface crack shape in bending fatigue using an inexpensive resonant fatiguing apparatus, Journal of Testing and Evaluation, vol. 6, pp. 183–188 (1978).
11. C. Yen and S. Pendleberry, Technique for making shallow cracks in sheet metals, Mater. Res. Stands, vol. 2, pp. 913–916 (1962).
12. Lee et al., Experimental research on surface crack propagation laws for alloy steel, Engineering Fracture Mechanics, vol. 16, pp. 105–113 (1982).
13. D. Corn, A study of craking technique for obtaining partial thickness of pre-selected depths and shapes, Engineering Fracture Mechanics, vol. 3, pp. 45–52 (1971).
14. G. Lloyd and J. Walls, Propagation of fatigue cracks surface flaw in austenitic type 316 butt welds, Engineering Fracture Mechanics, vol. 13, pp. 879–911 (1980).
15. L. Hodulak, H. Kordisch, S. Kunzelmann, and E. Sommer, In: Smith C. W. (Ed.), Growth of part through cracks, in Fracture Mechanics, pp. 399–410 (1979).
16. O. Vosikovsky and A. Rivard, Growth of surface fatigue cracks in a steel plate, International Journal Fatigue, vol. 3, pp. 111–115 (1981).

17. S. Holdbrook and W. Dover, The stress intensity factor of a deep surface crack, Engineering Fracture Mechanics, vol. 12, pp. 347–364 (1979).
18. A. Nagai, M. Toyosado, and T. Okamoto, A study on the fatigue cracks growth in 90% Ni steel plate, Engineering Fracture Mechanics, vol. 7, pp. 481–490 (1975).
19. T. Cruse, G. Meyers, and R. Wilson, Fatigue growth of cracks, in flaw growth and fracture. ASTM STP 631, pp. 174–189 (1977).
20. L. Hall, R. Shah, and W. Engstrom, Fracture and fatigue cracks growth behaviour of surface flaws and flaws originating at fastener holes, Boeing Aerospace, AD/A-001 597 (1974).
21. J. Newman and I. Raju, An empirical stress intensity factors equation for the surface cracks, Engineering Fracture Mechanics, vol. 15, no. 1–2, pp. 185–192 (1981).
22. K. Kobayashi, A. Narumoto, and M. Tanaka, Prediction of crack propagation life in axial loading fatigue of structural steel, Proceeding of the Third International Conference of Pressure Vessel Technology, ASME 11, pp. 807–813 (1977).
23. M. Jolles and V. Tortoriello, In: Lewis J. and Sines G. (Eds.), Geometry variation during fatigue growth of surface flaws, in Fracture Mechanics, ASTM STP 791, vol. 1, pp. I-297–I-307 (1983).
24. T. Boukharouba and G. Pluvinage, Prediction of semi-elliptical defect form, case of a pipe subjected to internal pressure, Nuclear Engineering and Design, 188, pp. 161–171 (1999).
25. Y. S. Yoo and K. Ando, Circonferential inner fatigue crack growth and penetration behaviour in pipe subjected to a bending moment, Fatigue and Fracture of Engineering, Materials and Structures, vol. 23, pp. 1–8 (2000).
26. E. Sommer and M. Ratwani, Experimental investigation of part-trougth cracks in paltes and thik walled shells, 2nd SMIRT (1973).
27. V. N. Shlyannikov, A. V. Tchadaev, and V. A. Kalatchev, Fatigue fracture of power engineering structures, ECF. 12. F. F.D, 1998, vol. 1, pp. 375–380.
28. I. S. Raju and J. C. Newman, Jr., Stress intensity factors for internal and external surface cracks in cylindrical vessels, Journal of Pressure Vessel Technology, vol. 104, pp. 293–298 (1982).
29. X. B. Lin and R. A. Smith, Crack propagation prediction of practical fatigue defects using a crack shape following technique, ECF. 12. F. F.D, vol. 1, pp. 121–126 (1998).
30. P. Paris and F. Erdogan, 1963, Trans. ASME, 528–534.
31. T. Boukharouba, Comparison of the fatigue behaviour of the semi-elliptical defects contained in plates and tubes, using various approaches, Contact Mechanics 2001, International Conference on Computational Methods in Contact Mechanics, 18–20 June 2001, Seville, Spain.
32. F. Corner, C. Mattheck, and D. Munz, Change in geometry of surface cracks during alternating tension and bending, Z. Workstoff Tech, no. 14, pp. 11–18 (1983).
33. K. Iida, Aspect ratio expressions for pat-through fatigue crack, II W Doc. XIII, pp. 967–980 (1980).
34. A. Carpinteri, Surface flaw stress intensity factor computation with quarter-point elements, Journal of Strain Analysis, vol. 28, no. 2, pp. 117–123 (1993).
35. A. Carpinteri, Propagation of surface cracks under cyclic loading, Handbook of Fatigue Crack Propagation in Metallic Structures, pp. 653–705 (1994).
36. M. A. Mahmoud, Quantitative prediction of growth patterns of surface fatigue cracks in tension plates, Engineering Fracture Mechanics, vol. 30, no. 6, pp. 735–746 (1988).
37. M. A. Mahmoud, Surface fatigue crack growth under combined tension and bending loading, Engineering Fracture Mechanics, vol. 36, no. 3, pp. 389–395 (1990).
38. I. S. Raju and J. C. Newaman, Improved stress intensity factors for wide range of semi-elleptical cracks in finite thickness plates, Engineering Fracture Mechanics, vol. 11, no. 4, pp. 817–829 (1979).

39. T. A. Cruse and P. M. Besuner, Residual life prediction for surface crack in complex structural details, Journal of Aircraft, vol. 12, pp. 869–887 (1983).
40. I. V. Varfolomeyev, V. A. Vainstok, and A. Y. Krazowsky, Prediction of part-through crack growth under cyclic loading, Engineering Fracture Mechanics, vol. 40, no. 6, pp. 1007–1022 (1991).
41. V. I. Letunov, I. V. Kramarenko, B. S. Shulginov, and V. A. Vainshtok, Relationships governing the propagation of surface cracks in a low-alloy steel in asymmetric cyclic bending, Report 2, Strength of Materials, vol. 18, pp. 13–16 (1986).
42. D. Hoeppner, D. Petit, C. Frayherson, and W. Hyler, Determination of flaw growth characteristics of Ti-6Al-4v sheet in the solution treated and aged condition, NASA CR-65811 (1968).
43. K. Nishioka, K. Hirakawa, and K. Kitaura, Fatigue crack propagation in behaviour of various steel, The Sumitarno Search, vol. 17, pp. 39–55 (1977).
44. H. Muller, S. Mullet, D. Munz, and J. Newman, Extension of surface cracks during cyclic loading in fracture mechanics. In: J. Lewis and G. Sine, (Eds.), ASTM STP905, vol. 1, pp. 625–643 (1986).

HYDROGEN EFFECT ON FATIGUE LIFE OF A PIPE STEEL

J. CAPELLE*, J. GILGERT AND G. PLUVINAGE
Laboratoire de Fiabilite Mecanique
Universite Paul Verlaine Metz et École NAtionale D'ingenieurs de Metz – France

Abstract: The adverse effect of hydrogen environment on notch resistance and fatigue life of pipeline steel is experimentally proved and quantified by about 70% reduction of life. The experiment is performed in an air and also in a hydrogen atmosphere by three-point bend testing, in specially designed device, applying specimens shaped from the pipe initial form of steel for pipeline application.

Keywords: hydrogen, fatigue test, electrolytic solution NS4

1. Introduction

Pipelines are today increasingly applied for the transport of energy from the extraction region to the region of consummation. In order to prevent explosion or leakage in pipeline which might pollute the environment and cause the loss of human lives mechanical properties of steel applied for pipes manufacture have to be specified properly. Hydrogen is new source of energy in more extended use and in some cases can be applied to replace the oil or the gas. It is necessary to determine the damage kind and level of applied steel in hydrogen environment as an important item in its specification.

1.1. FRACTURE CAUSES IN PIPES

The causes of the failures of the gas pipelines are various natures. They can appear either by a fracture, or by a leak (it depends of the nature of the fluid transported). The majority of these failures are caused by pitting corrosion or

* To whom correspondence should be addressed. Julien Capelle, Laboratory of Mechanical Reliability, National School of Engineers of Metz, île du Saulcy, 57045 Metz, France; e-mail: j.capelle@hotmail.fr

G. Pluvinage and M.H. Elwany (eds.), Safety, Reliability and Risks Associated with Water, Oil and Gas Pipelines, 205–217.

cracking by stress corrosion, but there are also problems related to the defects of welding. Movements of ground (landslip, earthquake) can also be the cause of damage on the buried pipelines. The owners of pipelines study these problems for a long time and have a good knowledge of the methods allowing to manage them.

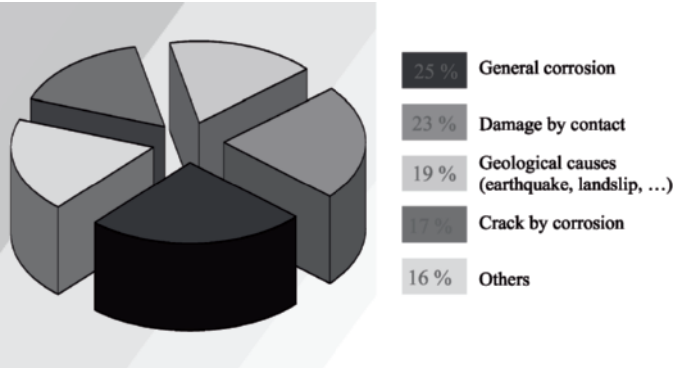

Figure 1. Causes of the fracture of pipelines in the course of exploitation recorded by the members of the ACPRÉ of 1985–1995 [1].

It is clear from Figure 1 that the failure caused by corrosion is most important, expressed in 56% cases. But also very important cause of failure is connected with mechanical damage due to soil digging or excavating by machines. Frequently happens that the notches are formed in the pipelines by machines used in ground removal during construction. Together with cracks caused by corrosion (general, pitting, stress corrosion) these notches are stress raisers, reducing the material resistance to fatigue and fracture. Stress concentration is considered as the origin in more than 90% of the failures in service.

This study is performed with the aim to get an insight in material response to variable loading (fatigue) in hostile environment of hydrogen (corrosion) and stress concentration by notch. Obtained data can be useful in life prediction of damaged pipes.

1.2. STEEL USED

The steel used is a steel intended for the manufacture of pipeline, employed in the Ukrainian network. The API X52 was the most common gas pipelines material for transmission of oil and gas during 1950–1960. The standard chemical composition and mechanical properties of this steel are shown in the Tables 1 and 2.

TABLE 1. Chemical composition of the steel (mass proportion in %) [2].

C	Mn	Si	Cr	Ni	Mo	S	Cu	Ti	Nb	Al
0.22	1.22	0.24	0.16	0.14	0.06	0.036	0.19	0.04	<0.05	0.032

TABLE 2. Mechanical properties of API X52 [3].

E (GPa)	σ_Y (MPa)	σ_U (MPa)	A%	n	K (MPa)
203	410	528	32	0.0446	587.3

where E, σ_Y, σ_U, $A\%$, n, and K are the modulus of elasticity, yield stress, ultimate stress, relative elongation, hardening exponent, and hardening coefficient, respectively.

The Ludwik [4] law will make it possible to introduce the real behaviour of steel into its plastic range, where the hardening parameter is *n*, and the resistance coefficient is *K*.

$$\sigma = K\varepsilon_p^n \tag{1}$$

2. Fatigue Test

2.1. SAMPLE USED

The view of sample taken from tested pipe (outer diameter 219.1 mm, wall thickness 6.1 mm) is presented in Figures 2 and 3. It is to notice that welded joint is avoided, since the data of parent metal were requested. Shape, dimensions, and view of machined specimen are given in Figures 4 and 5.

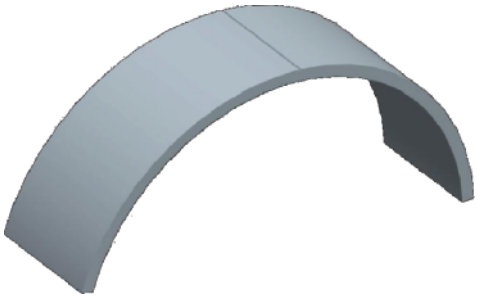

Figure 2. Curved sample used.

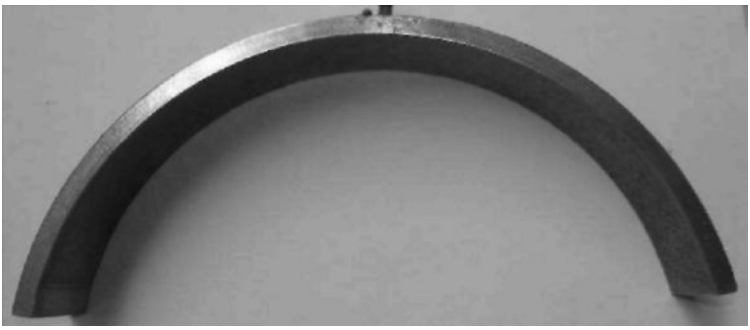

Figure 3. View of the sample cut from a pipe.

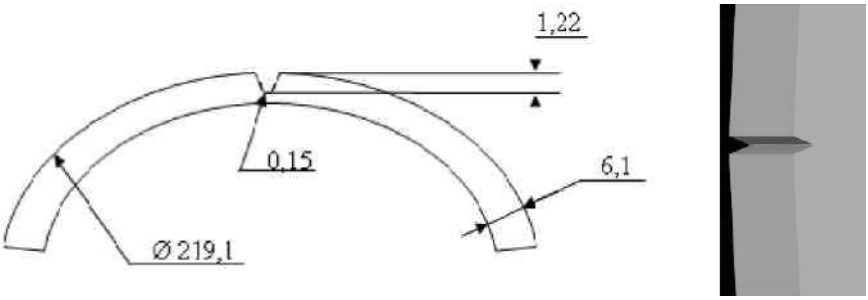

Figures 4 and 5. Shape, dimensions, and view of prepared specimen.

It was not possible to produce standard tensile or bending specimen from available sample of given diameter and low thickness. For that the form of circle arc, corresponding to central angle of 160°, long 60 mm, is accepted. The zone comprising the welding being avoided). The V notch of 45°, with root radius of 0.15 mm, is machined to a depth of 1.22 mm (about 20% of wall thickness), simulating the expected mechanical damage caused during the removal of ground for construction by excavator or digger.

2.2. ELECTROLYTIC SOLUTION

The electrolytic solution is used to achieve required hydrogen ion concentration around the notch tip. This standard solution Natural Soil 4 (NS4), applied in the experiment, produced the effect of stress corrosion caused by the soil surrounding the tested pipeline. Chemical composition of NS4 solution is given in Table 3.

TABLE 3. Chemical compound of the NS4 solution [5].

Chemical compound	Formula	Concentration (mg/L)
Potassium chloride	KCl	122
Sodium hydrogenocarbonate	$NaHCO_3$	483
Hydrated calcium chloride	$CaCl2,2H_2O$	181
Hydrated magnesium sulfate	$MgSO4,7H_2O$	131

This solution was prepared from these chemical compounds and distilled with demineralized water, the solution volume is about 17 l. Homogeneity of the solution during the test was saved applying the pump. The natural pH value of the solution is between 8 and 8.5, and in the first test the value of 8.56 was held. To be in the same condition that in reality, the pH is decreased until 6, 7 during the fatigue test. During all the test the level of the pH is controlled and regulated between 6, 6 and 6, 7, applying a bubbling of CO_2 gas. Another bubbling of N_2 gas is used to stabilize the solution and to take off oxygen inside. The bubbling of gas set out again in the following way: 80% of N_2 gas and 20% of CO_2 gas.

2.3. EQUIPMENT

2.3.1. *Fatigue Machine*

Specially designed three-point bending device was positioned on the closed loop hydraulic testing machine INSTRON 1341 (Figure 6) with a load cell of capacity 0–10 kN for operation in load or displacement control. The applied load, frequency, and the type of cycle (sinusoidal, trapezoidal, or rectangular) were monitored on the control panel. The set-up for bend test with variable load with positioned specimen is presented in Figure 7.

All testing device components were produced of stainless steel 316L, in order to avoid the problems with corrosion in NS4 solution. The specimen was exposed to variable load through a support A (Figure 7), and supporting rollers B and C allowed the bending of specimen. Support and rollers were produced of PVC for electrical insulation and reduced friction.

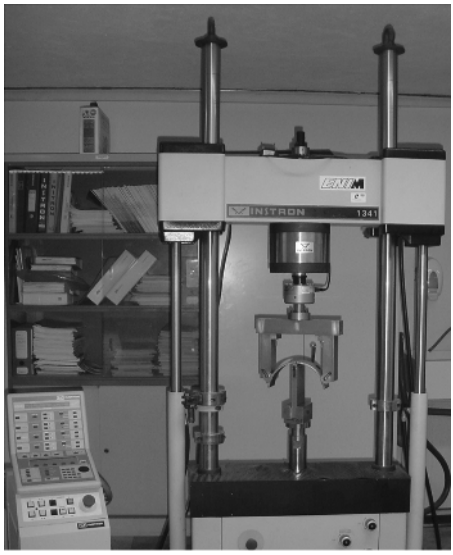

Figure 6. Hydraulic fatigue machine.

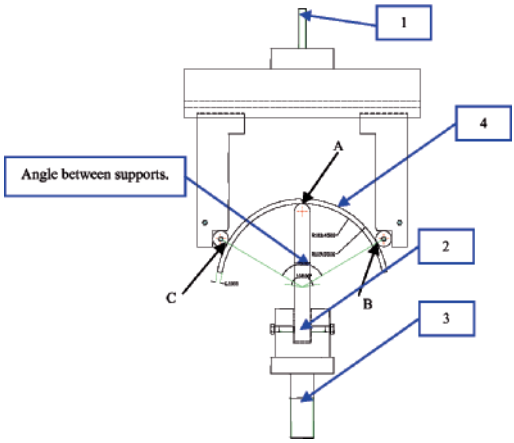

Figure 7. Design of set-up for three-point bend test with variable loading 1 – Connection of testing device to the load cell 2 – Transmitting component with rounded tip 3 – Connection to the machine bottom 4 – Curved specimen.

2.3.2. *Hydrogen Cell*

The hydrogen cell is a recipient containing the NS4 solution, sufficiently spaced to dispose three-point bending set-up in it (Figure 11). The recipient of open upper side was produced by welding of PVC plates. Potentiostatic device was used to control the electrolysis. Complete remote monitoring of the system was

enabled by used PC computer. The EC-Lab software allowed to process all the parameters and the data (i.e., work potential, test duration, signal type, limits). This electrolysis was performed with three electrodes:

- The working electrode (in blue on the Figure 8): is the curved sample because we want to make a reduction of this sample (hydrogen atom are adsorbed on the surface of the sample and with the time they can diffuse towards the interior of the sample).
- The counter electrode (in yellow on the Figure 8): is made with a stainless steel (platinum). It is used to measure the evolution of current during the fatigue test.
- The reference electrode (in red on the Figure 8): is saturated calomel (KCl) electrode. It is used to control the tension applied.

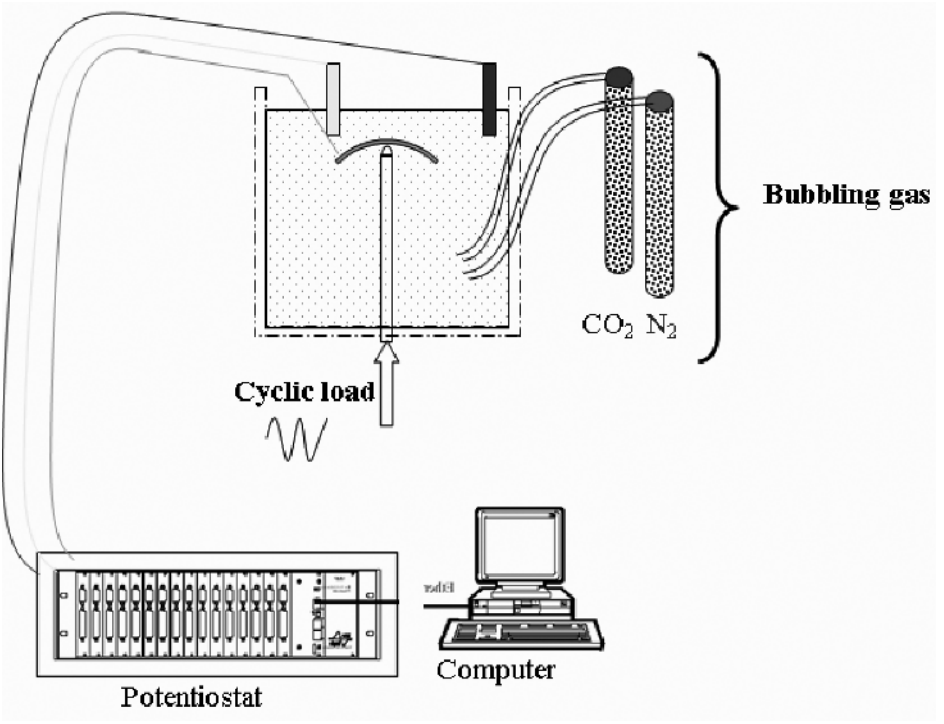

Figure 8. Assembly of the hydrogen cell.

The free potential of tested steel is –0.78 V_{sce} (Figure 9), is determined from experimentally obtained polarization curve. We have chosen to set the work potential at $-1V_{sce}$, at this potential we will certainly carry out a reduction of the sample near the notch (adsorption of hydrogen atom on the sample) [6]. The difference between oxidation and reduction is explained in the Figure 9, based on a chemical principle.

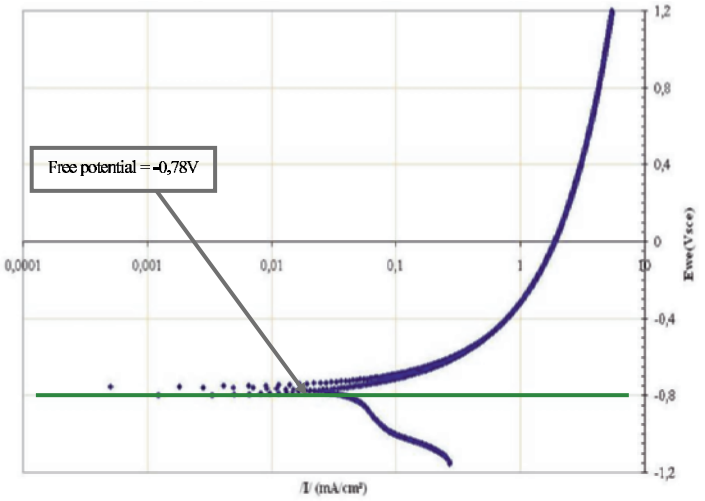

Figure 9. Free potential of steel used.

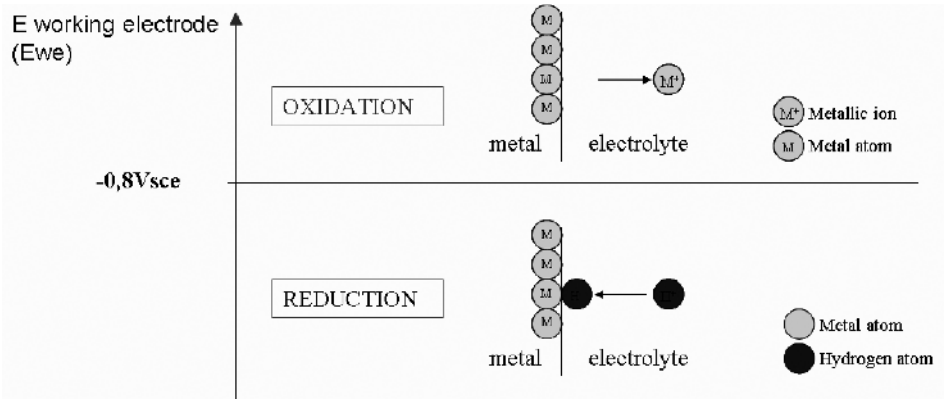

Figure 10. Difference between oxidation and reduction.

A pump is used to have always a homogeneous and a stable solution during the fatigue test which can last up to two months.

The Figure 10 shows the difference between the two great chemical principles that are the oxidation and the reduction. The first is characterized as being a loss of a metallic ion and the second as being an adsorption of a hydrogen atom (in our case).

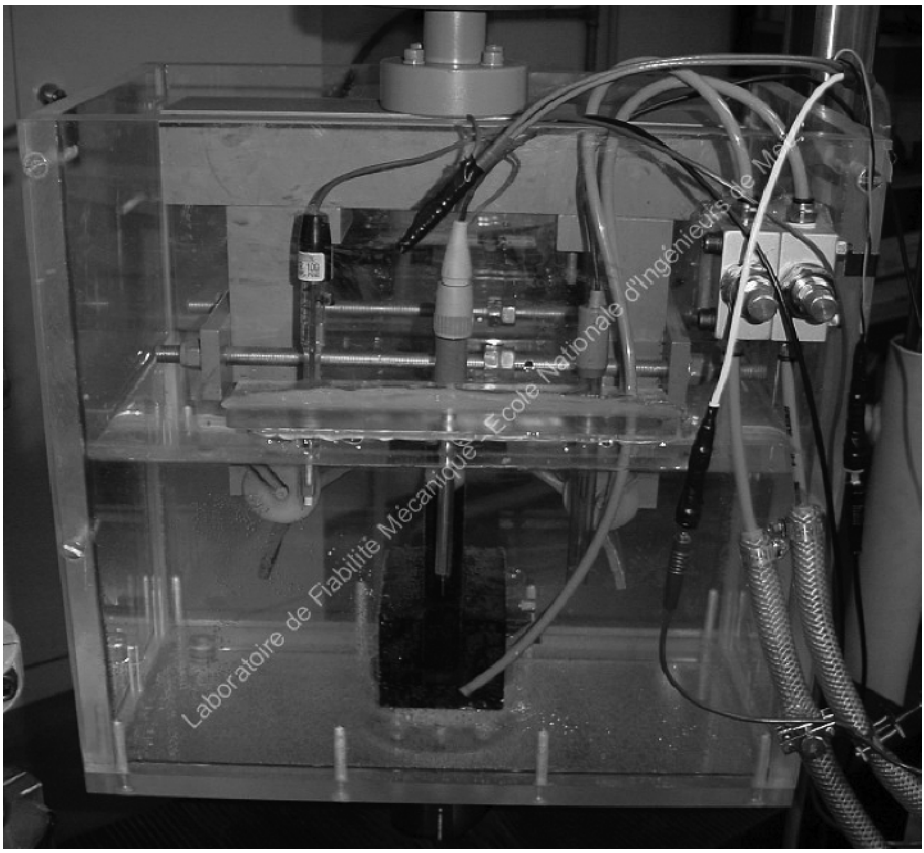

Figure 11. Hydrogen cell.

3. Results

3.1. TESTS IN AIR

For testing in air atmosphere sinusoidal loading cycle was selected, with the frequency of 7 Hz, and load ratio R = 0.5. The load ratio is defined by holding account owing to the fact that the pressure in pipeline fluctuates in average once a day between $P_{min} = 40$ bar and $P_{max} = 70$ bar:

$$R = \frac{P_{min}}{P_{max}} \quad (2), \qquad \text{So in our case we have: } R = \frac{40}{70} = 0.57$$

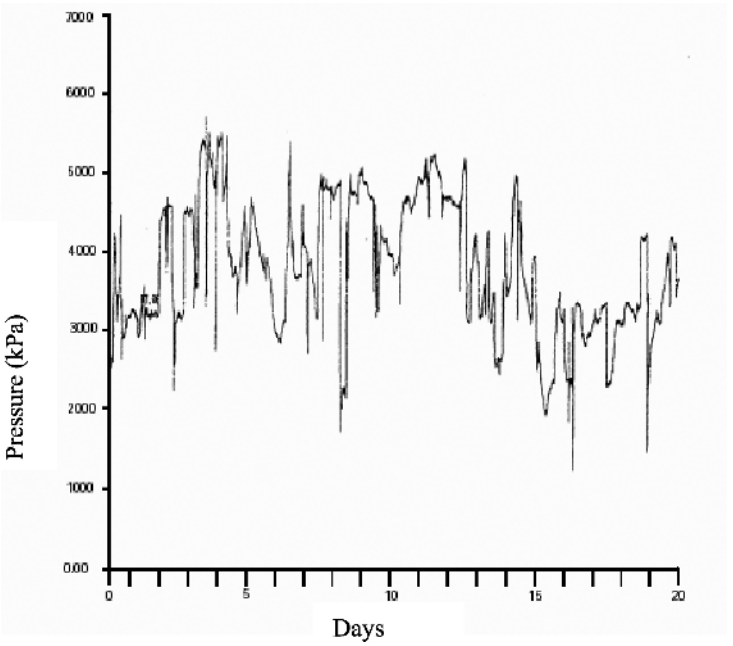

Figure 12. Profile of pressure during 20 days for a pipeline with liquid products [1].

The selected sinus amplitude of loading corresponded to the accepted pipeline life between 60,000 and 300,000 cycles. Approximate value of the amplitude was calculated based on Haigh's diagram and the relation of Basquin:

$$\sigma_a = C * N_R^b \tag{3}$$

We carried out 12 tests with six different amplitudes of loading, so there are two points by different tests.

3.2. TESTS IN HYDROGEN

Applying the same loading parameters (amplitude and ratio) (Figure 13) testing was performed in hydrogen environment, with the applied constant potential of electrolyse of –l V_{sce}. The frequency was reduced to 0.5 Hz, in order to achieve better diffusion of hydrogen atoms in the notch region of the specimen.

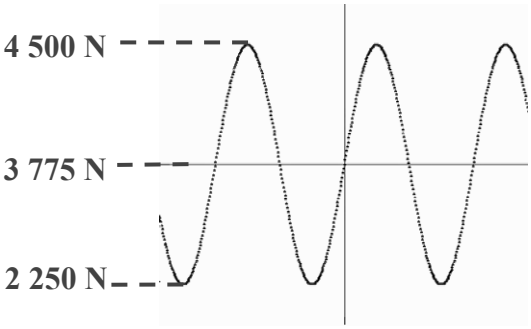

Figure 13. Shape of the cycle used during the fatigue test (load versus time).

3.3. COMPARISON OF RESULTS OBTAINED IN AIR AND HYDROGEN

For 12 performed tests with six different loading amplitudes it was possible to obtained two points for Wöhler's curves from each test performed in air and in hydrogen atmosphere, presented in Figure 14. It is clear from test results that the lifetime in presence of hydrogen is decreased by 70%.

The coefficient "b" in Basquin's relation (3) obtained for the test in air atmosphere was found to be –0.19. This value is close to referenced values for tested steel $(-0.2)^x$, so the obtained Wöhler's curves can be accepted as representative. In hydrogen atmosphere Basquin's coefficient "b" is found reduced by 42%.

The fracture surface appearance is shown in Figures 15 and 16 for both specimens, tested in air and in hydrogen atmospheres. The regions of fatigue and brutal fractures can be clearly recognized. The surface of fatigue crack is smooth and even. The surface of final, brutal fracture corresponds to brittle fracture, and which small region of blunting can be identified. The region of fatigue fracture is clearly smaller for the specimen tested in hydrogen, and this is expressed by the reduction of about 70% in crack length.

4. Conclusion

Detrimental effect of hydrogen on fatigue life of pipeline steel is experimentally evidenced and quantified by about 70%. Existing notch as a stress raiser has an important contribution to this adverse effect. Anyhow, the first results obtained are not sufficient, and next experiments are required in order to understand the effect of hydrogen environment on the crack initiation, what can be performed applying an acoustics emission device in similar tests.

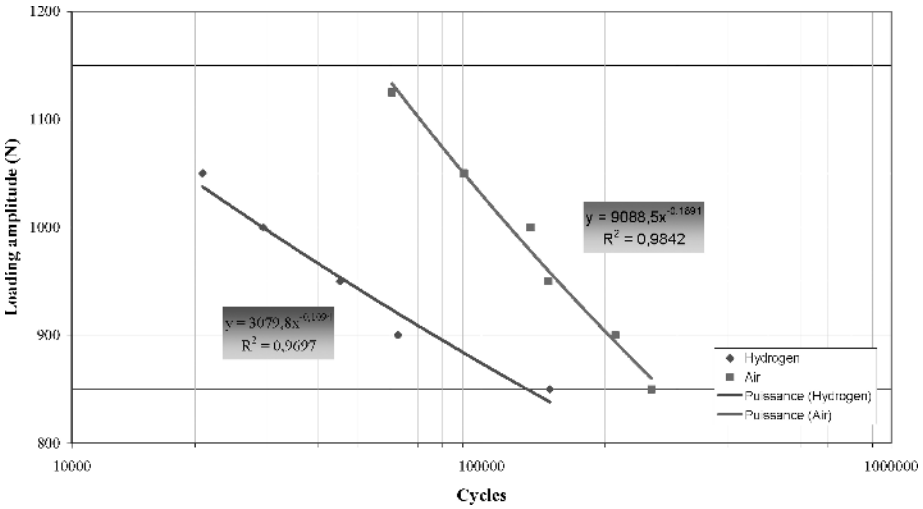

Figure 14. Wöhler curves in presence of air and hydrogen.

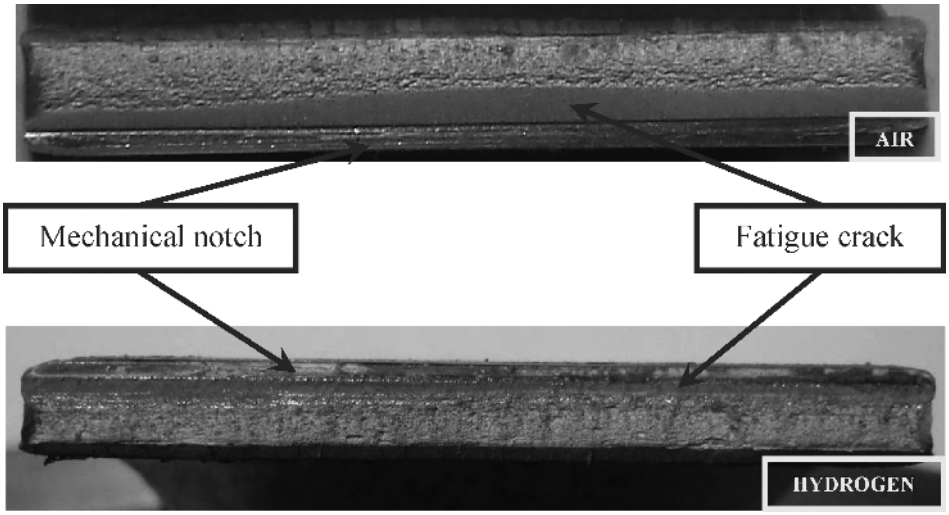

Figures 15 and 16. Fracture appearance after the fatigue test.

References

1. Rapport de l'enquête MH-2-95, Fissuration par corrosion sous tension des oléoducs et des gazoducs canadiens, Office National d'Energie (1996).

2. C. Monin, Etude de l'impact de l'hydrogène sur un défaut de soudage de canalisation par l'approche déterministe, Ecole Nationale d'Ingénieur de Metz (2001).
3. J. Capelle et al., Hydrogen Effect on Fatigue Life of a Pipe Steel, Paper presented at the conference ICMFM XIII (2006).
4. J. Capelle et al., A comparison of experimental results and computations for cracked tubes subjected to internal pressure, Materials and Technology, volume 40, 233–237 (2006).
5. A. Benmoussat and M. Hadje, Corrosion behaviour of low carbon line pipe steel in soil environment, JCSE, volume 17 (2005).
6. J. L. Crolet and G. Béranger, Corrosion en milieu aqueux des métaux et alliages, Techniques de l'Ingénieur, M150-4.

THE EXPERIENCE ON SAFETY, RELIABILITY AND RISK ASSESSMENT OF SOME UKRAINIAN, RUSSIAN AND LATVIAN TRANSITE PIPE LINES

A. J. KRASOWSKY
G. S. Pisarenko Institute for Problems of Strength, National Academy of Sciences of Ukraine, Timiryazevskaya St., 2 Kiev 01014 Ukraine

Abstract: The advanced Expert System (ES) "InfoPipeMaster" is developed for transit pipeline management incorporating databases (DB) "Objects", "Materials", "Defects", and "Loadings" with special attention to assist especially in defining the different materials damage processes during pipeline operation. Main results of ES application to the safety, reliability, and risk assessment are demonstrated for different pipelines: transit ammonia pipeline ø355.6 mm "Togliatty – Odessa" (territory of Ukraine), transit oil pipeline ø720 mm from Latvian oil corridor, transit gas pipeline ø1420 mm "Braterstvo", transit oil pipeline ø1020 mm "Kremenchug – Kherson" and other. Comparative analysis of diagnostics is provided for each pipeline using the nondestructive testing results of different time period. Special attention is paid to the geographic navigation system, to the pipeline inspections results, to the repair and mitigation amounts, to the materials degradation in service, to the calculation modules developed for stress–strain fields as well as for the flaw risks assessment. Existing Codes of different countries and fracture mechanics methods are used for flaw assessment and remaining lifetime prediction. Categorization of flaws method is proposed with respect to the safety factor to prescribe the repair terms for different defects in order to diminish reasonably the amount of repairs and inspections. Software complex "BucklingPipeMaster" is developed to solve the physically and geometrically nonlinear problems related to the large displacements of buried transit pipelines and its application is demonstrated to estimate the stresses due to the soil movement. Risk assessment is made for different pipelines.

Keywords: pipeline, reliability, flaw, risk, fracture, expert system

G. Pluvinage and M.H. Elwany (eds.), Safety, Reliability and Risks Associated with Water, Oil and Gas Pipelines, 219–231.

1. Introduction

The great number of transit pipelines in former Soviet Union was constructed many years ago mainly on the basis of the timely technological policy. The lifetime management of these pipelines has become of strategic importance for NIS countries, especially as the environmental and risk requirements are now more stringent. The territory of Ukraine, for instance, intersect about 35,000 km of transit gas pipelines, near 8,000 km of transit oil pipelines, and more than 1,000 km of transit ammonia pipeline. The great part of these pipelines has the age between 25 and 40 years whereas some of them are about 50 years old. Similar situation exists in some other NIS countries. This is why the safety, reliability, and risk assessment of these pipelines is thus a critical issue in NIS countries from both economical and environmental points of view.

The transit pipelines are territorially spread objects for which current monitoring of technical condition is a very difficult task with respect to the huge amount of information that has to be taken into consideration. The modern information technologies are only the way to solve correctly this problem. The development of ES for pipeline management requires a combination of data and expertise from different areas, for instance geography navigation, computer models derived from knowledge gained in studies of stress distribution, failures (due to corrosion, fatigue, stress corrosion cracking, corrosion fatigue, brittle fracture, or plastic collapse, etc.) and tested in the context of case studies of past failures and current state of pipelines.

The problem of life extension and risk assessment of the ageing transit pipelines is considered as a final goal of research. There is absent in Ukraine generally adopted approach to its solution, and a problem is complicated by the declared harmonization of the Ukrainian system of safety regulations with European one. The latter have moved away from prescriptive requirements to goal-setting ones to put the onus for safety back on the designer/builder/operator [1]. Thus, the western approaches and existing documents are considered with respect to three key questions: (1) the modern principles and limit state criteria for providing the safety at design; (2) the operational procedures and the usage of notion of risk in the safety management of existing pipelines; (3) the Fitness-for-Service procedures and criteria for analysis of the structural integrity of in-service component containing a flaw.

The strength calculations of transit pipelines are executed in the countries of former Soviet Union in accordance to code СНиП-2.05.06-85 [2]. Internal pressure is the basic loading factor, which results in the hoop stresses. To prevent the failure the sufficient wall thickness of pipe is provide taking into account the corresponding safety factors. Concerning the other specific loading factors (limit states) that result in the origin of considerable longitudinal stresses

from axial force and bending moment that can arise up during building and exploitation of pipelines (loss of stability, soil displacement and earthquakes, emerging, and other), domestic norms require their obligatory consideration by the use of methods of structural mechanics. However, traditionally, structural mechanics mainly operates by the concepts of the small displacements and, unfortunately, such practice is used for the calculations of buried pipelines. There is why the above mentioned requirement remains often only a declaration, as not only the concrete examples of calculations but also the methods of calculation of such important features in general are absent in standards.

Unfortunately, suggestions as to the improvement of norms in domestic literature are mainly concentrated to the clarification of safety factors related to the circumferential stresses. Indisputably, they substantially influence the price of new pipe building as well as the economic efficiency of operating pipelines. However, from the point of providing the reliability of pipelines the practice of exploitation and statistics of pipeline failures specify on the large role of exactly longitudinal stresses. For example, from the data of the European group on gas pipelines integrity only to the soil movement, as a reason of failure, belongs about 7% of pipes failures without flaws, whereas the circumferential stresses are the reason of failure only for pipes containing defects [3]. Therefore within the framework of this task we are thoroughly concentrated on the analysis of longitudinal stresses, especially for the case of the large displacements when a pipeline is characterized as both a flexible filament and a beam. It is necessary to point out that the pipe stability can be estimated correctly only on the basis of consideration of the large displacements and, main, can be described both its post-critical geometrical position and loading of pipeline on the direct and banded parts taking into account the movement of earth, the implementation of repair and building works, at presence of the water areas, etc.

2. The Expert System (ES) for Pipeline Management

The development of a considerably improved knowledge-based expert system for the accurate assessment and management of operating pipelines to enhance their reliability and for predictive maintenance is of utmost importance from technical, economic, and environmental viewpoints. In order to solve many problems related to the safety, reliability, and risk assessment of transit pipelines the ES “InfoPipeMaster” has been developed in the G. S. Pisarenko Institute for Problems of Strength, National Academy of Sciences of Ukraine. Main tasks of this system are as follows.Collection and storage (i.e., Integration) of all information about pipeline:

- Computer portrait, digital maps, schemes, drawings, photos of object, documents, etc.
- DB for materials, flaws, pipes, loading conditions, and soils
- The results of inspections
- The results of calculationsGlobal and local stress and strain fields calculations with respect to the real technical state and to the whole spectrum of loading conditions
- Comparative analysis using the inspection results of different time periods
- Technical reports and summary conclusion about the object conditions and risks. Safety declaration

2.1. MAIN COMPONENTS OF ES

- Information – search component (ISC)
- Geography information system (GIS)
- Automatic system for current documents Integration module for remote control and remote management

Expert modules for strength, reliability, remaining life and risk assessment, flaw assessment procedures (CODE's) existing in different countries;

- Component for actualization of DB distributed territorially
- Safety system and allowed information distribution

Integration of information is a key element of ES. It is an analytical process what attracts to the general consideration the information about design, construction, exploitation, maintenance, tests, diagnostics, etc. According to the code [4] the definition of the information sources is the first step of the data integration. Two special analytic modules are developed for ES, "3D position of object" and "Internal pressure calculation". The first one is prescribed for the pipeline attachment to the digital geography map, for creation of the situational trace plan (i.e., attachment of the objects to trace), for comparison the data from different sources, for creation the corrosion map. The module "Internal pressure calculation" is prescribed to calculate the internal pressure at each point of pipeline with respect to its real profile and to the transportation regime, which is governed by standard [2]. The procedures for internal pressure calculation are different for gas and for oil pipelines.

3. Databases (DB)

Special attention is paid to the structure of several Databases (DB) where all information is stored about pipeline and to their interactions. DB of unified

structure is incorporated into ES. The typical structure of some DB is pointed out at Tables 1 and 2.

TABLE 1. The structure of DB "objects".

Object position	Geometry	Loadings	Calculation results
• Object label	• Object type	• Pressure	• Displacements and angles
• Coordinates, GPS attachment, digital map	• Dimensions	• Temperature gradient	• Forces and moments
• Environment	• Schemes, photos, drawings	• Forces	• Stresses and strains
	• Documents	• Weight, etc.	

3.1. DB CONTENT:

- General information
- Linear part of pipeline
- Protection system against corrosion
- Previous diagnostics
- Repair and mitigation
- Earth and soils

DB "Loadings" contains information about all loading factors affected the pipeline.

As an example of such information the internal pressure variation is shown on Figure 1 during three years.

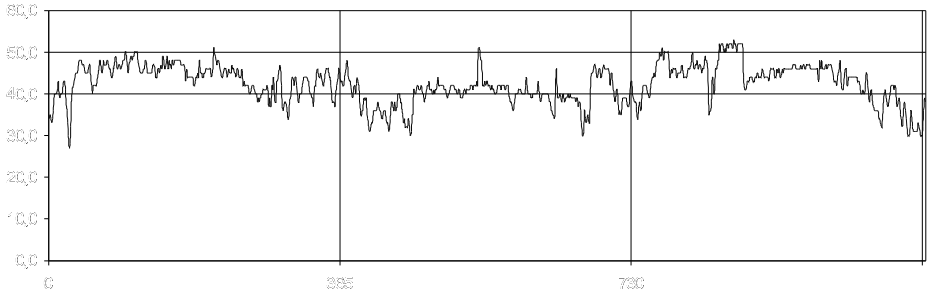

Figure 1. The internal pressure variation during period of 2000–2002 years. Transit gas pipeline "Ivankov - Chernobyl".

TABLE 2. The structue of DB “defects”.

Defect position	Geometry	Loadings	Calculation results
• Defect label	• Defect type	• Axial force	• Stress intensity factor
• Element number	• Dimensions	• Bending moments	• Reference stress
• Coordinates	• Position	• Pressure	• Safety factor
	• Schematization	• Corrosion rates	• Risks

DB “Materials” has the set of physical and mechanical properties of steels typical for given pipeline segments. Chemical composition typical for steel of given pipeline segment as well as some special physical and mechanical properties of steels can also be found in this DB. For instance, the Charpy V-notch energy characteristics are demonstrated on Figure 2 [5] of the pipeline steel 17GS degradation after 35 years of service, transit oil pipeline ø720 mm, Latvian oil corridor. This result shows essential aging of material: the brittle to ductile transition temperature shift is about 50°C due to the 35 years of service. In contrast, the Charpy U-notch energy of steel X46 (ammonia transit pipeline, 22-years old) versus temperature does not reveal significant shift of transition temperature.

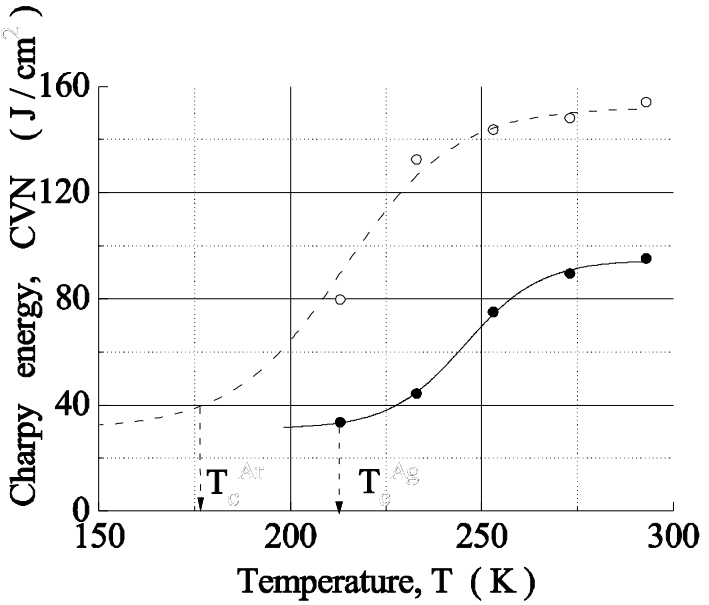

Figure 2. Degradation of pipeline steel 17GS after 35 years of service, transit oil pipeline Ø720 mm, Latvian oil corridor. Open points – as received material, black points – the same material after 35 years of service.

The Charpy energy is one of the most sensitive mechanical properties of material to the ageing process. In contrast, the fatigue crack growth rate shows less sensitivity to the ageing degradation (Figure 3). In spite of different structure, operation age, chemical composition the fatigue crack growth diagrams are quite similar for 8 materials variations, thus this properties can not be used as a good parameter to define the material degradation value.

4. Geography Information System (GIS)

This system contains huge amount of information about pipeline. It allows provide this information in the convenient digital cartography form with additional textual explanations, diagrams, and photos and connect the pipeline on map with the passport information at data banks. But the GIS is rather a provider of operative information but is not the instrument for creation of the management decisions.

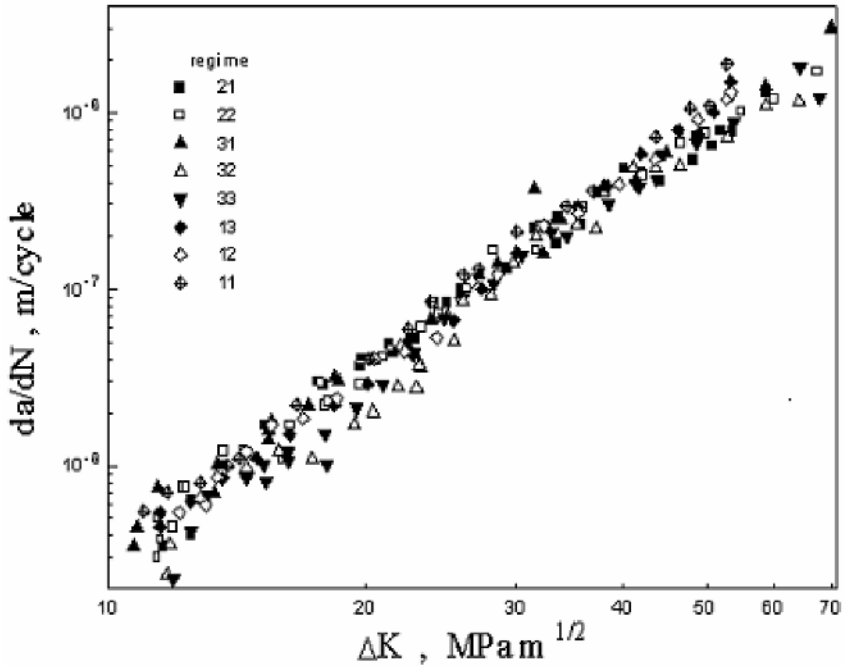

Figure 3. Fatigue crack growth rate versus stress intensity factor range for some pipeline steels and their welded joints of the Latvian oil corridor. 21 – pipeline NP-2 (D = 530 mm) after 26 years of service, pipes of Czech production, base metal; 22 – the same pipe, longitudinal welded joint; 12 – the same pipe, archival base metal; 31 – pipeline NP-1 (D = 720 mm) after 35 years of service, steel 17GS, base metal; 32 – the same pipe, longitudinal welded joint; 33 – the same pipe, circumferential welded joint; 13 – the same pipe, archival base metal; 11 – pipeline NP-3 (D = 720 mm) after 20 years of service, steel 16G2, base metal.

The image of ammonia pipeline "Togliatti – Odessa" (territory of Ukraine) is presented in lecture as an example of GIS technology in the ES "InfoPipeMaster". The whole length of this pipeline is 1,018 km. Another example of GIS technology demonstration is the attachment of data revealed during the repeated "Intelligent pig" diagnostics of the trace "Dolina – Rossosh" of transit gas pipeline Ø1,420 mm (Carpatian mountains region). This effective technology has been also used during the diagnostics of pipeline #1 (Ø720) mm of Latvian oil corridor. The results of recognizing along the trace "Ivankov – Chernobyl" of transit gas pipeline Ø325 mm are also presented in GIS component of developed ES. The GPS-attachment has been done as well for other different objects along the trace and the DB "Objects" has been created.

5. Large Displacements of Buried Transit Pipelines

Software complex "BucklingPipeMaster" is developed to solve the geometrically and physically nonlinear problems [6], related to great displacements of underground transit pipelines. The complex takes into consideration:

- Earth movements:
  - Longitudinal
  - Transversal
- Large displacements of pipe at buckling

The effective numerical iteration procedure is developed within the framework of implementation of task for the analysis of the stress–strain state of plain pipeline in an environment taking into account the possible presence of supports and pipe bifurcations. Raising equilibrium equations and geometrical equations are written down in the geometrically nonlinear statement and complemented by the boundary conditions found analytically for a semi-infinite pipeline at a longitudinally transversal resilient bend.

The possibilities of complex were demonstrated by analysis of both transversal (with respect to pipe axis) soil displacement and longitudinal soil displacement measured using the soil markers movement of ammonia transit pipeline "Togliatty-Odessa" near observatory "Stepove 2".

Another demonstration of the complex possibilities is the modeling of the installation process of new pipe ø720 mm into old one ø1020 mm at crossing of the river Dnepr [7] (the crossing length about 2 km, transit oil pipeline "Kremenchug – Kherson"). During this procedure the supporting plastic rings positions on the smaller pipe were optimized and the installation process was successfully finished.

The buckling was analyzed of buried pipeline at excavation of its part considering the effect of its solar heating. With the help of software complex "PipeMovement" the end position (after buckling) of pipe, large displacements, bending moments, and stress distribution were calculated. Similar problem was solved for the cases of transit pipeline in weak grounds (bogs, permafrost melting) when some supporting weights are lost.

As an example, the building of the see bottom pipeline with a ship has been considered, the task on emerging of pipeline, which has practical application at the gasket of submarine pipelines. The following example has been considered: it is necessary to know, what form will be taken by the pipe of defined length, one of ends of which is in sea bottom, and other one is fastened on a winch on ship and lift downward along the chamfer of some radius of curvature. The calculated equilibrated configuration of the pipeline and its curvature and stresses were defined. The geometries of the position are in good agreement with ones known from literature.

6. Risks Assessment

The risk-analysis starts from the stage of collection and storage (i.e., integration) of information about pipeline required for all procedures of the global stress calculation, the flaws danger and risk assessment as well as its components: failure probability and failure consequences. The analytical module "BucklingPipeMaster" has been developed [8–11] in order to calculate the global stress and strain fields of the complex 3D pipeline systems. The module allows to solve following problems:

1. Static stress calculation of multi-contoured 3D pipeline system (like pump station)
2. Stress and displacements of pipeline due to the soil movement
3. Buckling of buried and open pipelines
4. Taking into account the loading history (pressure, temperature, etc.)
5. Comparison of different procedures of intelligent pigging with respect to the pipeline 3D coordinates.

The results of such calculations are the input data for local stress and risks calculation for individual defects by ES.

Calculation module "Strength" of ES for flaw assessment is based on Ukrainian Code [12] what uses the philosophy of two criteria approach (like R6 Code) in fracture mechanics and the solutions [13–16]. The danger of defect is defined by the actual safety factor, Figure 4.

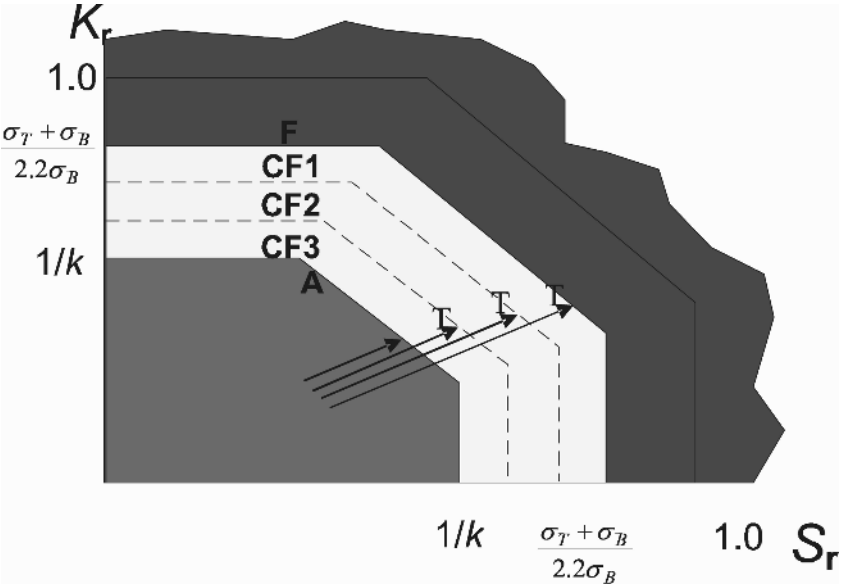

Figure 4. The "two criterion" assessment of the defect danger. Grey field corresponds to the laws that do not require the repair. White field corresponds to three kinds of flaws that can be repaired within the terms $T_2 > T_1 > T_0$, respectively. Black field requires immediate repair of flaw.

Fracture assessment diagram is presented in dimensionless coordinates $K_r = K_I/K_{Ic}$ and $S_r = P/P_{LL} = \sigma_r/\sigma_b$ where K_I and K_{Ic} are the calculated stress intensity factor and fracture toughness of material, respectively, P and P_{LL} are the generalized loading and the limit load of plastic collapse, respectively, σ_y, σ_b and σ_r are the yield stress, ultimate stress, and reference stress, respectively, k is the safety factor which represents the integral reliability coefficient of the considered pipe part. According to the results of flaws assessment the decision is taken concerning the repair term for each defect. Special method is developed in ES for this procedure (Figure 4). All flaws are divided into three categories depending on the field of FAD where the given defect is situated: F – forbidden to operate without immediate repair, CF – conventionally forbidden (there are three subcategories corresponding to different terms of repair) and A – allowed to operation without repair.

The efficiency of calculation module for the flaw risks assessments is demonstrated by analysis of limited internal pressure for each defect revealed during diagnostics of oil pipeline "Kremenchug - Kherson», ø1,020 mm (Figure 5). It has been shown by comparison of local operating pressure in pipeline with the limited internal pressure for each defect the possibility to graduate each defect with respect to its real safety factor and to prescribe the reasonable term for its repair. Such philosophy provides the possibility to diminish essentially the amount of required repairs. Categorization of flaws with respect to the safety

factor to prescribe the repair term has also been done for Latvian oil corridor, pipeline ø720 mm, 33 years using the comparison of Russian, and R6 Codes. Other demonstration of real flaw assessment and local integrity prediction using the codes of different countries has been done at the analysis of diagnostic results of gas pipeline "Ivankov – Chernobil" at excavated part No.6 (near Priborsk town) for the recognized longitudinal scar.

Statistics has been established of flaws recognized on the part "Dolina – Rossosh" by two diagnostics of transit gas pipeline "Braterstvo" ø1,420 mm as well as the comparison has been done of their results in order to estimate the accuracy of flaw detection. The calculation model for pumping station PS-13 of transit ammonia pipeline has been developed as an example in order to demonstrate the possibility of "Strength" module. Risk matrix was constructed for transit gas pipeline "Ivankov – Chernobyl" ø325 mm.

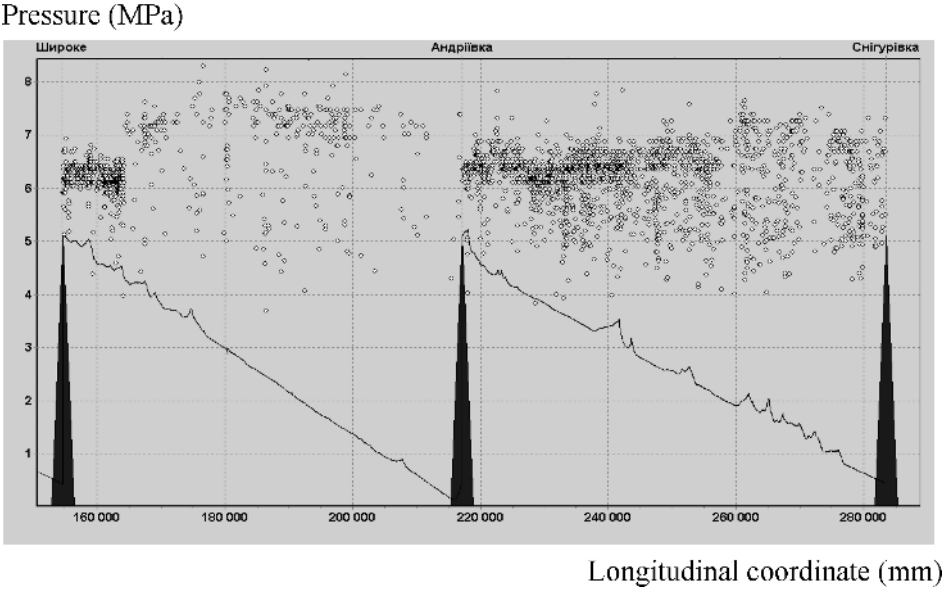

Figure 5. Diagnostics results of transit oil pipeline Ø1,020. Two inclined black lines between three pump stations represent actual internal pressure of pipeline. Each point corresponds to limit pressure (with respect to safety factor) for each revealed flaw. Note the high density of revealed defects in the region of high pressure just after pump stations.

7. Conclusions

1. The ES "InfoPipeMaster" is developed for transit pipeline management, flaws assessment, and risk analysis. Main tasks are realized in ES: the integration of all information about pipeline; global and local stress and

strain fields calculations; comparative analysis using the inspection results of different time periods; technical reports; and safety declaration about the object conditions and risks.

2. Special attention is paid to the DB realization where all information is stored about pipeline and its interactions. Several DB of unified structure are incorporated into ES.
3. GIS contains huge amount of information about pipeline. It allows provide this information in the convenient digital cartography form with additional textual explanations, diagrams and photos and connect the pipeline on map with the passport information at data banks.
4. Software complex "BucklingPipeMaster" is developed to solve the geometrically and physically nonlinear problems, related to great displacements of underground transit pipelines. The complex takes into consideration earth movements (longitudinal and transversal), pipe buckling, and provide the solution of different practical problems: static stress calculation of multi-contoured 3D pipeline system (like pump station); stress and displacements of pipeline due to the soil movement; buckling of buried and open pipelines; taking into account the loading history (pressure, temperature, etc.); comparison of different procedures of intelligent pigging with respect to the pipeline 3D coordinates.
5. The analysis of diagnostics results and risk analysis have been done for some transit pipelines of Ukraine, Russia, and Latvia.

Acknowledgment

This work has been partially supported by the Science and Technology Center in Ukraine.

References

1. Probabilistic methods: uses and abuses in structural integrity. Prepared by BOMEL Limited for the Health and Safety Executive. Contract research report 298/2001,2001, 216 pp.
2. СНиП 2.05.06 – 85. Transit pipelines. – Moscow, Gosstroj USSR, 1988, 52 pp.
3. Bolt, R. and Kuik, G. R., Safety in European Gas Transmission Pipelines; EGIG shows its continuing improving safety performance, 22nd IGU World Gas Conference, Tokyo, Japan, June 1–5, 2003.
4. ASME B31.8S – 2001. Managing system integrity of gas pipelines. Supplement to ASME B31.July 8, 2002 – New York: ASME, 2002, 66 pp.

5. Kotrechko S. O., KrasowskyA. J., Meshkov Yu. Yu.,and Torop V. M., Effect of long-term service on the tensile properties and capability of pipeline steel 17GS to resist cleavage fracture. *Int. J. Pres. Vessels a. Piping*, 81, pp. 337–344, 2004.
6. Orynyak I. V. and Radchenko S. A., Analytical and numerical solution for a elastic pipe bend at in-plane bending with consideration for the end effect. *Intern. J. Solids and Structures*, 44, pp. 1488–1510, 2007.
7. Orynyak I. V., Bogdan A. V., and Vasylyuk V. M., Simulation of the process of drawing a pipe through the pipeline with a larger diameter, *Proceedings of IPC2006 6th International Pipeline Conference,* September 25–29, 2006, Calgary, Alberta, Canada.
8. Orynyak I. V., Torop V. M.,and Romashchenko V. A. Strength of Materials, #2, pp. 87–100, 1998.
9. Orynyak I. V. and Radchenko S. A. Strength of Materials, #5, pp. 23–35, 2004.
10. Orynyak I. V. and Radchenko S. A. Strength of Materials, #4, pp. 93–101, 2003.
11. Orynyak I. V. and Bohdan A. V. Strength of Materials, to be published.
12. VBN B.2.3-00018201.04-2000, Naftogas of Ukraine, issued on May 01, 2001.
13. Orynyak I. V., Strength of Materials, #4, pp. 39–49, 1993.
14. Orynyak I. V. and Borodii M. V., The combined weight function method application for a hole emanated crack, *Engng. Fracture Mech*., 49, #2, pp. 287–294, 1994.
15. Krasowsky A. J. Makhutov N. A., Orynyak I. V.,and Torop V. M., *Problemy mashinostroenija i avtomatizacii*, #4/5, pp. 92–100, 1992 (in Russian).
16. Krasowsky A. J., Orynyak I. V.,and Torop V. M., The assessment of the limit state and the transition temperatures in hollow cylinders with axial cracks, #61, pp. R55–R59, 1993.

RELIABILITY ASSESSMENT OF PIPELINES USING PHIMECA SOFTWARE

A. AMIRAT[1*], B. BOUNAMOUS[1], R. KHELIF[1, 2],
A. MOHAMED CHATEAUNEUF[2] AND K.CHAOUI[1†]
[1]*LR3MI, Department of Mechanical Engineering, University Badji Mokhtar, BP. 12, Annaba 23000 Algeria;* [2]*LaMI – UBP & IFMA, Campus de Clermont-Ferrand, Les Cézeaux, BP. 265, F-63175 Aubière, France*

Abstract: The present work deals with lifetime management of underground pipeline for safe hydrocarbon transport. Reliability PHIMECA soft tool is used for assessing the tubular structure under active corrosion. Basically, three parts are presented. First, a theory of reliability methods is developed to make in evidence the design philosophy. Second, the concept of reliability analysis under PHIMECA soft is given to sort out the mechanical and probability models for a determined limit state function. Finally, a case study applied to an underground pipeline under severe loading and active corrosion is investigated in order to analyze the reliability. A PHIMECA report on the obtained result is given. The former approach concerns the experimental characterization of residual stress distribution in large diameter pipes to be coupled with a corrosion model. Along the pipe lifetime, the residual stress relaxation is involved due to the loss of pipe thickness as material layers are consumed out by corrosion.

Keywords: reliability, pipeline, residual stress, corrosion, PHIMECA soft

1. Introduction

Over the last 30 years, there has been an increased interest in the use of high-strength steel in automotive sector, offshore structures, ships, mining industry, pipeline applications and others. These steels derive their high strength from a

* amirat_abd@yahoo.fr
† chaoui_k@yahoo.fr

G. Pluvinage and M.H. Elwany (eds.), Safety, Reliability and Risks Associated with Water, Oil and Gas Pipelines, 233–259.

combination of mechanisms including solid solution, grain size, dislocation and precipitation hardening. However a good combination of strength, toughness, weldability and, for sour-gas service, also high resistance to hydrogen embrittlement (HE) corrosion have to be obtained. In the case of pipelines, increasing mechanical properties can allow the construction of larger tubes with the same inlet without increasing the thickness and weight of the tube [1, 2]. Therefore, the research tendency is oriented to the improvement of the material mechanical properties in terms of yield strength and toughness corrosion resistance [3, 4]. Meanwhile, mechanical problems of pressure pipes containing defects remain an important feature to solve despite considerable engineering and scientific efforts which have been devoted to the characterization of the damage response and the understanding of the mechanism of defect evolution. The need for such characterization and understanding is essential to pipe design, service life, risk, safety, economy and environment to avoid dramatic consequences [5].

In many cases, pipelines placed underground, under runways, railroads or roadways are required to resist the influence of the overlying soil and many surface traffic loads, accidents as well as the effect of corrosion attacks [5, 6]. In addition, the thermal and mechanical deformation manufacturing process of structures always generates residual stresses that should not be neglected since their effects are not evident until the structure is loaded or exposed to environmental hazards [7, 8]. Moreover, uncertainties associated with geometrical measurements, pipe manufacturing, operating conditions, rate of corrosion and nature of soil and load parameters can significantly affect the lifetime behavior of the pipe structure. How to incorporate, the effect of corrosion and residual stress in the structural analysis of a pipeline by handling the system uncertainties and fluctuations, is evidently of practical importance [1, 2, 9].

For this purpose, structural reliability analysis has significantly increased over recent years, because of computer facilities and powerful available engineering software [10–12]. The basic principals of the reliability approach are to calculate failure probabilities and to use them as a basis for demonstrating safe and economical operation over pipeline lifetime. The philosophy then consists, to identify the potential causes of failure, establish the mechanism, which leads to the failure mode and evaluate the risk associated to these failures.

The aim of this work is to present a reliability assessment of a buried pipeline structure. The application concerned the behavior of a pipeline under severe loadings. This is achieved by developing, a mechanical model where the loading parameters are included with both residual stresses and uniform corrosion. The analyses have been carried out using the reliability PHIMECA software [12]. Pipeline reliability is simulated in terms of corrosion damage over 50 years considering at the same time residual stress distribution.

2. Reliability-Based Methods

In any structural analysis the design philosophy is twofold. One design level is based on a deterministic approach, while the second level is related to a probabilistic approach. Both approaches should if used correctly, fulfill the basic safety requirements implicitly by the deterministic method and explicitly by the probabilistic method.

The mathematical models, which are derived, can be used in probabilistic approaches to assess the reliability of structures. The concept of the reliability-based method is well reviewed in the literature [13–16]. The scope comprises design, operation, requalification and abandonment of the structure [13, 14].

A reliability-based design systems analysis may be performed as [15–16]:

- Complete probabilistic designs check, i.e., the probability of failure is explicit, given and checked toward the acceptance criteria as the required target level, P_f.
- A calibration of partial design factors to be used together with a selected load and resistance factor design (LRFD) format, i.e., to develop the LRFD format and determine the safety factors.
- A re-calibration of safety factors in the LRFD format, i.e., the probability of failure is implicit in the acceptance criteria via safety factors and characteristic values. A redesign or requalification due to material deterioration and other lifetime changes of the design basis also comes into this group.

2.1. PROBABILISTIC DESIGN APPROACH

The probabilistic design approach consists then, in modeling the generalized stochastic load S and generalized stochastic resistance R [17–18], for a given limit state. As a simple illustration, the corresponding limit state function may be expressed in the form of:

$$G(x) = R - S \tag{1}$$

When the distribution functions for R and S are established through uncertainty analysis, the probability failure, as illustrated in Figure 1, is then calculated using Eq. 2:

$$P_f = \int_{G(x)\le 0} f_{R,S}(R,S)\,dRdS \tag{2}$$

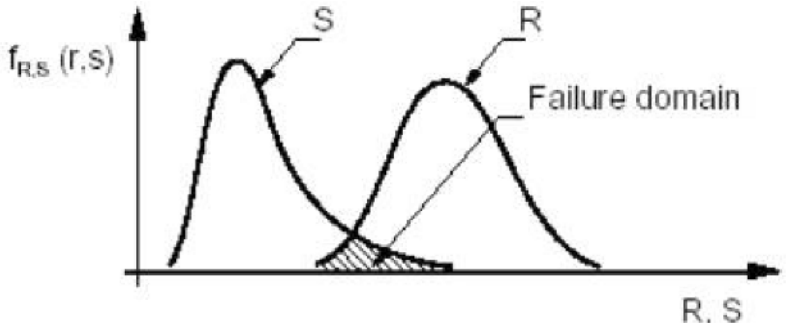

Figure 1. Domain of failure probability and random load and resistance.

which should be equal to or less than the required target level, $P_{f\ \text{target}}$, for a design to be accepted. A probabilistic design check can be then written as follows:

$$P_{f,calculated} \leq P_{f,\text{target}} \tag{3}$$

The probabilistic design approach includes the following steps:

- Identify and express all relevant failure modes, e.g., limit states
- Identify the physical variables
- Define the limit state function
- Uncertainty modeling of variables and properties
- Determine the target reliability
- Calculate the failure probability
- Compare against acceptable failure probabilities
- Evaluate results

2.2. RELIABILITY CALCULATION METHODS

The theory and methods of structural reliability have been developed significantly during the last two decades. Intensive research on both philosophical and conceptual issues as well as on computation methods has been performed. The field has now reached a stage where use of the developed methodology is becoming widespread. The methods and application of structural reliability theory have been documented in an increasing number of textbooks [10, 11, 19, 20], along with numerous papers dealing with the subject [21–24]. The reliability calculations are achieved by first calculating the failure probabilities. The probability of failure of a component P_f is defined by [20]:

$$P_f = \int_{G(x_i)\le 0} f_{x_1,x_2,...,x_n}(x_1,x_2,...,x_n)dx_1dx_2...dx_n \quad (4)$$

where x_i is a vector of stochastic variables, $f(x_i)$ is the joint probability density function and $G(x_i)$ is the limit state function where $G(x_i) < 0$ signifies failure. The function $G(x_i)$ may represent a single failure cause, i.e., single event function, or a system representation of several failure modes. Only few analytical solutions of the above integral exist, and formal numerical integration [18], Monte Carlo simulations [20] are very time consuming and costly due to high number of stochastic variables normally occurring in reliability applications.

Estimates of the failure probability may be obtained by the complementary approaches known as approximate analytical methods, first-order reliability method and second-order reliability method (FORM/SORM). The reliability of a component is defined by a limit state function $G(X_i) = 0$ of design variables X_i taken as random variables. Conventionally, two domains are chosen.

SAFETY DOMAIN:

3. $G(X_i) > 0$ and Failure Domain: $G(X_i) \le 0$

Hasofer and Lind [20] have shown that the reliability index should be taken in standardized Gaussian variable space, U_i. To do so, a transformation of the stochastic variables into a probability space of standardized independent normal variables must be defined such as:

$$U_i = T(X_j) \quad (5)$$

and the new limit state will be defined as:

$$H(U_i) = G(T\text{-}1(U_j)) \quad (6)$$

To approximate the failure probability a FORM or SORM can be used. The reliability index is therefore the minimum distance between the space origin of U_i variables and the domain failure space $H(U_i) \le 0$; in a simplified problem this can be written as follows:

$$\beta = \min\left(\sqrt{\{U\}^t\{U\}}\right), \text{for a limit state } H(U_i) \le 0 \quad (7)$$

The first proposition of the reliability index is due to Rzhanitzyn [21] in the 1950s. However, Cornell has popularized this index in the 1970s. Then, various propositions have been presented, but the most complete one is that of Hasofer and Lind [22].

RZHANTZYN-CORNELL INDEX [21]:

The proposed definition is very simple: the reliability index is obtained from the means (μ) and standard deviations (σ) of the characterized variables of the failure function (Z).

$$\beta_c = \frac{\mu_z}{\sigma_z} \tag{8}$$

However this definition is not invariant in all cases.

HASOFER-LIND INDEX:

This is the invariant definition and the reliability index can be given as a function of the probability of failure:

$$\beta = -\Phi^{-1}(P_f) \tag{9}$$

The reliability *R(t)* is hence defined as the complement of the probability of failure:

$$R(t) = 1 - P_f \tag{10}$$

In addition to the reliability index β, the cosines director α_i sensibility and elasticity factors are also obtained. α_i denotes the i-th component of the normalized gradient vector to the failure surface in the design point. The quantity α_i^2, is often denoted an (uncertainty) importance factor, which can be interpreted as a relative measure of the significance of the uncertainty of a basic variable (or a group of variables) for the problem, considered. The importance of these factors for a variable is to identify the effect of the variable variation on the mechanical system state. The aim of the investigation is therefore, selecting the most significant variables that can be optimized toward the mechanical behavior or the reliability.

A number of reliability analysis tools such as PHIMECA software [12] are at present time also available on the open market. The simplified methods are motivated by the fact that calculation of points on the failure surface in some cases is very costly, e.g., if for each iteration in normalized space a new time-consuming finite element analysis is required. It is therefore important to establish methods in which the number of *G(x)* calculations is kept, minimum. It should be mentioned that the number of interactions could in some cases be reduced by application of response surface techniques.

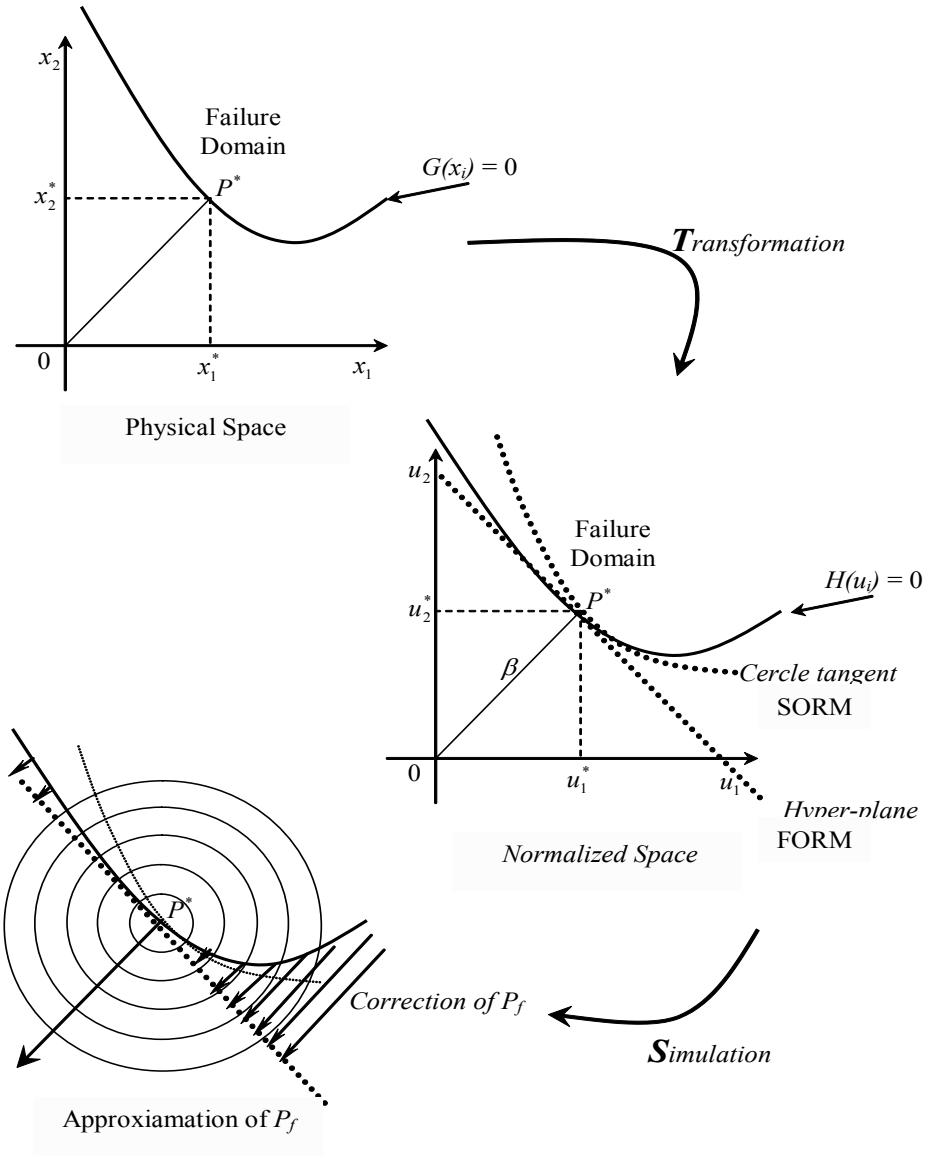

Figure 2. FORM/SORM approximate method. Hasofer-Lind reliability index [22].

3.1. PHIMECA SOFT FOR RELIABILITY ANALYSIS

PHIMECA [12] is general reliability analysis software that can be coupled to numerical code such FE codes, allowing a complete reliability-based design. This is very interesting for component and structural design and maintenance, when considering cost and safety parameters. However reliability analysis required a high scientific level making reliability tools less used in industry but reserved to research laboratories. Meanwhile, the need of using simple and convivial reliability tools is felt and expressed by system designers to evaluating the reliability of their structures. Therefore, the reliability tool tendency today, is oriented toward the development of sensitively easy tools for reliability calculations. PHIMECA soft offers this opportunity through a simple and convivial concept. Figure 3 shows the concept of PHIMECA soft for reliability calculations. The concept of PHIMECA integrates three parts:

The first part is a modeling part which consists in presenting the geometrical model, expressing the failure modes, identifying the physical variables together with their probabilistic distributions on the one hand, and in defining the limit state function according to the reliability target on the other. The former part allows to entering the mechanical model, the probabilistic model and the limit state function into PHIMECA software.

Once the models are introduced, the second part consists in calculations achieved through the physical analysis using deterministic approach and reliability analysis using probabilistic approach. FORM/SORM calculations are obtained through the direct method to determining the design point or the failure point. Surface response calculation gives a good approximation of the limit states around the design point. Monte Carlo simulations allow to obtaining references and control the second-order approximations. Then distribution and parametric reliability can be run.

The third part is the analysis part, in which interpretations of results should be done. The basic results of a probabilistic analysis comprise, failure probability or reliability index, design point giving the most likely values of the basic variables at failure and importance and sensitivity factors. The main purpose of an evaluation is to examine whether the design point is reasonable based on engineering judgement and experience from similar types of problems and that it is not in conflict with obvious physical knowledge or limitations. First, it has to be checked that the obtained point from the reliability analysis is a global minimum solution to the optimization problem rather than a local minimum. Further, the results from the reliability analysis also have to be

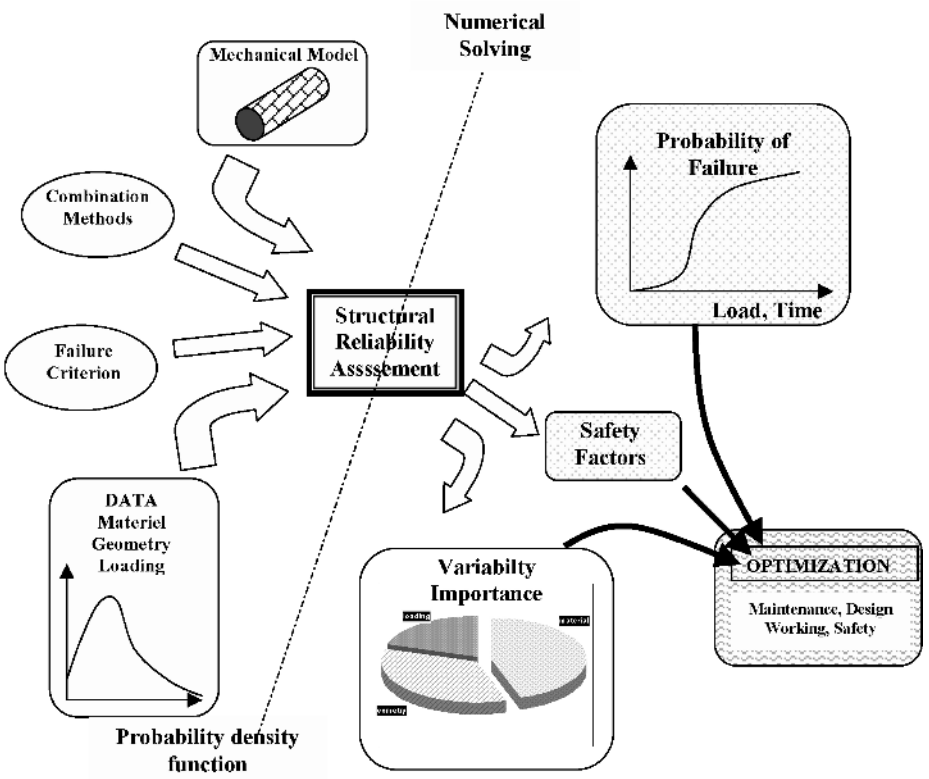

Figure 3. Concept of reliability analysis using PHIMECA software.

assessed by verifying that the design point corresponds to physically realizable outcomes of the stochastic variables. If a response surface technique is applied, it must be verified that the response surface performs satisfactorily in the neighborhood of the design point.

4. Case Study

The aim of this section is to present a reliability analysis of an uncoated buried pipeline under given pressure rating and incorporating hoop residual stresses using PHIMECA software.

4.1. MECHANICAL MODEL

Thin pipelines are mainly subjected to longitudinal and circumferential stresses as shown in Figure 4.

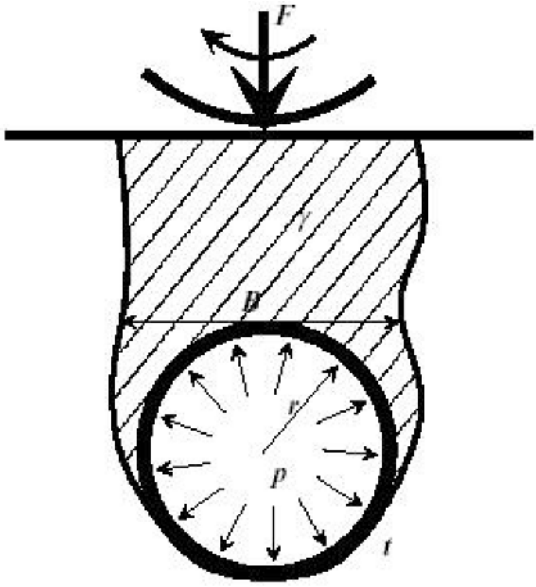

Figure 4. Underground pipeline configuration [25].

The mechanical model aims to define these stresses as a function of different applied loadings. The mechanical stress is directly obtained from von Mises equation applied to nonvanishing stresses: circumferential stress σ_c and longitudinal stress σ_l, leading to the following expression of equivalent stress:

$$\sigma_{equiv} = \sqrt{\sigma_c^2 + \sigma_l^2 - \sigma_c \, \sigma_l} \tag{11}$$

where σ_{equiv} is the von Mises equivalent stress. The circumferential and longitudinal stresses will be given in the following sections for uncorroded and corroded pipes.

4.1.1. *Uncorroded Pipes*

CIRCUMFERENTIAL STRESS

The circumferential stress σ_c is composed of four principal stresses:

$$\sigma_c = \sigma_{p_c} + \sigma_{s_c} + \sigma_{t_c} + \sigma_{res_c} \tag{12}$$

where σ_c is the total circumferential stress, σ_{p_c} is the stress due to internal pressure, σ_{s_c} is the soil loading, σ_{t_c} is the bending stress and σ_{res_c} is the residual stress; the subscript c indicates the circumferential component of stresses. These stresses will be developed in the following.

Under the hypothesis of thin tube, the circumferential stress σ_{p_c} due to internal pressure is evaluated by:

$$\sigma_{p_c} = \frac{p\,r}{t} \tag{13}$$

Where p is the internal pressure, r is the internal pipe radius and t is the pipe wall thickness. The overlying soi1 creates a bending deformation of the pipe in the circumferential direction; the corresponding bending stress is given by:

$$\sigma_{s_c} = \frac{6\,k_m\,C_d\,\gamma\,B^2\,E\,t\,r}{E\,t^3 + 24\,k_d\,p\,r^3} \tag{14}$$

where σ_{s_c} is the overlaying soil bending stress in the circumferential direction [9], B is the width of ditch at the level of pipe top, C_d is the coefficient for earth pressure, E is the modulus of elasticity, k_m is the bending moment coefficient depending on vertical load and associated reaction, k_d is the deflection coefficient and γ is the soil density. In the same manner, the traffic loads generate a bending stress in the circumferential direction:

$$\sigma_{t_c} = \frac{6\,k_m\,I_c\,C_d\,\gamma\,F\,E\,t\,r}{L_e\left(E\,t^3 + 24\,k_d\,p\,r^3\right)} \tag{15}$$

where σ_{t_c} is the circumferential bending stress due to traffic loads [9], I_c is the impact factor, C_I is the surface load coefficient and L_e is the effective length of the pipe on which load is computed.

LONGITUDINAL STRESS

The longitudinal stress is again determined from four principal stresses:

$$\sigma_l = \sigma_{f_l} + \sigma_{t_l} + \sigma_{B_l} + \sigma_{res_l} \tag{16}$$

where σ_{f_l} is the longitudinal tensile stress, as a result of Poisson's ratio effect from the outward radial action of the internal pressure:

$$\sigma_{p_l} = \frac{\mu\,p\,r}{t} \tag{17}$$

where μ is the material Poisson's ratio. σ_{t_l} is the longitudinal expansion or contraction stress [9], due to differences in operation and installation temperatures:

$$\sigma_{t_l} = \alpha\,E\,\Delta\theta \tag{18}$$

with α the thermal expansion coefficient and $\Delta\theta$ the temperature differential. The longitudinal stress due to external load bending σ_{B_l} is calculated by:

$$\sigma_{B_l} = E\, r\, \chi \tag{19}$$

with χ the longitudinal curvature of a bent pipe. Finally, σ_{s_t} is the longitudinal residual stress, as a result of Poisson's ratio effect:

$$\sigma_{res_l} = \mu\, \sigma_{res_c} \tag{20}$$

4.1.2. *Corrosion Model*

Simplified practical way in integrating the corrosion process in the mechanical model is to use a power law postulated for corrosion to model the loss of wall thickness *P* within the time of exposure:

$$t_c = k\, T^n \tag{21}$$

as t_c thickness of the corrosion layer and *T* is elapsed time.

The model is an engineering one where the multiplying factor *k* and the exponential constant *n* are obtained by fitting eq. (21) to corrosion data [9, 26]. In atmospheric pressure, the mean and standard deviation of *k* for these data were 0.066 and 0.037, respectively, and the corresponding values of *n* were found to be 0.53 and 0.14, respectively. If considering the net wall thickness instead of the original wall thickness of the pipeline then eqs. (13–15) will respectively take the following forms:

$$\sigma_{p_c} = \frac{pr}{t - kT^n} \tag{22}$$

$$\sigma_{s_c} = \frac{6k_m C_d \gamma B^2 Er\left(t - kT^n\right)}{E\left(t - kT^n\right)^3 + 24k_d pr^3} \tag{23}$$

$$\sigma_{t_c} = \frac{6k_m I_c C_d \gamma FEr\left(t - kT^n\right)}{L_e\left(E\left(t - kT^n\right)^3 + 24k_d pr^3\right)} \tag{24}$$

4.1.3. *Residual Stress Model*

Thin pipelines are mainly subjected to longitudinal and circumferential stresses. The mechanical model aims to define these stresses in function of different applied loadings.

CIRCUMFERENTIAL RESIDUAL STRESS

The residual stress was measured using the layer removal method based on Crampton technique [27], which consists in recording the relaxed strain generated after slitting longitudinally a tube. The distribution was determined through the pipe wall by removing incrementally layers of 2 mm from the parent tube of 12.7 mm thickness. Figure 5 shows the distribution of the circumferential residual stress through the pipe wall.

The maximum calculated residual stress reached 15% of the yield strength of the material and the law can be written in the form:

$$\sigma_{res_c} = -70\left(1 - \frac{2\,r_t}{t}\right) \tag{25}$$

σ_{res_c} is the circumferential residual stresses which are obtained practically for X60 API standard seamless steel tube [7, 8] and r_t corresponds to the radial coordinate of the design point.

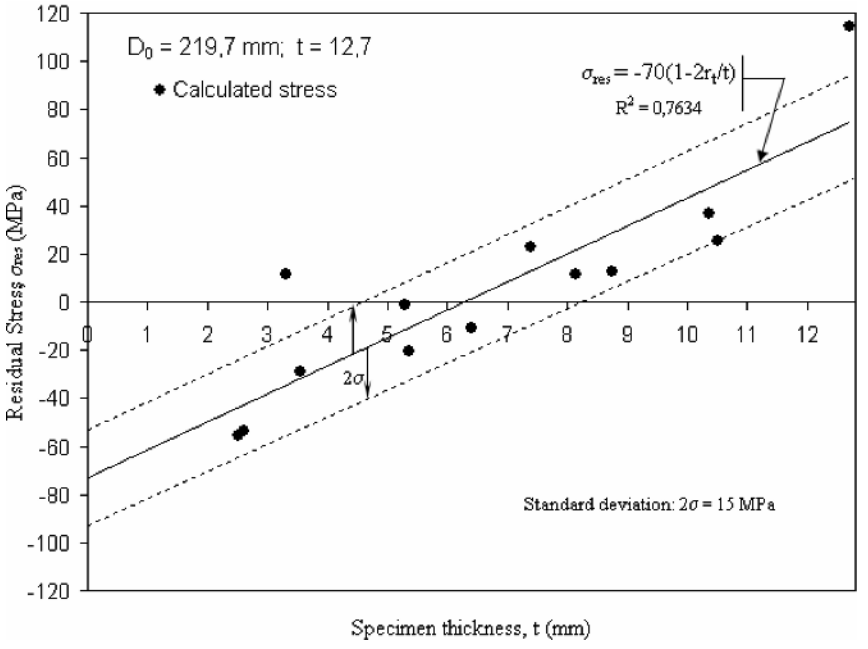

Figure 5. Residual stress distribution in a X60 Grade pipe [8].

LONGITUDINAL RESIDUAL STRESS

σ_{s_t} is the longitudinal residual stress, as a result of Poisson's ratio effect:

$$\sigma_{res_l} = \mu\, \sigma_{res_c} \tag{26}$$

$$\sigma_{res_c} = -70\left(1-\frac{2kT^n}{t}\right)\left(1-2\frac{r_t-kT^n}{t}\right) \tag{27}$$

Eq. (27) presents one of the important items in this study. In fact, when corroded layers of metal are removed a relaxation in residual strain occurs causing a redistribution of the residual stresses. The layer removal method used to determine the original distribution is very helpful to set a corrosion model when considering the net wall thickness instead of the original thickness, Figure 6.

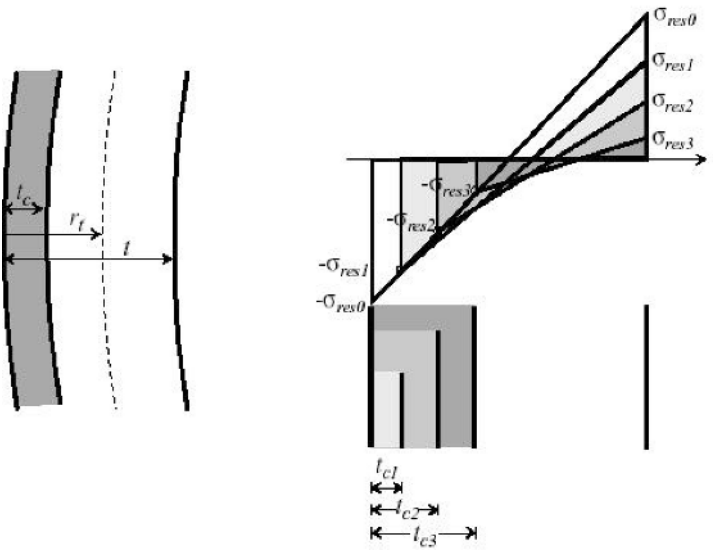

Figure 6. Net wall thickness for corroded pipes and residual stress relaxation scheme.

The model is therefore obtained from simple calculation as follows:

If r_t is the considered point for stress analysis, the net wall thickness is the difference between the original thickness of the pipeline wall to and the thickness of the corrosion layer t_c. The origin of the design point is displaced to t_c. When attributing the new origin of the design point $r_t + t_e$, Eq. (27) takes the form below:

$$\sigma_{res_1} = -70\left(1 - 2\frac{r_t - kT^n}{t}\right) \tag{28}$$

The new form of the residual stress in the equilibrium state will be:

$$\sigma_{res_2} = -\sigma_{res_1}\left(1 - 2\frac{r_t}{t - kT^n}\right) = -70\left(1 - 2\frac{r_t}{t - kT^n}\right)\left(1 - 2\frac{r_t - kT^n}{t}\right) \tag{29}$$

$$\sigma_{p_t} = \frac{\mu pr}{\left(t - kT^n\right)t} \tag{30}$$

4.1.4. *PHIMECA Mechanical Modeling*

As the mechanical model is defined, the next step is to write in PHIMECA soft. Figure 7 shows a part of the mechanical model program.

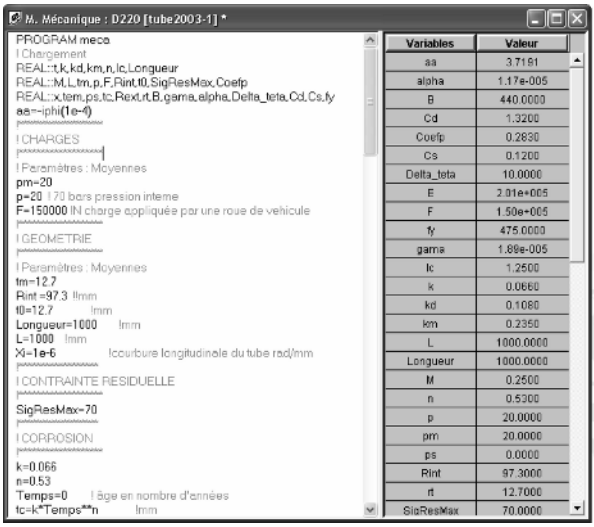

Figure 7. Sample of the mechanical model in PHIMECA soft.

4.2. LIMIT STATE FUNCTIONS

The reliability assessment for the pipelines considered in this study is mainly divided into two steps. On the one hand, the contribution of determined residual stress is obtained for an underground pipeline subjected to internal pressure and

externa1 loads and on the other hand, a corrosion model based on an empirically modeled power law (eq. 21) is used for the same pipeline under corrosion activation, with respect to residual stresses. Therefore two limit state functions *G(x)* are settled for reliability ca1culation according respectively to the case study:

$$G_{res} = f_Y - \sigma_{equiv} \tag{31}$$

For a corroded pipeline:

$$G_{cor} = f_Y - \sigma_{equiv} \tag{32}$$

The limit state function is introduced through the limit state window given by PHIMECA soft, as illustrated in Figure 8.

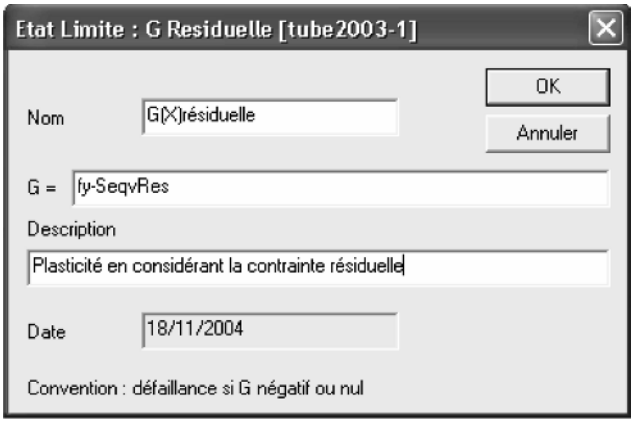

Figure 8. Conventional limit state function within PHIMECA software.

4.3. PROBABILISTIC MODELS

It is worth to note that in both limit state functions, the corrosion power law is used but for a noncorrosion case the ca1culation is made for times equals to zero. So, there are considerable uncertainties to be associated with the corrosion parameters k and n as described in the above stress expressions. All these uncertainties result from geometry, loading, manufacture coefficients and operating service of the pipeline. It is reported [9, 25] that the uncertainties associated to the effective 1ength L_o, impact factor I_c, and curvature χ are significant. The

coefficient C_d, C_s, k_d, k_m have moderate uncertainties associated with them since they need to be selected for a given situation on the basis on imperfect information. The geometrical parameters such as ditch width B_d, pipe radius and wall thickness contain uncertainties highly dependent on workmanship and quality control after ditch construction and pipe production process. Temperature differential depends on pipe bedding and seasonal variation of temperature relative to the lying process. The loading parameters in terms of internal pressure p and wheel load F are particularly difficult to define probabilistically as they depend on operational characteristics associated with the pipeline and its daily requirements. Properties of pipeline material such as Young's modulus *(E),* yield stress (σ_y), thermal expansion coefficient *(a)*, Poisson's ratio and of soil (for instance soil unit weight), are rather well defined and subjected to variable quantities. The residual stress is usually unknown, therefore neglected. The particular effort in this work is to emphasize on the residual stress by determining its distribution through the wall of the pipeline. The layer removal technique used for the residual strain measurements [8] is destructive and results in a large scatter calculated residual stresses for a series of given thickness, fluctuated between 20% and 30% of the mean value (Figures 5 and 6).

A probabilistic approach is then used to assess the reliability of the pipeline. Each design variable is therefore represented by a random variable with an estimated mean and standard deviation. For the present work, where available a probability density function is employed, and the normal distribution is the least-based distribution, Figure 9.

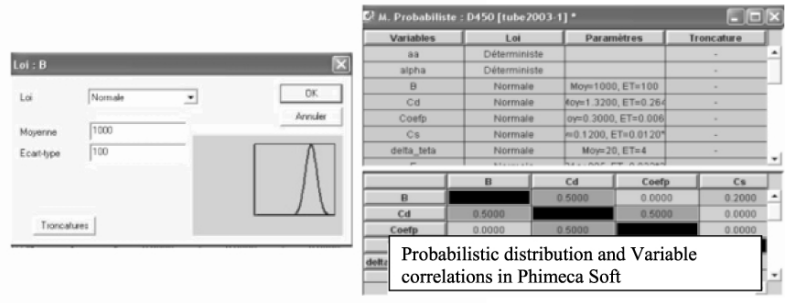

Figure 9. Probability density function and correlation of the variables.

4.4. UNDERGROUND PIPELINE RELIABILITY ASSESSMENT

4.4.1. *Pipeline Configuration and Uncertainties*

The pipe under the present investigation is an underground pipeline made from seamless tubes, passing under roadway. The pipeline is used to convey gas under

high pressures ranging from 7 MPa to 40 MPa. The wheel loading F of the traffic applied to the pipe length is that of maximum load during a given lifetime T. The effect of repeated loading that might lead to corrosion fatigue is not considered. The reliabilities calculations are carried out at the time where the wheel load is applied.

The random variable involved and their statistical distribution are given in Table 1. Numerical values are determined from measurements for geometrical parameters and from results on material testing for the properties; otherwise they have been obtained from literature [9, 26], where details about their importance and distribution are reported. The normal distribution has been adopted for all variables since only means and variances are available.

The probability of failure as discussed above is calculated for two limit state functions with regards to residual stresses.

4.4.2. *PHIMECA Reliability Report*

For a limit state function of eq. 31, a sample of PHIMECA reliability results are given in Tables 2, 3, 4, 5.

HASOFER-LIND RELIABILITY INDEX: β_{HL}=2.6106

The failure functions that are expressed in eqs. 31 and 32 satisfy the usual conditions, positive values of G imply safety and negative values imply failure. It is evident that the failure functions are then nonlinear with respect to their variables. It may also happen that the distribution of some of the variables is nonnormal. An iterative advanced FORM [20, 22] is well equipped to handle such problems and will be employed herein. In this approach, variables will be characterized by their mean value m_X and their standard deviations σ_X, or coefficient of variation (COV), Figure 9 and Table 1. In this case, it is assumed that these variables are statistically noncorrelated. For the purpose of applying the advanced FORM, the nonlinear limit state function must be linearized at some point on the surface $G = 0$. Here, the target is to find a point defined by the mean values of the variables. The point is known as the design point. An interaction is usually necessary in order to find this point. Once the design point is found, the mean m_G, and standard deviation σ_G of G can be used to determine the reliability index β, which is a measure of pipeline safety (see eqs. 8 and 9).

TABLE 1. List of 19 random variables.

Number	Variable	Value	Law	Mean	Standard deviation
1	B	440.00	Normal	440	44
2	Cd	1.3200	Normal	1.32	0.264
3	CoefP	0.2830	Normal	0.30	0.0069
4	Cs	0.1200	Normal	0.12	0.0120*1.5
5	Delta_teta	10.00	Normal	20	4
6	E	2.01E + 05	Normal	2.01E + 05	0.033*201,000
7	F	1.50E + 05	Normal	1.50E + 05	30000
8	Fy	475.00	Normal	475	24.5
9	Gamma	1.89E – 05	Normal	1.89E – 05	1.89E – 0.06
10	K	1.25	Normal	1.25	0.250
11	Kd	0.1080	Normal	0.1080	0.2*0.108
12	Km	0.2350	Normal	0.235	0.2*0.235
13	Length	1,000	Normal	1,000	100
14	N	0.53	Normal	0.53	0.053
15	P	40.00	Normal	40	4
16	Rint	97.30	Normal	97.3	0.04*97.3
17	SigResMax	70.00	Normal	70	15
18	T0	12.70	Normal	12.70	0.635
19	x_i	1.00E – 06	Normal	1.00E – 06	1.00E – 07

TABLE 2. Probability of failure.

FORM	P_f=4.52E-03
Hyper-sphere	P_f=4.52E-03
Breitung	P_f=4.52E-03
Tvedt	P_f=4.52E-03

4.4.3. *Reliability Analysis*

RELIABILITY AND RESIDUAL STRESS

Using PHIMECA software reliability approach to assess the pipeline safety in the case where the pipe is free from any flaws and when internal pressure is up rated, the reliability index β and probability of failure P_f are computed with

respect to residual stress distribution. Figure 10 illustrates the variation of reliability index β as a function of up rated pressure for two cases (i) the residual stress is not considered and (ii) the residual stress distribution follows a linear law according to eqs. (5 or 15).

Up rating pressure from 11 MPa to 45 MPa resulted in a decrease of the probability index β, in both cases. For instance, if acceptable probability of failure P_f ranges from 10^{-4} to 10^{-6} corresponding to an index of reliability β

TABLE 3. Design point in physical space and reduced space.

	Physical space	Reduced space		
Variable	X^*	U^*	α	α^2 %
B	441.59	0.0361	–0.0138	(–) 0.0192
Cd	1.3295	0.0360	–0.0138	(–) 0.0190
Coefp	0.2998	–0.0360	0.0116	(+) 0.013
Cs	0.1225	0.1364	–0.0523	(–) 0.2732
Delta_teta	19.6504	–0.0874	0.0335	(+) 0.1121
E	2.01E + 05	1.67E – 03	–6.41E – 04	(–) 4.10E – 05
F	1.55 E+ 05	0.1789	–0.0685	(–) 0.4696
Fy	444.6528	–1.2387	0.4745	(+) 22.5133
Gamma	1.89E – 05	0.0181	–6.93E – 03	(–) 4.80E-03
Lc	1.2947	0.1789	–0.0685	(–) 0.4696
Kd	0.1067	–0.0593	0.0227	(+) 0.0516
Kn	0.2450	0.2123	–0.0813	(–) 0.6612
Length	990.5906	–0.0941	0.0360	(+) 0.1299
N	0.5300	–2.51E – 14	9.60E-15	(+) 9.22E – 27
P	45.9636	1.4909	–0.5711	(–) 32.6156
Rint	100.0251	0.7002	–0.2682	(–) 7.1937
SigResMax	81.2152	0.7477	–0.2864	(–) 8.2029
T0	11.8347	–1.3626	0.5220	(+) 27.2459
X_i	1.00E – 0.06	0.0188	–7.19E – 0.03	(–) 5.17E – 03

from 4.753 to 3.7191, then the pressure decreases significantly. However with regards to residual stresses the probability index β is again fairly reduced. In fact for a given acceptable P_f, the pressure decreases of about 9 MPa. In this study, a probability of failure $P_f = 10^{-5}$ is adopted showing values of pressure equal to 40 MPa in the case where the residual stresses are not considered and 30 MPa when the residual stress distribution follows a linear law. The curves obtained followed similar trend. The evolution of the probability index β as a function of pressure coefficient of variation ρ_{pm} is plotted in Figure 11. A step of 5 MPa starting from 20 MPa is used to reveal the behavior of the probability index β when increasing ρ_{pm} from 0.1 to 0.3. It is evident that β decreases.

TABLE 4. Sensitivity and elasticity of the parameters.

Variable	Sensitivity σ	Elasticity σ	Sensitivity μ	Elasticity μ
B	−1.14E-05	−1.91E−04	−3.15E-04	−0.0530
Cd	−1.88E-03	−1.90E−04	−0.0522	−0.0264
Coefp	−0.0505	−1.33E−04	1.6745	0.1924
Cs	−0.3958	−2.73E−03	−2.9038	−0.1335
Delta_teta	−7.31E-04	−1.12E−03	8.37E−03	0.0641
E	−1.61E-10	−4.10E−07	−9.66E−08	−7.44E−03
F	−4.08E-07	−4.69E−03	−2.28E−06	−0.1312
Fy	−0.0240	−0.2249	0.0194	3.5238
Gamma	−66.3019	−4.80E−05	−3667.6047	−0.0266
Lc	−0.0490	−4.69E−03	−0.2741	−0.1312
Kd	−0.0624	−5.16E−04	1.0521	0.0435
Kn	−0.3669	−6.61E−03	−1.7301	−0.1557
Length	−3.39E−05	−1.30E−03	3.60E−04	0.1381
N	0.0000	0.0000	1.81E−13	3.68E−14
P	−0.2126	−0.3258	−0.1428	−2.1877
Rint	0.0482	0.0719	0.0689	2.5685
SigResMax	−0.0143	−0.0819	−0.0191	−0.5120
T0	−1.1190	−0.2722	0.8220	3.9990
X_i	−1348.4116	−5.17E−05	−71,905.4021	−0.0275

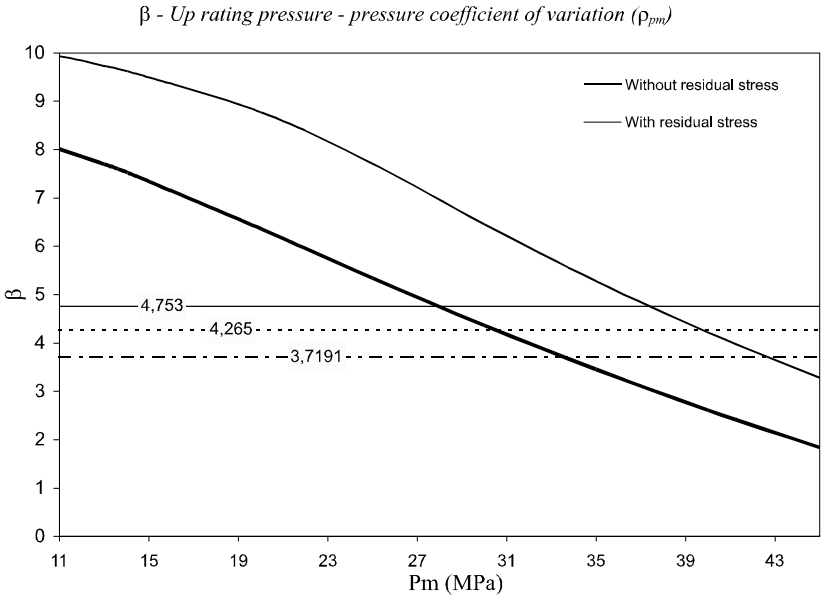

Figure 10. Variation of reliability index β as a function of up rated pressure [25].

RELIABILITY AND CORROSION

The assessment of reliability of underground pipeline with active corrosion is established with the model illustrated by Eq. 32. The model is used for atmospheric pressure [9]. In this case the corroded layer calculated for k = 0.066 and n = 0.53, in a period of 50 years is about 0.55 mm. To activate the corrosion process, a simulation based on increasing k is used. Therefore, for a pipe thickness of 12.7 mm, there will a process that involves a loss of half, a quarter and an eighth of the thickness. This is considered here as a very high corrosion rate, high corrosion, moderate corrosion and low corrosion which correspond to respectively to 1,000, 500, 250 and 100 years. The aim of this study then is to determine the reliability of the pipeline with regards to corrosion rates together with the residual stress.

Results on the reliability calculation as a function of elapsed pipeline lifetime are shown in Figure 12. The evolution of β as a function of the corrosion rate is presented for 30 MPa in the nonresidual stress case and in the presence of residual stress. As expected, the reliability index β decreases with T and correspondingly the nominal probability of failure increases with T. The effect of variation of T is investigated further more. For this purpose, the value of T is varied from 0 to 50 years. It is seen that the probability of failure increases nonlinearly with T. The higher the corrosion rates the higher the probability of failure. The nonlinearity is well expressed for higher corrosion

rate than the atmospheric corrosion. The influence of residual stresses observed in the beginning is decreasing with time, since after 20 years, the probability failure becomes less sensitive and converges to that obtained for a nonresidual case. In fact, as the corroded layers are created, the pipe wall thickness reduces thus the residual stresses relax and their effect is lost. One major advantage of these curves is to give the designer and the maintenance service a good picture of the level of the nominal risk of pipeline structural failure at various stages of pipeline elapsed time life with regard to corrosion rate. An example to consider is that for moderate corrosion rate in which, for a 30 MPa pressurized pipe, the probability of failure is acceptable for a range of 50 years whereas for a 40 MPa pressurized pipe this is not true since after 20 years the corroded pipeline could have blown up.

TABLE 5. Safety factors.

Variables	Partial safety factors
B	1.0036
Cd	1.0072
Coefp	−1.0007
Cs	1.0205
Delta_teta	−1.0178
E	1.0001
F	1.0358
Fy	−1.0682
Gamma	1.0018
Lc	1.0358
Kd	−1.0120
Kn	1.0425
Length	−1.0095
N	−1.0000
P	1.1491
Rint	1.0280
SigResMax	1.1602
T0	−1.0731
X_i	1.0019

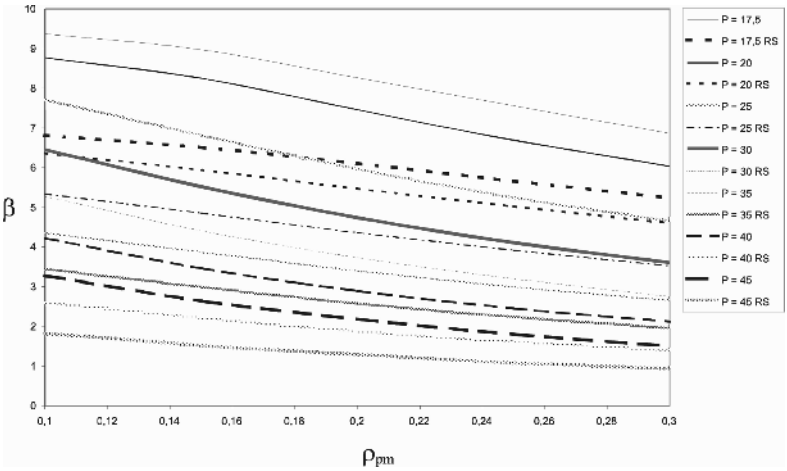

Figure 11. Variation of reliability index β as a function of pressure coefficient [25].

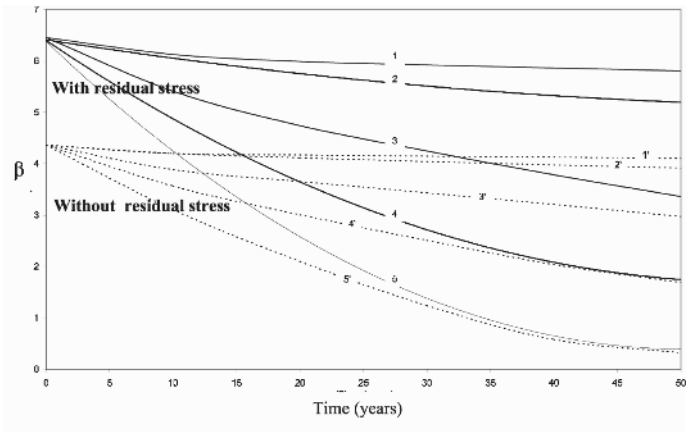

Figure 12. Reliability as a function of elapsed time.

VARIABLE IMPORTANCE

The relative contribution of the random variables to the pipe reliability is shown in Figure 13, for gas pressure increases from 11 to 40 MPa. The most important variables for the pipeline safety are the thickness, the yield stress and the applied pressure. When the mean value of residual stress is 15 MPa and the pressure is up-rated, the thickness and the yield strength dominate with more than 50%; the remaining part is equally divided between the other parameters. For an operating mean pressure up to 11 MPa, the contribution of all parameters is significant. The importance of the residual stresses increases with lower gas pressure; this importance is 8.5% for a pressure of 40 MPa and increases to 14.5% when the pressure is reduced to 11 MPa.

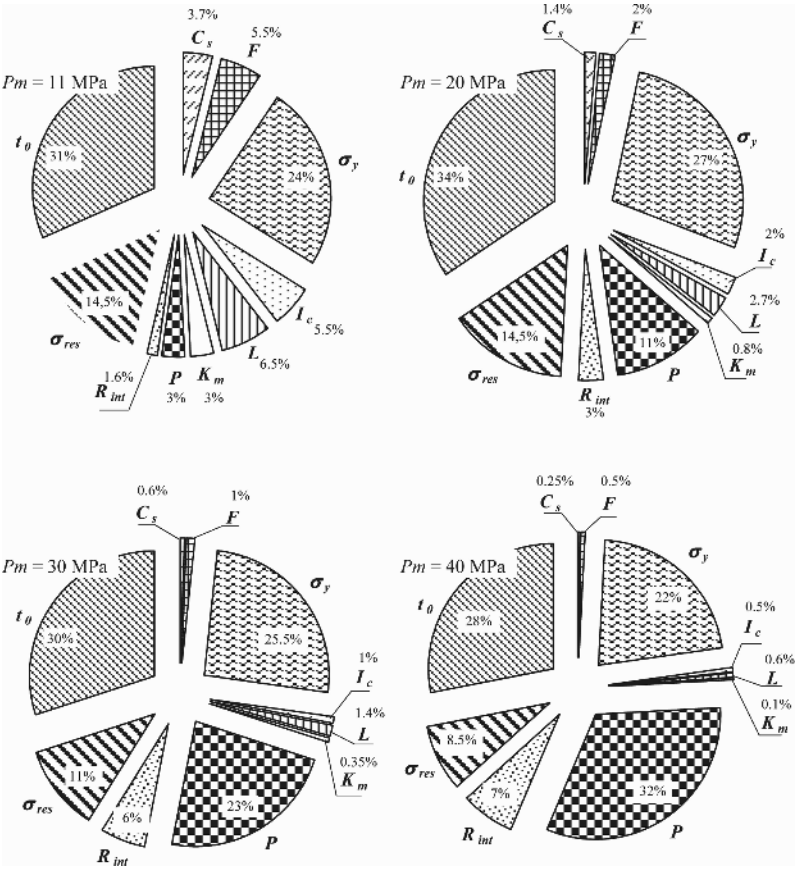

Figure 13. Variable importance on the pipe safety [25].

5. Conclusions

The reliability software PHIMECA has been used to assess the reliability of a pipeline under active corrosion with respect to residual stress. A corrosion model of the residual stresses is developed on the basis of experimentally determined distributions. The reliability is assumed to be a function of 20 independent variables. The main results are given below:

1. The residual stress increased the probability of failure. In terms of reliability index β, for an acceptable value of 4.265, the pressure is decreased from 40 to 30 MPa.
2. Increasing the coefficient of variation of pressure increased the probability of failure. The risk of failure does not exist for a pressure of 25 MPa for a coefficient of variation of 0.3 even when the residual stress is taken into account.
3. The most sensitive parameters are pressure, yield strength, internal radius, thickness, residual stress and the bending moment coefficient.
4. Two sensitivities followed opposite directions: that of the residual stress and that of the internal diameter.
5. For lower pressures up to about 20 MPa, the residual stress sensitivity was higher than that of the internal diameter.
6. As expected, corrosion rate caused the probability of failure to increase significantly.
7. The probability of failure P_f, is less sensitive in the presence of residual stresses.
8. The influence of the residual stress with time exposing is lost in less than 20 years.

References

1. R. N. Parkins. and R. R. Fesler, Line pipe stress corrosion cracking mechanisms and remedies, *Corrosion*, paper No. 320 (1986).
2. B. Leis and R. Parkins, Mechanics and material aspects in prediction: serviceability limited by stress-corrosion cracking, *Fatigue and Fracture of Engineering Materials and Structures*, 21, p. 583 (1998).
3. J. M. Gray and M. Pontremoly, Metallurgical options for grades X70 and X80 line pipes. *In the International Conference on Pipe Technology*, Rome, p. 171 (1987).
4. S. Endos and M. Nagae, Development of X100 UOE line pipe. *In the International Conference on Pipeline Reliability*, Calgary, p. 3, 4.1 (1992).
5. ASME-B31G, Manual for determining the remaining strength of corroded pipelines – a supplement to ASME B31G code for pressure piping. New York: American Society for Mechanical Engineers (1991).
6. H. P. Hong, Inspection and maintenance planning of pipeline under external corrosion considering generation of new defects, *Struct. Saf.*, 21, p. 203 (1999).
7. K. Chaoui and A. Amirat, Evaluation du champ de contraintes résiduelles dans les tubes aciers produits par l'entreprise SIDER. Projet de Recherche MESRS, Code J-2301/03/18/92 (1992).

8. A. Amirat, K. Chaoui, Z. Azari, and G. Pluvinage, Residual stress analysis in seamless API X60 steel gas pipelines, Revue Sciences et Technologie, de l'Université Mentouri de Constantine, No. 21B, p. 7–14 (2004).
9. M. Ahammed and R. E. Melchers, Probabilistic analysis of underground pipelines subject to combined stresses and corrosion. *International Journal of Pressure Vessels and Piping*, 19, p. 988 (1996).
10. O. Ditlevsen and H. O. Madsen, Structural Reliability Methods. Chichester: Wiley (1996).
11. A. Mebarki, D. Boissier, and D. Breysse, Fiabilité des matériaux et des structures, 2ème conférence nationale, JN-FIAB'98, Hermes (1998).
12. Pendola Phimeca Software, PHIMECA Engineering S.A. Romagnat, France (2001), contact@phimeca.com.
13. ISO 2394, Principes généraux de la fiabilité des constructions, Technical Report. ISO 2394-1986(F).
14. AFNOR. Eurocode 1: Bases du calcul et actions sur les structures et document d'application nationale. Technical Report XP ENV 1991-1, AFNOR.
15. SO 13623, Petroleum and natural gas industries-pipeline transportation systems. ISO 13623-2000(E).
16. SO 16708, Petroleum and natural gas industries-pipeline transportation systems. Reliability-Based limit state methods. ISO CD 16708-2000(E).
17. R. E. Barlow and F. Proshan, Statistical theory of reliability and life testing. Probability modes. New York: Holt, Rinehart and Wiston (1975).
18. K. Kolowrok, On asymptotic reliability functions of series-parallel and parallel-series systems with identical components. *Reliability Engineering and Systems Safety*, 41, p. 241 (1993).
19. R. E. Melchers and M. Stewart, Applications of statistics and probability – civil engineering and risk analysis. *Proceedings of the ICASP 8th Conference, Sydney, Australia*, Balkema, Rotterdam (1999).
20. M. Lemaire, J. L. Favre, and A. Mebarki, Applications of statistics and probability, volume I, II, III. *International Conference on Applications of Statistics and Probability*, ICASP7, Paris, Balkema, Rotterdam (1995).
21. R. A. Rzhanitzyn, Design of structures with considerations of plastic properties of materials. Stroivoenmorizdat (1949).
22. A. M. Hasofer and N. C. Lind, exact and invariant second moment code format. *Journal of Engineering Mechanics Division*, 100, p. 111 (1974).
23. T. Abdo and R. Rackwitz, A new beta-point algorithm for large time-invariant and time reliability problems. *In Reliability and Optimization of Structures*, 3rd WG 7.5 IFIP Conference,Berkeley, pp. 1–11 (1990).
24. O. Rollot, M. Pendola, M. Lemaire, and I. Boutemy, Reliability index calculation of industrial boilers under stochastic thermal process. *In proceedings of DETC'98, ASME Design Engineering Technical Conferences*, Atlanta, Georgia, USA (1998).
25. A. Amirat, A. Mohamed-Chateauneuf, and K. Chaoui, Reliability assessment of underground pipelines under the combined effect of active corrosion and residual stress. *International Journal of Pressure Vessels and Piping*, 83, pp. 107–117 (2006).
26. V. Kucera and E. Mattsson, Atmospheric corrosion. *In Corrosion Mechanics*, Mansfeld, F. (Ed.), New York: Marcel Dekker (1987).
27. J. J. Lynch, The measurement of residual stresses. *American Society for Metals*: *Residual Stress Measurements*, Cleveland, p. 42 (1952).

ON A NEW SOFTWARE PROJECT FOR WELDING SIMULATIONS OF PIPES (FABRICATION, REPAIRS) AND FOR THE EVALUATION OF FATIGUE BEHAVIOUR OF PIPES IN SERVICE

K. DANG VAN[1] AND FRÉDÉRIC ROGER[2]
[1]*Laboratoire de Mécanique des Solides, Ecole Polytechnique, 91128 Palaiseau;*[2]*ENSTA Paris, UME-MS, Batterie de l'Yvette, 91761 Palaiseau Cedex*

Abstract: Evaluation of fatigue behaviour of pipes in services necessitates the knowledge of the residual stress field after manufacturing and a specific multiaxial fatigue criterion for the life prediction. The modelling of the welding step is a major difficulty because of the multiphysics couplings. Indeed, it is necessary to take into account plasma physics, magnetohydrodynamics of the weld pool and metallurgical and thermomechanical behaviour of the structure. We have developed a global approach with numerical tools to cover all these phenomena and to predict weld shape, residual stress and strain. Fatigue evaluation of welded structure under multiaxial loadings with residual stresses is presented with applications in automotive and railway industries. Dang Van fatigue criterion associated with specific meshing rules allows to locate critical zone in fatigue.

Keywords: welding, fatigue, Dang Van criterion, pipes

1. Introduction

Safety and reliability of pipelines transporting inflammable fluids like oil or gas is of primary importance for companies and great efforts are done to understand the mechanisms of cracks initiation and propagation in order to be able to predict the remaining life duration of theses structures. These studies are based

G. Pluvinage and M.H. Elwany (eds.), Safety, Reliability and Risks Associated with Water, Oil and Gas Pipelines, 261–269.

on experimental approaches which necessitate performing a great number of tests, very often carried out on real structures. Generally the cracks start from defects which are introduced during manufacturing or repairing processes, and particularly by welding.

These defects are nuclei for fatigue phenomena: the initiation of the fatigue cracks occurs after a certain number of varying pressure service loadings and then they propagate until final failure. Evaluation of these defects and their evolution in relation with the loading conditions is very difficult because of the great number of factors which influence the different manufacturing processes and the fatigue phenomena. Among others, the welding operation which is the most important assembly process of pipe networks is until now quite poorly described by the present modelling (and consequently the derived computational software). For instance, it was not possible to predict with enough accuracy the geometry of the weld, the distribution of the residual stress, the leak of the weld penetration in relation with the welding parameters (voltage, intensity of the current, welding gas, welding speed). These parameters control the fatigue behaviour of the weld which is one of the most critical zones of pipes. This is the main reason of the little success of modelling to derive useful results for safety and reliability studies. It is then necessary to use difficult and expensive experimental approaches on pipes. Nowadays, the progress we have done in the modelling of the welding processes, and in the development of an efficient fatigue criterion applicable to welded structures permit to consider the problem in a different manner.

2. General Considerations for the Development of the Software

The main difficulties which must be overcome for an efficient welding modelling is to have a good description of the heat transfer during the process (GTAW, GMAW, SAW) in order to obtain a good predictive thermal history. This complex problem is until now not satisfactorily solved. Indeed, the heat transfer result of multiphysics coupling problem: plasma physics, magnetohydrodynamic, mass and heat transfer, thermomechanics, metallurgical transformations. Moreover, taking into account phase change in numerical simulation is very time consuming. Indeed, typical order of magnitude is one day for a 2D problem which is out of the scope of an industrial application. A second difficulty is the prediction of the weld shape with the parameters which intervene in the fatigue behaviour by inducing stress concentration. Finally, the prediction of fatigue behaviour of welded structure is not efficient with the present industrial softwares because they are not able to take account of complex residual stress field and multiaxial

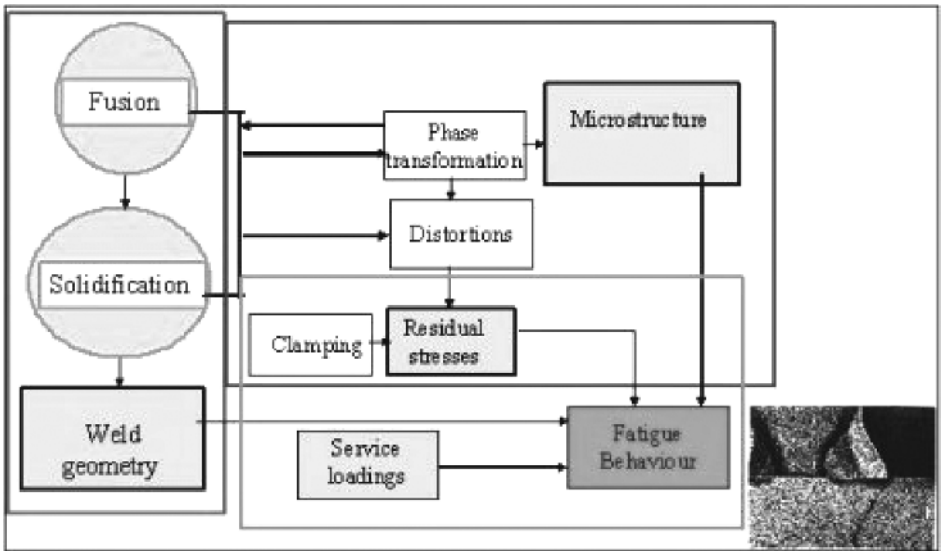

Figure 1. Description of the global modelling from the process to the life prediction.

stress due to loadings. Moreover, the structural effects due to the shape of the weld are poorly or not taken into account.

In the proposed approach, we considered the whole problem which is composed of three parts as it is shown in Figure 1.

3. Modelling of the Heat Transfer and Weld Pool Formation

The first part is the multiphysis modelling of the weld pool formation coupled with the arc plasma modelling. Indeed, heat flux from arc is the major melting heat source. This heat is due to electron flow and convection and radiation from the plasma. In GMAW, this heating is enhanced by overheated drops which bring up to 40% of the total welding power. It is why it is necessary to considered both heat and mass transfers.

The surface heat flux from the arc is generally assumed to have a Gaussian power density distribution which is not correct when you have complex geometry-like chamfer and electrode inclination (Figure 2).

We have developed a 3D modelling which is able to take into account arc plasma distribution with inclined electrode, complex geometry of the welding joint and welding gas mixture.

Mass transfer from welding electrode is also considered with calculation of droplet geometry, impact speed and depth of penetration.

The resulting weld shape is calculated by minimising surface energy of the weld pool subjected to arc pressure, drop impact and mass conservation. Figure 3

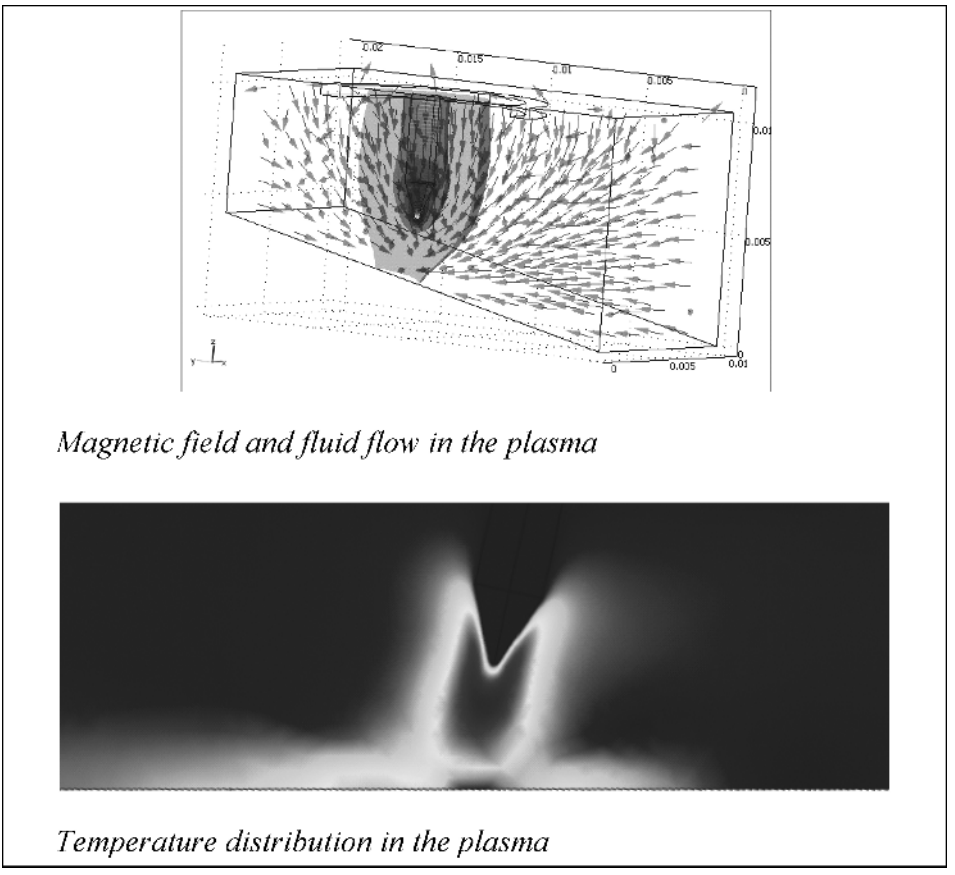

Figure 2. Example of modelling of the plasma with inclined electrode in GTAW.

shows the weld pool modelling in GTAW where convection in the weld pool is governed by gravity effects, Marangoni effects and electromagnetic body forces.

In GMAW, the melting electrode modifies the heat and mass transfer and the resulting shape in stationary is shown in Figure 4.

4. Thermomechanical and Metallurgical Modelling

Thermomechanical and metallurgical coupled constitutive equations which are necessary for predicting residual stress and strain and the final metallurgical state are based on phenomenological approaches. The classical kinetics models as Leblond or Koistinen-Marburger models are weakly coupled with thermomechanics. Calculations are quite time consuming. We have developed a new approach

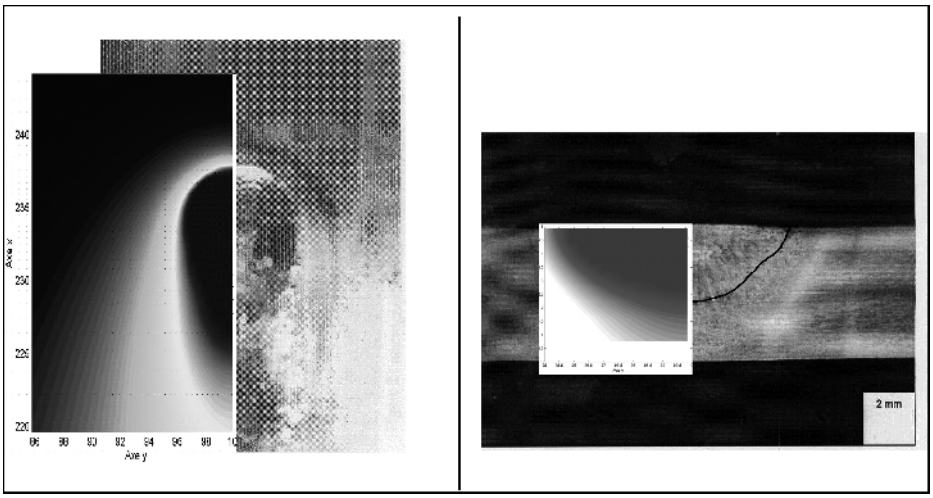

Figure 3. Example of weld pool modelling (temperature and fluid flow) in GTAW and comparison between prediction and macrograph [1].

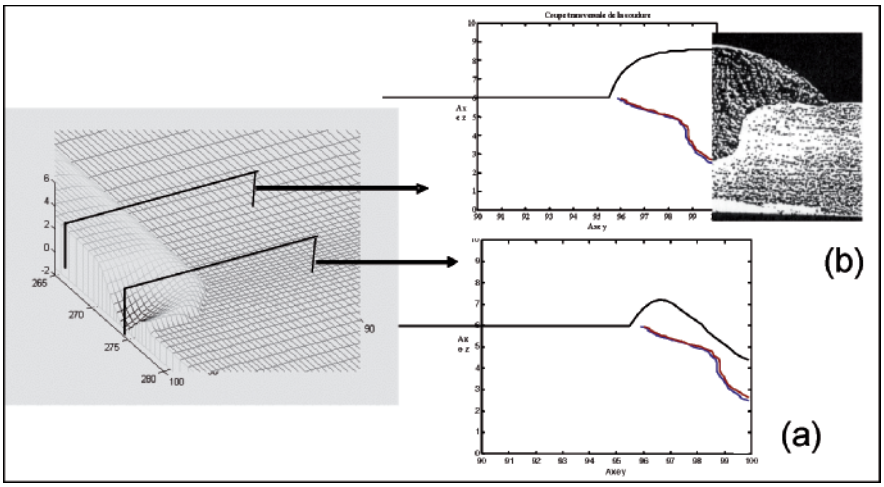

Figure 4. Prediction of the weld shape in the weld pool (a) and after solidification (b).

based on systematic thermodynamics formulation in the framework of generalised standard materials proposed by Q. S. Nguyen and B. Halphen. This approach leads to a systematic framework for developing thermomechanical and metallurgical constitutive equations fully coupled. Moreover, new integration algorithm permits short-time calculation (2 h for the welding of a 3D plate instead of one day for existing commercial softwares). An example of simulation of laser welding is given in Figure 5.

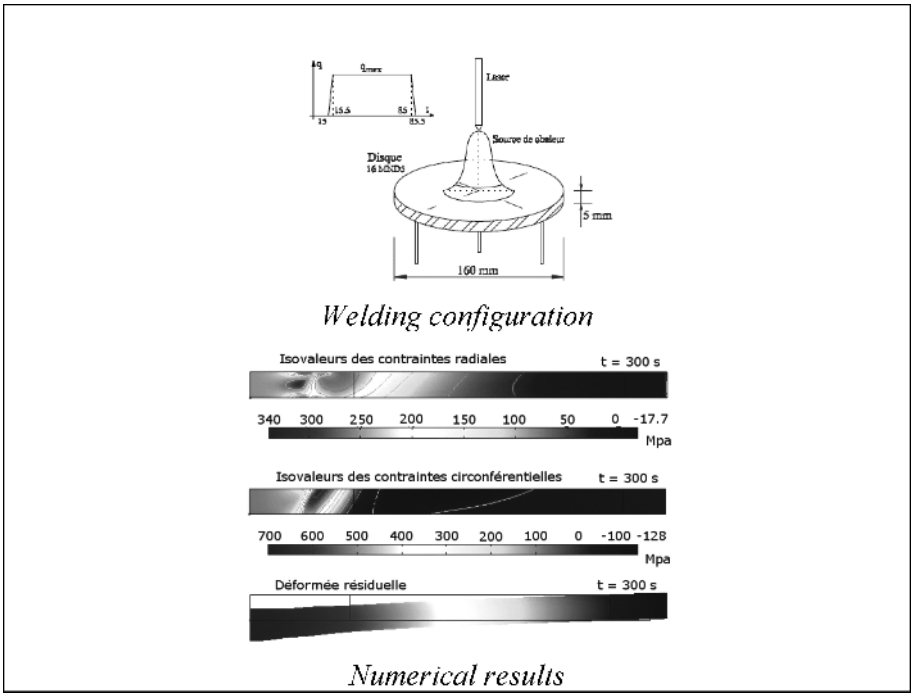

Figure 5. Simulation of the laser welding of a disk and residual stresses distribution after cooling.

5. Prediction of Fatigue of Welded Structure

Current practice in welded structure design is based on the use S–N curves, hot spot principal stress or structural principal stress limited to specific geometries. However, they are difficult to handle on complex shape components and for multiaxial loadings, which is the case in most of industrial structures. To overcome this difficulty, we come back to the structural approach with a clear definition of the design stress that can be transposed to multiaxial structural problems.

The classical introduction of the design stress is based on the extrapolation of far field stresses with unclear rules. In order to clarify the description of this design stress we propose an approach deriving from an analogy with the concepts, which are at the origin of the fracture mechanics. Actually, it is known that the mechanical state in the highly damaged crack tip zone, called the process zone, is inaccessible by the usual continuum solid mechanics. In this zone, the material is neither really continuous nor homogeneous and the local strains are not small. Nevertheless, the stress solution obtained from linear homogeneous and isotropic elasticity in small strains allows the correct description of the

mechanical state outside of the process zone. Although it is erroneous at the vicinity of the crack tip, it makes sense in terms of an asymptotic solution that allows the correct control and the interpretation of the phenomena produced in the process zone. Likewise, we will look for a way to build the asymptotic solution that allows the correct control and interpretation of the phenomena produced in the critical zone of the weld. For that purpose we adopt an approach with meshing rules taking into account the local rigidity due to the weld instead of the local geometry of the weld itself (as it is the case in fracture mechanics, where the actual geometry of the crack tip is not taken into account) that is a very hazardous data. Therefore, the fatigue design can be based on a structural stress calculation from a finite element shell analysis. On this basis we can establish design rules for welded structures with a structural stress, the asymptotic solution, which gives access to the fatigue strength through a unique S–N line where S is a local equivalent stress $\tau_0 = \tau - \alpha p$ defined from τ (mesoscopic shear which intervene in the Dang Van theory of fatigue [2]) and p is the hydrostatic tension at the Hot Spot.

In this approach, fatigue limit is related to elastic shakedown limit at all scale of material description.

This fatigue modelling is widely and successfully used in automotive and industry for the fatigue design. Applications to thicker welded structures (trains) lead also to very good life prediction (Figure 7). The complete theory is detailed in [2, 3].

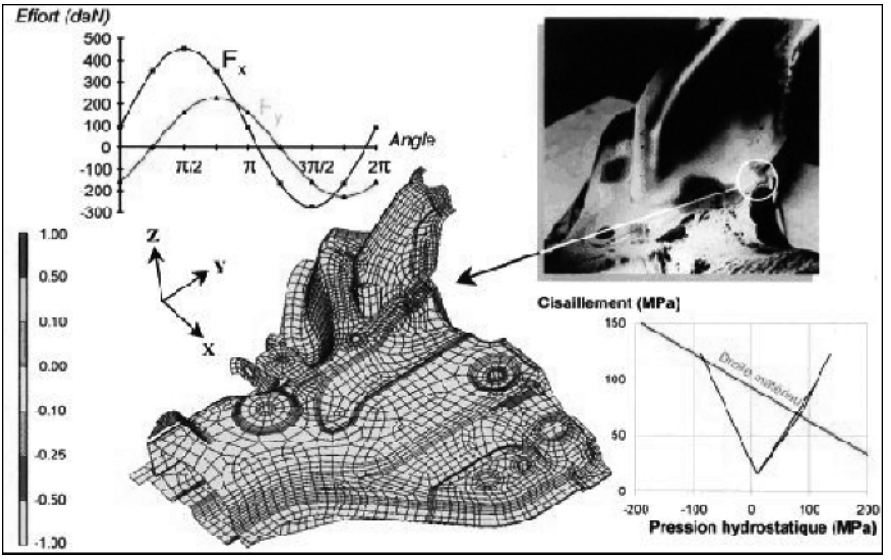

Figure 6. Application to automotive engine subframe under multiaxial out of phase loading. (Courtesy of PSA Peugeot Citroën.)

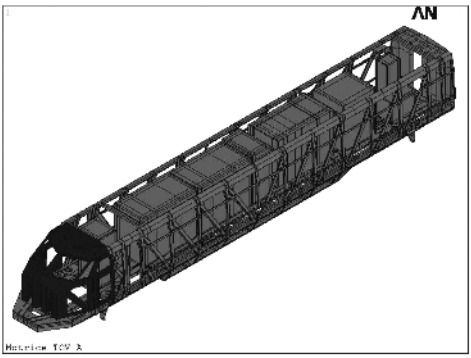

Prediction of fatigue cracks nucleation on a TGV locomotive after 15 years of service

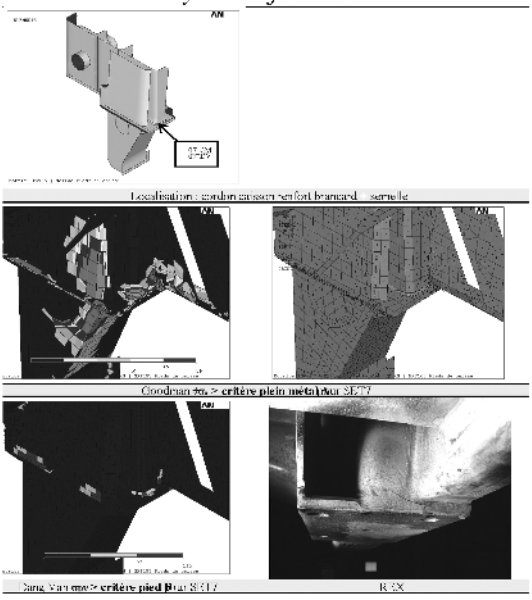

Example of critical zone identified and localisation of cracks

Figure 7. Railways application of the fatigue methodology.

J. L. Fayard et al. [3] developed an efficient numerical tool to evaluate the asymptotic mechanical field that defines precisely the design stress. On the basis of a shell model, a meshing rule was established [2, 3] with simple ideas: reproduce as precisely as possible the local rigidity induced by the weld,

simulate the stress flow from one sheet to another through the weld. (cf. ref [3] for meshing methodology).

In the following is shown two examples of industrial application:

- The first one shown on Figure 6 is related to the fatigue resistance assessment of an engine subframe undergoing multiaxial out of phase loading (Courtesy of PSA Peugeot Citroën).
- The second is the localisation of fatigue critical welded structures and evaluation of their life duration for the French TGV high-speed train. Comparisons between model predictions and cracks observed on the locomotive after 15 years of service prove the very good predictivity of the method.

6. Conclusion

In this paper, the main difficulties for the development of a software devoted to the evaluation of the safety and the reliability of welded industrials structures are presented. We have shown that these difficulties can be overcome with a multiphysics modelling of welding and a new fatigue methodology. We shall present specific application to pipes at the conference. Our intention is to develop a specific tool for pipes covering from the manufacturing processes including welding, the repair techniques and their influence on the fatigue life of these structures. We think that such a tool is very useful for the qualitative and quantitative understanding of the influence of the different process parameters and can help industry to develop a maintenance policy.

References

1. F. Roger, Etude et modélisation de la formation d'un cordon de soudure à l'arc, Ph.D. thesis, Ecole Polytechnique, December 2000.
2. Dang Van, K., Fatigue Analysis by the Multiscale Approach, High Cycle Metal Fatigue, From Theory to Applications, CISM Courses and Lectures No. 392, Ed. Ky Dang Van and Ioannis V., Papadopoulos, pp. 57–88, Springer 1999.
3. Fayard, J. L., Bignonnet, A., Dang Van, K., Fatigue Design Criterion for Welded Structures, *Fatigue Fract. Eng. Mater. Struct.*, vol. 19, pp. 723–229, 1996.

WELDED PENSTOCK, PRODUCED OF HIGH-STRENGTH STEEL AND APPLICATION OF FRACTURE MECHANICS PARAMETERS TO STRUCTURAL INTEGRITY ASSESSMENT

STOJAN SEDMAK[1*] AND ALEKSANDAR SEDMAK
[1]*Faculty of Technology and Metallurgy, Karnegijeva 4, 11000 Beograd, Serbia;*[2]*Mechanical Engineering Faculty, Kraljice Marije 16, 11000 Beograd, Serbia*

Abstract: Application of high-strength steel for welded penstock increased the probability of crack-like defects and in welded joint. Structural integrity assessment procedure is presented and applied to welded penstock produced of high-strength steel, comparing crack driving force and material crack resistance in terms of *J*-integral as fracture mechanics parameter. The safety and structural integrity of welded penstock are experimentally verified by testing of penstock models and precracked specimens, with special attention paid to matching effect and microstructural heterogeneity in HAZ.

Keywords: penstock, high-strength steel, welding, fracture mechanics, structural integrity, model, experimental testing

1. Introduction

The penstock in a hydroelectrical power plant is a responsible component, exposed to high stress. It is produced of steel by welding of bent segments. Poor welded joint quality can cause the failure of penstock. Appropriate welding quality has been required from early stage of welded structures manufacturing.

Welded joint quality is depended on welders' knowledge and skill, and quality assurance has to be proved by examination which has been introduced and

* To whom correspondence should be addressed: Prof. Stojan Sedmak, Faculty of Technology and Metallurgy, Karnegijeva 4, 11000 Beograd, Serbia; e-mail: sedmak@divk.org.yu

G. Pluvinage and M.H. Elwany (eds.), Safety, Reliability and Risks Associated with Water, Oil and Gas Pipelines, 271–286.

developed simultaneously with welding processes. Defect free manufacturing of welded structure is costly and probably impossible,[1] resulting in approach of defect acceptance criteria, based on experience. This approach is known as the fitness-for-service (FFS) assessment.

By introduction of ISO 9000 standards for quality assurance and ISO 9001 and ISO 9002 for quality systems the welding has been defined as "special process". In the case of welding, the quality cannot be verified on the product but has to be built in the product. Standard ISO 3834 defines quality requirements for welding, that prescribe the application of standards EN 287 for approval testing of welders and EN 288 for qualification of specified welding procedures for metallic materials. Acceptability criteria for welded joints are defined in standard ISO 5817 "Guidance on quality levels for imperfections". Cracks are not allowed defects in it, except cracks in crater of low quality welded joints and microcracks less than 1 mm^2 in cross section. However, it is generally accepted that welded joints can contain crack-like defects, so in service conditions they can operate with cracks and structural integrity should be assessed in order to prevent leakage by stable crack growth or burst after fast crack increase.

Development of fracture mechanics and standard test methods enabled the analysis of crack significance in structures using its parameters (stress intensity factor – K_I, crack opening displacement – COD or J-integral). The application of fracture mechanics to welded joints is natural, having in mind the possibility of crack occurrence. Fracture mechanics is based on homogeneous microstructure and uniform material properties and its application to welded joints is connected with many difficulties[2] due to very complex microstructure, consisting of parent metal (PM), weld metal (WM) and heat-affected-zone (HAZ). Popular Published Document PD 6493: "Guidelines on some methods for the derivation of acceptance levels for defects in fusion welded joints" is based on fracture mechanics analyses and experience with cracks in welded structure[3]. Further development ended by Structural Integrity Assessment Procedure (SINTAP).

Accepted design approach of welded structure is to define the allowable defect size except crack, for which structural integrity assessment is necessary. All efforts in material production and improvements in welding techniques, together with requirements in quality assurance, can not exclude the appearance of cracks during fabrication, hydrostatic proof tests or service, thereby making the use of fracture mechanics analyses inevitable.[1] It was for the first time formally applied in crack analysis of Trans Alaska Crude Oil Pipeline[4] for "fitness-for-service" assessment, reducing the expanses required for cracks repair.

Matching between PM and WM strength has an important role in the service of welded structures, particularly should high stress cause local plastic strain.[5] Welded joints are generally designed as overmatched, with the WM superior in strength compared to PM, when plastic deformation is expected in PM. The

situation turns to be complex in high-strength steel which should be welded as undermatched to prevent cold cracking,[6] when plastic deformation will start in WM, and PM can start to yield when WM strain hardening capacity is exhausted. Anyhow, in both cases HAZ of heterogeneous microstructure and non-uniform material properties is a weak region since its straining can be constrained and plane strain conditions can prevail, critical for brittle fracture.

In welded structure stress concentration caused by geometrical changes can produce local plastic strain, and the strain hardening capacity could be exhausted, affecting the behaviour of existing crack. Fracture mechanics parameter can be determined only approximately for welded joint, especially for HAZ.

Full-scale test of pressurized component or its model is the most informative and serves as final proof for the safety of a welded structure, because only it can give realistic answers about the response of loaded welded joints. Hydrostatic pressure proof test of pressurized equipment can be classified as full-scale test.

Necessity to introduce quality assurance system and full-scale model tests was recognized in the case of welded penstock of the Hydroelectric Pumping-Up Power Plant "Bajina Bašta". The penstock is about 7 km long and consists of differently stressed segments, produced of steels of different strength classes. The selection of a mild structural steel, with the yield strength up to 350 MPa for the most stressed segments of the penstock dictated the construction of two penstocks and two tunnels for the required water flow. This design alternative was very expensive. For only one penstock, a structural steel of 700 MPa yield strength class should be used for most stressed segments. Weldable, quenched and tempered, high-strength low-alloyed (HSLA) SUMITEN 80P (SM80P) steel, produced by "Sumitomo", of tensile strength 800 MPa and yield strength not less than 700 MPa was selected. At the time of plant design and construction the experience with this class of HSLA steel was not sufficient. For that, approval testing of welders and welding procedure specification had been required, similarly to now valid requirements in EN287 and EN288 standards. Penstock welding was to be partly performed in difficult field conditions, i.e., in tunnel under the slope of 45, and strict requirements could be satisfied only with trained and approved welders. A kind of "fitness-for-service" assessment had also been required, in order to understand better the crack significance. The penstock maximum wall thickness is 47 mm, and this was regarded as the upper limit in plate fabrication for this steel class. On the other hand, this thickness can contribute to plane strain condition, and for that the possibility of brittle fracture should be analyzed. The second problem requiring FFS assessment was low safety margin adopted according to German specification for the HSLA steel[7], i.e., safety factor of only 1.7 regarding PM yield strength.

2. Pressure Tests of Penstock Full-Scale Models

The full-scale model (Figure 1) was designed to simulate the most stressed penstock segment. Cylindrical mantle (1), designed with 5 knee as the penstock transition segment, was covered by two lids (2). Two stiffeners (3) were welded near circular weldments in order to minimize the effect of lids on the stress in the mantle. The support (4) consisted of three legs. The inner model diameter 4.2 m and wall thickness 47 mm corresponded to the penstock segment.

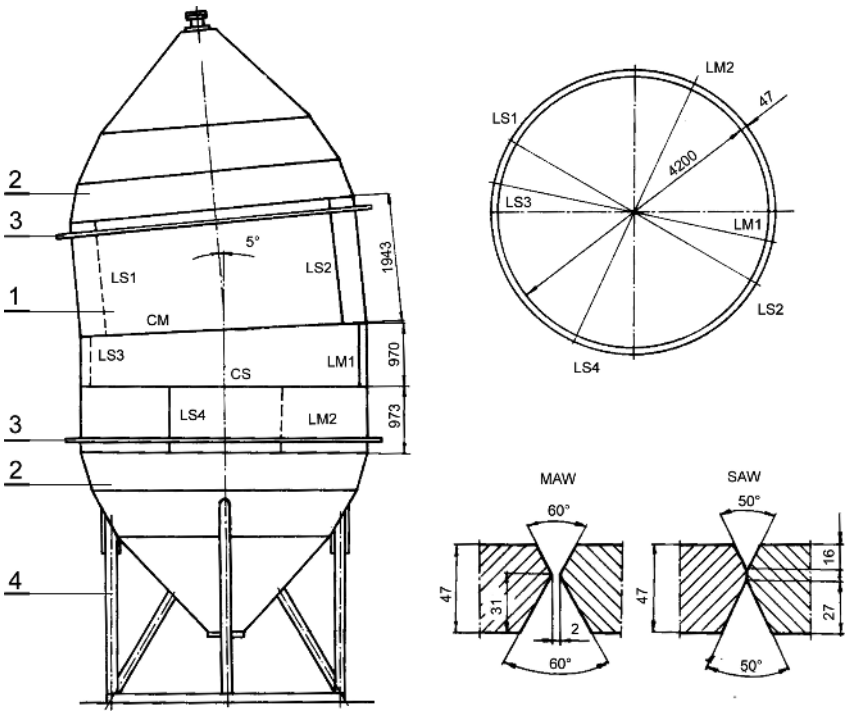

Figure 1. Design of penstock segment full-scale model: 1–mantle; 2–lid; 3–stiffener; 4–support. L–longitudinal, C–circular; MAW–manual arc welding (M); SAW–submerged arc welding (S).

2.1. FULL-SCALE PENSTOCK MODEL FABRICATION

Cylindrical mantle consisted of three segments (973, 970 and 1943 mm long). The steel plates, two for each segment, were rolled and welded. Welded joints, specified for penstock longitudinal (L) and circular (C) weldments with preparation given in Figure 1 were welded by manual arc welding (MAW) and submerged arc welding (SAW) procedures, The basic low hydrogen electrode LB118 for MAW and core wire U8013+M38F flux for SAW welding, produced by "Cobe Steel", were used. Certified welders welded the model and later the

penstock according to the qualified welding procedure specification (WPS). Trial samples for additional investigation were welded simultaneously with model. Typical chemical composition of applied SM80P steel and the weld metals is given in Table 1, and mechanical properties are given in Table 2.

2.2. STATIC PRESSURE TEST AND RESISTANCE TO CRACK INITIATION

The aim of this experiment was to analyze the behaviour of crack-free penstock under design loading and overloading by water hammer, and the effect of plastic strain on weldment toughness. This was achieved by comparing the results of mechanical and fast fracture tests (impact Charpy V, drop weight and explosion bulge tests) of specimens, taken from the model after local plastic deformation in weldments and undeformed trial samples, welded simultaneously.[5]

Static pressure test was performed at an ambient temperature (+6 to –3°C). Strains were monitored by strain gauges (Figure 2), and controlled by moiré grids. Acoustic emission sensors, positioned in stress concentration regions, enabled the control of crack initiation and prevention of failure. The model had been pressurized in two stages. In the first stage the pressure reached 90.2 bar (hoop stress σ_t = 399 MPa), corresponding to working pressure. After unloading, model was reloaded by the pressure 120.6 bar (σ_t = 533 MPa), that is expected maximum service pressure by additional effect of water hammer. Typical relationships strain versus pressure are given in Figure 3.

TABLE 1. Chemical composition of SM80P steel and of MAW and SAW weld metals.

Element		C	Si	Mn	P	S	Cu	Cr	Ni	Mo	V	B	C_{eq}
SM 80P		0.10	0.30	0.90	0.01	0.008	0.24	0.48	1.01	0.47	0.03	0.0016	0.5
Weld metal	MAW	0.06	0.53	1.48	0.011	0.005	–	0.24	1.80	0.43	–	–	–
	SAW	0.07	0.37	1.87	0.01	0.011	–	0.44	0.13	0.73	–	–	–

$$C_{eq} = C + \frac{Si}{24} + \frac{Mn}{6} + \frac{Ni}{40} + \frac{Cr}{5} + \frac{V}{14}$$

TABLE 2. Mechanical properties of SM 80P steel and of MAW and SAW weld metals.

Material	Direction	Tensile test			Charpy impact test	
		YS, MPa	UTS, MPa	Elongation, %	vE_{-40}, J	vT_{rs}, °C
SM 80P	rolling	755–794	804–834	24–29	156–224	–92
	cross rolling	755–794	795–834	22–23	60–147	–58
Weld metal	MAW	722	810	22	99	–5
	SAW	687	804	23	78	–18

YS – yield strength; UTS – ultimate tensile strength; vE_{-40}, J – absorbed energy by V notched specimen at –40°C; vT_{rs}, °C – transition temperature at 50% shear fracture in Charpy V test.

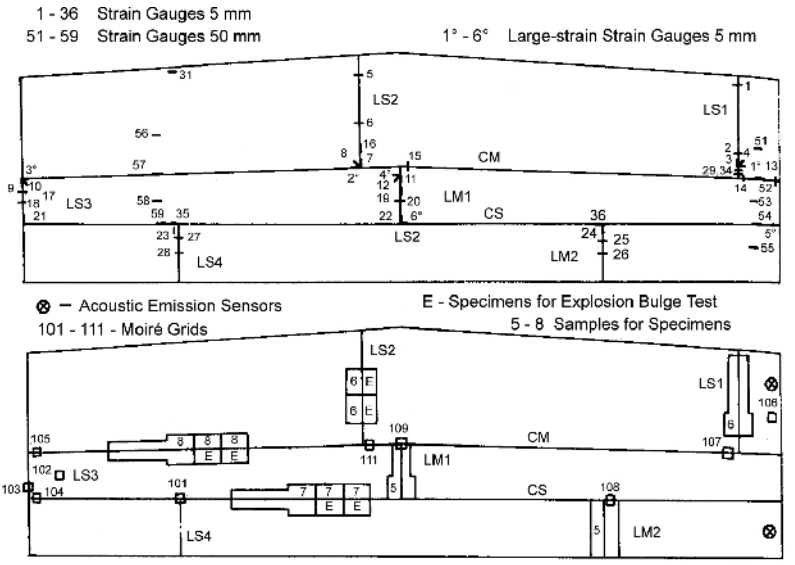

Figure 2. Instrumentation and specimens sampling in penstock model static pressure test.

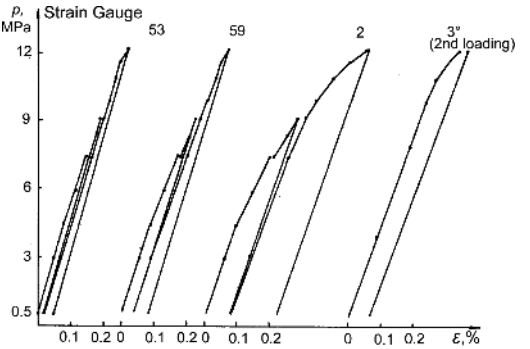

Figure 3. Typical relationship pressure versus strain during loading and unloading.

In parent metal material response is elastic, with negligible plastic deformation, strain gauge 53 (SG53). Total plastic strain of about 0.1% after pressurizing is found on circular CS weld metal (SG59). Plastic strain of 0.24% was found in weld metal LS1 (SG2, SG34). This plastic deformation indicated non-uniform behaviour of welded joints at stress concentration. Clearly undermatched yield strength is found in SAW weld metal (693 MPa compared to above 750 MPa for PM). Stress concentration in positions of SG2, SG29 and SG34 is involved by knee of transition segment and welded joint configuration.

Since performed mechanical and fast fracture tests of specimens of undeformed and deformed welded joints did not show any important difference,[5] the high quality of produced welded joints of the model is confirmed, with the high toughness regarding crack initiation. Important conclusion from performed test

is non-uniform behaviour and different local plastic deformation (Figure 3), indicating complex material response to loading. But it is not critical, since the behaviour of plastically deformed material in next loading will be elastic (Figure 3).

2.3. DYNAMIC PRESSURE TEST OF PRECRACKED MODEL

Pressure test was also performed with the precracked model for verification of resistance to fast fracture and crack arrest properties.[8] Three additional longitudinal SAW welded joints were made on the mantle bottom shell (Figure 4). The surface notches CS2 and CS3 were machined in model longitudinal weldments, from crossings with circular MAW weld (Figure 5), and sharpened by controlled explosion to cracks of final size (CS2: 2c × a = 180 × 4.3 mm; CS3: 50 × 6 mm). The embedded crack CS1 (40 × 3 mm) was intentionally made during welding.

The model was first pressurized statically in two steps by uniformly raising water pressure, achieving maximum pressure of 117 bar which corresponded to the hoop stress σ_t = 518 MPa in an ideal cylindrical vessel.

Next test was dynamic, performed by two successive explosions of controlled rate, starting from the static preloading of 60 bar (σ_t = 265 MPa). In this way the water hammer effect in the penstock caused by quick gate closing was simulated. The experiment was ended by the third static pressurizing, raising pressure up to 151 bar (σ_t = 668 MPa), with holding at the pressure 140 bar for 2 h. The instability for crack CS3 could be achieved at this pressure, since predicted critical pressure was 137 bar (σ_t = 606 MPa).

Detailed analysis revealed that fracture developed through brittle region in HAZ, close to fusion line, starting from precrack (Figure 5). Since the brittle

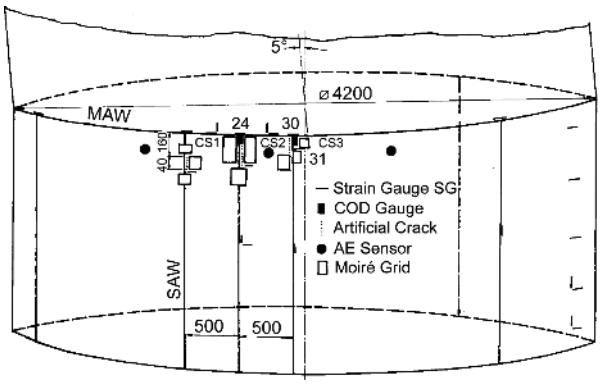

Figure 4. Artificial surface (CS2, CS3) and embedded (CS1) cracks in longitudinal SAW welds. Disposition of instrumentation (COD – Crack Opening Displacement; AE – Acoustic Emission).

region can be very narrow, it is clear that precrack tip can not be positioned accurately in it and some energy could be spent before fast fracture initiated.

The plastic deformation could follow the explosion loading rate, indicating stable crack growth, as confirmed by low acoustic emission. Only when approaching the pressure of 151 bar in third static loading, acoustic emission started to grow significantly, indicating unstable crack propagation.[8] The experiment was stopped, since the danger of fast fracture became obvious according to the experience from previous trial test, finished by bursting of the precracked model. The non-destructive testing showed that CS3 crack propagated for 28 mm in length (10 and 18 mm on sides, Figure 6), while CS2 crack did not propagate in length. Two new cracks, A and B, initiated during pressure test, Figure 6.

The most important conclusion from this test was that full-scale model and penstock can safely withstand the working pressure (90 bar) and an additional water hammer pressure (dynamic loading up to 120 bar) even in the presence of large flaw (CS3 crack 6 mm deep, 50 mm long did not grow) in spite significant misalignment of weldment. It should be mentioned that much smaller flaws can be detected by non-destructive testing. Although plastic strains were found in weld metal in the early loading stage (after unloading from 117 bar), they were of significant value in global sense only after unloading from 151 bar, as indicated by the change in periphery overall length. Extremely high plastic strain in

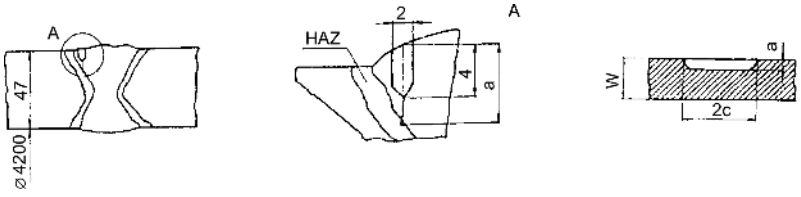

Figure 5. Scheme and geometry of surface crack CS3.

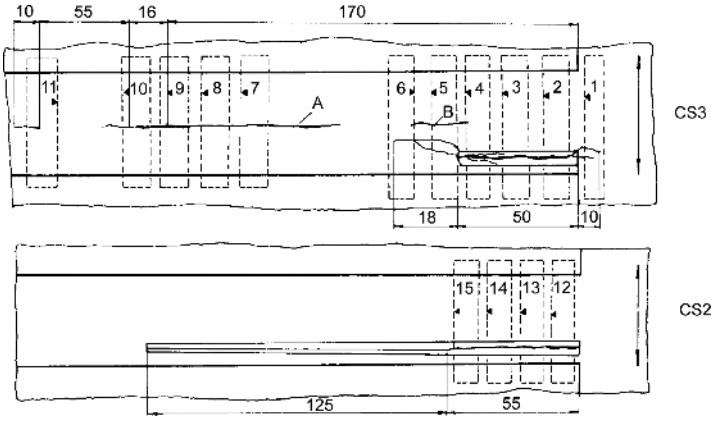

Figure 6. Schematic view of crack development during explosion test.

the weld metal, much larger than in defect-free model, was followed by crack propagation in depth and length (crack CS2) (Figure 3).

Performed test offered only the approximate solution for critical crack size and crack behaviour during loading, similar to service loading, since the most critical microstructure could not be reliably found. Anyhow, manufacturing of these models enabled qualification of welding procedure and welders training, that was of special importance for penstock construction.

3. Residual Strength Prediction of Cracked Penstock Model

After verified welding procedure specification and proved safety by experimental analysis of models, next step was the assessment of residual strength of cracked model and the resistance to stable crack growth. Path-independent contour *J*-integral was selected for this assessment, as the most promising fracture mechanics parameter due to its theoretical background, possible application beyond elastic range and developed direct measurement method.[9] The comparison of crack driving force, expressed by *J*-integral, and material resistance curve (J–R, relationship between applied *J*-integral and extension of initial crack) provides the possibility to determine the extend of the stable crack and the crack size critical for fast propagation. This approach is applied for residual strength evaluation of the model,[10] shown in Figure 1, presenting in the same time the assessment of structural integrity.

Crack driving force in cylindrical shell can be calculated using model, proposed by Ratwani, Erdogan and Irwin (REI).[11] They have introduced J^*, the form of *J*-integral normalized by elasticity modulus E, yield strength $R_{p0.2}$ and crack length $2c$ for a surface part-through crack of depth a, defined as:

$$J^* = J \cdot \frac{E}{2c \cdot R_{p0.2}^2} = \frac{2}{\sqrt{3}}\left[\frac{\delta_o}{d_1} + \frac{\theta_2}{d_2}\left(0.5 - \frac{a}{W}\right)\right]; d_1 = \frac{4c \cdot R_{p0.2}}{E}; d_2 = \frac{4c \cdot R_{p0.2}}{E \cdot W}$$

The ratios δ_0/d_1 and θ_2/d_2, can be found elsewhere,[11] with COD in the centre of crack plane, δ_0, and rotation angle of crack plane, θ_2, for wall thickness W, different pressure levels p and shell parameters

$$\lambda = \sqrt[4]{12(1-\nu^2)}\,\frac{c}{\sqrt{RW}}$$

where R is the mid-thickness shell radius and ν is Poisson's ratio.

Set of crack driving forces, defined by the ratio $pR/WR_{p0,2}$, are calculated for different pressures (Figure 7), with material yield strength $R_{p0,2}$ given in Table 2 for the PM – SM80P steel and SAW weld metal, and presented in $\sqrt{J}$ term.

Resistance curves for steel SM80P and SAW weld metal had been obtained by single-edge notched bend, SEN(B), specimens 22.5 × 45 × 180 mm according to standard ASTM E1152. They are adopted to the same plot with crack driving force curves in Figure 8. For the assumed ratio $a/W = 0.25$ (a = 11.75 mm) crack will grow in a stable manner for 3.75 mm in PM and 4.25 mm in WM, and critical pressure values for fast fracture will be 155 and 144 bar, respectively. For $a/W = 0.5$ (a = 23.5 mm) corresponding values are 6.1 mm and 104 bar for WM, 8.5 mm and 140 bar for PM.

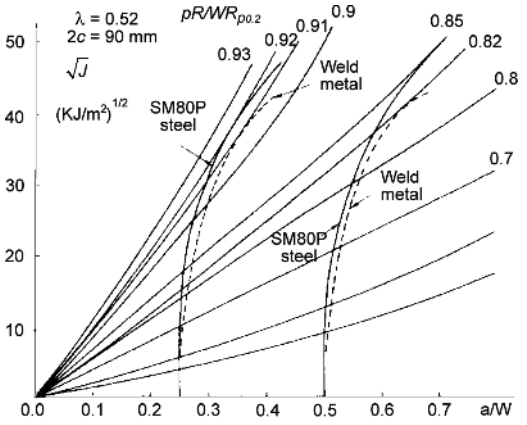

Figure 7. Residual strength prediction of cracked model, using crack driving force and J–R curves.

Obtained results had shown high crack resistance of SM80P and SAW weld metal. Although HAZ was not examined, the test of model precracked in HAZ (Figure 5) demonstrated its satisfactory behaviour. However, the behaviour of HAZ refers only to the microctructure of crack plane, and next investigation are necessary for better understanding the effect of HAZ heterogeneity.

The prediction of residual strength and structural integrity of cracked welded structure by comparing maximum crack driving force, and minimum material crack resistance should be conservative. Thus, it should be proved that applied REI model is conservative. With this aim experimental pressure vessel (Figure 8) of SM80P steel 16 mm thick plates was produced for the verification of REI model.[12] This was done using J-integral direct measurement[9] on fatigue precrack, positioned in SAW weld metal (Figure 8, II). Fatigue precrack was produced in the segment (180 × 380 mm), cut from the welded vessel. After machining part-through notch in the WM centre, fatigue precrack was produced and segment was rewelded on the pressure vessel. The instrumentation for J-integral measurement around selected contour DCBAB'C'D", Figure 8, III, consisted of strain gauges, Figure 8, IV and COD clip gauge.

It is interesting that during experiment crack developed in length, from initial value of 64.25 mm to 72 mm in first pressure stage and to the final value

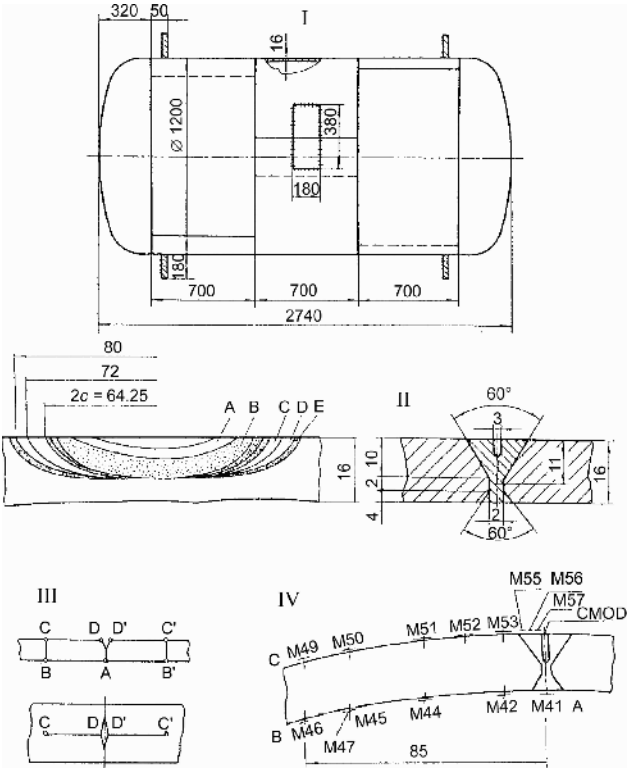

Figure 8. Experimental pressure vessel: I Shape and dimensions. II Details of the crack (A notch; B fatigue precrack; C, D stable crack growth; E final fatigue crack). III Integration contour. IV Distribution of strain gauges M (CMOD – Crack Mouth Opening Displacement).

of 80 mm, as measured after the test. Crack did not develop in depth, Figure 8, II.

For the crack length $2c = 64.25$ mm, shell radius $2R = 1184$ mm, wall thickness $W = 16$ mm, Poisson's ratio $\nu = 0.3$, the shell parameter is here $\lambda = 0.6$.

Crack driving force for an axial surface crack have been calculated by REI model for this λ value and plotted as set of lines in Figure 9, for different crack ratios a/W and different normalized pressures $pR/W\,R_{p0.2}$ ($R_{p0.2}$ is yield stress of WM, Table 2). Point "A" is experimentally obtained at the pressure 100 bar for crack depth $a = 11$ mm, measured after test on fractured segment (crack ratio $a/W = 0.69$). For that case crack driving force, calculated by REI model, is higher for 40% than experimentally determined in point "A". It means that the applied crack driving force, produced by pressure $p = 100$ bar, is clearly lower than the value obtained in experiment, showing that REI model is conservative.

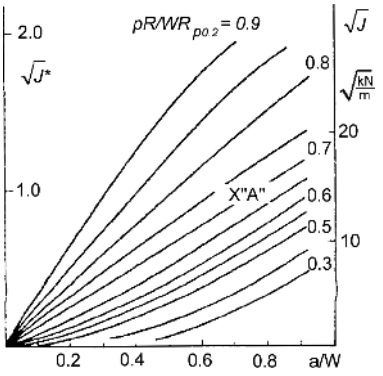

Figure 9. Set of crack driving forces with implemented point "A", obtained by *J*-integral direct measurement on experimental pressure vessel.

4. Effect of Matching and Microstructural Heterogeneity

Next problem in structural integrity assessment is how to define representative J–R curve for differently matched welded joints and HAZ. In order to investigate this, two welded joints of SM80 steel were produced: normal matched, with WM of slightly lower strength compared to PM, and undermatched, WM of significantly lower strength compared to PM. Third welded joint, overmatched one, was welded of SM60 steel (nominal yield strength 520 MPa) with consumable of higher strength, with WM superior in strength compared to PM.

Smooth specimens were produced as tensile panels of size given in Figure 10 but without crack). They were instrumented over PM and WM by normal strain gauges, and over HAZ by strain gauge chain measuring strains in close points. In this way non-uniform behaviour (Figure 3) and strain distribution were analyzed during loading. Although interesting, these results[12] are not directly connected with structural integrity assessment and are not considered here.

In this experiment precracked SEN(B) specimens (ASTM E1820) for single specimen compliance technique (Figure 10, I) were tested for crack growth measurement, and instrumented tensile panels (Figure 10, II) with surface crack – TP (Figure 10, III) were tested by *J*-integral direct measurement method.[9] Cross section of tensile panel (75 × 15 mm) was weakened by large crack (24 mm long, 5 mm deep) and small crack (16 × 2.5 mm). In both SEN(B) and TP specimens cracks were positioned in PM, WM and HAZ. The results are presented in detail elsewhere.[12] Some results, interesting for structural integrity assessment, are given here. Due to heterogeneity of microstructure and mechanical properties, HAZ is the most interesting welded joint constituent in structural

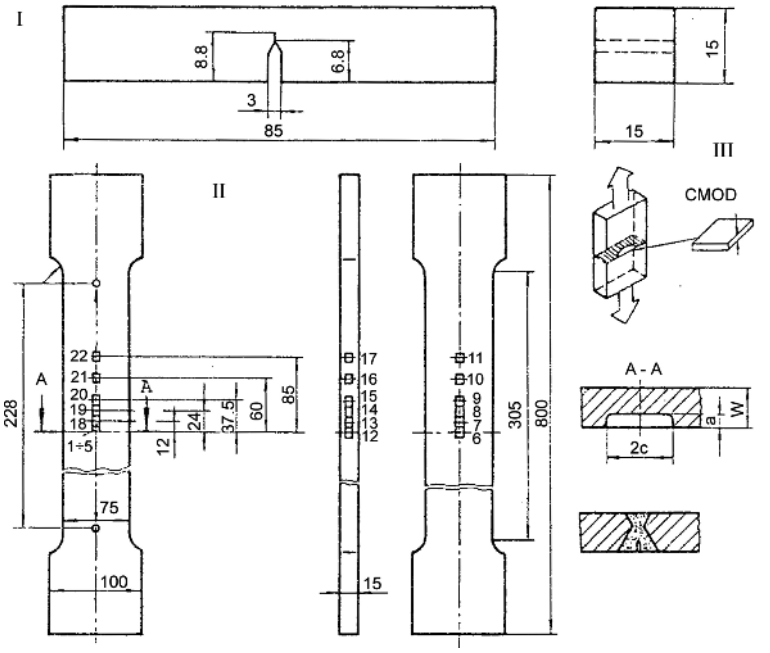

Figure 10. Precracked specimens (I – Single Edge Notched Bend, SEN(B), specimen; II – Tensile Panel – TP, III – details of surface cracks on TP; CMOD–)

integrity assessment and crack behaviour in it attracted the attention in this investigation.

Two typical plots load versus crack opening displacement are presented. They are of the uniform form for all TP and most SEN(B) specimens, Figure 11, I. Only SEN(B) specimens with short crack (*a/W* ratio 0.20 and 0.21) in HAZ plots are non-uniform, indicating a fast crack growth ("pop-in", Figure 11, II), but also material crack arrest capacity. It is clear that through crack in SEN(B) can develop more easily than surface crack in tensile panel due to constraint effect.

Typical J–R curves for crack positioned in HAZ are given in Figure 12 for TP with *a/W* ratios 0.14 and 0.37 and SEN(B) with five *a/W* ratios, including 0.20 and 0.21 values (pop-in). Structural integrity was assessed using J–R curves for both TP and SEN(B) specimens (Figure 13). The set of results for HAZ obtained by SEN(B) specimens was adopted by "lower bound" (LB) curve, the envelope of minimum values for crack resistance, including pop-in effect.

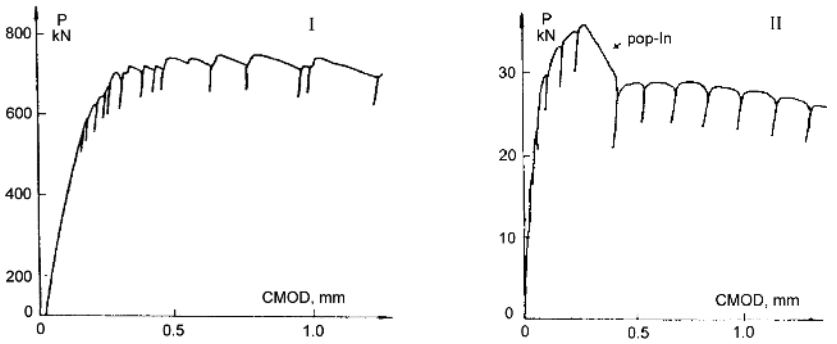

Figure 11. Typical plots load, *P* versus CMOD, obtained by single specimen compliance technique (I – Tensile Panel – TP; II – Single Edge Notched Bend SEN(B) specimen with short crack, exhibiting "pop-in" indicated by an arrow).

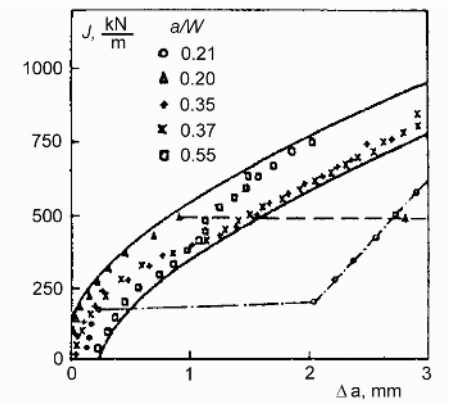

Figure 12. Set of J–R curves for crack in HAZ obtained by SEN(B) specimens.

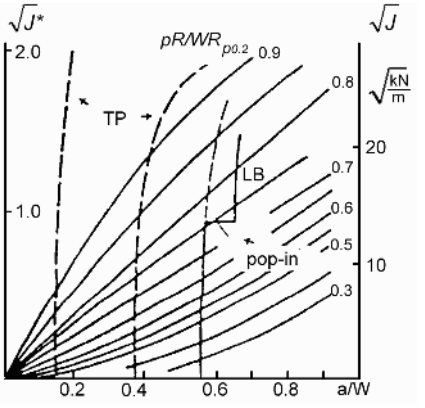

Figure 13. Structural integrity assessment using HAZ specimens.

Material crack resistance for *a/W* values in TP is clearly higher compared to the crack driving forces. Due to "pop-in" the behaviour of crack in HAZ is close to critical. For the crack ratio $a/W = 0.55$ (Figure 12,II), crack depth is $a_o = 8.77$ mm and the pressure $p = 120$ bar can produce an unstable crack extension for next 0.8 mm, before the crack tip enters the region of tougher material in which crack can grow with pressure increase, but in a stable manner.

5. Conclusion

Penstock is an element of simple design shape, but it is very responsible component in hydroelectrical power plant. Proof pressure test of pressurized equipment is decisive for introduction into operation, but experienced service failures in the form of leakage or even burst indicated that this is not completely reliable

approach. Many problems regarding service safety were considered for penstock of hydroelectrical pumping-up power plant "Bajina Bašta", produced of a HSLA steel, mostly connected with welded joint and HAZ in it as critical regions. This was achieved by experimental testing of penstock full-scale models and pressure vessel, on the one hand, and applying fracture mechanics parameter, *J*-integral, for residual strength prediction and structural integrity assessment. Experimental testing confirmed that welding quality according to welding procedure specification is satisfactory. It also allowed detailed analysis of penstock which revealed non-uniform strain distribution, attributed to matching effect, stress concentration and microstructural heterogeneity of welded joint. The important aspect of straining is that after experienced plastic deformation material behaviour will be fully elastic during next unloading and reloading up to previously achieved stress level, accounting also by strain redistribution in some extend. However, since cracks can not be completely excluded in welded joint (although not accepted by standard), structural integrity assessment is necessary for reliable penstock service when crack is detected or simply presumed. Performed analysis had shown that most critical are the cracks in heat-affected-zone, which is continuous metal, but of very complex microstructure and non-uniform properties strongly affecting crack behaviour. For that HAZ microstructural analysis, followed by local mechanical properties, not discussed here, is also important influencing factor for crack and failure occurrence and should be performed for heavy duty pressurized equipment. Simulation of HAZ could be very informative. Anyhow, high price of investigation in this area is limiting factor.

References

1. R. W. Nichols, The Use of Fracture Mechanics as an Engineering Tool, The 1984 ICF Honour Lecture. Sixth International Conference on Fracture, ICF 6, New Delhi, India (1983).
2. S. Sedmak, The evaluation of welded joint properties by testing of precracked specimens, in *Fracture Mechanics of Weldments*, edited by S. Sedmak (GOŠA, TMF, Beograd, 1985), pp. 281–306 (in Serbian).
3. F. M. Burdekin and M. G. Dawes, *Practical Use of Linear-elastic and Yielding Fracture Mechanics with Particular References to Pressure Vessels*, IIW Document X-641-71 (1971).
4. R. P. Reed, H. I. MacHenry, and M. B. Kasen, *A Fracture Mechanics Evaluation of Flaws in Pipeline Girth Welds*, Welding Research Council Bulletin, No. 245 (1979).
5. S. Sedmak, A. Radović, and Lj. Nedelković, The strength of welds in HSLA steel after initial plastic deformation, in *Mechanical Behaviour of Materials,* edited by K. J. Miller and R. F. Smith, (Pergamon Press/Oxford, New York, 1979), vol. 3., pp. 435–446.
6. K. Satoh and M. Toyoda, *Joint Strength of Heavy Plates with Lower Strength Weld Metal*, AWS (Translation from Japanese) (1975).

7. Dast Richilinie 011, *The Application of High Strength Weldable Fine-grained Structural Steels StE47 and StE70*, Deutscher Ausschuss fur StahIbau (1974) (in German).
8. I. Rak. V. Gliha, and J. Kuder, The testing of penstock model, welded of quenched and tempered structural steel for pumping-ap hydroelectric power plant Bajina Bašta, Metalna Strokovni bil. ’84/1, pp. 15–23 (1984) (in Slovenian).
9. D. T. Read, Experimental method for direct evaluation of the J contour integral, in *ASTM STP* 791, pp. 199–213 (1983).
10. M. M. Ratwani, S. Sedmak, and B. Petrovski, The assessment of residual strength of pressure vessel with surface crack by resistance curve, in *Fracture Mechanics of Weldments*, edited by S. Sedmak, (GOŠA, TMF, Beograd, 1985), pp. 131–162 (in Serbian).
11. M. M. Ratwani, F. Erdogan, and G. R. Irwin, *Fracture Propagation in Cylindrical Shell Containing an Initial Flaw*, Lehigh University, Bethlehem (1974).
12. B. Bozić, S. Sedmak, B. Petrovski, and A. Sedmak, Crack gowth resistance of weldment constituents in a real structure, Bulletin T. Cl de I’Academie serbe des Sciences at des Arts, Beograd, Classe des Sciences techniques. No. 25, pp. 21–44 (1989).

THE THERMAL AND MECHANICAL BEHAVIOR OF A JOINT PIPE SYSTEM CALCULATED BY FINITE ELEMENT METHOD

HUI-JI SHI, YAXIONG ZHENG, HONGGUANG YE AND LISHA NIU
FML, Department of Engineering Mechanics, School of Aerospace, Tsinghua University, Beijing 100084 China

Abstract: This paper investigated numerically the thermal and mechanical behavior of joint pipe system. The joint pipe system studied was subjected to the internal pressure and the thermal stress that came from the instantaneous temperature variation. A 3D finite element model is established to simulate the instantaneous process of pressurized thermal shock (PTS) in nuclear power station, however, it is also available to other pipe systems under thermomechanical load condition. The stress produced by thermal shock is much higher than that produced by pressure variation. The highest stress is situated at the joint of the injection pipe and the pressure vessel, and local plastic areas consequently occur in these places. The coupling effects of mechanical and thermal stresses have been analyzed and the influences of combined stress on the pressure vessel strength have been evaluated.

Keywords: joint pipe system, pressure vessel, finite element method, coupling of mechanical and thermal stress

1. Introduction

In pressurized water reactor (PWR) of nuclear power stations, nuclear pressure vessel will be influenced by pressurized thermal shock (PTS) in loss-of-coolant accidents. If the cooling water of high-pressure safety flooding system contacts the high heat in wall of the nuclear pressure vessel, the water will soon cool down the inner surface and generate thermal stress. And the re-boost caused by water injection will bring the coupling effects of mechanical and the thermal stresses to the pressure vessel system including the injection pipe. Because the surface of

G. Pluvinage and M.H. Elwady (eds.), Safety, Reliability and Risks Associated with Water, Oil and Gas Pipelines, 287–298.

nuclear pressure vessel is always irradiated by decrease, thus, study on integrity and safety of structures under the influence of PTS and the establishment of reliable analytic method and evaluating criterions become significant research subjects concerning reactor structural mechanics and reactor thermohydraulics. They are also key audit projects in reactor safety evaluation. [1–3].

The guide rule R. G. 1. 154 promulgated by the US Nuclear Administration Committee in 1987 made detailed specification of the background and purpose of safety analysis, range of analytic method, acquisition of data at the job site, analytic sequence of PTS, thermohydraulics, and fracture mechanics analysis. It also gave computing examples. After that, on the basis of new situation and achievements, the regulations of PTS safety analysis have been continuously embodied and completed. In order to analyze the formation mechanics of PTS, some major laboratories in America and other countries have put up one-fifth to full-scale simulating experiments. With numerical simulation technology, 3D model and damage and failure criterions going with PTS have been set up. Because of the complexity and importance of PTS incidents, many countries are carrying on the studies on this subject to establish adaptive criterions of structure safety analysis.

This paper mainly studies the instantaneous process of PTS on the nuclear pressure vessel. The coupling effects of mechanical and the thermal stresses have been analyzed and the influences of PTS events on the pressure vessel strength have been evaluated. A 3D finite element model is established to simulate PTS process and obtain its characteristic. According to the computing conditions, the finite element computing software Marc which can solve nonlinear 2D and 3D problems is chosen as the main tool to carry on the study.

2. Model Selection

Generally nuclear pressure vessels have complex structures, and the problem should be accordingly simplified. In this paper we only choose a system of a steam vessel and a cooling branch pipe and concentrate our attention on the joint of the vessel-pipe system. The damage part brought by thermal and mechanical loading defines a surrounding joint region where the high-pressure cooling water mixes with high-temperature steam and the stress level is higher than other regions. A similar system has been described by Kordisch et al. [3]. In our calculation model, height of the vessel is 0.6 m, outer diameter 1.6 m, and wall thickness 0.1 m. Length of the branch pipe is 0.20 m, outer diameter 0.13 m, and wall thickness of the branch pipe 0.015 m. The distance between the midline of the branch pipe and the bottom of the vessel is 0.4 m. The finite element mesh structure taken is the symmetric part which occupies one-fourth of the vessel and one-half of the branch pipe (Figure 1).

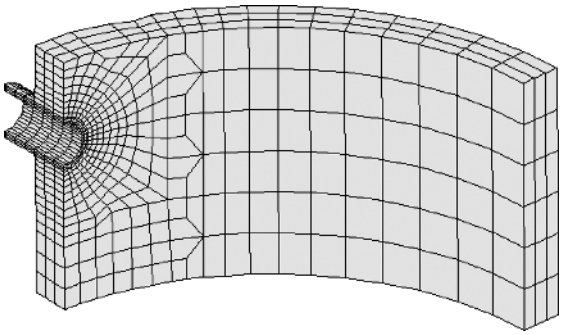

Figure 1. General view of the joint area of the connection pipe and the vessel with the finite element mesh.

As for the setting up of the boundary conditions, according to the symmetrical characteristic, in the interface of the vessel and the branch pipe, the normal displacement of lengthways cross section is given null. And on the other symmetrical side, the normal displacement of lengthways cross section is also given null. Considering the constraint of the axial rigid body displacement of the vessel, the normal displacement of the bottom cross section is set up to be zero. Thus, the top part can still freely move along the axial direction, so the model accords with the practical situation.

The load on the vessel can be classified as: (1) free convection at the vessel's outer surface contacting with the air; (2) convection at the vessel's inner surface contacting with the cooling water; (3) internal pressure caused by the expansion of the steam.

The condition of the convection at the vessel's outer surface contacting with the air is simple. Setting up the air temperature to be 20°C, when the temperature of the node which contacts the air is T, the convection transfer and the quantity of heat q is

$$q = h\left(T - T_{\infty}\right) = h\left(T - 20\right) \tag{1}$$

where T is temperature; h is coefficient of heat transfer.

The convection at the vessel's inner surface contacting with the water is complex, for the cold water is continuously heated and takes away a lot of heat when it flows through the inner wall of the vessel. Considering the duration of severe change of temperature is several minutes, so the time of the event simulation in this paper is only 200 sec (vessel are often cooled down to room temperature several hours later), the water temperature here can be considered as a fixed value. Now the water temperature is fixed to 50°C, and the heat transferred by convection can be obtained by relationship (1), at the instant $T_m = 50$.

Vaporization of the heating-up water coolant will cause pressure change of the vessel, which influences the whole inner wall of the vessel. The relation curve of inner pressure and during time adopted in this paper is shown in Figure 2. Under the influence of PTS, the initial condition of the model is that the temperature of all the nodes is 295°C.

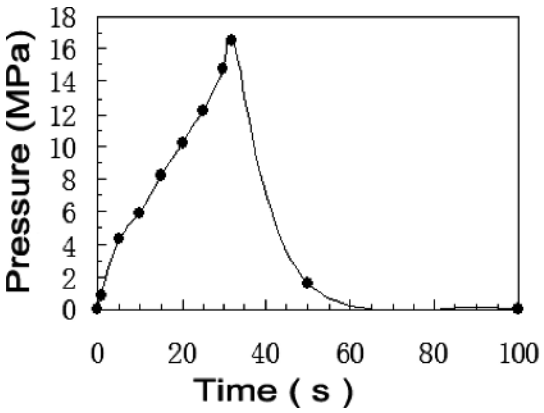

Figure 2. The relation curve of inner pressure and temporal time.

The material of the nuclear pressurized vessel is high-strength steel, the elastic ratio of which is 190 GPa, and the Poisson's ratio is 0.3. The physical properties of the material are shown in Table 1. The stress–strain curve is shown in Figure 3.

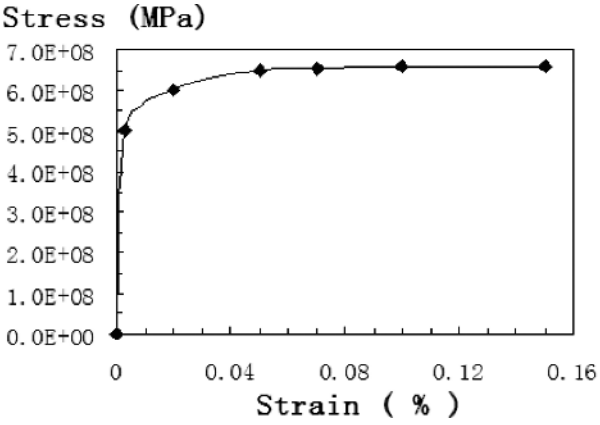

Figure 3. The stress-strain curve of the material.

TABLE 1. The physical properties of the material of the nuclear pressurized vessel.

Density (kg m^{-3})	Coefficient of thermal expansion (K^{-1})	Thermo conductivity (W m^{-1} K^{-1})	Specific heat (J kg^{-1} K^{-1})	Thermal diffusivity (m^2 s^{-1})	Coefficient of heat transfer (water-steel) (W m^{-2} K^{-1})	Coefficient of heat transfer (air-steel) (W m^{-2} K^{-1})
7833	1.45×10^{-6}	41.5	502.4	1.05×10^{-5}	5,000	20

3. Computing Principles

As for the computing principles, according to the characteristics of the analyzed problems, here are only some brief instructions on criteria of elastic-plastic yielding, the incremental relation of stress and strain and the computing methods of heat transference and thermal stress.

As the pressurized vessel is made of metal, Von Mises's yielding criteria are adopted in the elastic-plastic computing:

$$f\left(J_2'\right) = \sqrt{2J_2'} - \bar{\sigma} = 0 \tag{2}$$

Where J' is invariant of the second stress deviator, $\bar{\sigma}$ is average stress.

Prandtl-Reuss' model is adopted to show the relation between the increment of plastic strain and stress condition.

The strain is supposed to be the sum of elastic strain and plastic strain. Thus, the strain increment is the sum of the increment of elastic strain and the increment of plastic strain.

$$d\varepsilon_{ij} = d\varepsilon_{ij}^{p} + d\varepsilon_{ij}^{e} \tag{3}$$

Hooke's law is still appropriated for the elastic strain. As for the plastic strain, nonlinear hardening coefficient is adopted

$$H' = \frac{\partial \bar{\sigma}}{\partial \bar{\varepsilon}^{p}} \tag{4}$$

The relation between the increment of stress and the increment of strain is indicated as the following relationship:

$$d\sigma_{ij} = \left(C_{ijkl} - \frac{C_{ijmn}\sigma_{mn}\sigma_{pq}C_{pqkl}}{\sigma'_{ij}C_{ijkl}\sigma'_{kl} + \left(\frac{1}{2}\right)^2 H'} \right) d\varepsilon_{ij} \tag{5}$$

In computing the heat transfer, the following formula is adopted

$$M\frac{\partial T}{\partial t} + (K + F)T = Q + S \tag{6}$$

where

$M = \int_v N^T \rho C dv$, heat capacity matrix

$K = \int_v B^T K B dv$, heat transfer matrix

$F = \int_{s_3} N^T h N ds_3$, convection matrix

$Q = \int_v N^T Q dv - \int_{s_2} N^T Q ds_2 + \bar{Q}$, heat-flow vector

$\bar{Q}$ is heat flow of nodes

N is interpolating function

$B = \partial N_i / \partial N_j$

In nonlinear steady-state problems, coefficient matrices are generally concerned with temperature. Solutions of convergence can be obtained by iterations of several times.

The method of initial strain is used in the thermal stress computing procedure. The thermal strain caused by the increment of temperature is led in the equilibrium iteration formula as a simulating load. The relation of increment of thermal strain, increment of temperature ΔT and linear expansibility is as follows:

$$\Delta\varepsilon_{ij}^{th} = \sigma_{ij} \cdot \Delta T \tag{7}$$

The stress–strain relation is:

$$\Delta\sigma_{ij} = D_{ijkl}\left(\Delta\varepsilon_{kl} - \Delta\varepsilon_{kl}^{th}\right) \tag{8}$$

The simulating load item is:

$$\Delta F^{th} = \int_{v} B_{ij} D_{ijkl} \Delta \varepsilon_{kl}^{th} dv \tag{9}$$

4. Analysis of the Computed Results

To compute by adopting the boundary conditions, the initial conditions, material parameters, the regular pattern of variation of integer stress and integer strain field in the PTS process can be obtained. There is usually a great stress concentration at the joint of the connection pipe and the vessel, and so this area needs to be paid more attention. The locations of numbered nodes are shown in Figure 4. The computed results also indicate that the area, which has maximum stress is at the interface part.

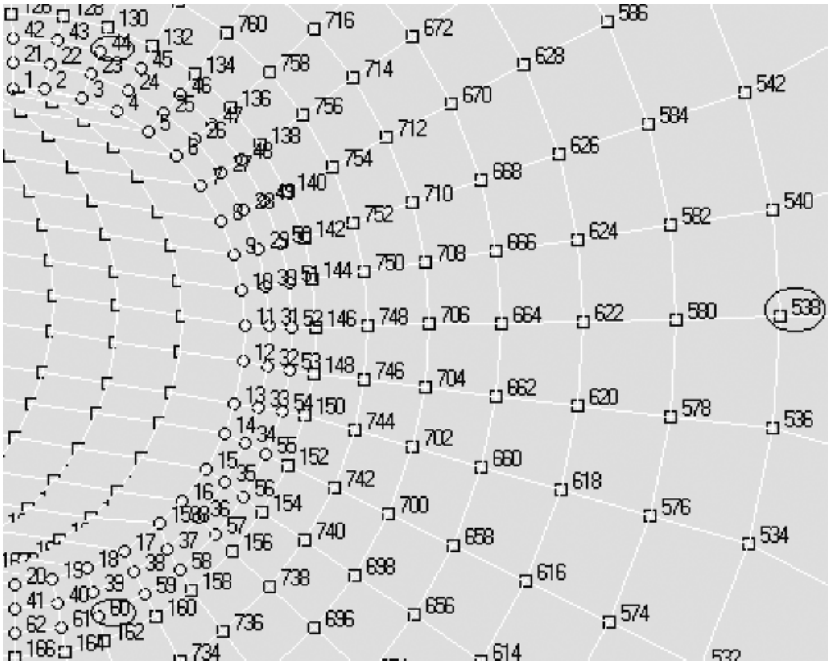

Figure 4. The locations and numbers of the nodes at the interface part.

Figure 5 shows the relation curve of stress and time at node No. 60 at the interface part which has the greatest stress under the pressure, the thermal shock and PTS respectively, from 0 to 30 sec, the stress fast increases in the case of PTS, and from 30 to 150 sec, the stress remains at a high level, and that of thermal shock separately, the stress generated by thermal shock is a few times greater

than that generated by the variation of pressure. When calculating the influence of PTS on the vessel strength, the stress generated by pressure and the stress generated by thermal shock are approximately coupled in the form of linear superimposing.

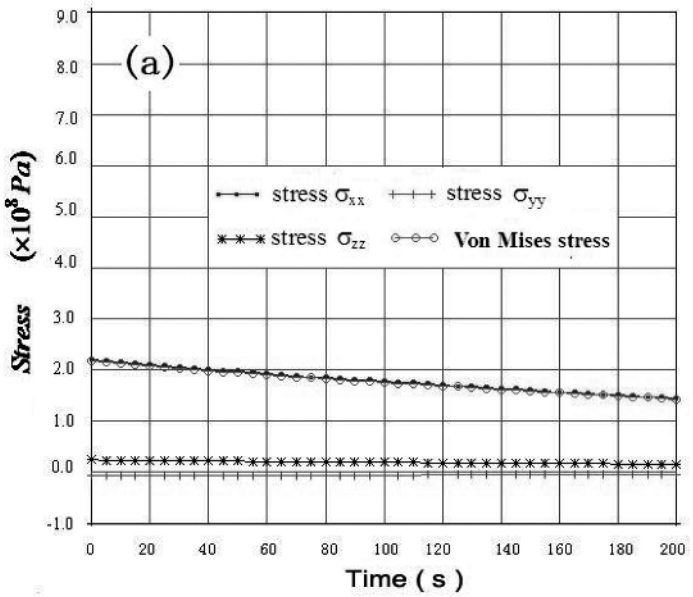

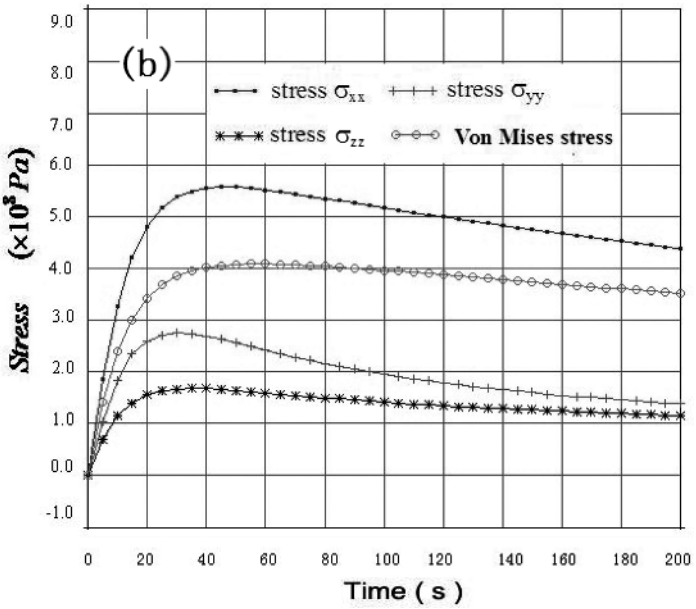

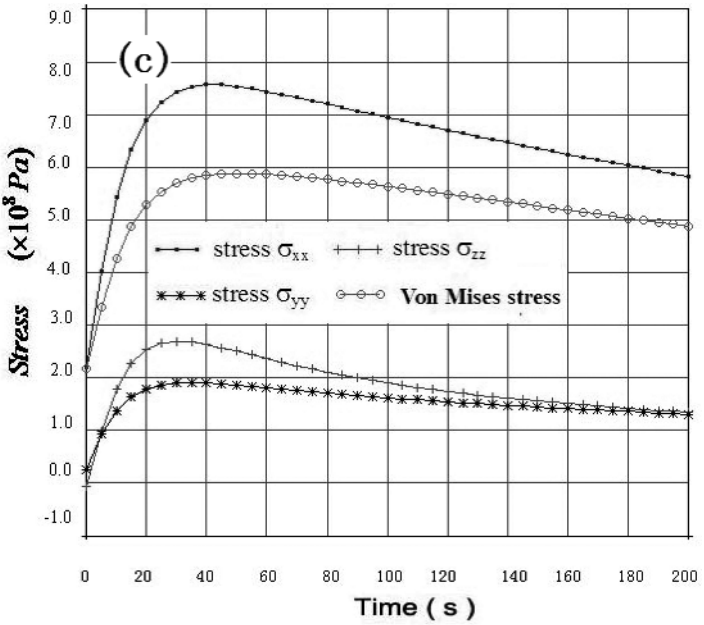

Figure 5. The stress–time hour curve of node No. 60 at the joint part (a) influence of inner pressure; (b) influence of thermal shock; (c) influence of PTS.

Figure 6 shows the distribution of every kind of stress under the influence of pressure, thermal shock and PTS in a pitch arc (composed of nodes from No. 60 to No. 44 in the finite element mesh), when the high-pressure safety water flooding system has been running for 100 sec. According to Figure 6, it is convenient to estimate the magnitude of the stress of every node by Von-Mises stress. Seen from the location of the connection tube, node No. 60 and node No. 44 are symmetric. But because of the asymmetry of heat transfer, the stress in the area of node No. 60 will be greater than the stress in the area of node No. 44, which is attributed to the influence of thermal shock.

Similarly, after the injection of cold water, the stream current will firstly contact the bottom of the vessel and generate thermal stress.

Local plastic areas occur in the place of the joint under the influence of PTS. Figure 7 shows the pattern of equipotential of Von-Mises stress distribution (100 sec, the joint area). The light-colored parts approximately represent the plastic areas. The plastic areas under the joint are a little bit larger than that above the joint.

With this method, the analyses of displacement distribution and temperature distribution of the PTS process have also been carried out.

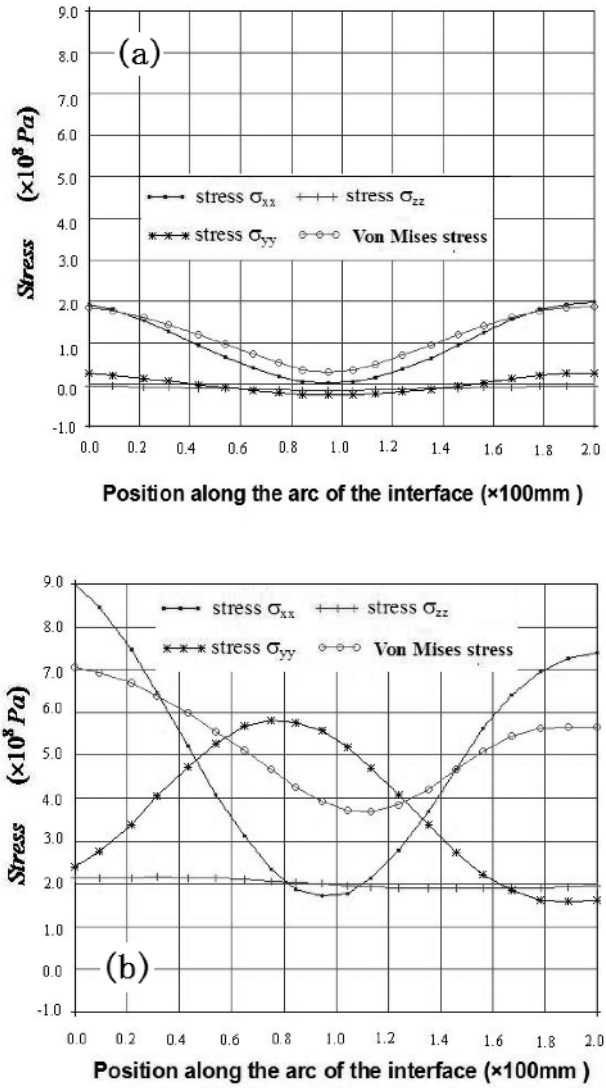

Figure 6. The stress distribution in the pitch of arc at the joint part (when the high-pressure safety water flooding system has been running for 100 sec) (a) influence of inner pressure; (b) thermal shock.

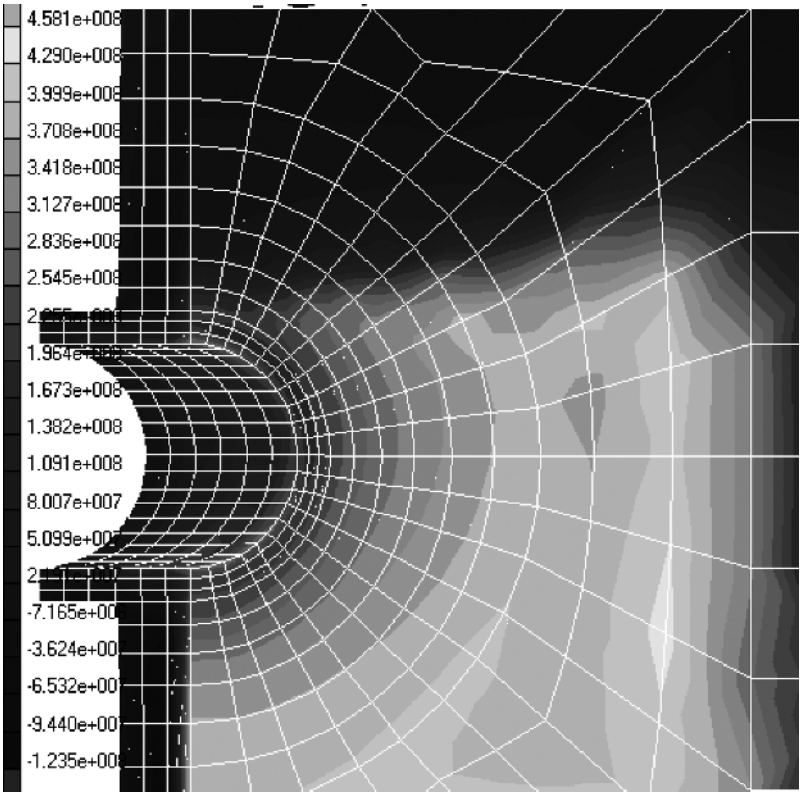

Figure 7. Pattern of equipotential of Von-Mises' stress distribution at the joint area at 100 sec.

5. Conclusions

It is of great significance to study the instantaneous process of PTS on the nuclear pressure vessel, to analyze coupling effects of mechanical and the thermal stresses and to evaluate influences of PTS events on the pressure vessel strength. The building of a 3D finite element model is able to simulate a PTS process and obtain its characteristic in the adjacent area of branch pipe. In the process of establishing the computing model, the plastic-elastic characteristic of the material, thermal transfer generated by the variation of the temperature and the coupling process of mechanics and the thermal stresses should be taken into consideration.

Under the effects of PTS, if the plastic area is not large enough, the coupling effects of mechanical and the thermal stresses are not obvious and the stress of PTS is nearly the same as the linear superimposing of the stresses generated by pressure and the thermal shock. The duration of PTS is about several hundred seconds. The highest stress is situated at the joint of the injection pipe and pressure vessel, and local plastic areas consequently occur in this place.

Acknowledgments

We are grateful for the financial support provided by the Chinese National Natural Science Foundation No. 50371042 and 10472049, the Special Funds for the Major State Basic Research Projects 2006CB605003.

References

1. Theofous T. G., Angelini H., and Yan S., Universal Treatment of Plumes and Stresses for Pressurized Thermal-Shock Evaluations. *Nuclear Engineering and Design*, **146**:1 (1996).
2. Okamura H. et al., Further Experimental Verification of WPS Effect under PTS. *Journal of Pressure Vessel Technology*, **118**(5): 174 (1996).
3. Kordisch H., Talja H., and Neubrech G. E., Analysis of Initiation and Growth of a Circumferntial Crack in the HDR-RPV-Cylinder under Pressurized Thermal Shock. *Nuclear Engineering and Design*, **124**: 174 (1990).

DEGRADATION OF THE PHYSICAL AND MECHANICAL PROPERTIES OF PIPELINE MATERIAL DEPENDING ON EXPLOITATION TERM

STEFAN VODENICHAROV
Institute of Metal science, Sofia, Bulgaria

Abstract: Failures and breakdowns of transport pipelines are especially dangerous because they are connected with enormous material losses, environment damages and very often with serious human casualties and injuries. The worldwide experience in the exploitation of hundreds of thousands kilometers of gas and oil pipelines shows that the number of failures and the probability of catastrophes in the pipelines grows with the increasing operation time due to pipeline material ageing. The object of this investigation is the behavior of C55E (09Г2С) pipeline steel subject to long-term model static loading. The structure and mechanical properties in initial state are compared to the steel characteristics after 15 years stay under static loading by internal pressure. Particular attention is paid to the changes of strength and toughness which are of special importance for the reliable pipeline operation in oil and gas transportation.

Keywords: degradation of the physical and mechanical, properties of pipeline material, depending on exploitation term

1. Introduction

The gas and oil pipelines operate in regions of various climatic conditions. The transport pipelines are subject to different additional loadings produced by sun heating, earthquakes, floods, cyclones, etc. The transported products possess huge reserve of potential energy which ranks the pipelines among the extremely dangerous energy systems. On a global scale over 5 million km of gas and oil pipelines are in exploitation – more than 400 thousand km in Europe, above 300 thousand km in Russia, and above 500 thousand km in USA.

G. Pluvinage and M.H. Elwany (eds.), Safety, Reliability and Risks Associated with Water, Oil and Gas Pipelines, 299–315.

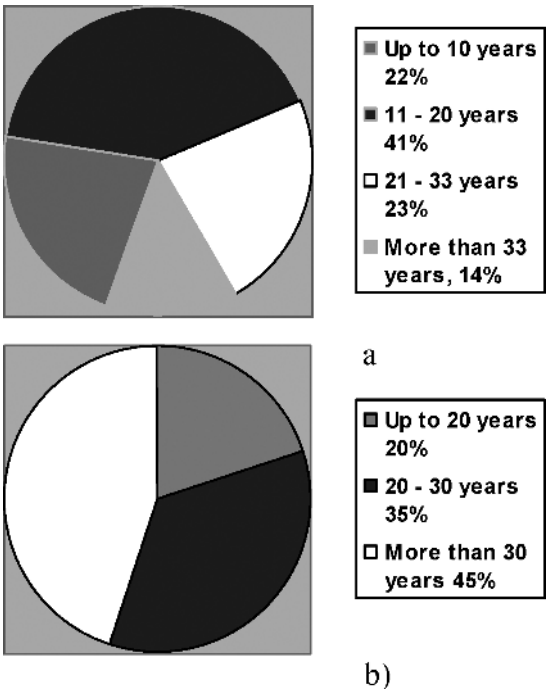

Figure 1. Pipelines distribution according to their age in Russia [12]: (a) gas mains; (b) oil trunk pipelines.

In Russia alone more than 50% of these pipelines are in operation beyond their designed term of exploitation exceeding their serviceable lifetime by 20–30 years [1, 2] (Figure 1).

A large part of the registered failures happen in consequence of exceeding pipelines lifetime. They cause irreparable damages to the environment, economy and lead to human losses.

2. Some Pipeline Failures

The pipeline failures have very often serious consequences. Some individual examples from the last decade are presented below.

On September 28, 2006 in the Volgograd region of Russia not far from populated area (the 442nd kilometer of the main gas pipeline "Middle Asia - Center") a pipe of 1,200 mm diameter breaks and the out flowing gas ignites causing explosion of about 75–80 m in diameter [12].

Figure 2. Explosion of gas pipeline in Dubois, Pennsylvania, USA.

On August 21, 2004 explosion of gas pipeline located not far from town of Dubois, Pennsylvania, USA, destroys the whole residential district and kills several inhabitants (Figure 2) [4].

On January 27, 2000, a 24-inches pipeline collapses producing crack 265 miles long near Winchester, Connecticut. As a result of the failure 11,644 barrels of oil are lost but fortunately there are no human casualties [5].

On July 21, 1997, a 20-inches gas pipeline property of citizens gas, breaks down not far from Indianapolis, Indiana state. As a result three people are killed and 75 injured, six houses are completely destroyed, and 65 are uninhabitable [6].

On August 15, 1997, a 28-inches pipeline located 45 miles to the north of Dallas, Texas, breaks down and 13,436 barrels of gasoline run out. The crack of 10-ft length causes enormous pollution.

On March 9, 2000, a pipeline breaks down near Greenville, Texas, and 13, 436 barrels of gasoline (over 18 million dollars) run out [3]. Fortunately, there are no human casualties.

The US Department of Transportation's Research, The Special Programs Administration and The Office of Pipeline Safety (RSPA/OPS) published data about USA national gas pipeline failures, their causes, and consequences. The data for the period 2002–2003 are presented in Table 1 [4].

TABLE 1. Accidents with national gas pipelines in USA for the period from January 1, 2002 to December 31, 2003 [4].

Failure cause	Number of accidents	% of the total number of accidents	Material losses	% of complete losses	Deaths	Injuries
Excavation works	32	17.8	$4,583,379	6.9	2	3
External forces	12	6.7	$8,278,011	12.5	0	0
Other forces	16	8.9	$4,688,717	7.1	0	3
Corrosion	46	25.6	$24,273,051	36.6	0	0
Equipment	12	6.7	$5,337,364	8.0	0	5
Material	36	20.0	$12,130,558	18.3	0	0
Management activities	6	3.3	$2,286,455	3.4	0	2
Others	20	11.1	$4,773,647	7.2	0	0
Total	180		$66,351,182		2	13

TABLE 2. Pipelines failures in Washington district, USA, from years 1977-1997. [4].

Year	Miles of PL	Accidents	Gallons spilled	Accidents[mi]	SPD[mile]	Gallons released[mi]
1977–1986				.001350		43.45
1986	153,462	209	9,215,346	.001362	104,44	60.05
1987	125,859	237	13,131,468	.001883	104.41	104.33
1988	152,547	193	4,798,542	.001265	212.49	31.46
1989	150,488	163	5,089,518	.001083	58.57	33.82
1990	149,008	180	2,295,486	.001208	105.50	15.41
1991	150,425	216	2,343,508	.001436	251.21	15.57
1992	152,595	212	2,887,164	.001389	253.29	18.92
1993	165.781	230	2,440,536	.001387	174.17	14.72
1994	155,208	244	4,718,700	.001572	363.73	30.40
1995	153,566	188	22,307,746	.001224	211.76	145.26
1996	154,863	195	4,037,922	.001259	320.96	20.07
1997	154,863	179	4,699,674	.001154	320.36	30.29

The pipeline failures in Washington district, USA, can be traced through the years in Table 2 [6]. The detailed analysis of the results shows that the accidents number in the different years varies in narrow ranges but the material losses are enormous.

According to data of The Energy and Utilities Board in Alberta, USA, over 700 failures are registered annually [7]. Most often the failure cause is internal

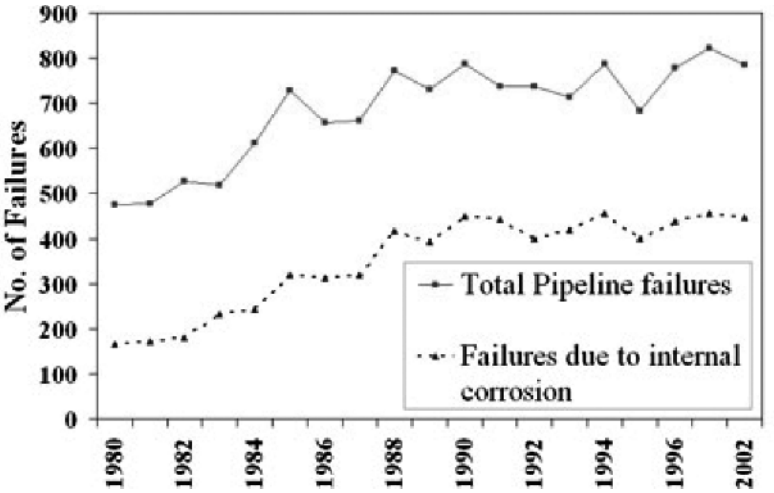

Figure 3. Oil pipeline failures in Alberta, USA in the years [7].

corrosion of the joint components of the pipelines (Figure 3). It is evident that the number of failures is growing in the recent years.

The Russian experience in the exploitation of several tens of thousands kilometers of gas pipelines shows [2, 10], that the number of failures grows with the increase of the exploitation time (Figure 4, 5). A peak of accident rate is established after 24–28 years of exploitation after which the failures number decreases.

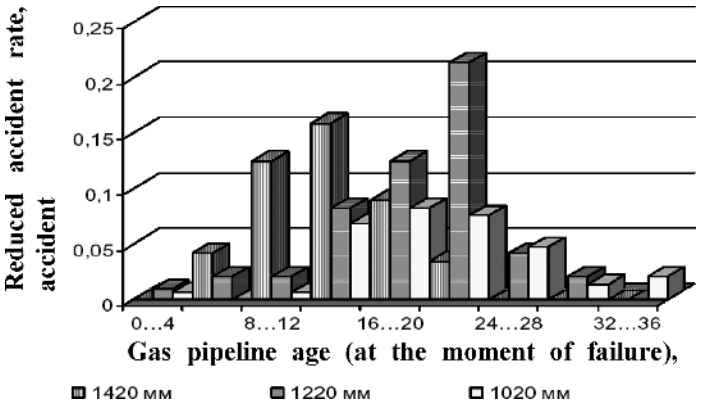

Figure 4. Failures of pipelines, property of Gazprom, Russia [2].

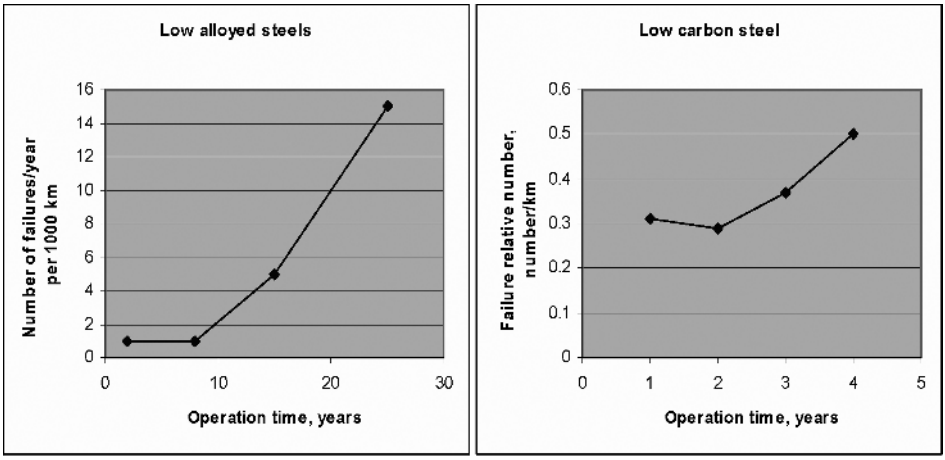

a) b)

Figure 5. Number of failures (a) main oil pipelines [2], (b) distribution gas pipelines [5].

The analysis of statistical data [1, 5] on failures of gas and oil pipelines in Russia (Figure 6) shows that the number of pipeline failures occurring in the exploitation period up to ten years varies between 1% and 7% of all analyzed cases. For the operation period between 10 and 15 years the frequency of failures sharply increases up to 32% and for the next period it decreases considerably.

The statistical data accumulated in England and Norway about failures in oil and gas pipelines in North Sea show continuous growth of the accidents with the increase of the exploitation time [11]. Table 3 presents information for the

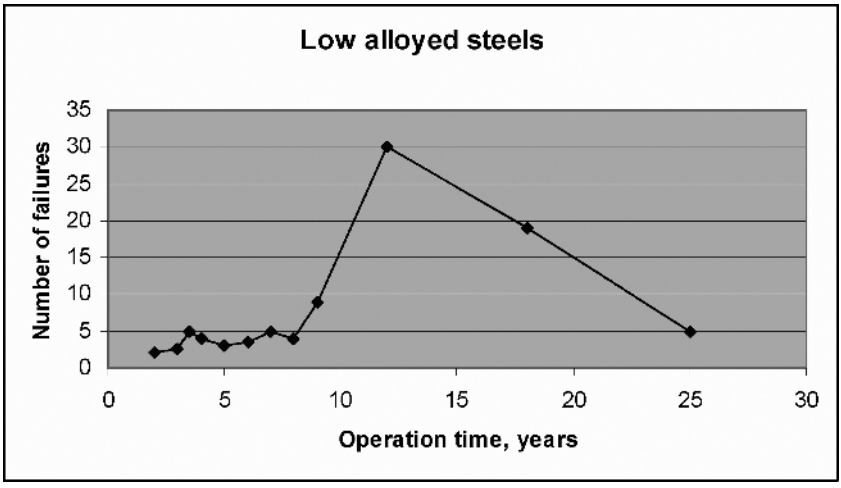

Figure 6. Distribution of failures number [%] of main gas pipelines depending of operation time [5].

period 1970–1995. The data are presented as probability for failure occurrence per 1 km of pipeline per year. In Russia the probability for failure occurrence is assumed to be 0.22 per 1,000 km per year. This value is 1.5 times higher than the probability for failure occurrence given in Table 3 and it corresponds to the actual number of failures in North Sea.

TABLE 3. Probability for failure occurrence per 1 km pipeline per year.

Corrosion and defects of pipeline material	Failures through third parties' fault	Other causes for failures	Total frequency of failures
9.29·10–5	3.61·10–5	2.5·10–5	1.55·10–4

According to the management of the Northwestern Regional Center of Russia there are 446 pipeline failures in 2005, 403 of them resulting on technogenetic reasons [13]. According to the prognosis of specialists from the Institute of Metal Physics (Russia) from 2008 on the number of pipeline failures will grow 2.5–3.5 times per year and toward 2010 it will reach 5.5 thousand accidents per year.

The safe operation assurance of the functional systems at different exploitation stages is only possible on the basis of developing modern safety methods in the processes of design, manufacture, building, exploitation, and scheduled technical diagnostics with competent assessment of the pipelines rest lifetime.

3. Causes for Pipeline Failures

The pipeline safe operation and high reliability depend on various factors – mechanical damages, fatigue cracks, material defects, weld cracks, improper welding, internal or external corrosion, presence of flokens – and most of all on the natural changes of the physical state of the pipeline metal and welded joints during their prolonged exploitation.

In compliance with the regulation documents the pipeline operation ability is determined by the strength and toughness margin of the pipeline metal structure that is the main construction component of any pipeline system. The above parameters are specified taking into account the pipes loading at uniform distribution of the stresses along the perimeter and the mechanical properties of the material. However, very often the change of the properties during long-term exploitation is not taken into consideration.

This could be explained by the absence of unified approach for assessment of the metal structure properties after long term of exploitation. Finding out the effects of the operation duration on the mechanical properties of the metal structures requires long-term research by several generations of scientists. The

now existing scheduled system for replacement of outworn equipment also contributes for the lack of data related to the actual condition of the installations.

According to the statistical data of US Department of Transportation's Research and Special Programs Administration [4] most often the failures of oil and petrol pipelines are due to fatigue cracks, corrosion damages, presence of cracks and hydrogen flakes, or structure inhomogeneities in the metal.

According to other authors [12, 15] the main reason for the growing number of failures in the oil pipelines are the accumulation of fatigue damages and the deformation ageing in combination with the irreversible microplastic damages of the structure.

According to [16] the main reason for pipeline failures are the internal and external corrosion processes.

However, in most of the cases the pipeline failures are due to complex reasons – deterioration of the pipeline design parameters and change of metal properties during operation. The damages caused by human error or vandalism are not infrequent also.

4. Materials Used for Pipes Production in Russia

The steels used for pipes production could be divided into several generations:

- First generation (up to 1947 г.) – steels Ст3, Ст4, 20
- Second generation (1947–1960) – steels 19Г, 09Г2С, 14ХГС
- Third generation (1960–1975) – steels 17ГС, 17ГС1, 17ГС-У
- Fourth generation (from 1975) – low-alloyed steels with carbonitride inclusions produced by controlled rolling – 15Г2СФ, 12Г2СБ, 09Г2ФБ, 09ГНФБ, 10Г2ФБ.

The steels of first, second, and third generations are most widely applied for manufacture of pipes and pipelines and they have been already in operation for 15–40 years. The operation life of fourth generation gas pipelines has been not longer than 20 years. Very limited data on the material behavior during long-term exploitation can be found in the available publications. For example, the pipes of fourth generation steels of 1,420 mm diameter operating under pressure of 7.5–10 MPa are not yet examined. The analysis of the published data indicates that the initial properties of the pipe metal change during long-term exploitation.

5. Change of the Metal Mechanical Properties

The results on the changes of the mechanical properties occur in the metal of main pipelines made of steel 09Г2С are reported in [1, 2, 15]. The strength properties (yield strength R_e and tensile strength R_m) increase (Figure 7, a) but

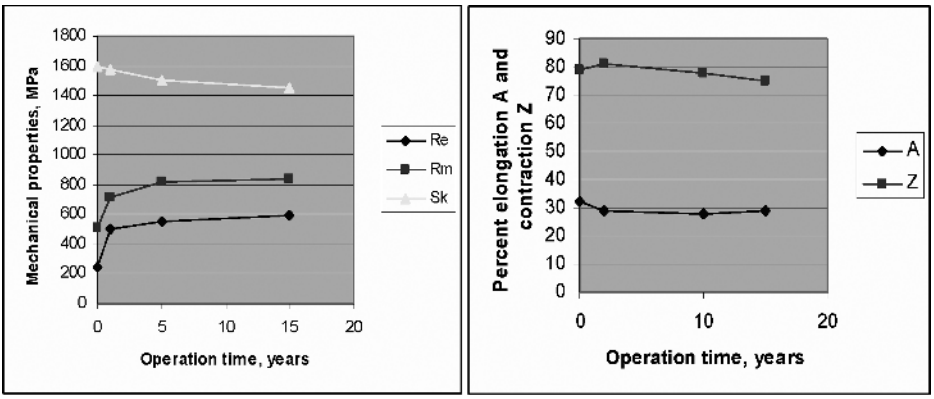

a) b)

Figure 7. Effect of operation time on the metal mechanical properties: (a) material strength properties, (b) C55E steel plastic properties [1].

the true stress S_k, the elongation A [%] and the contraction Z [%] slightly decrease (Figure 7, b) with the operation duration.

The impact toughness of the steel decreases during the operation A (Figure 8) [1]. The decrease during the first ten years of operation is insignificant, but after that period begins an intensive degradation of the metal impact toughness. The same trend is found also in pipeline of X70 steel, which is in exploitation at minus temperatures in Urengorsk, Russia, where the impact toughness drops by 16–25% after nine years of operation.

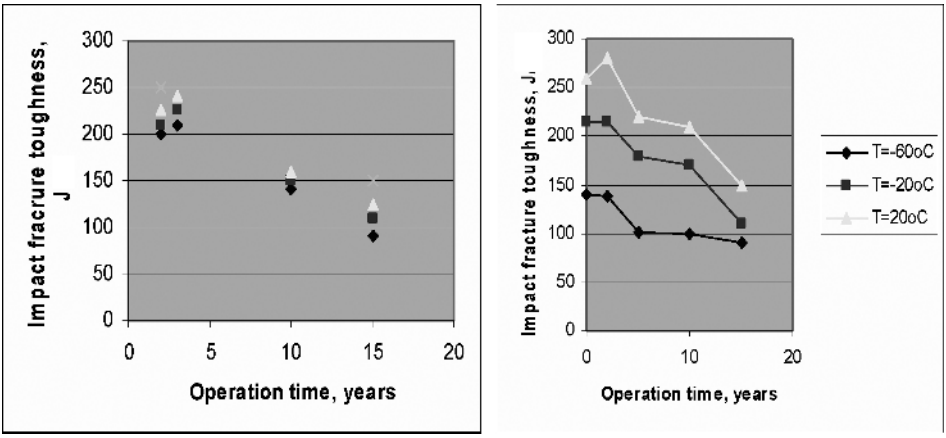

Figure 8. Change of the impact fracture toughness of steel 09Г2С [1] in dependence of the operation time.

The impact fracture toughness of 09Г2С steel specimens taken from pipelines after long term of operation decreases in the whole temperature range of testing. It should be noted that the degradation rate is different depending on the test temperature. For the first five years of operation it decreases by 15–30% compared to the reference state. The degradation after the 9th year goes slower and practically no degradation is observed in the temperature range –40/–60°C.

Two types of ageing of steels with the operation time have been reported for a number of pipelines materials [2]: natural ageing, resulting on microstructure nonequilibrium, and deformation ageing, which is due to overloading. Both types of aging are accompanied by strengthening and embrittlement of the steels that favors the low energy fracture of the pipelines.

The crack resistance of specimens taken from 530 mm diameter pipeline of 09Г2С steel subject to long-term operation in the severe conditions of Yakut is studied in [1]. Significant degradation of the material resistance to crack growth is found after five and ten years of operation. The effect of the operation time on the material mechanical properties of 820 mm diameter main gas pipelines of steel 19Г at operation pressure of 5.0 MPa is discussed in [2]. The properties of pipeline material after 29.5 years of operation are compared to the properties of pipe which has spent the same time in warehouse. The test results show, that the strength properties of the operating pipe R_e and R_m have increased by 11% and 30%, respectively, but the impact toughness has decreased by more than 40%. These changes of the mechanical properties are explained with the severe restriction of dislocations mobility in the metal.

Particularly unique investigations of 914 mm diameter/9.9 mm wall thickness pipe subjected to 24 h action of internal hydraulic pressure are reported in [17]. A notch of 84 mm length and 5 mm depth was made on the wall surface prior to testing. The stress in the wall was $1.02R_e$. A plastic yield was established at the notch tip as well which led to formation of small crack. After six months loading of the pipe at $0.9\ R_e$ no plastic yielding was found, but the subsequent increase of the stress to $1.03\ R_e$ caused immediate fracture. This test shows that the long-term loading by average stress close to the yield strength (R_e) the atomic bonds break due to deformation concentration at the notch tip, the crack slowly grows and finally leads to fracture.

Cyclic stresses develop in the pipe metal due to fluid transport of flow during operation. They are an essential reason for the growth of the existing ones and formation of new defects in the metal. Localized plastic deformation develops around the mechanical damages in the outer surface layers of the wall. In many cases fatigue cracks nucleate very often around these stress concentrators and their further growth results in pipe failure. The statistical data analysis [18] verifies the conclusion that the main cause for the increasing number of pipeline

failures with operation time is the accumulation of fatigue damages in combination with the accumulation of irreversible microplastic deformation of metal.

The external corrosion of the pipes is of particular importance for the fracture of pipelines operating in cold climatic conditions (e.g., West Siberia, Alaska, etc.) [1, 2, 15, 16]. Many of these pipelines are insulated by different anticorrosion means. In Russia bitumen is commonly applied whose durability is 12–15 years. Some pipeline connections are insulated by insulation tapes with protection lifetime of 20 years. The short service life of these insulation materials is one of the reasons for the intensive external corrosion of the pipelines made before 1980 (they are more than 85% of all pipelines). 65% of the pipes of the contemporary gas pipelines have polymer insulation. The proper laying of this insulation depends on the skill of the builder and can additionally restrict the life of the insulation (it is eight to ten years).

The action of the transported fluid causes formation of erosion pits on the inner surface of the pipe. In the recent years the different countries succeed to limit the internal corrosion damages by active corrosion control and prevention [15, 16]. USA applies inspection method called “smart pigs”. Extremely sensitive devices travel inside the pipe and register the presence of even the smallest corrosion pits.

The relatively high number of pipeline failures is due to defects of welding origin. Examinations are carried out on pipes of steels 17ГС, 17Г1С, and 09Г2С after manual electric arc and contact spot welding [1]. Samples are prepared from these welded pipes and subjected to long-term loadings on special stands of 20 kN normal force. The significant change of the mechanical properties of the manually electric arc welded steels grade 17Г1С and contact welded steels 09Г2С is found out after the loading. It is proven that the tensile strength properties considerably increase with the duration of the loading. The metal impact toughness of the weld metal strongly decreases in the whole operation temperature range (from -60^{o}C to $+20^{o}$C). It is established that the heat affected zone metal is more susceptible to crack growth and deformation ageing processes in comparison to the weld metal. The investigations show phases precipitation in the weld area as well as lower mobility of dislocations, which are blocked by the phases and interstitials atmospheres.

6. Object of Investigation

The determination of the rest lifetime and crack resistance of the dangerous technogenetic systems for petrol and gas transport, taking into account their long-term exploitation, is particularly sophisticated research problem. From the analysis of the available sources the conclusion could be made that at present the knowledge about the effect of the time factor on the kinetics, mechanism,

and morphology of the deformation and fracture of the pipe and pipeline constructions are at the stage of experimental database accumulation. There is no unified scientific conception describing the physical nature of the material mechanical properties dependence on the exploitation duration. There is no sufficient experimental base for assessment of the pipeline and material service properties. In this respect the information about the change of the pipelines crack resistance during their operation is particularly valuable. Unfortunately, such data are almost not found.

The steels grades 19Г, 09Г2С, 14ХГС are the most largely applied for pipes and pipelines production since 1947 and their operation time varies from 15 to 40 years. In the published sources the data about the properties changes of that steel grade after long term of operation in pipelines are extremely scanty.

Object of investigation of the present paper is steel C55E (EN10083) equivalent to 09Г2С (GOST 19281-89). The purpose is to investigate the changes of mechanical properties of seamless pipe of 133 mm diameter and 5 mm wall thickness subjected to static internal pressure of 20 MPa for 15 years.

7. Experimental Method

Table 4 presents the chemical composition and Table 5 – the mechanical properties of as received 09Г2С seamless pipe of 133 mm diameter and 5 mm wall thickness. Short parts of the examined pipe are subjected for 15 years to loading by internal static pressure produced by hydraulic stand at nominal pressure 20 MPa. Standard samples for tensile test at room temperature and for three-point impact bending test at temperatures of -60^{o}C, -20^{o}C, and 20^{o}C are made of as received pipes and of pipe parts after the loading.

The dislocation structure in initial state and after the 15 years loading is examined by transmission electron microscopy. The TEM specimens are prepared parallel to pipe axis. The fracture morphology of the impact fractured specimens is analyzed by scanning electron microscopy.

TABLE 4. Chemical composition of C55E (09Г2С) steel.

C, %	Si , %	Mn , %	Ni, %	S, %	P, %	Cr, %	N, %
0.10	0.72	1.64	0.3	0.04	0.035	0.3	0.008

TABLE 5. Mechanical properties of C55E steel in initial state.

Re	Rm	A_5	Z	KCU
MPa	MPA	%	%	J/sm^2
368	518	34	80	110

8. Experimental Results

8.1. MECHANICAL PROPERTIES

The tests show that after 15 years loading by static pressure the strength properties of the steel practically do not change; only the yield strength R_e increases very slightly (Figure 9).

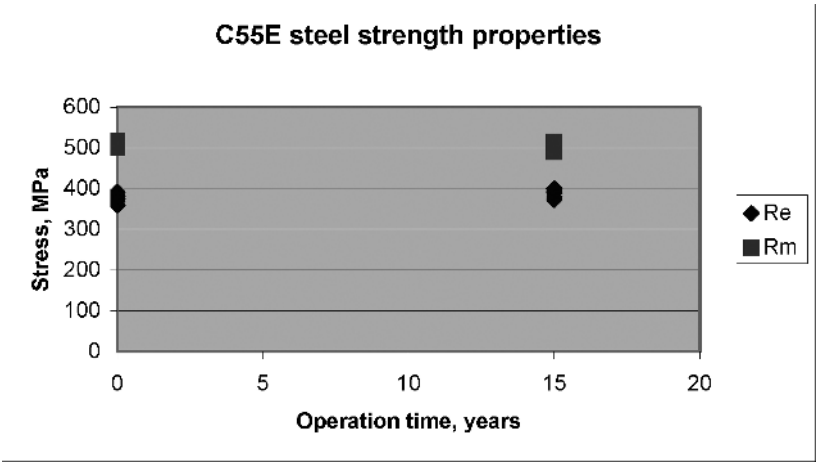

Figure 9. Change of the strength properties of steel 09Г2С after long-term loading.

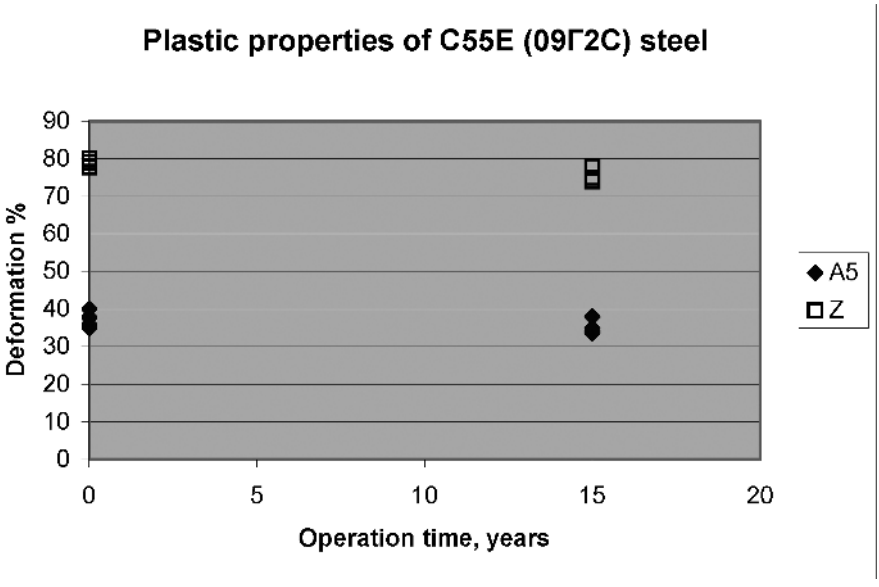

Figure 10. Change of the plastic properties of steel 09Г2С after long-term loading.

The relative elongation A5 and contraction Z decrease more visibly after the loading (Figure 10).

The results of three-point impact bending test show very slight decrease of the impact toughness after the stay of the pipes under internal static pressure for 15 years (Figure 11, 12). The values of the fracture energy obtained for the three test temperatures (+20°C, –20°C, and –60°C), correspond to the energy of the

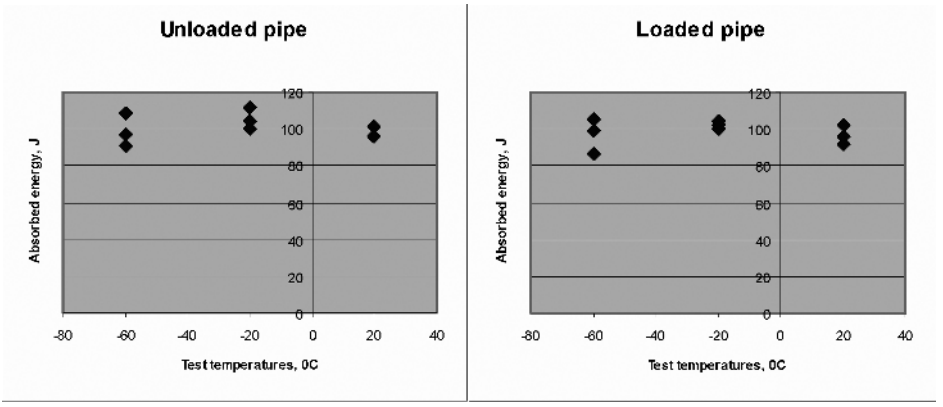

Figure 11. Impact fracture toughness of 09Г2С pipe: (a) as received; (b) after 15 years under static loading.

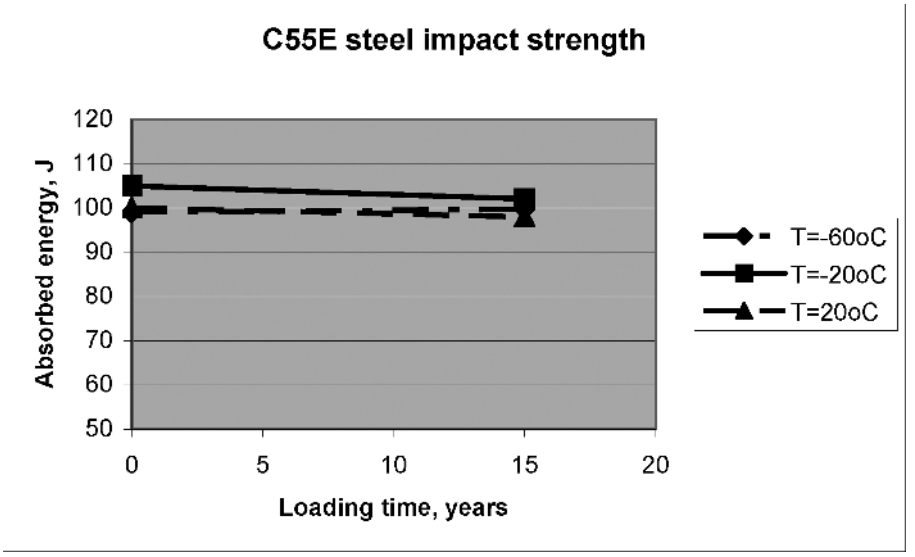

Figure 12. Impact fracture toughness of 09Г2С pipe as received and after 15 years under internal static pressure.

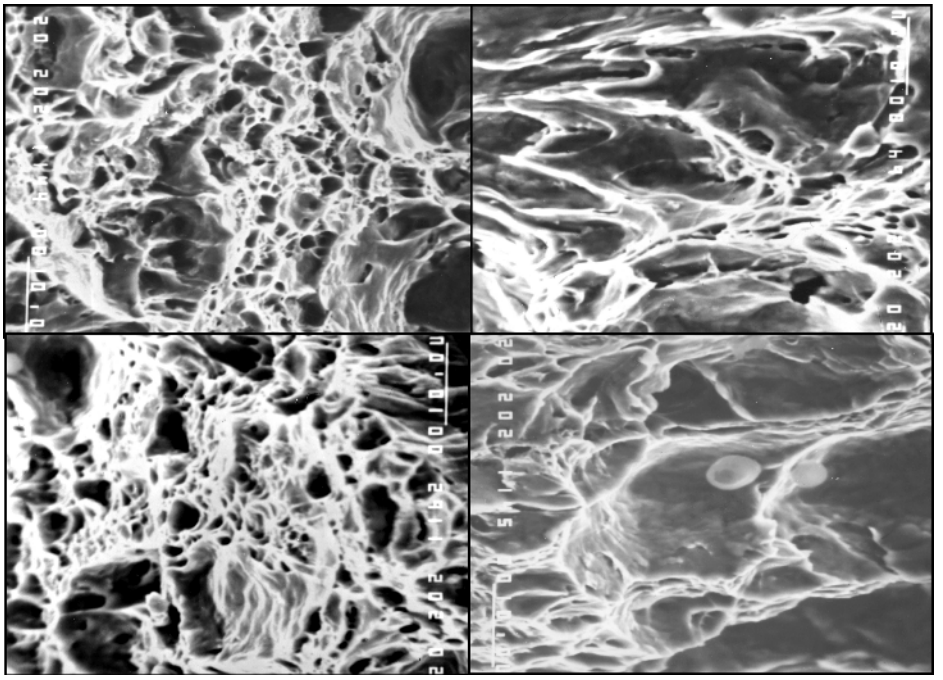

Figure 13. Fractured surface morphology of 09Г2С pipe specimens tested by three-point impact bending: (a) as received; (b) after 15 years under internal static pressure.

Charpy's curve upper shelf. That proves that the fracture of the metal, both as received and after long stay under static pressure occurs by ductile mechanism in the whole test temperature range.

The visual examination of the impact fractured surfaces shows strongly expressed wave-like relief and lateral expansion of the specimens. The observation by scanning electron microscopy reveals the presence of tear dimples with highly deformed walls (Figure 13). No elements of brittle fracture are registered. This fracture morphology is found both in the samples in as received state and the sample tested by internal static pressure for 15 years and does not change depending on impact test temperature.

The observed character of the fractured surface is typical for ductile fracture and confirms the conclusion that at any testing temperature the fracture runs in the area of the Charpy's curve upper shelf.

8.2. STRUCTURE CHARACTERISTICS

The examination by transmission electron microscopy shows ferrite-pearlite structure with relatively low dislocation density both in the as received samples and in the samples after 15 years internal static pressure (Figure 14). No changes

of dislocations density and distribution are registered after the long-term action of pressure (Figure 14b). This behavior is easy to explain having in mind that the stresses in the pipe wall under the action of 20 MPa internal pressure are much below the yield strength of the steel. The absence of effect on the dislocation structure is in a good agreement with the absence of changes of tensile properties after the long-term loading of the steel. The established slight increase of Re and decrease of impact fracture toughness could be due to initial stage of ageing processes – e.g., formation of atmospheres of interstitial atoms.

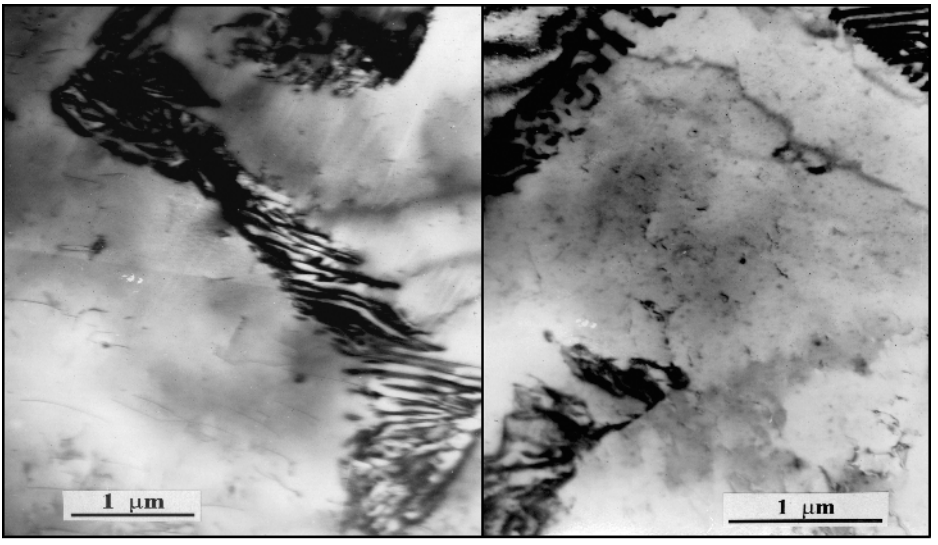

Figure 14. Microstructure of 09Г2С pipe: (a) as received; (b) after 15 years under static pressure.

9. Conclusions

- The influence of long-term internal static pressure on the behavior of seamless pipe of 09Г2С/GOST 19281–89 steel (equivalent to C55E/EN10083) designed for usage in gas or oil pipelines was investigated.
- The comparison of mechanical properties of the pipe steel in initial condition and after 15 years long action of 20 MPa internal static pressure showed no significant changes.
- It was established that the long-term action of internal pressure does not affect the dislocation structure of the steel. This is explained by the fact that the stresses produced by the 20 MPa internal static pressure in the pipe wall are far below the yield strength of the pipe steel.

- The absence of dislocations movement and recombination and the absence of new dislocations indicate that no defects can develop by dislocation mechanism in the structure during the long-term action of the pressure.
- The performed investigation shows that a fracture of pipeline loaded by 20 MPa internal static pressure can be expected only if defects of critical size are present in the pipe material in initial state. These defects can serve as stress concentrators around which the real stresses may exceed considerably the material yield strength and lead to crack growth.

References

1. Pashkobv, Y. and Georgiev, M., Effect of exploitation term on the change of the pipeline metal mechanical properties Влияние срока, Proceedings of Technical University Plovdiv, vol. 7, Engineering Sciences, 2001 (in Russian).
2. Myasnikov, V., Assessment of the design reliability parameters of long term exploited pipelines in West Siberia, TGNGU, 2004 (in Russian).
3. Pipeline failure causes, 2005.
4. Pipeline Failures, www.efsec.wa.gov.
5. Failures of pipelines, www.materialsengineers.com.
6. Causes of Pipeline Failures, www.inga.com.
7. Dahlberg, E. and Bruno, T., Analysis of gas pipeline failure, NG-20, Report 125, December, 1990.
8. Bonasso, S., Pipeline Safety, October 9, 2003.
9. Giedon, R. and Smith, D., An analyses of reportable incidence for natural gas transmission and gathering lines 1970 through 1978, NG-18, Report 121, September 1980.
10. Goncharov, V., Analysis of North-European gas pipeline effects on the environment in the process of exploitation, J. Economics and Investment, VIIth International Ecological Forum Baltic Sea Day (in Russian)
11. Prusenko, B., Analysis of failures and accidents in Russia pipeline transport, 2005 (in Russian).
12. www.engr.sjsu.edu.
13. Zvyagin, Y., How to avoid technogenetic catastrophes, International Conference "Current problems of industrial safety", Sanct-Petersburg, 2005 (in Russian).
14. Kelley, C., Pipeline safety, United state Senate, May, 2000.
15. Arulanandam, S. J., Wilson, D. J., and Hrudey, S. E., Accounting for Uncertainty in Predicting the Risk of Pipeline Failure, University of Alberta, Edmonton, AB T6G 2G8, 2004.
16. www.corrosion-doctors.org.
17. Mochernyuk, N. et al., Effects of operation time and gas pressure on physical-mechanical characteristics of pipeline steel 19Г, Gas Industry, No. 3, 1991 (in Russian).
18. Yamaliev, K., Aging of pipe metal in the process of oil pipeline exploitation, VNIIOENG, series Oil transport and storage, 1990 (in Russian).

DEFORMATION CHARACTERISTICS OF CARBON STEELS UNDER HIGH TEMPERATURES

RAZMIK BARSEGHYAN[1] AND ARTAK BARSEGHYAN[2]

[1]*State Engineering University of Armenia (SEUA), 105 Teryan, Yerevan, 0009, Republic of Armenia;*[2]*AREV Scientific-Industrial CJSC, 1st Adana,*
Yerevan 0082, Republic of Armenia

Abstract: The temperature influence on mechanical properties of the carbon steels is discussed. Under high temperatures the steel structures, moreover the pipes, can lose their structural strength.

Keywords: elasticity modulus, elastic characteristics, carbon steels, high temperatures, strength

1. Introduction

In some critical situations (fire, explosion, etc.) particular part of the pipeline can be in the sphere of high temperature. Under high temperatures the steel structures, moreover the pipes, can lose their structural strength. The reasons of this loss can be the changing of material strength characteristics or short-time creeping phenomenon. The latter is a topic for another study. The influence on mechanical properties of the carbon steels is examined.

It is common knowledge that the increase of the body temperature leads both to the changes of physical characteristics of the lattice and the development of complicated physical and chemical processes, so the deformation properties of the material changes. The higher the temperature, the more important is the temperature influence. The threshold of accounting the temperature influence is approximately 200^{o}C.

The existing experimental investigations show that under high temperatures and low deformation (for short-time interval when creep deformations are small) the steel satisfies the isotropic elastic body model, the elasticity modulus and Poisson's ratio being its temperature functions.

G. Pluvinage and M.H. Elwany (eds.), Safety, Reliability and Risks Associated with Water, Oil and Gas Pipelines, 317–324.

According to papers [1, 2] when temperature of steel is high, the Poisson's ratio, tends to one half, and in engineering calculations it is expedient to accept one half. This allows simplifying the mathematical development of the solution, and the small increase for values of stress to be calculated increases the safety factor of the structure.

The temperature dependence of the carbon steel elasticity modulus in different loading conditions is studied in papers [3–7]. In article [4] setting and the method of measuring the steel elasticity modulus at high temperatures is proposed. All the experimental investigations show that the steel elasticity modulus is a monotonously decreasing function of temperature, practically tending to zero at steel melting point. Spreading of experimental results obtained is, as a whole, connected with using different methods of the experimental process.

Elastic steel characteristics in static loading were studied by specialists from "Nippon Steel" firm [7], Morozinsky [8], Puringer [9], and Ghali [10].

Various approximating expressions are used by different researchers for presenting experimental results of elasticity modulus dependence on the temperature. Polynomial [11] and experimental [12] approximating expressions are used more frequently.

In article [7] the influence of various admixtures (copper, tin, sulfur) on steel elastic properties at high temperatures is discussed. Elastic steel dependence on chemical inhomogeneity is considered in detail by Yefimov [11]. He proposed an approximating formula for the elasticity modulus accounting the influence of carbon, silicon manganese, phosphor, and sulfur concentration under high temperatures. In all probability, this elasticity modulus expression can be applied to limited interval of temperature change close to the steel melting point, and therefore it has no practical value for structures or their elements calculations of strength analysis and longevity.

During long loading effect, in particular, high temperatures, creeping deformation becomes important in general deformation. The elasticity theory and long-term strength development has recently been accelerated. Continuous accumulation of new experimental results, general relationship development of continuous medium mechanics and expanding possibilities of computer engineering stimulate this development. An important contribution in elasticity theory and long-term strength development of metals was made by Shesterikov [13], Ilushin and Pobedria [15], Kachanov [16], Goldenblat, et al. [17], Odqvist [18], Garofalo [19], etc.

Shesteriklov and Lokoshchenko [20] made most detailed review of the literature devoted to creeping phenomenological theories of common character. Here and in book [13] ageing, flows, strengthening, hereditary theories, as well as thermodynamic problems of elasticity theory are scrutinized.

There are numerous monographs, reviews, and materials in which physics of processes resulting in macroelasticity of metals are examined. However they have a theoretical character and are not suitable for using in engineering calculations.

The fundamental theory of short-term creeping of metals is elaborated by creeping of metals Rabotnov and Mileyko [21]. An interesting dependence of high temperature steel creeping is proposed by Sorimachi and Brimacomba [22].

In article [23] an attempt to give a particular physical sense to coefficients of different temperature–time parameters is made.

Unfortunately, the elasticity of carbon steels which are not used as structural material working under high temperatures is studied comparatively little. For this class of steels the main experimental results and their theoretical treatment are carried out jointly by Muradian [24].

2. Elastic Properties and Coefficient of Thermal Expansion Under High Temperatures

As it was mentioned before, on the basis of existing experimental research the steel behaves under high temperatures and as an elastic isotropic body and its properties are functions of temperature. The revealing of functional dependence of real metals with elastic properties on temperature by means of theory apparatus physics of metals is practically impossible.

Consequently, under temperature changing interval $\left(200^{o}C \le T \le 1000^{o}C\right)$ that interests us the elastic characteristics can be specified only by existing experimental results.

According to [1] Poisson's ratio for carbon steels working under high temperatures is accepted as 0.5. Simplifying mathematical calculations in solving practical tasks such an approximation results in insignificant increase of value stresses to be calculated, and therefore it is desirable in strength and longevity analyses.

The experimental research results of the steel elasticity under high temperatures are given in Figure 1 [27]. As it follows from the given graphs, the experimental result spreading mentioned by different authors reaches the maximum value for temperature over $1000\,^{o}C$.

Figure 2 shows the results of experimental investigation made by Yefimov [11] under high temperatures.

Considering the results of recent experimental researches in defining elastic properties of carbon steels under high temperatures [3, 7] and investigations for specifying other deformation characteristics (creeping and plasticity) [20, 22,

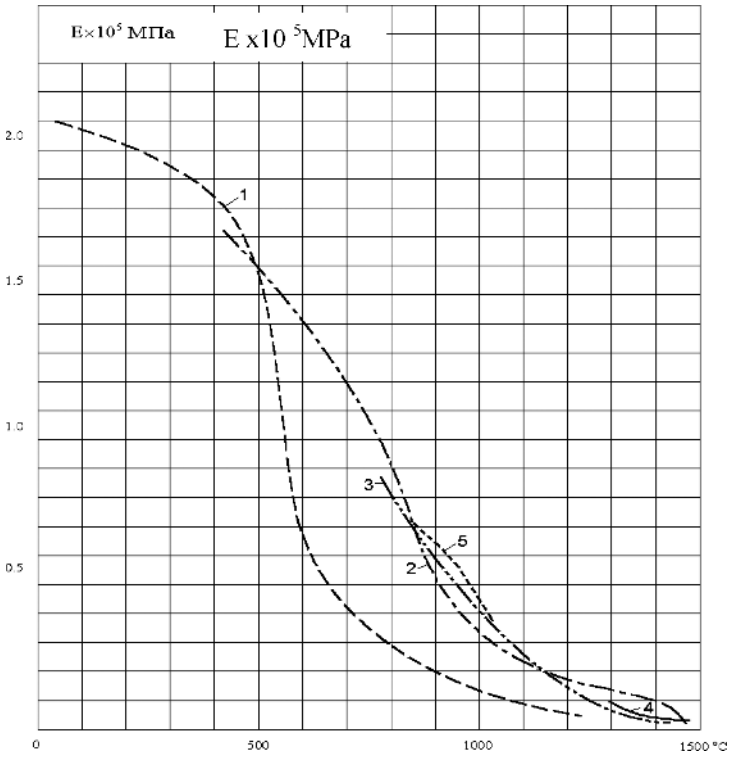

Figure 1. Perimental results of steel elasticity modulus investigations under high temperatures [27] according to: 1. "Zakk" firm, 2. "Nippon Steel" firm, 3. Puringer, 4. Morozinsky, 5. All-Union Scientific Research Institute of Met Engineering Industry.

25–27] for constructing functional dependence, it is necessary to take into account the following basic aspects.

The carbon steel elasticity modulus can be changed within the next trusting interval for high temperatures to be examined:

$$200^{o}C...185 \div 190GPa$$

$$400^{o}C...160 \div 170GPa$$

$$600^{o}C...120 \div 140GPa$$

$$1000^{o}C...20 \div 25GPa$$

$$1200^{o}C...10 \div 15GPa$$

$$1400^{o}C...0.5 \div 0.5GPa$$

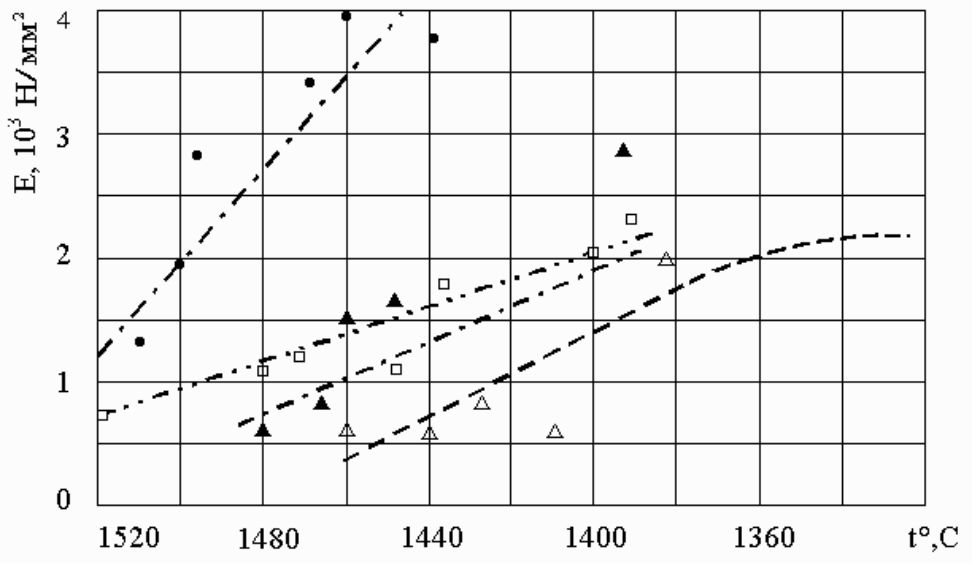

Figure 2. The dependence of elasticity modulus on temperature for steels with various contents of carbon in percentage: 1. □ – 0.06…0.08 2. ● – 0.19…0.21 3. ▲ – 0.30…0.37 4. △ – 0.48…0.54

1. The influence of relative concentration of M_n/S on the steel elasticity modulus is more strongly felt under $900 \div 1200^{\circ}C$ in $M_n/S \le 20$ relationships. This phenomenon can be presented as follows:

$$\left(\frac{M_n}{20S}\right)^n \left(\frac{T_C}{T}\right)^m; \quad n,m>1, \quad M_n \le 20S,$$

which can be neglected in approximation of the carbon elasticity modulus.
2. The influence of carbon concentration is more strongly felt under temperatures close to the temperature of the pearlite formation solidus in intergrain boundaries.
3. The influence of the temperature can be expressed by a polynomial or exponential function with regard to the temperature (Figure 1).

Proceeding from the above mentioned, the approximating function of the carbon steel elasticity modulus is to be accepted in the form of mathematical expression:

$$E(T,C,M_n/S)=E_0^{'}+E_1\frac{T}{T_C}-E_2\left(\frac{T}{T_C}\right)^2+E_3\left(\frac{T}{T_C}\right)^3\left(\frac{M_n}{20S}\right)^2+\left(E_4C-E_5C^2\right)\left(\frac{T}{T_C}\right)^2$$

where C is carbon concentration of $\le 0.5\%$ T_C is the temperature of steel solidus.

The constants E_0, E_1, E_2, E_3, E_4, and E_5 are defined from the condition of the presence of elasticity modulus maximum with concentration of carbon $0.18\div 0.2\%$,

$$E_0^{'}=1.8\cdot 10^5\,MPa,\ E_1=25.07\cdot 10^5\,MPa,\ E_2=58.85\cdot 10^5\,MPa$$

$$E_3=30.85\cdot 10^5\,MPa,\ E_4=0.823\cdot 10^4\,MPa,\ E_5=2.286\cdot 10^4\,MPa$$

Sometimes it is more convenient to make use of the following approximating elasticity modulus expression:

$$E=E_0^{"}e^{-\lambda_1 T}+E_1Ce^{-\beta_1 C}$$

where $E_0^{"}=2.10^5\,MPa$, $.\lambda_1=0.0024521/^{\circ}C$, $\beta=5$, $E_1=1500MPa$

For engineering calculations the expression of the elasticity modulus can be simplified as follows:

$$E=\overline{E}_0e^{-\lambda T-\beta C}$$

$$\overline{E_0}=2.10^5\,MPa,\qquad \lambda=0.0024521/^{\circ}C,\qquad \beta=0.0001.$$

Considering that for structural steels the carbon concentration in average equals ~2% we will definitely obtain

$$E=E_0e^{-\lambda T}$$

where

$$E_0=1.996\times 10^5\,MPa,\quad \lambda=0.0024521/^{\circ}C$$

In solving temperature problems for mechanics of continuous deformation medium and, in particular, thermal elastic problems we clash with a physical parameter specifying linear temperature expansion. It should be mentioned that the high temperature also influences the coefficient of linear steel expansion. It is known that under low temperatures this ratio is a constant quantity, however in this interval it changes depending on temperature increase. It is expedient to use the relationship of the following form for the coefficient of thermal expansion [27]:

$$\alpha=\alpha_0+\alpha_2T,$$

where α_0, α_2 are constants to be specified from experiments having the following values for particular class of steels:

$$\alpha_0 = 0.115 \times 10^{-4}\, 1/^{\circ}C \quad \alpha_0 = 0.1 \times 10^{-7} \left(1/^{\circ}C\right)^2$$

The proposed approximation expressions for the carbon steel elasticity modulus and coefficient of thermal expansion can be applied in strength analyses, and it will really estimate "workability" of the pipeline in critical situations. On the ground of experimental research results of deformation properties in structural steel under high temperatures $\left(T > 200^{\circ}C\right)$ the functions of the steel elasticity modulus are constructed. The relationships describing the change in the steel elasticity modulus under high temperatures suitable for solving engineering problems are obtained.

References

1. N. I. Nikitenko and N. R. Snovida, The temperature dependence of Poisson's ratio and its influence on solids stress condition. *Teplofizika I Teplotekhnika*, No. 29, 38–41 (1975) (in Russia).
2. I. E. Prokopowich, *Influence of long-term processes on construction stress and deformation conditions* (Gosstrojizdat, 1963) (in Russian).
3. N. I. Bezukhov, N. I. Bajanov, I. I. Goldenblat, N. A. Nikolajenko, and A. M. Sinjukov, *Durability, stability and vibration calculation in high temperature environment* (Mashinostroenie Moscow, 1965), pp. 567 (in Russian)
4. S. A Golovin, A. A. Morozjuk, et al., Plant for steel Young modulus measurement under high temperature, in *Book Vzaimodejstvie defektov kristallicheskoj reshotki I svojstva metallov*, Tula, pp. 90–93 (1980) (in Russian).
5. N. N. Guglin, A. A. Novikova, and B. B. Guljaev, Study of mechanical properties of steels under temperature near-crystallization point, *Kristalizatsija metallov*, 126–134 (1960) (in Russian).
6. E. A. Leonova, Mechanical properties of steels about a crystallization temperature, *Uprugost I neuprugost*, No. 1, 221–250 (1971) (in Russian).
7. Tetsu to Hagane. Influence of copper, tin and sulfur on mechanical properties of 0.25% carbon steal under high temperatures, 66, No. 4, 170 (1980) (in Russian).
8. L. I. Morozinski and O. A. Mitaev, Physicochemical and thermal-physic processes of bar steel crystallization, *Tr. II konferentsii po slitkam*, 438–447 (in Russian).
9. O. P. Puringer, Forming of uninterruptedly-casted feedworks, *Chornie metallic*, 6–7, 3–8 (1967)
10. A. Ghali and E. Elliott, Pre stressing of circular tanks, *ACI Structural Journal*, 88, No. 6, 721–729 (1991).
11. V. L. Yefimov, Steel pouring and crystallization, *Metallurgia*, Moscow, 552 (1976) (in Russian).
12. L. M. Muradyan, The plane problem of thermal creep under high temperatures, *DAN. ArmSSR,* LIV, No. 1, 74–85 (1972).

13. Yu. N. Rabotnov, *Creep of construction element* (Moscow, Nauka, 752, 1966) (in Russian).
14. S. A. Shesterikov et al., *Rules of creep and long-term durability* (Moscow, Mashinostroenie, 101, 1983) (in Russian).
15. A. A. Ilushin and B. E. Pobedria, *Mathematical fundamentals of thermoviscoelastic theory* (Moscow, Nauka, 280, 1970) (in Russian).
16. L. M. Kachanov, *The theory of creep* (Fizmatgiz, Moscow, 455, 1960) (in Russian).
17. I. I. Goldenblat et al., *Structural analysis on thermal effects* (Moscow, 566, 1969) (in Russian).
18. F. K. G. Odqvist, *Mathematical theory of creep and creep rupture* (Oxford, Clazendon Press, 1974).
19. F. Garofalo, *Fundamentals of creep and creep-rupture in metals* (New York, 1965).
20. S. A. Shesteriklov and A. M. Lokoshchenko, *Creep and long-term stability of steels*, in Book Itogi nauki I tekhniki. Ser.Mekh. def.tverd.tela, 13, 3–186 (1980) (in Russian).
21. Yu. N. Rabotnov and S. T. Mileyko, *Short-term creep* (Moscow, 222, 1970) (in Russian).
22. K. Sorimachi and I. K. Brimocomba, Improvements in mathematical modeling of stress in continuous casting of steel, *Ironmaking and Steelmaking*, 4, 240–245 (1977).
23. V. K. Adamovich, I. I. Mints, and R. V. Yancer, About the nature of temperature-time parameters used during prediction of long-term stability steels and alloys, *Problemi prochnosti.*, No. 1, 34–38, (1976) (in Russian).
24. L. M. Muradyan and V. A. Vardanyan, About carbon steels creep under high temperatures, *Izvestia AN ArmSSR,* ser. tekh. Nauk, TXLIV, No. 4 (1991) (in Russian).
25. S. A. Palmers, Mechanical properties of steels under high temperature as a checker of continuous casting, *Met. oboz.*, 53, 23–32 (1978) (in Russian).
26. H. Fudzi, M. Oda, et al., Steel plasticity near-crystallization temperature, *Tetsu to Hagane*, 68, No. 14, 2148–2157 (in Russian).
27. R. N. Barsegyan, Thermal stress condition of hollow cylindrical shell with liquid nardening core, *Dis… kandid. Tekh. Nauk*, YrPhI, Yerevan, 99 (1985) (in Russian).

FRACTURE MECHANICS ANALYSIS OF REPAIRING A CRACKED PRESSURE PIPE WITH A COMPOSITE SLEEVE

PHILIPPE JODIN
Laboratory of Mechanical Reliability, University of Metz and ENIM
Île du Saulcy, F-57045 Metz cedex, France

Abstract: Pressure pipes may be externally damaged in different ways: corrosion or notch due to diving machines. These defects may initiate a fatigue crack, which will be first part-through, then through the thickness. This results in a weakened region of the tube, then in leak of the pressure fluid contained in the pipe. There are several ways to repair the tube: changing the portion of tube, welding of extra metal in the defect, putting a welded metal sleeve, or gluing a composite sleeve. This last solution seems to be the easiest and the cheapest. The advantage is that the repairing sleeve is made on site and can be put with a given pre-tension. The work presented here is the numerical study of the fracture mechanics parameters of a part-through crack in a tube submitted to internal pressure and repaired with a composite sleeve. As there is a transfer of loading from the cracked tube to the repairing sleeve, the fracture mechanics parameters of the crack such as *J*-integral or opening of the crack lips will be modified. The study can be used as a design procedure for such repairing sleeves.

Keywords: pipes, defects, composites, fracture mechanics, finite elements

1. Introduction

The price of the transportation of fluids (gas or liquids) in pipes may be seriously increased when there is a leak, due to the waste of fluid. Moreover, the fluid may be dangerous for environment and health, if it is toxic or explosive. Leak is generally caused by brittle fracture of the pipe, or by the opening of the defect, depending on the nature of the material and on the environmental conditions.

G. Pluvinage and M.H. Elwady (eds.), Safety, Reliability and Risks Associated with Water, Oil and Gas Pipelines, 325–333.

Defects may have several kinds of origin, but are generally due to welding defects, corrosion pitting, manufacturing defects, or damage caused by diving tools or machines, in case of works on the place of the pipe.

When the defect is detected, its harmfulness is asserted and, if necessary, a repairing procedure is initiated. There are several possibilities to repairing a tube portion [1, 2, 3]:

- To replace the portion by a new one
- To weld, if applicable, a patch over the damaged zone
- To weld a metallic sleeve around the damaged zone
- To wrap a composite sleeve around the damaged zone

The first solution is certainly the most efficient, but also the most expensive, as it needs very important works and interruption of service of the pipe. The second and the third ones are less expensive and do not need interruption of service, but are only applicable to steel pipes which can be welded. In this work, we will present the last solution, which is applicable to all materials in any kind of situations. Moreover, it does not need a large quantity of works and does not need interruption of service of the pipe.

2. Presentation of the Mechanical Problem

The situation which is here studied is that of pressure pipe exhibiting a semi-elliptical longitudinal part-through crack. It is represented on Figure 1, where the crack plane is parallel to the axis of the tube. The crack is assumed to have been initiated from a defect on the outer surface of the tube, for instance a notch caused by a diving machine during works. Under fatigue loading, the crack has been initiated and it propagates, taking progressively a semi-elliptical shape.

When the crack is detected and repairing decided, a sleeve made from pre-impregnated unidirectional fiberglass fabrics is wrapped around the defect zone. The sleeve has a width of 1.5–2.0 times the length of the crack.

In a previous work [4], a similar situation has been presented, but for a straight through-the-wall crack. It has been shown that a drastic reduction of the *J*-integral maximum value was obtained by this repairing process.

To study the fracture conditions of such a situation, we have computed the *J*-integral along the front of the crack.

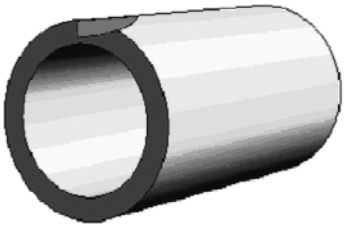

Figure 1. Schematic view of a portion of the cracked tube.

3. Finite Elements Computation of The *J*-Integral

The finite elements computation has been done using the CAST3M program delivered by the French Atomic Energy Agency (CEA). Only a quarter of the tube has been meshed, including a lip of the crack. The sleeve, if any, is considered as glued or only in contact with the tube. The actual situation is probably intermediate, depending on the properties of the surface where the sleeve is glued. Both situations will be computed, giving the upper and lower boundaries of the solution. A view of the mesh is given in Figure 2.

Figure 2. General view of the mesh of the quarter of the tube.

The detail of the crack meshing is given on Figures 3 and 4.

The mesh around the crack front line is automatically generated by a procedure, where the number of elements, their shape, and the number of concerned layers of crack elements are given. The quarter of cylinder is therefore generated from the initial cracked block.

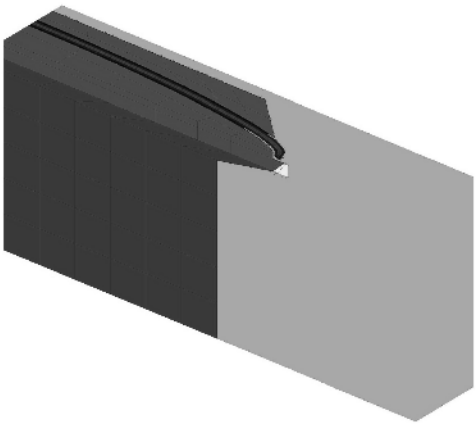

Figure 3. View of the crack meshing.

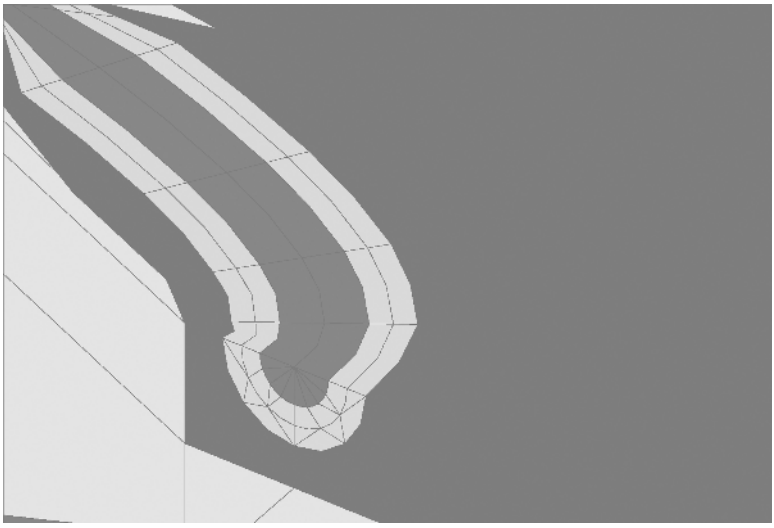

Figure 4. Detailed view of the crack front meshing.

TABLE 1. Combinations of sleeve thickness and width for calculations.

		Sleeve width (mm)		
	Sleeve thickness (mm)	No sleeve	36	48
Elastic	No sleeve	X		
Nonglued	5		X	X
	10		X	X
glued	5		X	X
	10		X	X
	10		X	X

In a previous work [4], it has been shown that there was little difference between elastic and elasto-plastic calculation (1.8% between maximum *J*-integral values). Therefore, in this work, only elastic computations have been done.

The different combinations of sleeve thickness and width are given on Table 1.

Materials used in the computation are given in Table 2. They are a standard pipe steel used in France for gas distribution and a standard fiberglass-epoxy composite.

E_1 is the Young's modulus along the fibers direction

E_2 is the Young's modulus across the fibers direction

ν_{12} is the Poisson's ratio measuring the transverse contraction when pulling in the fibers direction

G_{12} and G_{12} are shear modulus in two orthogonal planes containing the fibers direction axis

G_{23} is the shear modulus in the plane perpendicular to fibers direction

σ_y is the yield stress of the steel

σ_u is the ultimate stress of the steel

4. Results

Results are given in terms of maximum crack lip opening and evolution of *J*-integral along the crack front line, from the deepest point to the surface point.

Crack lips opening. The opening of the lips is computed at the upper lip point, which is located on the axis of symmetry of the crack. The results are presented on Figure 5.

TABLE 2. Materials data for computation.

Property	Steel	Composite
E1 [MPa]	203,000	49,400
E2 [MPa]	–	18,000
ν, ν12	0.28	0.4
G12 [MPa]	–	7,800
G23 [MPa]	–	6,760
G13 [MPa]	–	7,800
σ_y [MPa]	410	–
σ_u [MPa]	528	–
Elasto-plastic behavior law	$\sigma = 587.3*\varepsilon^{0.045}$	–

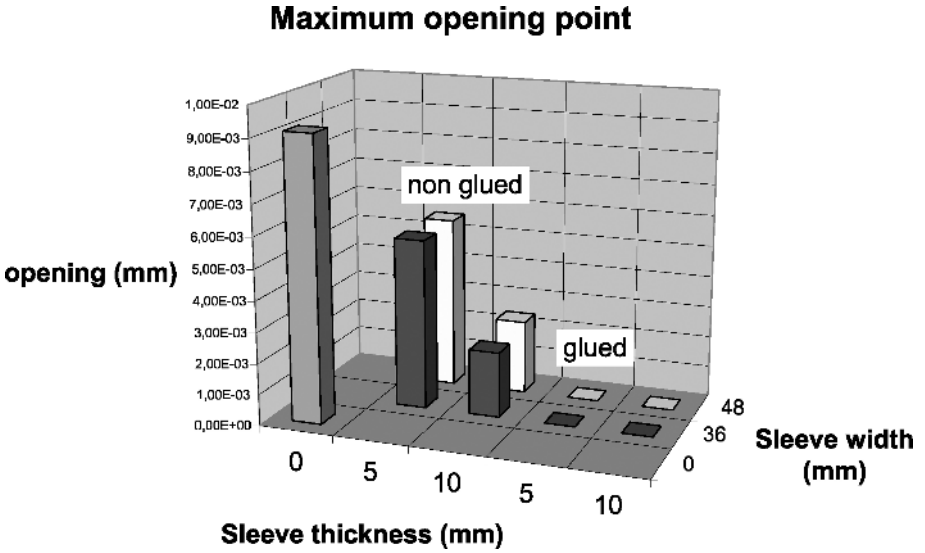

Figure 5. Maximum crack lip opening value in different cases.

It is observed that there are great differences between different sleeve-tube joining conditions, when sleeve width seems to have minor effects. This is clearly demonstrated in Figure 5.

J-integral values. *J*-integral is automatically computed by the FE program at the first available contour, with respect to the crack tip meshing, then to the second one, and then to the third one. As the first contour calculation exhibits instabilities due to meshing, the second one seems to be more consistent, and

the third one has few differences with respect to the second one. Finally, it is decided to retain the values obtained on the third contour, which seems to be the most stable. The evolutions of the *J*-integral are given on Figure 6.

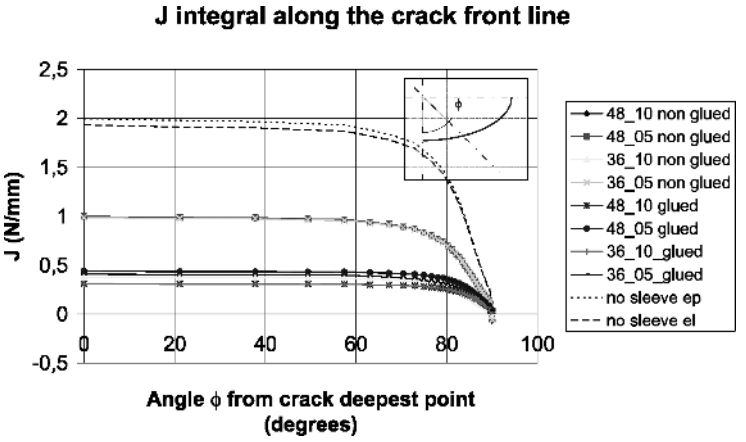

Figure 6. Evolution of *J*-integral values along the crack front line.

It is clearly seen on that figure that the *J*-integral value is, at least, divided by two when fitting a sleeve and that it is quite constant on the main part of the front line and decreases to near zero when reaching the outer surface of the tube. The maximum *J*-integral values are reported on Figure 7. It is obvious that the sleeve has a strong effect on the maximum *J*-integral value, but, there is a slight influence of sleeve width and thickness.

5. Analysis of Results

The reductions of the opening of the lip and of maximum *J*-integral value are given in Tables 3 and 4, with respect to the no-sleeve condition.

It is obvious that there is a strong effect of the sleeve on the fracture mechanics parameters, i.e., crack opening and *J*-integral. This effect is maximum for the thickest sleeve. However, the width of the sleeve seems to have non-significant effect or slightly negative effect. The most important effect is obtained when the sleeve is glued on the pipe. But this depends highly on gluing conditions. In any case, this demonstrates the interest to repair damaged pressure pipes with this technique.

TABLE 3. Maximum opening of the crack lip percentage of reduction with respect to no-sleeve case.

		sleeve width		
	sleeve thickness (mm)	0	36	48
No sleeve	0	9.14E–03		
Nonglued	5		–40.1%	–39.4%
	10		–77.0%	–74.1%
Glued	5		–100.0%	–100.0%
	10		–100.0%	–100.0%

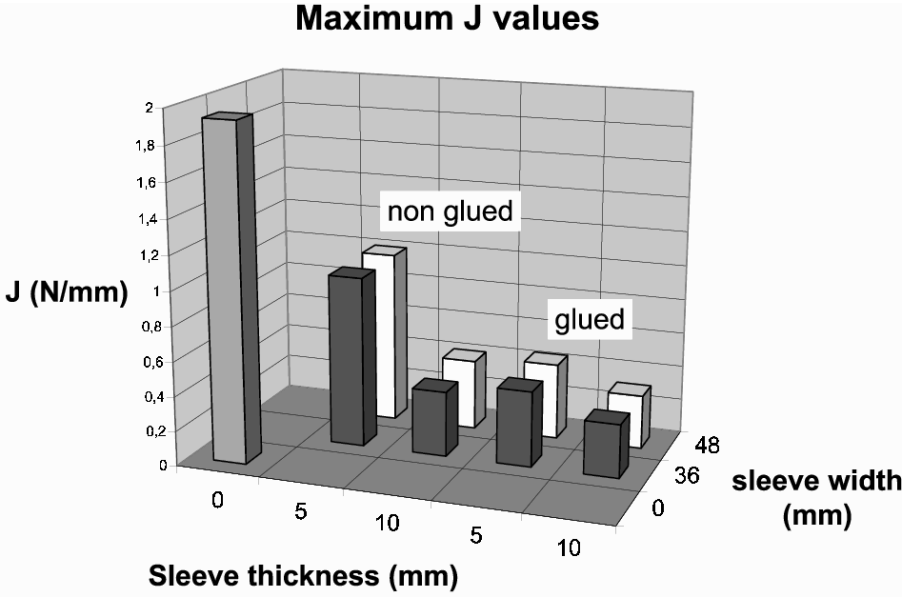

Figure 7. Maximum *J*-integral values in different cases.

In a previous study [4], the stresses in the composite sleeve have been computed. They grow up to 140 MPa. This value should be quite lower in the present studied cases.

TABLE 4. Maximum values of *J*-integral reduction with respect to the no-sleeve situation.

		Sleeve width		
	Sleeve thickness (mm)	0	36	48
No sleeve	0	1.9336		
Nonglued	5		–48.9%	–48.3%
	10		–80.5%	–78.9%
Glued	5		–77.4%	–77.2%
	10		–84.0%	–83.9%

As conclusion, we can recommend trying to repair damaged tube with a composite fiberglass fabric, which will be easy, cheap, and safe. Moreover, if a pretension is applied, an improvement of the tube capacities could be obtain, preventing unexpected effects of peak of pressure, or dilatation due to temperature variations.

References

1. Frassine, R., "Long-Term Performance of a Polymer Composite Repair System for Gas Pipelines", *Advances in Polymer Technology*, vol. 16, no. 1, pp. 33–43, 1997.
2. Alexander, C. R. and Wilson, F. D., Assessing the Use of Composite Materials in Re-rating Liquid and Gas Transmission Pipelines, *Proceedings of the ASCE National Conference on Environmental and Pipeline Engineering 2000*, pp. 343–347, Kansas City (Mis.), July 23–26, 2000.
3. Palmer-Jones, R. and Paisley, D., Repairing Internal Corrosion Defects in Pipelines – A Czse Study, *Proceedings of the 4th International Pipeline Rehabilitation and Maintenance Conference*, pp. 1–25, Prague, September, 2000.
4. Jodin, Ph., An Elastoplastic Fracture Mechanics Study of a Pressurized Steel Pipe Repaired with Fiberglass Reinforced Composite Sleeve, *Proceedings of the NT2F5 Congress*, Bari (Italy), May 9–10, 2005 (to be published) jodin@univ-metz.fr.

REVIEW OF GAS TRANSMISSION PIPELINE REPAIR METHODS

REMI BATISSE
Gaz de France – Research and Development Division
361, Avenue du Président Wilson-BP 33, 93211 Saint-Denis la Plaine Cedex – FRANCE

Abstract: Repair methods are key operations for the integrity management of pipelines. The parameters guiding the repair decision are briefly reminded. A nonexhaustive external and internal repair techniques are described, notably grinding and weld deposition techniques, metallic and various composite sleeves which are developed for 25 years. The main advantages of different repair techniques are summarized in conclusion and perspectives are given.

Keywords: pipeline, repair, weld deposition, grinding, metallic sleeve, composite sleeve, internal repair, defect, flaw

1. Context

During the last 50 years, gas transmission pipelines have become significant networks to transmit high energy quantities on long distances from gas deposit to consumption areas. Considering European Transmission Pipelines only, the onshore network mileage has been multiplied by more than three times between 1970 and 2004. But, despite the growing of the gas transmission pipelines mileage, the failure frequencies by leak or rupture have been reduced by five in Europe in the same time (EGIG report [1]).

This improvement of pipelines integrity management along the years is partially the consequence of high-technical developments like systems for the aggressions prevention and detection, inspection tools, repair techniques. When a defect is identified, operators must ask:

- Is the defect acceptable without repair? If yes, the external coating is restored. If the defect is temporarily acceptable, the defect can be immediately repair

G. Pluvinage and M.H. Elwady (eds.), Safety, Reliability and Risks Associated with Water, Oil and Gas Pipelines, 335–349.

or repair after a time requiring a next inspection. The choice is often lead by a cost competition between the immediate repair and the delayed repair with an additional inspection.

- If not acceptable, is the defect repairable? And what is the more adapted repair technique? If not repairable, the extreme decision to replace the damaged pipe or segment is taken requiring an interruption of gas transit and so a loss of earnings.

This paper focuses on repair technologies for gas transmission pipelines. After a remind of the main parameters to guide a repair decision, a nonexhaustive external and internal repair techniques are described.

2. Main Parameters to Guide the Repair Decision

Before to repair, the operators have to check a list of parameters to make the best choice of repair techniques. If any of these parameters are unknown, the operators have to opt for the conservative assumption. These parameters are following:

- Pipeline geometries and materials
- Pipeline operating characteristics
- Pipeline configuration and location
- Nature and extend of the defect to be repaired

2.1. PIPELINE GEOMETRIES AND MATERIALS

- *Pipe Geometries*

The pipe diameter must be considered to select the appropriated external repair by sleeves whereas the pipe thickness is a limiting parameter for repair techniques requiring welding on pipe as welded sleeves or weld deposition.

- *Pipe Materials*

The steel strength and toughness determine the residual resistance of the damaged pipe section necessary to quantify the amount of reinforcement which must be sustained by the repair. Otherwise, the steel grade is a metallurgical indicator for the repair techniques involving welding which can be limited for high-grade steels more tricky to weld. The presence of girth weld or seamweld in or near the damaged area can be also a limiting parameter and the welding process has to be known.

2.2. PIPELINE OPERATING CHARACTERISTICS

The repair technique chosen must ensured the full integrity of the pipeline during its remaining lifetime in operating conditions. So:

- The Maximal Allowed Operating Pressure (MAOP) must be restored after the repair of the damaged section.
- The repair must sustain the pressure fluctuations during the pipeline lifetime. In consequence, a profile of pressure variation during the time in terms of amplitude, frequency, and mean pressure must be estimated to define the repair of defect.
- In certain cases, the pipe temperature can increase up 60°C for example at the exit of compression station or in opposite decrease to –40°C during a decompression; The choice of the repair method can be affected by the temperature like the durability of organic materials (composite sleeves) decreasing at elevated temperature whereas metallic materials becoming more brittle at cold temperature (weld deposition, welded metallic sleeve).
- A pressure drop is sometimes required during the repair for some techniques. The possibility or not to decrease temporary the pressure influences the choice of the repair technique.

2.3. PIPELINE CONFIGURATION AND LOCATION

The pipeline configuration also affects the choice of the repair method. A pipeline buried deeply or in a strong slope contains significant additional stresses to primary stress created by the internal pressure. The repair method has to take into account this supplementary stresses. The presence of bends and elbows can exclude certain repair techniques.

The pipeline location is also a constraint. The pipelines accessibility in a high density of population area is sometimes very restricted, and can lead to prevent an excavation for the repair. So repair technique without excavation could be the only one solution if all other parameters are satisfied.

2.4. NATURE, ORIENTATION, AND SIZE OF THE DEFECT

The nature of the defect (external or internal corrosion, plain dent, gouges, gouge in dent, cracks, lack of penetration), the orientation (axial or circumferential), and the size (length and depth) are the important parameters to choose and to design the repair technique. The determination of these parameters requires an excavation to proceed to size the defect as accurate as possible by None Destructive Techniques (US, radiography).

In view to guide the choice on repair techniques, the EPRG [2] has produced in December 2000, repair specifications applicable for any kind of permanent repair technique for natural gas onshore pipelines. These specifications refer to three areas:

- Generic functions
- Application range
- Defect type

For each area, different functions or application ranges or defect types are listed with a required level which is nonnegotiable or negotiable or optional. For example:

- Duration of repair is a generic function. “Less than a day” is a required level which is negotiable
- Repair lifetime is also a generic function. “≥ 50 years” is a required level which is nonnegotiable
- Steel grade is an application range. “L220-L485” is a required level which is nonnegotiable
- Hot bends is also an application range. “Radius of curvature ≥ 5*Diameter” is an optional required level

This EPRG method allows a first approach to select the choice of repair technique candidate without to forget specifications we need. After this approach, the remaining repair candidates can be evaluated comparing other factors like the cost, the availability, or how easy to bring on field.

3. Review of Repair Techniques

3.1. EXTERNAL REPAIR TECHNIQUES

3.1.1. *Cut Out and Replace*

The cut out and replace is an extreme option, but conservative and safe since the damaged pipe section is removed and replaced by a sound pipe. However, this solution is expensive because it requires an interruption of the transit gas in the pipe to be repaired involving a loss of earning and could lead to review the contractual requirements with the end-customers. After the replacement, a new inspection is needed, notably for the girth weld, and an hydrostatic test can be required before to resume the gas transit.

3.1.2. *Bypass (Hot-tapping and Grouted tee Connection)*

The hot-tap process can be used to bypass the damaged pipe section. A new pipeline branch surrounding the damaged section is welded on the pipeline in service. Then, the pressure is applied in the pipeline branch and stopped in the damaged section which can be cut. So the gas transit interruption is avoided. Nevertheless, certain conditions are recommended or required as to weld the branch out of girth weld or seamweld. The branch pipeline with its welds must hold the service pressure. In addition, workmen must be qualified to weld, and pipe steels easily to weld on field. Lastly, Advantica [3] has developed a connection system called "Grouted tee", which is an alternative to welded tee connection. The need of skilled welders and the dependence of metallurgical aspects are removed. This is a great advantage in terms of effective cost and of application areas (diameters, high-grade steels, greater ovality).

3.1.3. *Grinding*

Grinding is a technique widely used to repair superficial defects removing:

- The harmful stress concentration effect of defect
- Hardened material and other damages near the defect like micro-cracks

However, following conditions are required:

- The operating pressure should be reduced to 80% during the repair process.
- Grinding shall not be used as the sole means of permanent repair of an indented defect. The aim of the grinding is to remove the stress concentration of a gouge or scratch in the dent before to apply a reinforced sleeve (metallic or composite).
- If the crack or the affected material near the defect do not entirely removed by grinding, an alternative repair technique must be applied instead.
- The removal of all cracks must be verified by NDT after grinding.
- The limits for metal removal for nonindented defects must be in agreement with ASME B31G [4] criterion corrosion and removal by grinding of more than 40% of the nominal wall thickness is not accepted.

Due to the restricted conditions of ASME B31G, pipeline operators have qualified their own optimized grinding methods to increase the application range. For example, Gaz de France has qualified its optimized grinding by several experimental fatigue and burst tests validated by finite elements analysis using the Dang Van fatigue criteria [5]. Figure 1 shows an example of optimized grinding.

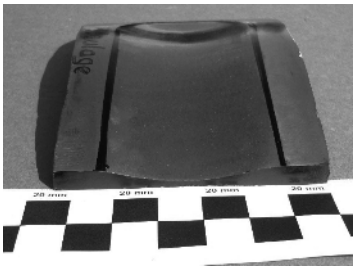

Figure 1. Optimized grinding.

3.1.4. *Weld Deposition*

A weld deposition (Figure 2) can be applied to rebuild the full wall thickness of pipe after a metal loss has occurred by corrosion, gouging, or after grinding. The weld deposition is adapted for bend sections or fittings where the use of sleeves is often inhibited. In addition, the weld deposition can be a cost effective compared to the sleeve cost and the time involved the sleeve installation. Nevertheless, the application range of the weld deposition is limited:

- The first limit is imposed by the burn-through which can occur when the pipe metal under the molten weld pool is insufficient to contain the internal pressure. In consequence, pipes with thin thickness are often out of the weld deposition application range.
- A second limit is the risk of hydrogen cracking which can occur when the steel microstructure is susceptible to hydrogen which is introduced during the welding and tensile stress acting on the weld. The condition of hydrogen cracking must be eliminated minimizing hydrogen level by low-hydrogen electrodes or low-hydrogen process.
- The third limit is the need of skilled welders.

Detailed guidelines for weld deposition repairs in the field are given by W. A Bruce [6] and in the Appendix B of API 1104 [7].

3.1.5. *Full Encirclement Sleeves*

TYPE A STEEL SLEEVES

Type A sleeve is attractive because it can be installed without welding on the pipe where a defect has to be repair. Two halves of a cylinder of pipe are placed around the pipe at the damaged area and after positioning, are joined by welding the side seams. The major advantages of a type A sleeve are following:

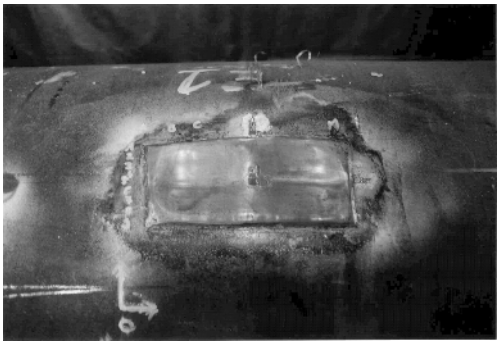

Figure 2. Weld deposition.

- For short flaws, the thickness of the sleeve can be reduced to two thirds of the thickness pipe, assuming that the sleeve is at least as strong as the pipe material because the sleeve does not carry much hoop stress. A short flaw is defined by a length "L" less or equal to $(20Dt)^{0.5}$ where "D" is the pipe diameter and "t" the thickness.
- For the longer flaws, the sleeve thickness should be equal or greater than the pipe thickness if the sleeve is at least as strong as pipe material.

In the two cases of flaw length, the A sleeve can be fabricated simply and requires no rigorous nondestructive inspection.
The minor disadvantages of the type A sleeve are listed below:

- It can not be used for circumferentially oriented defects because it can not sustain the axial stress.
- It can not be used to repair leaking defects because it cannot sustain the service pressure.

CSA Z662 [8] gives the use of steel compression A sleeves attractive for repairing longitudinally oriented crack-like defects.

TYPE B STEEL SLEEVES

This type of steel sleeve (Figure 3) is able to contain the maximum allowable operating pressure (MAOP) and to carry a longitudinal stress imposed on the pipeline by lateral loads. So, the type B sleeve can be used to repair leaks and to reinforce the circumferentially oriented defects.

The type B sleeve consists of two half pipes welded together and placed over the pipe section containing the defect. The ends of the sleeve are welded onto the pipe with full encirclement fillet welds. If a weld is present on the pipe

Figure 3. Type B sleeve repair.

section to be repaired, the sleeve's inner surface can be machined to accommodate the weld. Since the thickness of the sleeve must be designed to contain the MAOP, its nominal value t is determined versus the MAOP "P", the external pipe diameter "D", the pipeline design factor "F" and the Specified Minimum Yield Strength "SMYS" :

$$T = PD/[2F(SMYS)]$$

Because welding to the carrier pipe is required, the same precaution taken for weld deposition is applied to weld the type B sleeve onto the pipe (API 1104 [7]). In addition, the remaining wall thickness of the carrier pipe where welding is to be performed must be determined by ultrasonic inspection before the repair. After the repair, the sleeve welds should be inspected to ensure the integrity.

3.1.6. *Composite Sleeves*

Composite sleeves have been developed during the past years. Notably, Gas Research Institute, GRI contributed with a large effort during the 1990s [9, 10]. A state of the art assessment of composite systems used to repair transmission pipelines has been provided by Chris Alexander and Bob Francini [11]. Composite sleeves offer great advantages:

- Restoring the full strength of a damaged pipeline
- Increasing the stiffness of the repaired pipe section and so reducing the local strain induced by internal pressure on the defect area
- Favoring leak-before-break failure modes and arresting crack propagation
- Inhibiting external corrosion phenomenon, the composite acting like an external coating

The drawback of composite sleeves is the ageing. The mechanical properties decrease with the time. This decrease of mechanical properties is taken into account in the qualification for permanent repair techniques. The lifetime target is at least 50 years in the standard specifications (CSA Z662 [8]). The ASME B31.8 [12] does not accept the repair of injurious dents or mechanical damage, "unless proven through reliable engineering tests and analysis". Lastly, Chris Alexander and Franz Worth P. E. [13] have shown that dent with gouge removed by grinding could be repaired by composite sleeves.
Two main techniques are used to elaborate composite wraps for pipeline repair:

- One is based on precured and prefitted to standard pipe diameters composite coils
- The other, referred as "wet-tape" technology is cured on site

The precured composite sleeves are made of prefitted composite panels which are wrapped on the section of pipe to be repaired, and hold in place by an adhesive which is placed between the successive composite layers during application. Due to the elaboration in a factory, the curing of the matrix is accurately controlled and this process also allows the use of polyester as the composite matrix which is less sensible to the ageing process compared to epoxies. However, this process is not adapted to repair specific pipeline configurations others than straight and slightly ovalized sections.

For the "wet-tape" technology, the impregnation of the fiber reinforcement is performed on site during the implementation of the repair. The advantage is that the final composite wrap can be designed according to the severity of the defect to repair. However, the performances of "wet-tape" are more sensitive to implementation conditions during the on-site impregnation of the fibers like the control of the volume fraction of reinforcement and the accuracy of its homogeneity.

CLOCK-SPRING SLEEVE

This product is distributed by Clock-spring Co. [14]. Clock-spring is a precured composite sleeve composed with a polyester matrix and a type E glass fibers reinforcement, prefitted, and prestrained in a cylindrical coil of eight layers (Figure 4).

Clock-spring is used since more than 15 years, due to its use of implementation (limited workforce) and its wide application range. However, it cannot be applied to repair bends or ovalized pipe sections and to provide axial reinforcement of the damaged section.

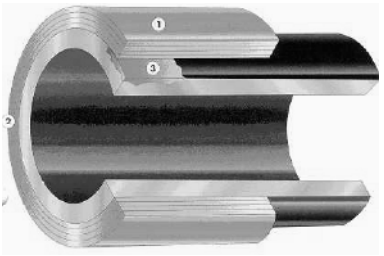

Figure 4. Clock-spring.

PERMAWRAP AND WELDWRAP SLEEVES

These products, very similar of Clock-spring composite, are offered by the Wrapmaster company [15]. The main differences compared to Clock-spring are the insertion of metallic material to allow the detection by a MFL inspection tool of an already installed wrap (Figure 5). In addition, a specific product, called weldwrap, has been validated to repair defects near or on filled welds.

Figure 5. Implementation of a Permawrap sleeve.

ARMOR PLATE PIPE WRAP SLEEVE

The Armor Plate Pipe Wrap sleeve [16] is a “Wet-tape” technology consisting in a primary bonding resin applied on the defect area with a high stiffness resin used to transfer the load from the defect to the sleeve, glass fibers mats and an epoxy resin used for the impregnation of the fibers. This technology allows to repair in specific configurations, like on a bend or on a “T” connection (Figure 6).

Figure 6. Plate Pipe Wrap on a bend and a connection.

TECHNOWRAP 2K SLEEVE

The Technowrap 2K composite wrap is a "wet tape" permanent repair distributed by Walker Technical Resources [17] (Figure 7). The main advantage of Technowrap 2K is the difference of fibers orientations (one in the axial direction and the others at ±45°) which offers an axial reinforcement in addition of the reinforcement in the hoop direction, by a significant fraction of aramid fibers.

Figure 7. Technowrap 2K sleeve.

STRONGBACK SLEEVE

The strongback sleeve composite, distributed by Strongback Corporation [18] is a "wet tape" technology based on three components (Figure 8):

- A primary bonding made of a blend of epoxy and polyamine to enhance the cohesion between the pipe and the wrap
- A high-stiffness resin used to transfer the load from the defect to the composite wrap
- Glass and Kevlar fibers panels, preimpregnated with a resin whose curing process is activated by water

Figure 8. Implementation of strongback sleeve on field.

The use of a water activated curing process for the resins of the strongback sleeve system allows its implementation under flooded conditions, such resins being also less sensitive to humidity-induced ageing.

3.1.7. *Epoxy Sleeve Repair (ESR)*

The epoxy sleeve Repair (ESR) [19], is distributed by PII. Two oversized steel half-shells are joined to encircle the damaged area leaving an annular gap (Figure 9). The annulus is sealed at each end of sleeve with a fast-setting material, and then filled at very low pressure with a stiff epoxy-based compound.

The epoxy grout compound forms an excellent bond at both steel interfaces, providing an high reinforcement of the damaged section, in the axial and circumferential directions. Welding on the pipe is not required, and the need of skilled welders is not necessary. ESR has been used on major pipeline networks for more than 20 years and has been validated by numerous tests in terms of internal pressure loading and fatigue cycles. ESR can repair all types of nonleaking defects such cracks, dents, gouges, corrosion, and manufacturing defects, also in girth welds or seam welds. In most of cases, the repaired area is stronger than the adjacent sound pipe.

Figure 9. Schematic view of epoxy sleeve Repair (ESR).

3.2. INTERNAL REPAIR TECHNIQUES

Internal repair techniques consist to introduce an internal liner in the damaged section pipe to reinforce it. These techniques are often trenchless. It is a benefit in urban areas reducing the annoyance of residents, the traffic obstruction, the damage to the environment and minimizing the time of repair. Unfortunately, the most of them are restricted in range application for gas distribution or for low pressure below 20 bar. Nevertheless, we can mention the "Starline-HPL" [20], produced by Karl Weiss Technologies. Starline-HPL is a composite linear made up of polyester fibers impregnated by polyurethane or polyethylene resin. The implementation can cover up 600 m length in trenchless condition (Figure 10).

Figure 10. Implementation of Starline-HPL.

Starline-HPL was awarded by the German DVGW VP404 certificate [21] in 2002 for a Maximum Allowable Operating Pressure of 30 bar. It has been used for bridging corrosion pits up to 50 mm (2") in diameter or to reinforce damaged section containing cracks or severe defects in girth welds.

4. Conclusions and Perspectives

This nonexhaustive review exhibits a lot of available repair techniques. V. Diaz et al. [22] and PRCI [23] have established first matrix to indicate the repair techniques which can be applied to various types of defects. The results show:

- Type B sleeve is the repair method which is adapted for any kind of defects such as external and internal corrosions, gouges, dents in body or in welds (girth weld and seamweld), cracks, and girth weld defects because it is able to contain the service pressure and to reinforce the axial and circumferential stresses. This repair technique requires skilled welders to join the sleeve on pipe body.
- ESR is also an interesting repair technique for all types of nonleaking defects with the benefit to avoid the welding requirements.

- The composite sleeves reinforce the hoop stress but not the axial stress, except few of them like Technowrap 2K sleeve. So, they are adapted to repair axial-oriented defect but they cannot be used for circumferential defect or damaged section of pipe loaded by other forces creating complementary axial stress (ground movement). We can also mention the trick of Permawrap sleeve inserting detectable metallic material to indicate the presence of a repair during a MFL inspection.
- Weld deposition is limited for external corrosions, gouges, and shallow cracks after removing cracks by grinding. Obviously, this method requires skilled welders and is more sensitive to the high-grade steel pipe.

Nevertheless, in perspective two improvements should be implemented:

- There is a need to validate with more accuracy the application range of repair techniques in many cases of defects. Notably, the range of dent repair by metallic or composite sleeves is known with partially limits.
- There is also a need to compare the costs between different repair techniques for a same defect to repair.

For the future, the repair techniques shall be checked for the new emerging pipelines like grade X100 and the pipelines used to transport gas involving hydrogen in natural gas [24] or pure hydrogen like an energetic vector.

References

1. 6th Report of European Gas Pipeline Incident Data Group, December, 2005, 6th EGIG-Report 1970–2004, *Gas pipeline Incidents*, 2–31 – http://www.EGIG.nl.
2. V. Diaz, M. Zarea, S. Torun, and P. Riou, December 27, 2000, *State-of the-art on existing repair techniques for damaged pipelines,* on behalf of EPRG workshop “fitness for purpose”.
3. Advantica, www.advantica.biz, Furmanite, www.furmanite.com.
4. ASME B31G, 1991, *Determining Remaining Strength of Corroded Pipelines: Supplement to B31 Code-Pressure piping.*
5. R. Batisse, H. Di Fant-Jaeckels, F. Curie, and J. M. Virely, Biaxial High Cycle Fatigue Tests On A Gas Transmission Pipeline Steel, *Fatigue Fracture Engineering Material Structures*, vol. 19, No. 10, pp. 1231–1238.
6. W. A. Bruce, 1998, *Guidelines for Weld Deposition Repair on Pipelines*, American Gas Association, Arlington, VA, Catalog No. L51782.
7. API STD 1104 *Welding Pipelines and Related Facilities*, 19th Edition, American Petroleum Institute, Washington DC, October 31, 2001.
8. CSA Z662, *Oil and Gas Pipeline Systems*, Canadian Standards Association, Mississauga, Ontario, June, 2003.

9. C. J. Kuhlman, U. S. Lindholm, D. R. Stephen, T. J. Kilinski, and R. B. Francini, *Long-Term Reliability of Gas Pipeline Repairs by Reinforced Composites*, Final Report to the Gas Research Institute, Chicago, IL, GRI-95/0071, December 1995.
10. D. R. Stephen and T. J. Kilinski, *Field Validation of composite Repair of Gas Transmission Pipelines*, Final Report to the Gas Research Institute, Chicago, IL, GRI-98/0032, April 1998.
11. C. Alexander and B. Francini, *State of the Art Assessment of Composite Systems used to Repair Transmission Pipelines*, 6th International Pipeline Conference, Calgary, Canada, IPC2006-10484, September 2006.
12. American Society of mechanical Engineers, 2003 Edition, *Gas Transmission and distribution piping Systems*, New York, ASME B31.8.
13. C. Alexander and B. Franz Worth, *Assessing the use of Composite Materials in Repairing Mechanical Damage in Transmission Pipelines*, 6th International Pipeline Conference, Calgary, Canada, IPC2006-10482, September 2006.
14. Clock-Spring, www.clockspring.com.
15. Permawrap and Weldwrap sleeves, www.wrapm.com.
16. Armor Plate Pipe Wrap sleeve, www.armorplateonline.com.
17. Technowrap 2K sleeve, www.technowrap.net.
18. Strongback corporation, www.strongbackcorp.com.
19. GE power Systems_PII Pipelines Solutions, www.gepower.com/prod_serv/serv/pipeline/en/field_serv_repairs/repair_tech/esr.htm.
20. Karl Weiss technologies, www.starlinett.com.
21. DVGW VP 404 “Rehabilitation von Gas-Hochdruckleitungen mit Gewebeschläuchen im Druckbereich über 4 bar bis 30 bar”, www.dvgw.de/service/neuerscheinungen2005.html.
22. V. Diaz, M. Zarea, S. Torun, and P. Riou, , *State of the Art Review on Existing Repair Techniques for Damaged pipelines (EPRG Report)*, 14th Biennal Technical Meeting on Pipeline Research, Berlin, Germany, Paper-29, May 2003.
23. C. E. Jaske, B. O. Hart, and W. A. Bruce, *Updated Pipeline Repair Manual*, Pipeline Research Council International, report R2269-01R, August 2006.
24. Naturalhy Project, European 6th FrameWork Programme FP6, www.naturalhy.net.